UNIVERSITÉ DE GRENOBLE

THÈSE

Pour obtenir le grade de

DOCTEUR DE L'UNIVERSITÉ DE GRENOBLE

Spécialité : **Sciences de la Terre, de l'Univers et de l'Environnement**

Arrêté ministériel : 7 août 2006

Présentée par

William VICARS

Thèse dirigée par **Joël Savarino**

préparée au sein du **Laboratoire de Glaciologie et Géophysique de l'Environnement**
dans **l'École doctorale Terre, Univers, Environnement**

Transfert de l'anomalie isotopique portée par l'ozone dans la troposphère : Vers une interprétation quantitative de la composition isotopique en oxygène du nitrate atmosphérique

Thèse soutenue publiquement le **19 avril 2013,**
devant le jury composé de :

M. Matthew JOHNSON
Professeur a l'Université de Copenhague, Rapporteur
M. Slimane BEKKI
Directeur de Recherche CNRS, LATMOS, Rapporteur
M. Christof JANSSEN
Chargée de Recherche CNRS, UPMC, Examinateur
M. Erik KERSTEL
Professeur à l'Université Joseph Fourier, Examinateur
M. Michel LEGRAND
Directeur de Recherche CNRS, LGGE, Examinateur
M. Joël SAVARINO
Chargée de Recherche CNRS, LGGE, Directeur de thèse

Université Joseph Fourier / Université Pierre Mendès France / Université Stendhal / Université de Savoie / Grenoble INP

Résumé

L'ozone (O_3) possède une anomalie isotopique en oxygène qui est unique et caractéristique, offrant ainsi un précieux traceur des processus oxydatifs à l'œuvre dans l'atmosphère moderne mais aussi ceux ayant eu lieu dans le passé. Cette signature isotopique, dénotée $\Delta^{17}O$, se propage au sein du cycle atmosphérique de l'azote réactif ($NO_x = NO + NO_2$) et est préservée lors du dépôt du nitrate (NO_3^-) présent dans l'aérosol, par exemple. L'anomalie isotopique en oxygène portée par le nitrate, $\Delta^{17}O(NO_3^-)$, représente ainsi un traceur de l'importance relative de l'ozone ainsi que celle d'autres oxydants dans le cycle des NO_x. Ces dernières années, de nombreux travaux de recherche ont été dédiés à l'interprétation des mesures de $\Delta^{17}O(NO_3^-)$. Pourtant, les processus atmosphériques responsables du transfert de l'anomalie isotopique de l'ozone vers le nitrate ainsi que leur influence globale sur la composition isotopique du nitrate à différentes échelles spatiales et temporelles sont encore mal compris. De plus, la magnitude absolue ainsi que la variabilité spatio-temporelle de $\Delta^{17}O(O_3)$ sont peu contraintes, car il est difficile d'extraire de l'ozone de l'air ambiant. Cet obstacle technique contrecarre l'interprétation des mesures de $\Delta^{17}O$ depuis plus d'une décennie. Les questions scientifiques posées au cours de ce travail de thèse ont été choisies dans le but de combler ces lacunes. Le principal outil d'analyse utilisé dans ce travail est la « méthode bactérienne » associée à la spectrométrie de masse en flux continu (CF-IRMS), une combinaison de techniques qui permet l'analyse de la composition isotopique totale du nitrate (c'est-à-dire, la mesure de $\delta^{15}N$, $\delta^{18}O$ et $\Delta^{17}O$). Cette méthode a été employée pour l'analyse isotopique d'échantillons de nitrate obtenus pour deux cas d'études : (i) une étude des variations spatiales de la composition isotopique du nitrate atmosphérique sur la côte californienne à l'échelle journalière; et (ii) une étude du transfert du nitrate et de sa composition isotopique à l'interface entre l'air et la neige à l'échelle saisonnière sur le plateau Antarctique. En outre, cette méthode a été adaptée à la caractérisation isotopique de l'ozone via la conversion chimique de ses atomes d'oxygène terminaux en nitrate. Au cours de cette thèse, un important jeu de données rassemblant de nombreuses mesures troposphériques de $\Delta^{17}O(O_3)$ a été obtenu, incluant une année entière de mesures à Grenoble, France (45 °N) ainsi qu'un transect latitudinal de collecte dans la couche limite au-dessus de l'océan Atlantique, entre 50 °S to 50 °N.

Ces observations ont permis de doubler le nombre de mesures troposphériques de $\Delta^{17}O(O3)$ existantes avant cette thèse et d'accroître de manière conséquente notre représentation globale de cette variable isotopique essentielle. Enfin, les deux cas étudiés et présentés dans ce document révèlent des aspects nouveaux et inattendus de la dynamique isotopique du nitrate atmosphérique, avec d'importantes conséquences potentielles pour la modélisation de la qualité de l'air et l'interprétation de l'information isotopique contenue dans les carottes de glace prélevées aux pôles.

Mots clés: isotopes stables, nitrate atmosphérique, ozone, anomalie isotopique, oxygène, azote

Abstract

The unique and distinctive ^{17}O-excess ($\Delta^{17}O$) of ozone (O_3) serves as a valuable tracer for oxidative processes in both modern and ancient atmospheres. This isotopic signature is propagated throughout the atmospheric reactive nitrogen (NO_x = NO + NO_2) cycle and preserved in nitrate (NO_3^-) aerosols and mineral deposits, providing a conservative tracer for the relative importance of ozone and other key oxidants involved in NO_x cycling. However, despite the intense research effort dedicated to the interpretation of $\Delta^{17}O(NO_3^-)$ measurements, the atmospheric processes responsible for the transfer of $\Delta^{17}O$ to nitrate and their overall influence on nitrate isotopic composition on different spatial and temporal scales are not well understood. Furthermore, due to the inherent complexity of extracting ozone from ambient air, the absolute magnitude and spatiotemporal variability of $\Delta^{17}O(O_3)$ remains poorly constrained, a problem that has confounded the interpretation of $\Delta^{17}O$ measurements for over a decade. The research questions that have been pursued in this thesis were formulated to address these knowledge gaps. The primary analytical tool used was the bacterial denitrifier method followed by continuous-flow isotope ratio mass spectrometry (CF-IRMS), which allows for the comprehensive isotopic analysis of nitrate (i.e., $\delta^{15}N$, $\delta^{18}O$, $\Delta^{17}O$). This method was applied to the isotopic analysis of nitrate samples in two case studies: (i) an investigation of the diurnal and spatial features of atmospheric nitrate isotopic composition in coastal California; and (ii) a study of the seasonality and air-snow transfer of nitrate stable isotopes on the Antarctic plateau. Furthermore, the method was adapted to the isotopic characterization of ozone via chemical conversion of its terminal oxygen atoms to nitrate. During the course of this thesis, a large dataset of tropospheric $\Delta^{17}O(O_3)$ measurements has been obtained, including a full annual record from Grenoble, France (45 °N) and a ship-based latitudinal profile from 50 °S to 50 °N in the Atlantic marine boundary layer (MBL). This observational dataset represents a two-fold increase in the number of existing tropospheric $\Delta^{17}O(O_3)$ observations and a dramatic expansion in the global representation of this key isotopic variable. Additionally, the two case studies presented reveal novel and often unexpected aspects of the isotope dynamics of atmospheric nitrate, with potentially important implications for air

quality modeling and the interpretation of isotopic information preserved in the polar ice core record.

Keywords: stable isotopes, atmospheric nitrate, ozone, ^{17}O-excess, oxygen, nitrogen

Acknowledgements

First, I would like to thank Matthew Johnson and Slimane Bekki for having accepted to evaluate this manuscript, as well as Christof Janssen, Erik Kerstel, and Michel Legrand for their participation in the jury.

The research presented in this thesis could not have been possible without the support and active involvement of many people. Above all, I acknowledge my advisor, Joël Savarino, for all of the support, encouragement, and insight that he has given me throughout this experience. His scientific skill and imagination is implicit in all of the work described here and I thank him deeply. I would also like to express sincere gratitude to all of my other advisors, coauthors, and collaborators. I thank S. K. "Bhatta" Bhattacharya for his encouragement and help at the early stages of this thesis. His assistance and expertise were instrumental to the success of the vacuum line experiments described in Chapter 2. I would also like to thank Joseph Erbland, a patient and generous instructor and guide in the laboratory, whose curiosity and meticulous attention to detail sparked many thought-provoking discussions, some of which can be found paraphrased in this text. I am deeply grateful to Samuel Morin, who has provided a tremendous amount of support and encouragement throughout this thesis, particularly with regards to the CalNex study described in Chapter 4. I also express gratitude to my lab and officemate, Tesfaye Berhanu, for his active involvement and interest in this work. I thank Steve Brown, Nick Wagner, Eric Williams, Brian Lerner, and our other collaborators from the National Oceanic and Atmospheric Administration (NOAA) Earth Systems Research Laboratory for the opportunity to participate in the CalNex field campaign. I equally thank the scientific crews of both the R/V *Atlantis* and R/V *Polarstern*. I would like to express gratitude to Jean Martins and Erwann Vince of the Laboratoire d'Etude des Transferts en Hydrologie et Environnement (LTHE) for preparing the bacterial cultures used for all of the nitrate isotope analyses reported in this study. They have been exceedingly accommodating and generous with their time and I thank them sincerely. I acknowledge the OPALE scientific team, particularly Michel Legrand, Susanne Preunkert, Bruno Jourdain, Markus Frey, and Alexandre "Sacha" Kukui, for all of their hard work during the 2011 - 2012 field campaign at Dome C. They have graciously agreed to allow me to include in Chapter 5 an analysis based on their

unpublished results, for which I am extremely grateful. I would like to thank the INTRAMIF (INitial TRAining network in Mass Independent Fractionation) scientific network, both the students for their camaraderie and support, and the professors and senior researchers for their time and encouragement. I am particularly grateful to Thomas Röckmann and his students for hosting me at their laboratory in Utrecht to participate in experiments on their vacuum line. The Environnement S.A.™ ozone monitor used for experiments in Chapter 2 was graciously provided by Jean-Luc Besombes of the Université de Savoie. I would also like to thank Becky Alexander, Sergey Gromov, Meredith Hastings, Jan Kaiser, and several anonymous reviewers for helpful suggestions and comments on this work at various stages of its development.

The research presented here is deeply indebted to the efforts of those who came before me. I would like to particularly acknowledge the groundbreaking work of Mark Thiemens and his colleagues, which has profoundly influenced the course of the research described in this thesis.

The research leading to these results has received funding from the European Community's Seventh Framework Programme (FP7/2007-2013) under grant agreement n° 237890. The Agence Nationale de la Recherche (ANR) is gratefully acknowledged for its financial support through the OPALE project (Contract NT09-451281). LEFE-CHAT, a scientific program of the Institut National des Sciences de l'Univers (INSU/CNRS), has also provided partial funding for this study.

Table of contents

Abstract ---------- **iii**

Acknowledgements ---------- **vii**

Table of contents ---------- **ix**

Chapter 1: Introduction ---------- **1**

1.1 Principles of stable isotope geochemistry ---------- 6

1.1.1 Definitions and concepts ---------- 7

1.1.2 Isotope fractionation processes ---------- 8

1.2 The "anomalous" isotopic properties of ozone ---------- 20

1.2.1 Tropospheric chemistry of ozone and related species ---------- 21

1.2.2 Experimental and theoretical developments ---------- 26

1.2.3 Atmospheric measurements ---------- 34

1.2.4 Applications in atmospheric research and beyond ---------- 38

1.3 Isotope dynamics of atmospheric nitrate and its precursors ---------- 43

1.3.1 The atmospheric reactive nitrogen (NO_x) cycle ---------- 44

1.3.2 Isotopic composition of atmospheric nitrate ---------- 49

1.3.3 $\Delta^{17}O$ mass balance for nitrate ---------- 52

1.3.4 Nitrogen stable isotopes in the NO_x-nitrate system ---------- 61

1.4 This thesis ---------- 64

Chapter 2: Measurement of the ^{17}O-excess ($\Delta^{17}O$) of tropospheric ozone using a nitrite-coated filter ---------- **69**

2.1 Introduction ---------- 70

2.2 Experimental ---------- 73

2.2.1 Rationale ---------- 73

2.2.2 Reagent preparation and filter coating procedure ---------- 74

2.2.3 Preliminary tests of ozone sampling apparatus ---------- 75
2.2.4 Isotope transfer experiments ---------- 76
2.2.5 Ambient ozone collections ---------- 77
2.2.6 Sulfamic acid treatment ---------- 80
2.2.7 Nitrate concentration analysis ---------- 80
2.2.8 Isotopic measurements ---------- 81
2.3 Results and discussion ---------- 85
2.3.1 Efficiency of ozone collection ---------- 85
2.3.2 Nitrate blanks and interferences ---------- 88
2.3.3 Accuracy of isotopic measurements ---------- 90
2.3.4 Isotope transfer during the $O_3 + NO_2^-$ reaction ---------- 96
2.3.5 Isotopic composition of ambient samples ---------- 99
2.4 Conclusions and recommendations ----------110

Chapter 3: Quantitative constraints on the ^{17}O-excess (Δ^{17}O) signature of surface ozone: Ambient measurements from 75 °S to 50 °N ----------112

3.1 Introduction ----------113
3.2 Experimental ----------117
3.2.1 Sample collection ----------118
3.2.2 Sample extraction and isotopic analysis ----------123
3.3 Results ----------123
3.3.1 Isotopic composition of nitrate in filter extracts ----------123
3.3.2 Isotopic composition of ozone ----------129
3.4 Discussion ----------131
3.4.1 Comparison to “cryogenic” measurements ----------131
3.4.2 Annual $\Delta^{17}O(O_3)$ record from Grenoble, France ----------136
3.4.3 $\Delta^{17}O(O_3)$ from 50 °S to 50 °N in the Atlantic MBL ----------140
3.5 Summary and conclusions ----------141

Chapter 4: Spatial and diurnal variability in nitrogen oxide chemistry as reflected in the isotopic composition of atmospheric nitrate: Results from the CalNex 2010 field study ----------144

4.1 Introduction ----------145
4.2 Methods ----------150
4.2.1 High-volume air sampling ----------150
4.2.2 Nitrate extraction and chemical analysis ----------152
4.2.3 Isotopic analysis ----------152
4.2.4 Complementary data ----------153
4.3 Results ----------154
4.3.1 Atmospheric nitrate concentration and complementary data ----------155
4.3.2 Isotopic composition of nitrate ----------159
4.4 Discussion ----------165
4.4.1 Interpretation of $\Delta^{17}O(NO_3^-)$ measurements ----------165
4.4.2 Interpretation of $\delta^{15}N(NO_3^-)$ measurements ----------180
4.5 Summary and conclusions ----------186

Chapter 5: Nitrogen and oxygen isotope dynamics of nitrate in the surface snow and boundary layer of the East Antarctic plateau ----------191

5.1 Introduction ----------192
5.1.1 Site description and scientific background ----------195
5.2 Methods ----------199
5.2.1 Snow and atmospheric sampling ----------199
5.2.2 Isotopic analysis ----------200
5.3 Results ----------201
5.3.1 Nitrate concentrations in the atmosphere and skin layer ----------201
5.3.2 Isotopic measurements ----------202
5.3.3 Intensive snow collections ----------204

5.4 Discussion ----------206
5.4.1 Seasonal variations ----------206
5.4.2 Dynamic equilibrium at the air-snow interface ----------210
5.4.3 Nitrate isotope mass balance during OPALE ----------214
5.5 Summary and conclusions ----------223

Chapter 6: Conclusions and outlook ----------226

6.1 The $O_3 + NO_2^-$ reaction as an isotopic probe for ozone ----------227
6.2 Temporal and spatial variations in $\Delta^{17}O(O_3)$ ----------230
6.3 Diurnal variability in atmospheric nitrate isotope ratios ----------230
6.4 Impact of snow photo-denitrification on nitrate isotopes ----------231
6.5 Application to modeling studies ----------232

Bibliography ----------235

Summary of activities ----------263

Chapter 1

Introduction

The *troposphere* is the lowest region of the atmosphere, extending from the Earth's surface to an altitude of 10 - 18 kilometers. Although the troposphere accounts for only a small fraction of the atmosphere's total height, it contains about 90% of its mass. It is within this thin gaseous layer that terrestrial ecosystems have evolved and are sustained. The troposphere is well mixed and composed primarily of the gases N_2 (78%), O_2 (21%), and Ar (1%). The remaining gaseous constituents represent less than 1% of total tropospheric mass; however, while these *trace species* exist at low concentrations, their presence in the troposphere has several important implications. Most significantly, trace species exert a profound influence on the Earth's energy balance by absorbing and reradiating terrestrial radiation. The trace species also largely determine the chemical activity of the atmosphere, whereas the major gases are comparatively nonreactive. Furthermore, while the abundances of the major atmospheric constituents fluctuate only over geologic timescales, the concentrations of the trace species can be extremely variable in space and time and are presently increasing globally at an extraordinary rate in the case of some species. Increases in trace gas abundance observed over the last two centuries can be mostly attributed to human activities such as fossil fuel (oil and coal) combustion, industry and agriculture, biomass burning, and deforestation. The environmental implications of this increase in trace gas abundance are numerous and include increased acid deposition, air pollution, eutrophication of aquatic ecosystems, stratospheric ozone loss, and global climate change. The atmospheric dynamics of trace gases and the evolution of these dynamics over time have therefore become major research priorities in the earth and atmospheric sciences.

The majority of the trace species found in the atmosphere are emitted from the surface into the troposphere where they undergo a complex series of chemical and physical transformations that determine their overall lifetime. These transformations serve as loss pathways, or "sinks," for reduced gaseous species injected into the troposphere via biogeochemical activity (e.g., methane and other hydrocarbons,

gaseous sulfur emissions from the oceans and volcanic activity, etc.) and also act as *in-situ* sources of oxidized secondary species. An analogy is often drawn between the chemistry of the troposphere and a low temperature combustion system in which organic molecules, methane (CH_4) being the simplest, are oxidized to yield carbon dioxide (CO_2), with the overall reaction given by:

$$CH_4 + 2O_2 \rightarrow CO_2 + 2H_2O \qquad \text{(R1.1)}$$

However, unlike a combustion reaction, tropospheric chemistry is driven by complex photochemical cycles in which the interaction of sunlight with photolabile molecules leads to the production of free radical species that in turn exert a significant influence on the ultimate composition of the atmosphere. In general terms, the photo-dissociation of trace species and the subsequent reactions involving the products of photo-dissociation can be considered the primary drivers of the majority of the chemical processes occurring in the atmosphere. Due to their extremely high reactivity, the abundances of the free radical species are very small, typically less than one hundred parts per trillion (ppt = pmol mol^{-1}) of air. However, despite their exceptionally low concentrations, it is the free radicals that determine the transformation and loss pathways of most trace species in the troposphere. Understanding the processes and rates by which trace species are transformed via oxidation (i.e., the *oxidative capacity* of the atmosphere) is crucial for assessing the link between global atmospheric composition and climate. Furthermore, global and regional simulations of air quality are highly dependent on an accurate representation of tropospheric oxidation chemistry.

The production, cycling, and removal of trace species are often coupled through a complex system of chemical and physical interactions that can be difficult to evaluate and quantify. As a result of these intricate relationships, a change in the concentration of one species can often lead to significant changes in the concentrations and lifetimes of other trace species, which can subsequently result in feedbacks that either amplify or dampen the original perturbation. Tropospheric ozone (O_3) and the reactive nitrogen oxides ($NO + NO_2 = NO_x$) play central roles in these interconnected oxidation processes, acting as initiators, reactants, and products in many important tropospheric reactions. To demonstrate the complexity involved in this chemistry, a more detailed representation of the basic oxidative pathway simplified in R1.1 has been presented schematically in **Figure 1.1**, which shows the generation of photochemically produced radicals and ozone that accompanies the oxidation of CH_4

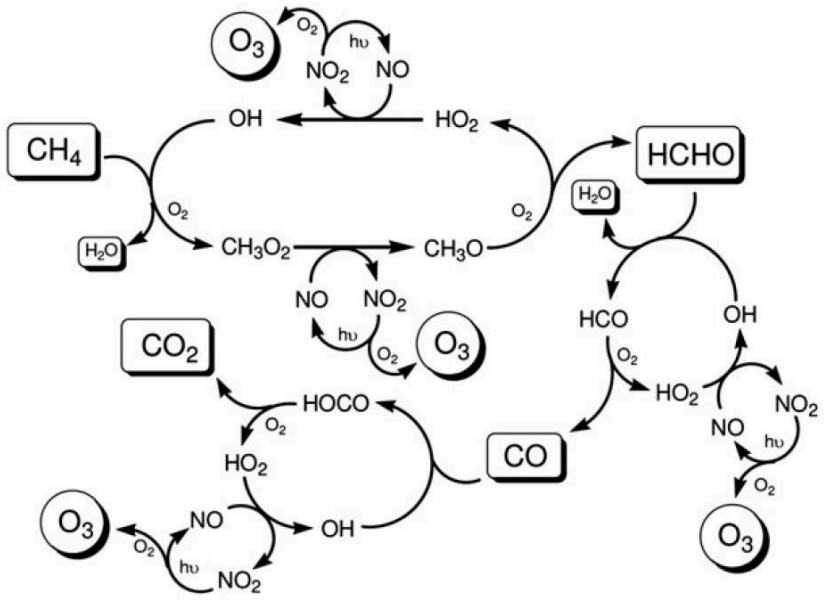

FIGURE 1.1 - Schematic representation of the photochemical oxidation of methane (CH_4) in the troposphere, a cycle initiated by the hydroxyl radical (OH) and catalyzed by reactive nitrogen oxides (NO and NO_2). The reaction sequence shows the formation of formaldehyde (HCHO) and CO as intermediate oxidized products. The complete sequence results in the formation of four ozone molecules (Jenkin *et al.*, 2008).

in the atmosphere. This oxidation sequence is initiated by the homogeneous gas-phase reaction of CH_4 and the hydroxyl (OH) radical:

$$CH_4 + OH \rightarrow CH_3 + H_2O \qquad (R1.2)$$

which operates at a rate that depends on the concentration of OH. R1.2 consumes about 25% of all OH globally and thus represents an important sink for this key tropospheric radical. R1.2 also represents an important *in-situ* source of ozone: the methyl radical (CH_3) that is produced in R1.2 reacts rapidly with O_2 to produce a methyl peroxy radical (CH_3O_2), which may then oxidize NO to NO_2, forming formaldehyde (HCHO) and resulting in the formation of ozone as a by-product. In the presence of sunlight, ozone photolyzes to produce excited O(^1D) atoms, which drive OH formation via reaction with water vapor. Intuitively, this production of OH suggests the potential for a positive feedback, as OH also participates in R1.2. However, the HCHO produced from CH_4 oxidation subsequently undergoes photo-oxidation to form carbon monoxide (CO), which is also an important sink for OH that competes with the CH_4 pathway in the troposphere:

$$CO + OH \rightarrow CO_2 + H \qquad (R1.3)$$

Therefore, by influencing the tropospheric ozone and CO budgets, the CH_4 oxidation

chain affects the concentration of OH, the very species that initiates the sequence of reactions.

From inspection of **Figure 1.1**, it is clear that the troposphere is an extremely complex reactive system in which numerous interconnected processes occur simultaneously. Ambient concentration measurements have been instrumental in deciphering many of the key processes involved; however, such measurements offer only a snapshot of atmospheric conditions at a particular point in time and space and thus provide limited information regarding the dynamics of the underlying processes. Over the past decades, alternative approaches based on stable isotope measurements have been pursued in an effort to obtain concentration-independent information relevant to atmospheric processes. This research effort has been driven in part by analytical developments in isotope ratio mass spectrometry (IRMS), particularly the combination of IRMS and gas chromatography (GC), which has allowed for precise isotope measurements of nano-mole quantities of trace gases. Variations in the isotopic composition of atmospheric trace species have been found to act as novel indicators of important earth system processes, often serving as source markers for gases and aerosols and providing both qualitative and quantitative constraints on the chemical and physical pathways that determine their fate. Isotope ratio measurements can offer direct insight into the nature and magnitude of the fluxes associated with different processes, thus providing unique information regarding phenomena that are often difficult to quantify from concentration measurements alone. Stable isotope analysis has been particularly useful in the development of global trace gas budgets, a tool that has important applications in earth systems research and climate modeling. Furthermore, systematic variations in isotopic composition associated with the production and removal of trace species provide a means for identifying and evaluating the relative importance of different chemical pathways in the atmosphere.

Research within the atmospheric isotope community in recent years has become increasingly focused on ozone (O_3). The reason for this is partly historical: the gas-phase ozone formation reaction endows ozone with a distinctive and “anomalous” isotopic composition, which was immediately recognized upon its identification in the early 1980s as a breakthrough discovery of a previously unknown process occurring in the atmosphere. An understanding of this puzzling isotope effect has been the driving force behind a broad range of experimental and theoretical developments in physical chemistry. The second reason for the intense research focus on ozone arises

from the fundamental role it plays in atmospheric chemistry. In conjunction with its photochemical counterpart the OH radical, ozone is central to the chemistry of the troposphere and is closely coupled to the oxidative cycles of most atmospheric trace species. The unique isotopic composition of ozone is propagated throughout the atmosphere through these oxidation processes and has now been detected in a broad range of atmospheric gas and aerosol species, thus providing a powerful research tool in studies of atmospheric chemistry with several emerging applications. Particularly encouraging developments have been made in the study of the oxygen isotope dynamics of nitrate, an important secondary species resulting from the oxidation of NO_x. The isotopic signal transferred from ozone to nitrate provides a marker for the relative importance of the various sink mechanisms in the atmospheric nitrogen cycle. Due to the relatively high concentrations of nitrate preserved in polar snow and ice, there also exists the possibility of extending this tracer into the past using deep ice core records of nitrate, which could allow for an evaluation of the link between climate and atmospheric oxidation chemistry over glacial/interglacial time scales and during rapid climate change events.

The following chapters are largely focused on the isotopic composition of ozone (Chapters 2 - 3) and its transmission to nitrate via the atmospheric reactive nitrogen cycle (Chapters 4 - 5). Stable isotope ratio measurements compromise the majority of the observations reported herein; therefore, this introductory section begins with a brief discussion of the fundamental concepts, definitions, and notations encountered in stable isotope geochemistry. This is followed by an introduction to *mass-dependent fractionation*, a diverse group of isotope effects that encompass the majority of chemical and physical processes known to lead to natural variability in stable isotope abundances. Examples used to illustrate basic concepts are drawn primarily from the fields of atmospheric chemistry and paleoclimatology. Wherever possible, oxygen is used as the model isotope system. After this overview of stable isotope basics, the concept of *mass-independent fractionation* is introduced followed by a brief history of the elucidation of this effect in the ozone formation reaction. A wealth of experimental and observational data has been collected in an attempt to better understand this singular isotopic phenomenon. These scientific pursuits are briefly reviewed here, with particular attention given to the existing field measurements of ozone isotopic composition. The focus is then shifted to the intricate coupling of ozone to the atmospheric NO_x cycle, which is reflected in the oxygen and nitrogen

isotopic composition of nitrate in ways that are complex and not well constrained. After reviewing the current theoretical framework for interpreting the isotopic variability observed in nitrate, the existing field measurements and modeling studies are reviewed with regards to major implications and open questions.

1.1 Elements of stable isotope geochemistry

Atomic nuclei consist of protons and neutrons. The number of positively charged protons in the nucleus determines the atomic number *Z* of the atom, which establishes its position on the periodic table. The sum of protons and neutrons together determines the mass number *A*, typically given as a left superscript of the elemental symbol (e.g., ^{16}O). *Isotopes* are atoms whose nuclei contain the same number of protons but a different number of neutrons; i.e., atomic species that occupy the same position in the periodic table but have different masses. For example, every oxygen atom has 8 protons in its nucleus; however, while approximately 99.8 % of oxygen nuclei contain eight neutrons (^{16}O), some contain nine or ten neutrons (^{17}O and ^{18}O, respectively). Naturally occurring oxygen contains all three isotopes; therefore, any sample that contains oxygen includes nuclides with three different masses.

The chemical reactivity of an element is determined principally by its electronic configuration. Because isotopes of an element contain the same number and arrangement of electrons, they are often considered to be essentially identical in terms of behavior. However, while isotopes of an element indeed share a chemical identity, they exhibit distinct physicochemical properties arising from their atomic mass differences. These subtle differences, commonly referred to as *isotope effects*, induce small but often detectable variations in natural isotope abundances that result from the divergent behaviors of isotopically substituted molecular species, or *isotopologues*. Because theses effects scale with the relative mass difference between isotopes, they are typically most pronounced among the light elements (e.g., H, C, N, O, S) in naturally occurring compounds. Beginning with the research on deuterium by Harold Urey and coworkers (Urey et al., 1932), differences between isotopologues have served as useful research tools for exploring the chemical and physical properties of molecules in the laboratory. Today, research fields as diverse as medicine, agriculture, planetary science, anthropology, and physical chemistry all benefit from the

application of isotope systems. These powerful techniques stem largely from the gradual development of a quantitative representation of the mechanisms producing variability in the stable isotope composition of atoms and molecules, a suite of processes referred to collectively as *isotope fractionation*. Before discussing these processes, we will first briefly introduce the prerequisite notations for reporting isotope abundances in natural samples.

1.1.1 Definitions and concepts

An isotope ratio R for a particular compound is conventionally defined as the atomic abundance ratio of a less abundant, or "rare," isotope of an element to the most abundant isotope of that element. In the case of oxygen, which possesses three stable isotopes, two isotope ratios must be specified: ^{17}R = n (^{17}O) / n (^{16}O) and ^{18}R = n (^{18}O) / n (^{16}O). Because stable isotope variations in nature tend to be exceptionally small, isotope ratios for samples are normally expressed as isotopic enrichments (δ) in per mill (‰ = parts per million or "ppm") relative to an *international measurement standard*:

$$\delta = \frac{R_{sample}}{R_{reference}} - 1 \qquad (1.1)$$

The reasons for reporting isotope ratio measurements relative to a reference are quite practical. In short, the accuracy at which absolute isotope abundances can be measured is significantly lower than the precision at which relative differences in isotope abundances between two samples can be determined. Therefore, by reporting the measured isotope ratios of a sample as relative deviations from a co-measured standard, any proportional errors arising from mass spectrometry or sample preparation can be corrected. For the comparison of isotopic measurements from different laboratories, internationally accepted standard references have been produced which have established the relative scale on which isotopic enrichment values are compared. In the original data reported in this thesis, the reference used for oxygen isotopes is Vienna Standard Mean Ocean Water (VSMOW) and the reference used for nitrogen is atmospheric N_2 gas. For historical reasons, not all δ values found in the literature are given relative to a single standard and often several standards of one element are in use. While the choice of reference standard is in some sense

arbitrary, the same standard should be used when comparing different measurements. For the majority of ozone isotopic measurements reported for previous experimental studies and ambient collections, oxygen isotope enrichments ($\delta^{17}O$ and $\delta^{18}O$), are reported relative to air O_2 and are therefore not directly comparable to measurements expressed on the VSMOW scale. To convert the δ-values of a substance from one isotopic reference scale to another, the following equation may be used:

$$\delta_{X/A} = \delta_{X/B} + \delta_{B/A} + \left[\delta_{X/B} \times \delta_{B/A}\right] \quad (1.2)$$

where X represents a sample and A and B represent two different SRMs used to express the relative isotopic enrichment of sample X.

An important mathematical property of δ values that will be encountered throughout this manuscript concerns mixing between isotopically distinct reservoirs. This is a process that is capable of inducing changes in the isotopic composition of a chemical reservoir that are independent of fractionation effects. When the relative abundance of the rare isotope of interest is sufficiently low compared to the most abundant isotope of that element, which is the case for oxygen and nitrogen, the δ value of a mixture of multiple reservoirs can be expressed as the sum of the δ values of each reservoir multiplied by the fractional contribution of each reservoir to the mixture:

$$\delta_{mixture} = \sum_{i=1}^{n} x_i \times \delta_i \quad (1.3)$$

where n is the number of reservoirs contributing to the mixture and x is the atomic fraction of each reservoir. In essence, Equation 1.3 describes the fundamental means by which isotope ratios may be used in conjunction with concentration measurements to resolve sources and pathways in atmospheric geochemistry. The mixing of reservoirs is a concept that is implicit throughout Chapter 2, where contributions from an analytical blank must be considered in relation to their quantitative impact on an ozone isotope measurement technique. In Chapter 4, Equation 1.3 will form the basis for a general mass-balance equation used in the interpretation of oxygen isotope ratios of nitrate.

1.1.2 Isotope fractionation processes

Processes that generate variations in isotope abundance lead to recognizable patterns that can be discerned in nature given that the process in question is well understood

and quantitatively constrained. The nuclear decay of radioactive (i.e., unstable) isotopes is one such process. Unstable nuclides undergo nuclear decay continuously at a rate that is unique for a given nuclide. All nuclear decay obeys a first-order rate law and can thus be treated mathematically to give Equation 1.4, which relates the number of nuclei, N, to time, t, for a first-order decay process:

$$N = N_0 e^{-\lambda t} \tag{1.4}$$

where N_0 is the number of radioactive atoms present at $t = 0$ and λ is a proportionality constant known as the decay constant. Equation 1.4 conveys a convenient means for determining the age of a natural sample containing radioactive isotopes, which forms the basis of *radiometric dating*. Indeed, if the initial concentration and λ value of the decaying element are known, then the age of a sample can be calculated upon measurement of N. Scientific efforts to constrain the age of the Earth and solar system have been based almost entirely on this technique, and radiocarbon (^{14}C) analysis is used routinely to determine the age of organic materials, an important isotope application in many different disciplines. Furthermore, radioactive isotopes can provide novel tracers for unconstrained physical and chemical processes in the atmosphere. For example, ^{35}S is a cosmogenic radionuclide that is produced naturally in the atmosphere where it readily reacts to form $^{35}S(SO_2)$. $^{35}S(SO_2)$ may undergo gas or aqueous-phase oxidation to $^{35}S(SO_4^-)$ or may be simply removed from the atmosphere via deposition. Due the enhanced production rates of ^{35}S and the extended residence times of the gas and aerosol ^{35}S species in the stratosphere, the ^{35}S of tropospheric sulfate serves as a sensitive marker for stratospheric-tropospheric exchange (STE); furthermore, due to its relatively short lifetime in the troposphere, $^{35}S(SO_4^-)$ also reflects boundary layer oxidation capacity by tracking the efficiency of the SO_2 to sulfate conversion (Priyadarshi *et al.*, 2011). Cosmogenic isotopes have also been applied successfully in the determination of interhemispheric exchange, cross-Equator mixing, and the removal rates and lifetimes of various gas and aerosol species in the troposphere (Lal and Baskaran, 2011). However, while radionuclides are an important class of isotopes, a thorough discussion of their atmospheric applications is beyond the scope of this introduction, which will be focused entirely on stable isotopes of the light elements, particularly oxygen and nitrogen.

Variations in the abundances of stable isotopes are produced only via *isotopic fractionation*, a diverse group of chemical and physical processes that partition

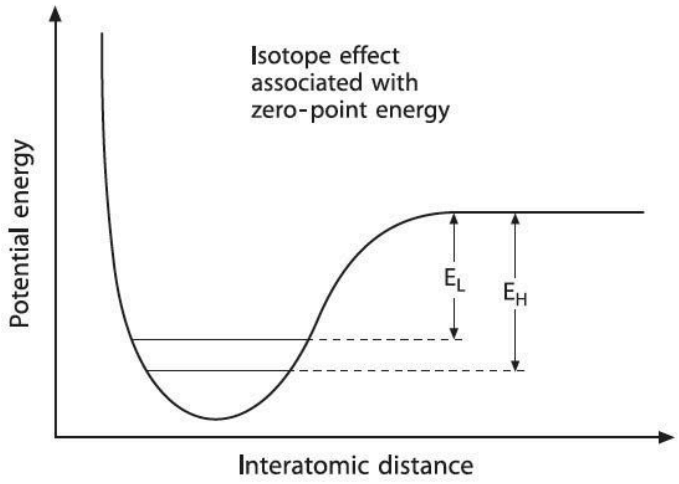

FIGURE 1.2 - Schematic potential energy curve for the interaction of two atoms in a stable molecule or between two molecules in a liquid or solid (after Bigeleisen, 1965).

isotopes between substances or between phases of a substance to a degree that is dependent on the relative mass difference between isotopes. Isotopic fractionation arises from quantum mechanical effects related to the impact of the mass of an atom on the vibrational frequency of the bond that it forms. This is represented schematically in **Figure 1.2**, which shows the potential energy surface of a diatomic molecule as a function of bond length. According to quantum theory, the energy of a molecule is restricted to discrete levels with the lowest level (zero-point energy) being above the minimum of the potential energy surface by a distance that is dependent on the vibrational frequency of the molecule. In other words, even at a temperature of absolute zero, a molecule continues to vibrate at its characteristic frequency, which is mass dependent. Because heavy isotopes vibrate at lower frequencies, heavy isotopologues therefore possess lower zero-point energies than their isotopically light counterparts. This is shown in **Figure 1.2**, where the upper horizontal line (E_L) represents the dissociation energy of the light isotopologue and the lower line (E_H), that of the heavy one.

The difference in zero-point energy between isotopologues has an important consequence: bonds formed by the heavy isotope require greater energy input for cleavage of the bond to occur. Therefore, molecules bearing the light isotope will typically participate in chemical reactions at a slightly higher rate than those with a heavy isotope substitution. Phenomena that lead to isotope fractionation are typically divided into two different classes: (i) *equilibrium fractionation*, in which there is no

net reaction, but only a change in the distribution of isotopes between different species, between different phases, or between individual molecules of a species; and (ii) *kinetic isotope effects* (KIEs) that result primarily from the differences in chemical reaction rates among isotopologues of a given molecular species.

1.1.2.1 Equilibrium fractionation

The term equilibrium fractionation, also referred to as *isotope exchange*, encompasses a wide range of processes with various physicochemical mechanisms. Here we will outline the basic concepts of equilibrium fractionation and introduce the notations used to describe this group of isotope effects using classic examples of isotope systems with applications in the earth and atmospheric sciences.

Chemical equilibria. Let us consider the ^{18}O exchange equilibrium between water and calcite, the principal mineral component of marine limestone:

$$CaC^{16}O_3 + H_2{}^{18}O \leftrightarrow CaC^{16}O_2{}^{18}O + H_2{}^{16}O \quad \text{(R1.4)}$$

Isotope exchange reactions are a special case of general chemical equilibrium. For reaction R1.4, the equilibrium constant is given by:

$$K = \frac{\left(CaC^{16}O_2{}^{18}O\right)\left(H_2{}^{16}O\right)}{\left(CaC^{16}O_3\right)\left(H_2{}^{18}O\right)} \quad (1.5)$$

Harold Urey (1947) and Bigeleisen and Mayer (1947) demonstrated using statistical quantum mechanics that isotope exchange equilibrium constants, such as the one shown in Equation 1.5, have values that are slightly different from unity. It was shown in these pioneering studies that ln K, as for any equilibrium constant, can be expressed as a function of temperature in the form $a' + (b'/T) + (c'/T^2)$. It can be seen from this simple relationship that, as temperature increases, K approaches a'. In other words, isotope fractionation approaches zero at very high temperature and generally increases with decreasing temperature. Recognizing the significance of the temperature dependence measured for R1.4 ($d\alpha/dt \approx$ -0.23 ‰ K^{-1}), Urey and coworkers concluded that $\delta^{18}O$ measurements of ancient carbonate sediments could be used to determine water temperature at the time the sediment was precipitated, thus giving birth to the field of paleoclimatology. The carbonate "paleothermometer" approach has since proven to be instrumental in the development of an understanding

of Earth's dynamic climate history and remains one of the major accomplishments of the field of stable isotope geochemistry (Marshall, 1992; Miller *et al.*, 2005b).

For isotope exchange reactions in geochemistry, the equilibrium constant K is often replaced by the fractionation factor α, which is defined as the ratio of any two isotopes in one chemical compound (A) divided by the corresponding ratio for another chemical compound (B):

$$\alpha_{A-B} = \frac{R_A}{R_B} \tag{1.6}$$

If the isotopes can be assumed to be randomly distributed over all possible positions in these compounds, then α is related to the equilibrium constant K by:

$$\alpha = K^{1/n} \tag{1.7}$$

where n is the number of atoms exchanged. For simplicity, isotope exchange reactions are often written such that only one atom is exchanged. In these cases, the equilibrium constant is equal to the fractionation factor. For example, the exchange of ^{18}O and ^{16}O between water and $CaCO_3$ is expressed as follows:

$$\tfrac{1}{3}CaC^{16}O_3 + H_2{}^{18}O \leftrightarrow \tfrac{1}{3}CaC^{16}O_2{}^{18}O + H_2{}^{16}O \tag{R1.5}$$

with fractionation factor defined as:

$$\alpha_{CaCO_3-H_2O} = \frac{\left(\frac{^{18}O}{^{16}O}\right)_{CaCO_3}}{\left(\frac{^{18}O}{^{16}O}\right)_{H_2O}} \tag{1.8}$$

Because α values are typically extremely close to one, it has become common practice in recent years to replace the fractionation factor with ε, the *enrichment factor*, which is defined as:

$$\varepsilon = \alpha - 1 \tag{1.9}$$

where ε is reported in ‰, thus allowing for direct comparison with δ values. Equation 1.8 can be rewritten as:

$$\ln(1+\varepsilon) = \ln(1+\delta^{18}O_{CaCO_3}) - \ln(1+\delta^{18}O_{H_2O}) \tag{1.10}$$

If the values of ε and $\delta^{18}O$ are much less than one, this equation can be approximated as follows:

$$\varepsilon \approx \delta^{18}O_{CaCO_3} - \delta^{18}O_{H_2O} \tag{1.11}$$

In essence, Equation 1.11 is an expression of the fractionation factor as the difference in $\delta^{18}O$ between molecules in the two compounds considered.

Physical equilibria. Equilibrium fractionation is observed not only in case of isotopic exchange between different chemical species, but also for phase changes among molecules of the same species. A classic example of isotope fractionation accompanying a physical equilibrium is the concentration of heavy isotopes of oxygen in liquid water relative to water vapor. At the gas-liquid interface, isotopic exchange occurs as follows:

$$H_2{}^{16}O_{gas} + H_2{}^{18}O_{liquid} \leftrightarrow H_2{}^{18}O_{gas} + H_2{}^{16}O_{liquid} \quad \text{(R1.6)}$$

The fractionation factor at equilibrium is expressed as:

$$\alpha_{gas-liquid} = \frac{\left(\frac{^{18}O}{^{16}O}\right)_{H_2O_{gas}}}{\left(\frac{^{18}O}{^{16}O}\right)_{H_2O_{liquid}}} \quad (1.12)$$

The fractionation factor for R1.6 can also be expressed in terms of the partial pressure of the two isotopologues. The partial pressure of a gas is:

$$P_{gas} = P_{total} \times X_{gas} \quad (1.13)$$

where X_{gas} is the molar fraction of the gas. The gas-liquid equilibrium obeys Henry's law. Therefore, when water evaporates, the vapor is enriched in the light isotope. If the water vapor can be considered a perfect gas, we can write:

$$P(H_2{}^{16}O) = X_{H_2{}^{16}O} \times \rho^0(H_2{}^{16}O) \quad (1.14)$$

$$P(H_2{}^{18}O) = X_{H_2{}^{18}O} \times \rho^0(H_2{}^{18}O) \quad (1.15)$$

where P is the total pressure, X designates the molar fractions in the liquid, and $\rho^0(H_2O)$ is the saturated vapor pressure. The fractionation factor can then be given as a function of the saturated vapor pressures of the two isotopologues:

$$\alpha_{gas-liquid} = \frac{\rho^0(H_2{}^{18}O)}{\rho^0(H_2{}^{16}O)} \quad (1.16)$$

Because $H_2{}^{18}O$ is the denser and less volatile liquid, $\rho^0(H_2{}^{18}O) < \rho^0(H_2{}^{16}O)$ and $\alpha < 1$. This is commonly referred to as the *vapor pressure isotope effect*. Like all fractionation factors, α in Equation 1.16 is temperature dependent: from the Claudius Clapeyron equation it can be shown that ln α can be written in the form $(a'/T) + b'$. The temperature effect on α to a large extent determines isotopic composition of water vapor in the atmosphere and its seasonal and geographic features. This equilibrium

isotope effect applies also to the D/H ratio of H_2O. In fact, a close correlation between D/H and $^{18}O/^{16}O$ can be observed in surface precipitation, a linear relationship known as the meteoric water line (MWL): $\delta D(H_2O) = m \times \delta^{18}O(H_2O)$, with $m \approx 8$ (Craig, 1961). The isotopic variability induced by the vapor pressure isotope effect forms the basis for using H_2O stable isotopes as tracers of the hydrological cycle, an active field of research since the early 1960s (Dansgaard, 1964) that has progressed markedly in recent years through the application of $^{17}O/^{16}O$ measurements and numerical models (Zahn *et al.*, 2006).

Open and closed systems. When isotopic fractionation occurs within a closed system, a balance effect is imposed by the conservation of mass and the isotopic composition of the system as a whole thus remains constant. In the case of a system composed of a liquid phase and a vapor phase:

$$\delta_{vapor} = \delta_{system} + f\varepsilon \tag{1.17}$$

where f represents the mass fraction of the liquid reservoir relative to the total mass of the system. Therefore, if the system is entirely in the vapor form, then $\delta_{\text{vapor}} = \delta_{\text{system}}$. Conversely, as the vapor in the system becomes progressively condensed, then δ_{vapor} approaches the value of the term $\delta_{\text{liquid}} + \varepsilon$.

Earth systems are rarely closed. For example, in the case of condensation during raindrop formation, the liquid phase is progressively removed from the system through rainfall and the mass balance effect does not apply. Any isotope fractionation that occurs in such a way that the products are isolated from the reactants immediately after formation will show a characteristic trend in isotopic composition. Such an isotopic separation process can be treated theoretically in terms of fractional distillation or condensation under equilibrium conditions as expressed by the Rayleigh (1896) equation. For a condensation process, this equation is:

$$R/R_0 = f^{\varepsilon} \tag{1.18}$$

where f represents the fraction of the residual vapor, R_0 is the isotope ratio of the initial bulk composition, and R is the instantaneous isotope ratio of the residual vapor. Expressed in δ, the Rayleigh formula is:

$$\delta = (1+\delta_0) \times f^{\varepsilon} - 1 \tag{1.19}$$

In plain words, Equations 1.18 and 1.19 predict that, as condensation proceeds, the residual vapor will become progressively depleted with respect to the heavy isotope,

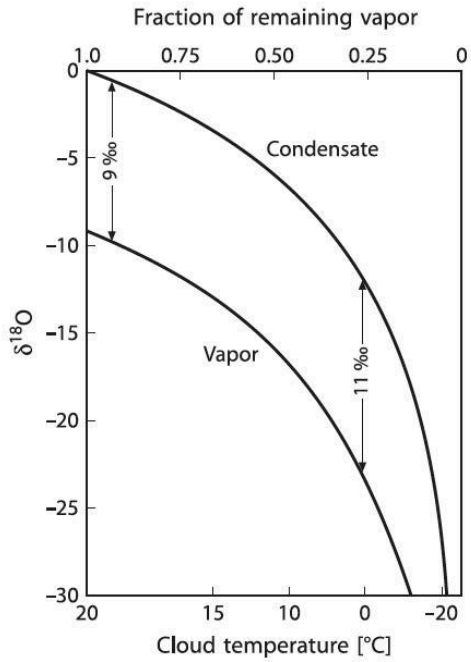

FIGURE 1.3 - Rayleigh process between vapor and condensate in a cloud for $\delta^{18}O$. The liquid phase is removed continuously as rain. The temperature of the cloud is shown on the lower axis and the increase in fractionation with decreasing temperature is taken into account (after Dansgaard, 1964).

thus resulting in a progressively depleted condensate. The resulting decrease in $\delta^{18}O$ in both the residual vapor and the raindrops released from the cloud are shown in **Figure 1.3** as a function of the fraction of vapor remaining in the cloud. Note that the difference in $\delta^{18}O$ between the condensate and vapor increases at low values of *f*.

1.1.2.2 Kinetic isotope effects

Isotopically different molecules react chemically at different rates, with lighter molecules generally reacting more readily than their heavy isotopologues. This arises from two combined causes: first, light molecules move faster than heavy molecules and thus collide more often; second, heavy molecules are more stable than light ones because of their lower zero-point energy. During collisions, molecules carrying heavy isotope substitutions will be dissociated less often and will thus be less reactive. This differential reactivity among isotopologues results in variations in isotopic composition between reactants and products. This form of isotope fractionation, which falls into the class of *kinetic isotope effects* (KIEs), often provides useful tracers of atmospheric chemistry, as these effects often accompany the removal of trace species, mainly via reaction with OH or photolysis. Unlike equilibrium isotope

fractionation, such as the ^{18}O exchange between H_2O and $CaCO_3$, this process is not reversible. Therefore, KIEs fractionate the unreacted trace gas remaining in the atmospheric reservoir, causing it to gradually acquire a different isotopic composition (Kaye, 1987). For example, let us consider the reaction of CH_4 and OH, an important reaction in troposheric oxidation chemistry (**Figure 1.1**). In terms of carbon stable isotopes, there are two reactions to be considered:

$$^{12}CH_4 + OH \rightarrow {}^{12}CH_3 + H_2O \quad \text{(R1.7)}$$

$$^{13}CH_4 + OH \rightarrow {}^{13}CH_3 + H_2O \quad \text{(R1.8)}$$

These two reactions occur at different speeds, with two kinetic constants, ^{12}k and ^{13}k. The isotopic fractionation factor, α, in this case also referred to simply as the "KIE," is taken to be the ratio of the respective reaction rate constants:

$$\alpha_{KIE} = \frac{^{12}k}{^{13}k} \quad (1.20)$$

It should be noted that, given the convention of defining the ratio R as the rare over the most abundant isotope, it would be more consistent to use the inverse definition for the KIE (i.e., $^{13}k/^{12}k$). However, for most kinetic fractionations processes, this would imply a negative value for the enrichment factor, ε (Equation 1.9), as the reaction rate for the heavier molecule is normally smaller relative to its light isotopologue. For the CH_4 + OH reaction, the resulting ε value is positive in most cases, meaning that the atmospheric CH_4 reservoir becomes enriched in ^{13}C because $^{13}CH_4$ reacts less readily and $\alpha_{KIE} > 1$. Laboratory measurements have determined α_{KIE} values for the CH_4 + OH reaction of 1.0039 and 1.0054, corresponding to ε values of 3.9% and 5.4‰, respectively. This isotope effect thus provides a quantitative tracer for the CH_4 + OH pathway provided that the $^{13}C/^{12}C$ of the original bulk methane (i.e., the "source signature") is known.

1.1.2.3 Mass independent fractionation

The isotopic effects that have been discussed so far fractionate isotopes according to laws proportional to the difference in mass between isotopologues. Therefore, in the $H_2O/CaCO_3$ exchange reaction (R1.5) or during the evaporation of water (R1.6), $^{18}O/^{16}O$ fractionation is approximately twice that of $^{17}O/^{16}O$ fractionation. In an oxygen three-isotope plot, most terrestrial and lunar materials thus fall along a line with a slope ≈ 1/2, known as the *mass-dependent fractionation* (MDF) line (**Figure 1.4**), a result predicted by the theories of Urey (1947) and Bigeleisen and Mayer

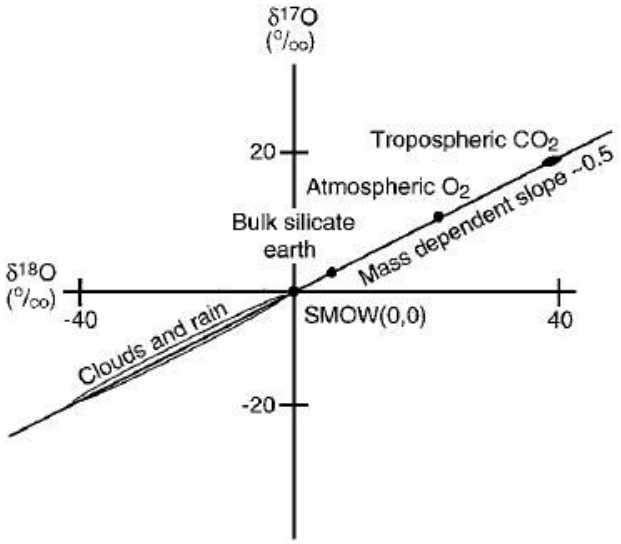

FIGURE 1.4 - Oxygen three-isotope plot showing the mass-dependent relationship for a variety of terrestrial materials (Thiemens, 1999).

(1947). However, in the first triple-oxygen isotope ratio measurements, reported by Clayton *et al.* (1973), it was observed that the oxygen isotopes of inclusions from the carbonaceous meteorite Allende did not obey the expected relationship $\delta^{17}O = 1/2 \times \delta^{18}O$. In fact, equal enrichments were observed (slope ≈ 1). Assuming that no chemical mechanism could produce a variation of stable isotopes in a manner independent of mass, Clayton *et al.* (1973) argued that the $\delta^{17}O \approx \delta^{18}O$ relationship must reflect a nucleosynthetic process (MacPherson and Thiemens, 2011). However, Thiemens and Heidenreich (1983) later demonstrated that such a relationship could be produced chemically. In a simple experiment, they observed equal ^{17}O and ^{18}O enrichments in ozone produced from molecular oxygen via electrical discharge, rather than the expected mass dependent value of ~1/2 (**Figure 1.5**). This observation was quickly recognized to be a breakthrough discovery of a previously unknown fractionation process. A theoretical explanation of this strange isotope effect and its non-adherence to the expected mass-dependent fractionation line became a major research objective in the decades following its original discovery by Thiemens and Heidenreich (1983). During this time, anomalous oxygen isotopic compositions were also detected in a wide range of trace species in the Earth's atmosphere (**Figure 1.6**), indicating that the effect is widespread in nature. The observation of this effect in nitrate and sulfate aerosol particles was a particularly interesting result, as it indicated

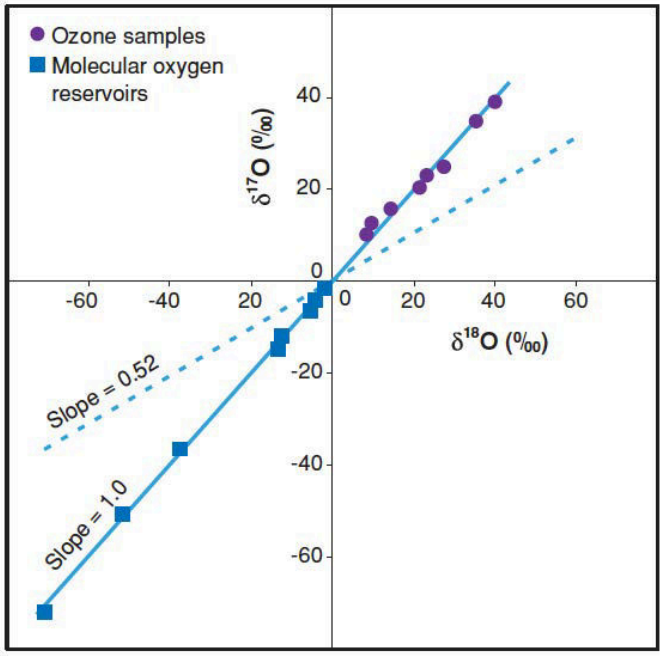

FIGURE 1.5 - The isotopic fractionation of ozone formation (Heidenreich and Thiemens, 1983; Thiemens and Heidenreich, 1983). The original oxygen isotopic composition is at 0,0 per mil. The residual oxygen is denoted by squares and the product ozone by circles. The dotted line is a mass-dependent fractionation line passing through the original oxygen isotopic composition (Thiemens, 2006).

that the $\delta^{17}O \approx \delta^{18}O$ relationship can be preserved in solids and thus transferred from the atmosphere to crustal minerals.

The nearly identical behavior of ^{17}O and ^{18}O in ozone has become commonly referred to as *mass-independent fractionation* (MIF). This expression is somewhat of a misnomer, as it cannot be said that the fractionation observed during ozone formation is truly independent of mass. Indeed, *non-mass-dependent fractionation* (NOMAD) is almost certainly a more appropriate term. However, for brevity we will use the more common expression MIF (MIF signature, MIF composition, etc.) to indicate all deviations from strict mass dependence, which have been detected at various levels of magnitude for several species. The precise definitions used to quantify these variations are introduced in the next section.

Definitions of MIF. Deviations from the MDF line are expressed in "cap delta" (Δ) or delta over baseline notation as:

$$\Delta^{17}O = \delta^{17}O - \lambda \times \delta^{18}O \qquad (1.21)$$

where λ, the slope of the MDF line, was originally taken to be 1/2. This definition gives an approximate measure of *^{17}O-excess* (i.e., the abundance of ^{17}O over that

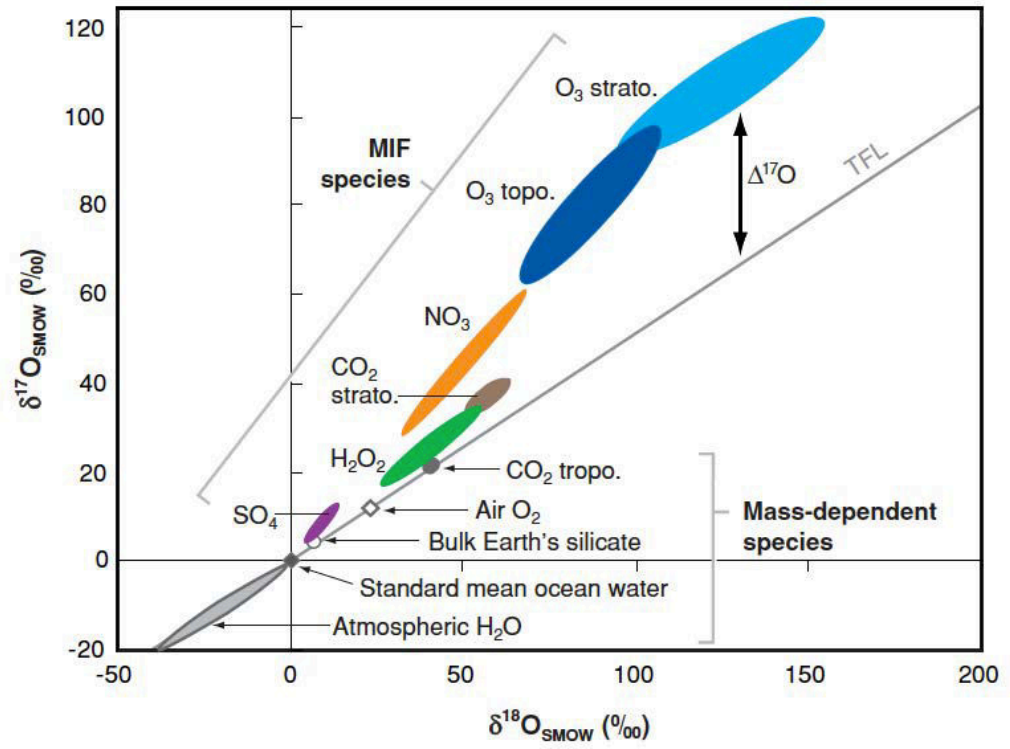

FIGURE 1.6 - Oxygen three-isotope plot summarizing measurements of the mass-independent isotopic compositions of atmospheric ozone, nitrate, sulfate, CO_2, and hydrogen peroxide (H_2O_2) (Thiemens, 2006).

expected based on a mass-dependent relationship); however, it has significant limitations. First, the slope of the MDF is not exactly 1/2, with the exact value depending on the underlying fractionation process. For some materials, the mass-dependent slope has been well established through the analysis of samples from a wide range of origins. For example, the relationship between the $\delta^{17}O$ and $\delta^{18}O$ of meteoric waters forms a robust mass-dependent relationship with a λ value of 0.5281 (Meijer and Li, 1998). λ values ranging from 0.51 to 0.53 have been reported in various other studies of terrestrial rock and water samples, which have been reviewed in detail by Miller (2002). Because λ can attain different values for different mass dependent fractionation processes, a representative value has to be chosen for operational purposes. In the vast majority of studies of ^{17}O-excess in ozone and nitrate, a slope of 0.52 has been used for the definition of $\Delta^{17}O$, which represents an approximate average of the various λ values reported in the literature. However, other authors prefer $\lambda = 0.528$, a more precise value based on the most recent measurements of meteoric waters (Assonov and Brenninkmeijer, 2003; Kaiser, 2009). For species carrying large ^{17}O-excesses ($\Delta^{17}O > 20‰$), the slope value chosen has little relative

impact on the resulting $\Delta^{17}O$ value; however, interpreting small and precisely determined $\Delta^{17}O$ values as a deviation from an assumed mass-dependent fractionation line is not nearly as straightforward, which will be seen below.

The second limitation of Equation 1.21 is that it is based on an approximation of a power law function to a linearized form. A more rigorous derivation of the $\delta^{17}O$ and $\delta^{18}O$ relationship leads to the following expression for $\Delta^{17}O$ (Kaiser *et al.*, 2004):

$$\ln(1+\Delta^{17}O) = \ln(1+\delta^{17}O) - \lambda \ln(1+\delta^{18}O) \quad (1.22)$$

or the equivalent expression:

$$\Delta^{17}O = \frac{1+\delta^{17}O}{(1+\delta^{18}O)^{\lambda}} - 1 \quad (1.23)$$

Equation 1.23 provides an expression of $\Delta^{17}O$ that is independent of the reference adopted for reporting isotopic measurements, which is very useful for the inter-comparison of data reported in the literature. However, for large values of ^{17}O-excess, the difference between the $\Delta^{17}O$ values calculated with Equations 1.21 and 1.23 is quite small. For example, using Equation 1.23 and a λ value of 0.528 yields a $\Delta^{17}O$ value that is only ~0.5‰ different from that calculated with Equation 1.21 and a λ value of 0.52. The linearized expression will be used in this manuscript on account of its simplicity and the ease of its application in mass balance calculations. Furthermore, a λ value of 0.52 will be used, a definition that is consistent with the majority of the previous studies of $\Delta^{17}O$ in nitrate (Michalski *et al.*, 2002; 2003) and sulfate (Bao *et al.*, 2000; Savarino *et al.*, 2000; Lee *et al.*, 2001), thus ensuring the comparability of the data reported here with that in the literature.

1.2 The "anomalous" isotopic properties of ozone

Ozone plays a central role in the chemistry of the atmosphere and, as we have seen in the preceding section, it carries a distinct isotopic signature (i.e., ^{17}O-excess or $\Delta^{17}O$) due to MIF during its formation process. An understanding of the cause or causes of this phenomenon at the molecular level has been the objective of a tremendous amount of experimental and theoretical work, which will be reviewed briefly in this section. This research effort has important implications for atmospheric isotope geochemistry: the $\Delta^{17}O$ signature of ozone is transferred through oxidation reactions to other oxygen bearing compounds such that the $\Delta^{17}O$ of atmospheric species acts as

a marker of the influence of ozone in their chemical formation. This isotopic fingerprint, although it is subject to dilution, cannot be removed or altered via subsequent mass-dependent fractionation processes and is thus conserved during atmospheric transport and processing. The ^{17}O-excess of ozone thus provides a useful conservative tracer of atmospheric oxidation pathways and, since it's discovery in the early 1980s, numerous techniques have been developed for the measurement of ^{17}O-excess in many different atmospheric trace species, some of which are shown in an oxygen three-isotope plot in **Figure 1.6**. After a short introduction to the atmospheric chemistry of ozone, we will briefly consider the laboratory and theoretical work on isotope fractionation in ozone formation and dissociation processes. The existing atmospheric observations of isotope enrichments in ozone will then be discussed.

1.2.1 Tropospheric chemistry of ozone and related species

The basic mechanism underlying the production of ozone in the atmosphere was originally proposed by Chapman (1930) and this sequence of reactions is now commonly referred to as the *Chapman mechanism*. Chapman proposed that ozone in the atmosphere is formed in a three-body recombination reaction between atomic and molecular oxygen in the presence of a third molecule M (i.e., N_2 or O_2):

$$O + O_2 + M \rightarrow O_3 + M \qquad \text{(R1.9)}$$

R1.9 is indeed, for all practical purposes, the only ozone production reaction that occurs in the atmosphere. In the stratosphere, atomic oxygen for R.9 is supplied from the photolysis of molecular oxygen:

$$O_2 + h\nu\ (\lambda < 242\ \text{nm}) \rightarrow O + O \qquad \text{(R.10)}$$

In the troposphere, where solar UV radiation of wavelengths < 242 nm is absent and O_2 does not photolyze, the source of atomic oxygen is the photolysis of NO_2 or, as will be seen below, ozone itself.

The ozone molecule strongly absorbs radiation in both the stratosphere and troposphere and its photolysis yields both ground-state and excited singlet oxygen species, denoted $O(^1P)$ and $O(^1D)$, respectively:

$$O_3 + h\nu\ (\lambda = 400 - 600\ \text{nm}) \rightarrow O(^1P) + O_2 \qquad \text{(R1.11)}$$

$$O_3 + h\nu\ (\lambda < 315\ \text{nm}) \rightarrow O(^1D) + O_2 \qquad \text{(R1.12)}$$

The ground state oxygen atom produced in R1.11 reacts rapidly with O_2 to reform ozone via R1.9. The majority of the $O(^1D)$ produced via R.12 is immediately quenched to ground-state atomic oxygen by collision with N_2 or O_2:

$$O(^1D) + M \rightarrow O(^1P) + M \quad \text{(R1.13)}$$

Therefore, photolysis of ozone essentially leads to the production of $O(^1P)$, which then recombines with O_2, thus forming a "null" cycle (i.e., no net reaction). However, a certain fraction of the $O(^1D)$ produced in R1.12 reacts with water vapor to yield two hydroxyl (OH) radicals:

$$O(^1D) + H_2O \rightarrow 2OH \quad \text{(R1.14)}$$

The photolysis of ozone by ultraviolet light in the presence of water vapor is the primary global source of OH in the troposphere The fraction of $O(^1D)$ atoms that react to form OH is dependent on pressure and the absolute concentration of water vapor. Highest OH concentrations are found in the tropics, where elevated humidity and solar radiative flux leads to a high rate of OH production year-round. Atmospheric chemistry models typically predict OH concentrations approximately 20% lower in the Northern Hemisphere as a result of the large amounts of CO produced by human activities, which serves as a sink for OH via R1.3, as previously discussed.

The OH radical does not react with any of the major atmospheric gases (e.g., N_2, O_2, CO_2, H_2O); however, it is the most important species in chemistry of the troposphere. OH controls the removal and, therefore, the tropospheric concentrations of many trace gases, including most volatile organic compounds (VOCs), CO, sulfur dioxide (SO_2), NO_2, and organic sulfur species. The total atmospheric burden of OH, its associated species (HO_2, H_2O_2, etc.), and its precursor (i.e., ozone), are thus the primary determinants of atmospheric oxidative capacity (Thompson, 1992; Bloss *et al.*, 2005), which is often taken to mean the "total global OH." The OH radical is ubiquitous throughout the troposphere owing to the widespread abundance of ozone and water. Furthermore, by initiating radical-chain oxidation processes, illustrated previously using the example of CH_4 oxidation, OH is regenerated in catalytic cycles, leading to sustained concentrations on the order of 10^6 molecules cm^{-3} during daylight hours.

In relatively unpolluted regimes, the main fate of the hydroxyl radical is reaction with either CH_4 (R1.2) or CO (R1.3) to produce peroxy radicals, such as HO_2 and CH_3O_2 (**Figure 1.1**). Under low NO_x conditions, such as those found in the unpolluted marine boundary layer (MBL), HO_2 can react with ozone and then lead to further

catalytic ozone destruction through a chain sequence involving the production of hydroxyl radicals:

$HO_2 + O_3 \rightarrow OH + 2O_2$ (R1.15)

$OH + O_3 \rightarrow HO_2 + O_2$ (R1.16)

Alternatively, HO_2 can self-react to form hydrogen peroxide (H_2O_2):

$2HO_2 \rightarrow H_2O_2 + O_2$ (R1.17)

R1.17 is essentially a chain termination reaction in the unpolluted atmosphere where H_2O_2 acts as an effective sink for HO_x (i.e., OH and HO_2). However, under the high NO_x conditions associated with the polluted urban atmosphere, the peroxy radicals HO_2 and CH_3O_2 can catalyze the oxidation of NO to NO_2. In the case of HO_2:

$NO + HO_2 \rightarrow NO_2 + OH$ (R1.18)

R1.18 and the analogous reaction involving CH_3O_2 are extremely important pathways in tropospheric chemistry as they lead to the production of ozone via NO_2 photolysis:

$NO_2 + h\nu\ (\lambda < 420\ \text{nm}) \rightarrow NO + O(^1P)$ (R1.19)

followed by the subsequent reaction of the atomic oxygen thus produced to form ozone via R1.9. Furthermore, R1.18 reforms OH, which can then reinitiate the CH_4 and CO oxidation chains, leading to the further peroxy radical production, *et cetera*. However, depending on the concentration of NO_2, OH may also react to form nitric acid (HNO_3), a key pathway in tropospheric chemistry that represents an effective loss mechanism for both HO_x and NO_x:

$NO_2 + OH + M \rightarrow HNO_3 + M$ (R1.20)

Clearly, NO_x chemistry plays a central role in tropospheric oxidation and photochemical processes. As will be seen Section 1.3.1, the concentration of NO_x in the troposphere ultimately determines the catalytic efficiency of ozone production and establishes the magnitude and sign of net photochemical ozone production or destruction.

1.2.1.1 Isotopic processes in the atmospheric chemistry of ozone

Hypothesis regarding the isotopic composition of ozone and its relationship to the atmospheric processes summarized above predate the measurement of ozone isotopic composition in the laboratory and atmosphere. These theoretical discussions were originally centered on the isotopic exchange reactions between the "odd" oxygen ($O_x = O + O_3$) and "even" oxygen reservoirs. This exchange occurs during the ozone

formation reaction R1.9, which proceeds according to an energy-transfer mechanism, consisting of three steps:

$O + O_2 \rightarrow (O_3)^*$ (R1.21)

$(O_3)^* \rightarrow O + O_2$ (R1.22)

$(O_3)^* + M \rightarrow O_3 + M$ (R1.23)

In R1.21, a vibrationally excited intermediate is formed, which may either dissociate spontaneously to reform O and O_2 (R.22) or yield a stabilized ozone molecule via energy transfer to an inert atmospheric molecule (R1.23). These association and dissociation dynamics lead to oxygen isotope exchange reactions between O and O_2, two of which represented below:

$^{18}O + {}^{16}O{}^{16}O \leftrightarrow {}^{18}O{}^{16}O + {}^{16}O$ (R1.24)

$^{17}O + {}^{16}O{}^{16}O \leftrightarrow {}^{17}O{}^{16}O + {}^{16}O$ (R1.25)

These exchange reactions are rapid compared to ozone formation, recycling O-atoms between O and O_2 many times before a stable ozone molecule is formed via three-body collision (R1.23). These isotope exchange reactions contribute to the observed isotope enrichments in ozone, because they determine the distribution of the three isotopes, with ^{17}O and ^{18}O being always lower than what would be expected from a statistical distribution of isotopes in molecular oxygen (Janssen *et al.*, 2001). The relative abundance of oxygen isotopes in turn determines the production of ozone isotopologues and, consequently, $^{16}O^{16}O^{17}O$ ($^{49}O_3$) and $^{16}O^{16}O^{18}O$ ($^{50}O_3$) should be depleted in oxygen. Early investigators were thus met with great surprise when enrichments of over 400‰ were reported for the first measurements of the ^{18}O isotopic composition of stratospheric ozone (Mauersberger, 1981). This observation suggested that KIEs during ozone formation reaction are the primary determinant of ozone isotopic composition and, while these very high enrichments were never confirmed in later experiments, the early measurements of stratospheric ozone generated great interest in the field, triggering many subsequent studies.

KIEs during ozone formation arise from the isotopic dependency of the third-order rate coefficient for the three-body recombination reaction (R1.9), which varies depending on the specific ozone isotopologue formed. Early theoretical discussions were focused on the following reactions:

$^{16}O + {}^{16}O{}^{16}O + M \rightarrow {}^{16}O{}^{16}O{}^{16}O + M$ (R1.26)

$^{18}O + {}^{16}O{}^{16}O + M \rightarrow {}^{16}O{}^{16}O{}^{18}O + M$ (R1.27)

$^{16}O + {}^{18}O{}^{18}O + M \rightarrow {}^{16}O{}^{18}O{}^{18}O + M$ (R1.28)

$^{18}O + {}^{18}O^{18}O + M \rightarrow {}^{18}O^{18}O^{18}O + M$ (R1.29)

The kinetic effects in the ozone formation reaction have been extensively studied and a wealth of experimental data has been obtained regarding the relative rate coefficients of the various ozone formation reactions and their temperature, pressure, and third-body (i.e., N_2, O_2, Ar, etc.) dependencies. While no completely satisfying theoretical framework has yet emerged that can account for the anomalous isotopic composition of the ozone molecule, many interesting experimental discoveries on kinetic isotope effects in ozone formation have been made. First, as discussed in Section 1.1.2, the bulk composition of ozone is nearly equally enriched in ^{17}O and ^{18}O with respect to the composition of the O_2 gas from which it is formed, thus not following the mass-dependent slope of ~1/2 (**Figure 1.5**). The magnitude of isotope fractionation in ozone, including the MIF signal (i.e., $\Delta^{17}O$), exhibits a positive relationship with temperature and decreases with increasing pressure. For selected isotopic substitutions of the reactants, a very large difference in rate coefficient is observed (Mauersberger *et al.*, 1999; Janssen *et al.*, 2001). For example the rate coefficient ratio of R1.28 relative to the standard R1.26 reaction is 1.50, while the R1.27 pathway is at a kinetic disadvantage, possessing a rate coefficient ratio of 0.92. Consequently, different formation rates result in the specific intra-molecular distribution of the ozone *isotopomers* (i.e., molecular species having the same number of each isotopic atom and thus the same relative molecular mass but differing in the position of the substitution). In particular, asymmetric isotopomers become more abundant, which disproportionately impacts the isotopic composition of the terminal oxygen atoms of ozone.

In addition to the KIEs of ozone formation and the isotopic exchange between O and O_2, ozone decomposition processes have also been proposed to influence the isotopic composition of ozone in the atmosphere. However, as discussed by Brenninkmeijer *et al.* (2003), cycling within the O_x reservoir proceeds rapidly compared to source or sink reactions for the odd oxygen species and, consequently, the reaction pathways capable of producing significant isotope fractionation in ozone are limited. As previously discussed, the photolysis of ozone in the stratosphere leads ultimately to a null cycle, as the $O(^1D)$ produced in R1.12 is quenched rapidly to the same ground-state $O(^1P)$ as produced in R.11, which then reform ozone via R1.9. This rapid photolytic cycling leads to an equilibration of the isotopic compositions of O and O_3; however, even this kinetic effect is ultimately diluted by the rapid oxygen

isotope exchange reactions between ground-state O and the virtually infinite O_2 reservoir (R1.24, R1.25). Therefore, the KIEs in the formation reaction become the dominant effects determining the isotopic composition of ozone. The other ozone-related reactions, namely oxygen cycling in the HO_x and NO_x families and the sink reaction with atomic oxygen:

$$O_3 + O \rightarrow 2O_2 \qquad \text{(R1.30)}$$

are often ruled out as sources of fractionation in ozone as well, because the rates of these processes are at least 1 or 2 orders smaller than the rate of the odd oxygen cycling reactions.

1.2.2 Experimental and theoretical developments

Published research pertaining to the physical chemistry of MIF, particularly in ozone, is extensive and associated with a diverse range of experimental and theoretical approaches. The aspects of the literature most relevant to the work described in this manuscript will be introduced in this section; however, this body of research cannot be reviewed exhaustively here. For example, measurements of the isotope-specific reaction rate constants and their interpretation will not be treated here. For detailed discussions of the various experiments and their implications, the reader is referred to excellent and extensive reviews by Thiemens (1999; 2006), Weston (1999), Janssen *et al.* (2001), Brenninkmeijer *et al.* (2003), Chakraborty and Bhattacharya (2003a) Mauersberger *et al.* (2003; 2005), and Marcus (2008).

1.2.2.1 Isotope effects of ozone formation

A considerable number of laboratory studies have been performed to investigate the isotopic composition of ozone following its production from molecular oxygen. The basic experimental approach was originally developed by Mark Thiemens and John Heidenreich and reported in two simultaneous papers in 1983 (Heidenreich and Thiemens, 1983; Thiemens and Heidenreich, 1983). In their method, which is still widely used today (see Chapter 2), ozone is produced via electric discharge in oxygen gas and immediately condensed at liquid N_2 temperature (~ 77 K), followed by conversion to O_2 using molecular sieve pellets. The $\delta^{17}O$ and $\delta^{18}O$ values of both the O_2 reservoir and the decomposed ozone are then measured using an isotope ratio mass spectrometer in classical dual-inlet mode. Thiemens and Heidenreich measured

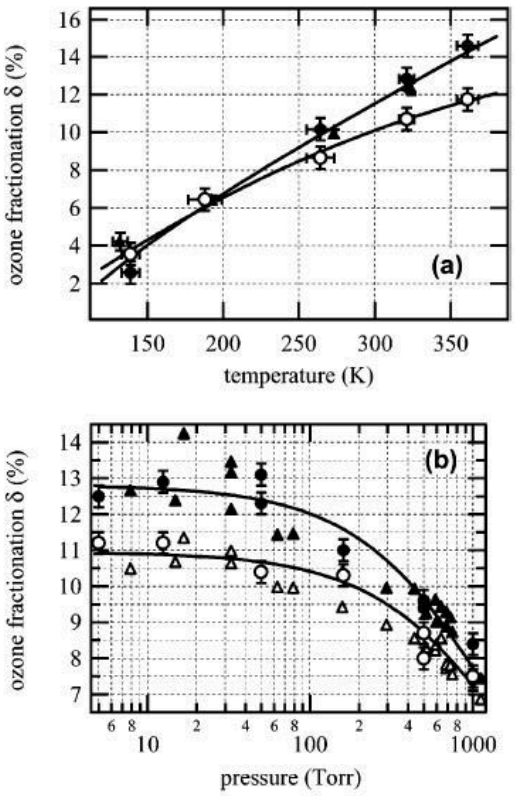

FIGURE 1.7 - (a) Measured temperature dependencies of $\delta^{17}O$ (white symbols) and $\delta^{18}O$ (black symbols) enrichments in ozone reported relative to the O_2 gas used in the experiment. Measurements conducted by Morton *et al.* (1990) (circles) were performed at a constant oxygen pressure of 50 Torr. Triangles represent measurements performed at 45 Torr by Janssen *et al.* (2003). Error bars indicate the 2σ statistical uncertainties reported for the measurements. The best-fit curves were established by Janssen *et al.* (2003). (b) Measured pressure dependency of $\delta^{17}O$ (white symbols) and $\delta^{18}O$ (black symbols) enrichments in ozone formed from O_2 gas. Experiments by Morton *et al.* (1990) (circles) were conducted at a constant temperature of 321 K. Triangles indicate measurements performed under room-temperature conditions (Thiemens and Jackson, 1988; 1990).

maximum ozone enrichments relative to the experimental O_2 of 39‰ and 40‰ for $\delta^{17}O$ and $\delta^{18}O$, respectively, in the first studies using this method. However, the most important result of these studies was the slope of 1.00 observed between $\delta^{17}O$ and $\delta^{18}O$ in a three-isotope plot (**Figure 1.5**), which provided the first direct observational evidence of MIF associated with a chemical mechanism. Subsequent studies in the Thiemens laboratory (Bains-Sahota and Thiemens, 1987; Thiemens and Jackson, 1987; 1988; 1990) were focused on the pressure dependence of isotopic effects during ozone formation. Results obtained in these studies for ozone produced at room temperature and over a wide range of gas pressures are shown in **Figure 1.7b**. Maximum $\delta^{17}O$ and $\delta^{18}O$ enrichments of ca. 110‰ and 130‰, respectively ($\Delta^{17}O \approx$ 42‰), were measured for ozone produced in the low-pressure regime (< 200 Torr), while the intermediate pressure range (200 - 600 Torr) yielded ozone with $\delta^{17}O \approx$ 80‰ and $\delta^{18}O \approx$ 90‰ ($\Delta^{17}O \approx$ 33‰). Above 450 Torr, $\delta^{17}O$ and $\delta^{18}O$ first decrease moderately and then drop off sharply within the high-pressure (> 1000 Torr) regime.

Subsequent experiments revealed that the temperature of the gas from which ozone is formed also plays an important role in determining its isotopic composition. In a major development in the study of the physical chemistry of MIF effects, Morton *et*

al. (1990) developed an experimental method for studying the ozone formation reaction under controlled temperature and pressure conditions and determined the temperature dependence of the ozone formation KIE. In their approach, the photolysis of ozone serves as the source of ground state oxygen atoms for R1.9, rather than electrical discharge. Due to rapid isotope exchange reactions (R1.24, R1.25) following photolysis, oxygen atoms produced in this manner equilibrate with the molecular oxygen reservoir before reacting to reform ozone. Ozone therefore acquires an isotopic composition that is a function only of the composition of the O_2 reservoir and the fractionation processes involved in the formation and photolytic destruction of ozone. Large temperature-dependent enrichments were observed by Morton *et al* (1990) at a constant oxygen pressure of 50 Torr (**Figure 1.7a**), with ozone enrichments values increasing from $\delta^{17}O \approx 36‰$ and $\delta^{18}O \approx 26‰$ ($\Delta^{17}O \approx 23‰$) at 130 K to $\delta^{17}O \approx 117‰$ and $\delta^{18}O \approx 146‰$ ($\Delta^{17}O \approx 41‰$) at 360 K.

The datasets of Thiemens and Jackson (1988; 1990) and Morton *et al.* (1990) provide a useful benchmark for atmospheric studies as they allow for an approximation of the $\delta^{18}O$ and $\Delta^{17}O$ values of ambient tropospheric ozone. A quantitative understanding of the isotopic composition of ambient ozone is crucial for constraining atmospheric interpretations based on oxygen isotope measurements of secondary species, such as nitrate (Alexander *et al.*, 2009), that carry oxygen atoms transferred from ozone . The experimental pressure dependencies of the $\delta^{18}O$ and $\Delta^{17}O$ of ozone formed at 321K can be fitted to an equation in terms of P. For typical tropospheric pressures (500-800 Torr), a linear regression of the data reported by Morton *et al.* (1990) yields the following equation for $\delta^{18}O(O_3)$:

$$\delta^{18}O(O_3) = -0.028 \times P(Torr) + 112 \quad (1.24)$$

An analogous equation for the temperature dependency of $\delta^{18}O(O_3)$ (at 50 Torr) can also be generated from a regression of the measurements reported by Morton *et al.* (1990):

$$\delta^{18}O(O_3) = 0.52 \times T(K) - 45 \quad (1.25)$$

The pressure dependency study of Morton *et al.* (1990) was performed at a reference temperature of 321 K; therefore, a temperature correction must be applied to estimate the δ values of ozone formed under standard surface conditions. Furthermore, the enrichments determined by Morton *et al.* (1990) were reported relative to the initial O_2 composition. In the atmosphere, where air O_2 is +23.5‰ relative to VSMOW

(Kroopnick and Craig, 1972), an additional standard correction factor must be applied to the fitted data when using VSMOW as the reference (Equation 1.2):

$$\delta^{18}O(O_3) = \left(-0.028 \times P(Torr) + 134.8\right) + 0.52 \times \left(T(K) - 321\right) \quad (1.26)$$

Because the temperature dependence was measured at 50 Torr, the enrichment values in the low-pressure plateau (< 300 Torr) can be easily corrected using this approach. However, an extrapolation of the low-pressure temperature dependency data to the surface pressure regime is presently speculative. Assuming that the temperature correction is valid at higher pressures, a $\delta^{18}O(O_3)$ value of 101.6‰ relative to VSMOW is predicted for 298 K and 760 Torr.

The experimental temperature and pressure dependency data can also be used to estimate $\Delta^{17}O(O_3)$ and assess its potential variability for ambient tropospheric conditions. Fitting these data sets yields the following pressure and temperature $\Delta^{17}O$ equations:

$$\Delta^{17}O(O_3) = 78.8 \times P(Torr)^{-0.122} \quad (1.27)$$

$$\Delta^{17}O(O_3) = 0.06 \times T(K) + 16.2 \quad (1.28)$$

Correcting for the experimental temperature gives:

$$\Delta^{17}O(O_3) = \left(78.8 \times P(Torr)^{-0.122}\right) + 0.06 \times \left(T(K) - 321\right) \quad (1.29)$$

Using Equation 1.29 and the assumptions outlined above, a $\Delta^{17}O$ value of 33.7‰ is calculated for ozone formed under standard temperature and pressure conditions. In Section 1.2.3, the $\delta^{18}O$ and $\Delta^{17}O$ values estimated here will be compared to the existing ambient measurements.

1.2.2.2 The role of symmetry in the MIF effect in ozone

Many theoretical attempts have been made to provide a physical explanation for the large mass-independent isotope effect associated with ozone formation. The theory most successful at reproducing experimental results is that of Gao and Marcus (2001), which uses a modified version of the Rice–Ramsperger–Kassel–Marcus (RRKM) theory of unimolecular decomposition to treat the ozone formation reaction. In their theoretical framework, ozone formation is conceptualized as a time-dependent competition between unimolecular decomposition (R1.22) and the stabilization of $(O_3)^*$ via collision with a third-body (R1.23). Following the formation of $(O_3)^*$ in R1.21, an energy redistribution ("intramolecular energy randomization") occurs among the vibrations and rotations of the $(O_3)^*$ molecule. If energy is distributed

statistically among all vibrational-rotational modes of the $(O_3)^*$ complex, its lifetime is extended, which means that there is a larger chance of its being stabilized by loss of energy in a collision via R1.23. It has been suggested that the asymmetric ozone isotopomers (i.e., those with heavy isotope substitutions in the terminal position) dissociate in R1.22 more slowly than symmetric isotopomers due to a larger number of symmetry-allowed mode couplings, which promotes intramolecular energy redistribution in the asymmetric isotopomer. Therefore asymmetric isotopomers have longer lifetimes relative to symmetric species, which leads to the equal enrichment of ^{17}O and ^{18}O in the product ozone.

The theoretical model of Gao and Marcus (2001) implies that the MIF is driven by a symmetry effect, largely in agreement with the mechanism originally proposed by Heidenreich and Thiemens (1985). This suggests that the non-zero $\Delta^{17}O$ resides only in the molecules of type OOQ (asymmetric) and not in type OQO (symmetric), where Q is either ^{17}O or ^{18}O. Any enrichment observed in the symmetrical molecules (like OQO) should follow the mass dependent fractionation relationship. In other words, the $\Delta^{17}O$ of the terminal oxygen atoms should be related to the $\Delta^{17}O$ of bulk ozone as follows:

$$\Delta^{17}O(O_3)_{terminal} \approx 1.5 \times \Delta^{17}O(O_3)_{bulk} \tag{1.30}$$

This hypothesis has been tested experimentally by exploiting chemical reactions in which ozone transfers a terminal oxygen atom to form a stable product. The transfer function between the bulk ozone and its reaction product establishes the isotopic composition of the terminal oxygen atoms of ozone. This technique for investigating the intramolecular distribution of ^{17}O-excess in the ozone molecule has been applied to three such transfer reactions to date: (i) $2Ag_{(s)} + O_3 \rightarrow Ag_2O_{(s)} + O_2$ (Bhattacharya *et al.*, 2008); (ii) $NO + O_3 \rightarrow NO_2 + O_2$ (Savarino *et al.*, 2008); and $NO_2^-{}_{(aq)} + O_3 \rightarrow NO_3^-{}_{(aq)} + O_2$ (Michalski and Bhattacharya, 2009). In all three experiments, the relationship observed between the $\Delta^{17}O$ of bulk ozone and that of the atom transferred during the reaction was equivalent to that shown in Equation 1.30 within the uncertainty of the measurements. The hypothesis of the anomalous ^{17}O enrichment residing only in the terminal position thus appears to be generally valid. This has important implications for the interpretation of $\Delta^{17}O$ measurements for atmospheric trace species: the central and terminal oxygen atoms of ozone are not chemically equivalent in terms of reactivity, with the terminal oxygen atoms generally having a

greater probability of being transferred. Therefore, because the ^{17}O-excess of ozone resides exclusively on its terminal oxygen atoms, the $\Delta^{17}O$ value transferred through bimolecular reactions, denoted $\Delta^{17}O(O_3^*)$, will be a factor of 1.5 higher than $\Delta^{17}O$ of the bulk reacting ozone, or $\Delta^{17}O(O_3)_{bulk}$. Indeed, $\Delta^{17}O(O_3^*)$ appears to be a more relevant measure for the source strength of the ^{17}O-excess of ozone, which is a critical variable needed for interpreting isotope transfer processes in the atmosphere (Janssen, 2005; Morin *et al.*, 2011).

As noted by Michalski and Bhattacharya (2009), isotope transfer reactions are not only useful tools for studying the intramolecular distribution of ^{17}O and ^{18}O in ozone, but may also serve as chemical probes for determining the isotopic composition of ozone in the ambient atmosphere. As we will see in Section 1.2.4, the paucity of information regarding the isotopic composition of tropospheric ozone remains a major barrier to the interpretation of oxygen isotope measurements for other atmospheric species. A major objective of the original research described in this manuscript has been the development of a method that exploits the aqueous-phase ozone/nitrite reaction as an experimental approach for assessing variability in tropospheric $\Delta^{17}O(O_3)$ (see Chapters 2 and 3).

1.2.2.3 Isotope effects of ozone dissociation

Dissociation processes are key pathways in the atmospheric ozone budget. Therefore, in addressing the issue of isotopic enrichments in ozone, it is necessary to determine the potential isotopic effects associated with the various dissociation channels, which include: (i) photo-dissociation; (ii) thermal dissociation; (iii) surface-induced dissociation; and (iv) dissociation via chemical reactions.

Photo-dissociation has long been expected to impact the isotopic composition of atmospheric ozone; however, a quantitative understanding of this effect has not yet been achieved, despite the large amount of research effort directed in this area. Several experiments have been performed using artificial light sources to induce photo-dissociation (R.11 and R.12) followed by the isotopic analysis of the residual ozone. However, an extrapolation of the existing experimental results to atmospheric ozone is uncertain due to the experimental difficulties inherent in separating the photolysis reactions from the subsequent ozone destruction reactions involving the photoproducts (e.g., R1.30). In addition to this limitation, most reported fractionation factors for ozone dissociation rely on measurements with narrow-band light sources

only, while experiments with simulated solar radiation are currently lacking. The two existing studies of ozone isotope fractionation during photo-dissociation in the UV and visible wavelengths (Morton *et al.*, 1990; Chakraborty and Bhattacharya, 2003c) report conflicting results. For example, Morton *et al.* (1990) reported the first data on the effect of visible light photolysis on ozone isotopic composition. They used a tungsten lamp equipped with optical filters to photo-dissociate ozone at λ = 590 nm and observed no significant change in the δ values of the residual ozone, suggesting that photolysis has a negligible impact on the isotopic composition of ozone. In a subsequent study, Chakraborty and Bhattacharya (2003b) found that photolysis at both 520 and 630 nm led to the production of isotopically light oxygen and an enrichment of the residual ozone reservoir, with α values of 1.008 and 1.015 for ^{17}O and ^{18}O, respectively. Furthermore, while photo-dissociation at visible wavelengths displayed a mass-dependent slope in this sudy, UV dissociation exhibited a mass-independent character (slope of 0.63 in a three-isotope plot). However, these results were later questioned by Cole and Boering (2006), who assert that the apparent MIF observed in the Chakraborty and Bhattacharya (2003c) study can be explained by non-negligible ozone formation during the UV photolysis experiments, which results in a slope > 0.52 due to simple mixing. The results of Chakraborty and Bhattacharya (2003c) were further questioned by Brenninkmeijer *et al.* (2003), who suggested that the measurements in this study were likely affected by the heterogeneous loss of ozone on the walls of the reaction chamber due to the long irradiation times used. Therefore, any quantitative prediction of the overall isotopic effect induced by ozone photolysis cannot presently be derived from the laboratory experiments due to their inability to single out the fractionation factors which are associated with the individual steps of photo-dissociation. A ε value of approximately 20‰ is often assumed for ozone photolysis based on measurements obtained for Hg resonance lamp-induced photo-dissociation (λ = 590 nm) (Bhattacharya and Thiemens, 1988; Wen and Thiemens, 1991; Chakraborty and Bhattacharya, 2003c). However, a recent analysis of experimental ozone absorption spectra reveals that photolysis at all wavelengths yields large wavelength-dependent isotopic fractionation, with photochemical modeling suggesting a ε value of approximately 45‰ in the middle stratosphere (Miller *et al.*, 2005a).

Various attempts have been made to determine the isotope fractionation effects associated with the thermal decomposition of ozone, the reverse of the ozone formation reaction:

$O_3 + M \rightarrow O + O_2 + M$ (R1.31)

Experimental approaches to the study of gas-phase ozone decomposition are complicated because oxygen atoms produced in R1.31 may react with ozone via R1.30. The combined isotopic effect of these two reactions was first investigated in a series of experiments by Wen and Thiemens (1990; 1991). In experiments conducted at room temperature, the observed rates of ozone loss exceeded the accepted rate coefficient for thermal dissociation by several orders of magnitude, an observation that was attributed to the surface-induced dissociation of ozone on the walls of the glass reaction chamber during the experiments. For these room temperature experiments, isotopically light ozone molecules decomposed preferentially at the surface of the reactor walls leading to product oxygen molecules depleted in the heavy isotopes in a mass-dependent manner. Above 90°C, the observed rate of ozone decomposition is consistent with the accepted values; furthermore, there is a reversal in the isotopic effect, with the product oxygen becoming enriched in the heavy isotopes. The enrichment of the oxygen formed via ozone thermal dissociation exhibits a mass-independent character, although substantially less than that for the ozone formation reaction. Isotopic fractionation associated with the surface-induced decomposition reaction (i.e., the process identified by Wen and Thiemens (1990) for room temperature experiments) was later studied by Chakraborty and Bhattacharya (2003b), who found that the products of ozone dissociation were enriched in heavy oxygen isotopes in a mass-independent fashion. However, the significance of these results was later strongly disputed by Janssen (2003), who suggests that the apparent MIF behavior observed by Chakraborty and Bhattacharya (2003b) can be explained solely by a violation of the assumption of mass balance during the experiments.

Isotope fractionation associated with chemical transformation pathways may contribute to the observed ozone enrichments in the atmosphere; however, these processes have received very little attention thus far. The dissociation of ozone by reaction with NO was studied recently by Chakraborty (2003). The residual ozone was observed to follow a normal mass-dependent enrichment in this study. The fractionation factor observed in this study is relatively large ($\alpha = 1.031$), suggesting that the $NO + O_3$ reaction has the potential to impact the relative variations of ozone

isotope enrichments under different atmospheric contexts (i.e., low NO_x and high NO_x). Additional studies of other atmospherically relevant reactions are needed.

To summarize, the existing experimental results may be interpreted as an indication that decomposition effects will be significantly smaller in magnitude than isotope fractionation during ozone formation (Liang *et al.*, 2006). Nevertheless, these processes may have an impact, particularly in the stratosphere (Johnson *et al.*, 2000; Miller *et al.*, 2005a), and are thus deserving of further study.

1.2.3 Atmospheric measurements

1.2.3.1 Stratosphere

Measuring the isotopic composition of ozone produced in the laboratory is relatively straightforward; however, atmospheric data are much more difficult to obtain and the initial results for stratospheric samples were consequently sparse and carried large uncertainties (Mauersberger, 1981; Mauersberger, 1987). Following the development of a balloon-borne cryosampler by Schueler *et al.* (1990) and the improvement of spectroscopic techniques, such as far-infrared emission spectroscopy (FIRES) (Johnson *et al.*, 2000), the observational dataset for stratospheric ozone was greatly expanded. The entirety of this published record will not be discussed here; however, it is constructive to consider the most recent stratospheric measurements, which were obtained via laboratory analysis of returned samples during the period 1998 - 2005 using a O_3/CO_2 cryosampling system (Stehr *et al.*, 1996). A total of 42 samples were collected during this period. All samples were collected at an altitude range of 20 to 38 km during balloon flights at three locations: Aire-sur-l'Adour, France (44°N), Kiruna, Sweden (68°N), and Teresina, Brazil (5°S) (Krankowsky *et al.*, 2000; 2007; Mauersberger *et al.*, 2001; Lammerzahl *et al.*, 2002). Both the $\delta^{17}O$ and $\delta^{18}O$ of ozone were measured with improved precision over previous campaigns and the very high enrichments observed in earlier flights were not confirmed, leading Mauersberger *et al.* (2001) to conclude that the early measurements were erroneous and should be disregarded. Enrichment values reported for these samples average 80 ± 15‰ and 89 ± 22‰ for $\delta^{17}O$ and $\delta^{18}O$, respectively (relative to air O_2), and range between 52 ± 5‰ and 104 ± 6‰ for $\delta^{17}O$ and between 51 ± 3‰ and 130 ± 4‰ for $\delta^{18}O$, with errors indicating the statistical uncertainty at the 95% confidence level. Krankowsky *et al.* (2007) have demonstrated that the ozone enrichments observed during these collector

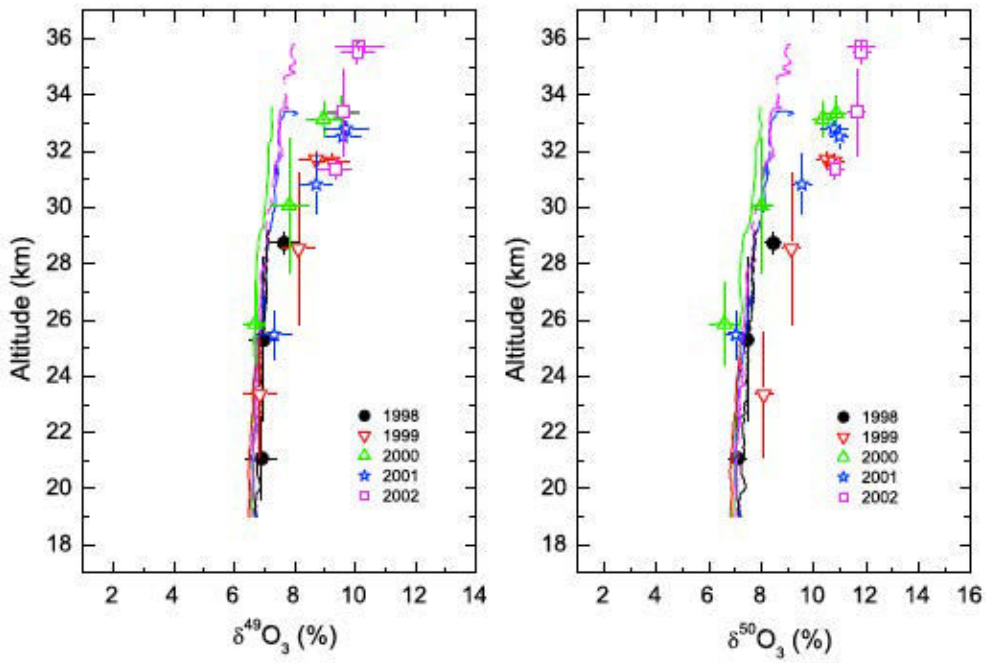

FIGURE 1.8 - Altitude profiles of the $\delta^{17}O$ (left) and $\delta^{18}O$ (right) of ozone measured during five balloon flights at a mid-latitude site (Aire-sur-l'Adour, France). Horizontal error bars indicate 2σ errors while the vertical bars indicate the height range over which the sample was collected. The lines represent the enrichment expected from measured atmospheric temperature profiles and the experimentally determined temperature dependency of isotope fractionation in ozone formation (Krankowsky *et al.*, 2007).

flights are clearly linked to stratospheric temperatures and pressures. **Figure 1.8** shows a comparison of the enrichment values obtained for the Aire-sur-l'Adour flights compared to the enrichments expected from measured atmospheric temperature profiles and the known temperature dependence of isotope fractionation in ozone formation (Morton *et al.*, 1990; Janssen *et al.*, 2003). The agreement between the observations and the predicted values is quite robust, lending credence to the low-pressure temperature dependency data. As the temperature in the stratosphere increases with increasing altitude, the isotope ratios are observed to increase as well, from 65‰ at 20 km to about 75‰ at 28 km for $\delta^{17}O$ and from 70‰ to 80‰ for $\delta^{18}O$. The presence of an additional isotope effect is clear from the difference between observations and expected values at high altitudes. This effect can be interpreted quantitatively in terms of the altitude dependency of isotopic fractionation during ozone photolysis (Miller *et al.*, 2005a; Liang *et al.*, 2006). $\Delta^{17}O(O_3)$ values calculated for the 1998 - 2005 stratospheric ozone data (Krankowsky *et al.*, 2007) average 33 ± 4‰, in excellent agreement with the low-pressure temperature dependency data, which would predict a $\Delta^{17}O(O_3)$ value of approximately 30 - 33‰ for International Standard Atmosphere (ISA) average temperatures between 20 and 32 km altitude.

However, a large degree of variability is observed in the $\Delta^{17}O(O_3)$ values, which range between 25 and 41‰. This variability in $\Delta^{17}O(O_3)$ is significantly correlated with altitude (r = 0.64), with $\Delta^{17}O(O_3)$ increasing between 20 and 32 km.

1.2.3.2 Troposphere

Due to the inherent complexity of extracting ozone from surface air, the observational record for tropospheric ozone isotopes remains quite small, despite the effort that has been devoted to the study of the various oxygen bearing atmospheric trace species carrying the isotopic signature inherited from ozone. Until now, only two studies (Krankowsky *et al.*, 1995; Johnston and Thiemens, 1997) have reported measurements of the isotopic composition of ozone collected from the troposphere. These landmark investigations were performed using a cryosampling technique in which ozone is trapped using liquid helium and subsequently converted to molecular oxygen for isotopic analysis. Krankowsky *et al.* (1995) collected and analyzed 47 ozone samples from ambient air outside of the German city of Heidelberg and found (mean ± 1σ) $\delta^{17}O$ and $\delta^{18}O$ values of 72 ± 11‰ and 91 ± 6‰, respectively (relative to air O_2). In a subsequent study using the cryogenic method, Johnston and Thiemens (1997) analyzed a total of 42 samples collected from three sites in the U.S. Southwest and found $\delta^{17}O = 70 \pm 7$‰ and $\delta^{18}O = 84 \pm 7$‰ (**Figure 1.9**). The $\Delta^{17}O$ of ozone, which can be readily calculated from the individual δ measurements reported, compare quite well for these two datasets in terms of average value: 25 ± 11‰ and 26 ± 5‰ for the Krankowsky *et al.* (1995) and Johnston and Thiemens (1997) studies, respectively (**Figure 1.10**). However, the magnitude of variability in $\Delta^{17}O(O_3)$ observed in the cryogenic data greatly exceeds the expected quantitative effects from variations in the pressure and temperature of ozone formation, indicating a likelihood of random errors, possibly associated with low collection efficiency and interference from xenon (Mauersberger *et al.*, 2003). Furthermore, while the two datasets appear to be in good agreement when comparing average $\Delta^{17}O(O_3)$, the average values observed (i.e., 25 - 26‰) are not quantitatively consistent with the $\Delta^{17}O(O_3)$ value predicted from the measured temperature and pressure dependencies for the ozone formation reaction, which is on the order of 34‰ for average surface conditions (see Section 1.2.2). This discrepancy between predicted and observed tropospheric $\Delta^{17}O(O_3)$ may arise from the analytical deficiencies of the cryogenic method;

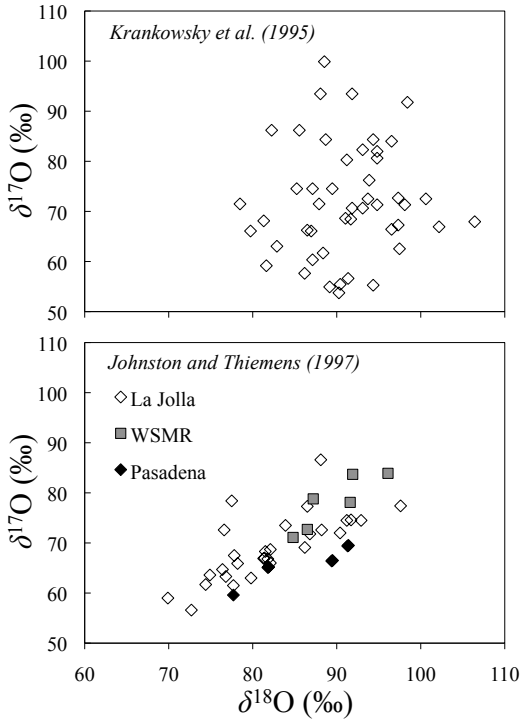

FIGURE 1.9 - Three-isotope plot showing the triple-oxygen isotopic composition ($\delta^{17}O$ and $\delta^{18}O$) of tropospheric ozone as measured by Krankowsky *et al.* (1995) and Johnston and Thiemens (1997) using the cryogenic trapping method. The ozone δ values are reported relative to air O_2, which is enriched by +23.4‰ relative to VSMOW (Kroopnick and Craig, 1972).

however, uncertainty also exists in the extrapolation of the laboratory data to ambient conditions, which is presently speculative as no experimental data for the impact of ozone formation temperature on $\Delta^{17}O(O_3)$ exists for the surface pressure regime. Therefore, debate persists regarding the true value of $\Delta^{17}O(O_3)$ in the troposphere (Brenninkmeijer *et al.*, 2003; Morin *et al.*, 2007b; Michalski and Bhattacharya, 2009).

The $\Delta^{17}O$ of ozone in the troposphere, should it be found to exhibit systematic variability, may also convey quantitative information regarding the balance between ozone production and loss in different environmental contexts. In the study of Krankowsky *et al.* (1995), no correlation was found between the $\delta^{17}O$ and $\delta^{18}O$ values of ozone, suggesting that the large degree of variability observed for $\Delta^{17}O$ is an artifact resulting from statistical scatter of the individual δ measurements. These results are therefore not inconsistent with the hypothesis that the tropospheric value of $\Delta^{17}O(O_3)$ is constant. However, the data of Johnston and Thiemens (1997) reveal a systematic variability in the relationship between $\delta^{17}O$ and $\delta^{18}O$, with data from the different sites aligning on different slopes in a three-isotope plot. The authors of this study concluded that the observed variability resulted from differences in ozone transformation pathways between the three sites. Because the magnitude of the diurnally averaged trend in ozone concentration was observed to decrease with

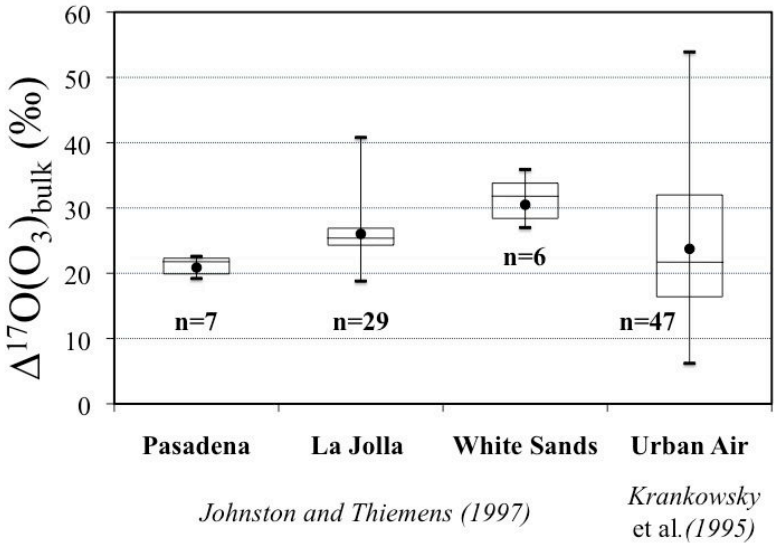

FIGURE 1.10 - Overview of existing measurements of $\Delta^{17}O(O_3)$ in the troposphere. The box plot indicates the median (line), inter-quartile range (box), maximum, and minimum values. The mean value is displayed (circle), as well as the number of data-points for each site (Krankowsky *et al.*, 1995; Johnston and Thiemens, 1997).

increasing $\Delta^{17}O$ (i.e., Pasadena > La Jolla > White Sands), Johnston and Thiemens (1997) suggested that the degree of photochemical control on the local ozone budget was a potential determining factor for MIF in tropospheric ozone. If this is indeed a valid assertion, then measurements of the triple-isotope composition of ozone could be useful in constraining the tropospheric ozone budget. However, the conclusions of Johnston and Thiemens (1997) were later questioned by Brenninkmeijer *et al.* (2003), who argued that the differences in slope are not statistically significant and that the apparent variability in $\Delta^{17}O$ detected between the three sites is therefore simply a measurement artifact.

1.2.4 Applications in atmospheric research and beyond

Ozone is a highly reactive species that transfers oxygen atoms to secondary atmospheric molecules. It is therefore perhaps not surprising that simultaneous measurements of ^{17}O and ^{18}O in many molecular species have shown that nonzero $\Delta^{17}O$ anomalies are common in the atmosphere and other environmental compartments. Indeed, almost all oxygen-bearing species in the atmosphere are now known to exhibit mass-independent oxygen isotope compositions and ozone is the overwhelmingly predominant source of this unique isotopic signal. In contrast to conventional enrichment values (δ), which are impacted by equilibrium and kinetic

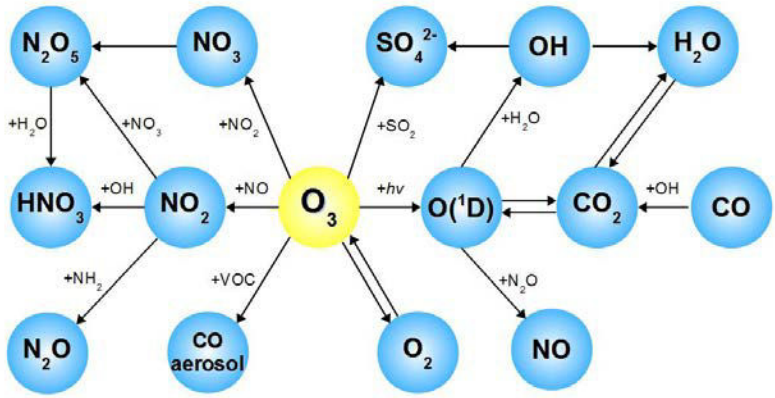

FIGURE 1.11 - The propagation of ozone's anomalous $\Delta^{17}O$ signature via chemical and isotope transfer reactions in the atmosphere.

isotope fractionation processes, the anomalous $\Delta^{17}O$ signature of ozone is insensitive to mass-dependent fractionation. Because the vast majority of chemical reactions induce mass-dependent fractionation, which in general does not strongly modify $\Delta^{17}O$, it can be reasonably assumed that $\Delta^{17}O$ is transferred quantitatively during oxidation reactions in the atmosphere. As a result, the $\Delta^{17}O$ of a given species reflects the fractional importance in its elemental composition of oxygen atoms inherited from ozone, either directly or indirectly (e.g., via $O(^1D)$ reactions). This unique behavior of the $\Delta^{17}O$ signature provides a unique approach for exploring atmospheric oxidation mechanisms using $\Delta^{17}O$ measurements in the atmosphere. Furthermore, $\Delta^{17}O$ measurements of atmospheric trace species preserved in ice cores and terrestrial sediments present the possibility of extending these interpretations to the glacial and geologic time scales.

Various oxidation processes resulting in $\Delta^{17}O$ transfer in the atmosphere are shown in **Figure 1.11**. The role of ozone in the oxygen isotopic dynamics of atmospheric nitrate (HNO_3 gas and particulate NO_3^-) and its precursor molecules (NO_x, NO_3, OH, H_2O, etc.) will be discussed in detail in the next section. Other various developments in the interpretation of $\Delta^{17}O$ measurements and their applications in the earth sciences will be briefly introduced below.

1.2.4.1 Carbon dioxide

Following the discovery of large mass-independent isotope enrichments in stratospheric ozone (Mauersberger, 1987; Schueler *et al.*, 1990), a lesser yet

substantial enrichment was also observed in stratospheric CO_2 (Thiemens *et al.*, 1995). Yung *et al.* (1991) subsequently proposed a mechanism for the transfer of the anomalous $\Delta^{17}O$ signature from ozone to CO_2 in which $O(^1D)$ radicals generated from the UV photolysis of ozone (R1.12) and CO_2 ($\lambda < 315$ nm) form a short-lived CO_3* intermediate, which dissociates rapidly to yield CO_2 and ground-state oxygen. Yung *et al.* (1991) showed that, when included in a photochemical model, this mechanism could reproduce the observed ^{18}O enrichments in stratospheric CO_2, which increase with altitude from the tropopause:

$$O(^1D) + CO_2 \rightarrow CO_3^* \rightarrow CO_2 + O(^1P) \qquad \text{(R1.32)}$$

R1.32 provides the basis for a number of promising atmospheric applications. The source of the $\Delta^{17}O(CO_2)$ signal is the upper stratosphere, where $O(^1D)$ production rates are maximized, and its primary sink is mass-dependent isotope exchange with liquid water in the ocean and biosphere. Because the $\Delta^{17}O(CO_2)$ signal has insignificant sinks in the stratosphere, it represents a long-lived stratospheric tracer and can thus be used to examine stratosphere-troposphere exchange. In the stratosphere itself, the value of the anomaly increases as CO_2 ascends to higher altitudes; therefore, $\Delta^{17}O(CO_2)$ be regarded as a tracer for R1.32 and thus used to assess $O(^1D)$ levels (Boering *et al.*, 2004). The R1.32 pathway also produces an interesting effect in the isotopic composition of atmospheric O_2: the high ^{17}O and ^{18}O enrichments associated with ozone formation lead to a residual O_2 that is correspondingly depleted. Without transfer of the isotope anomaly to CO_2, the heavy oxygen atoms would simply be cycled through the O_x reservoirs as part of the Chapman cycle. However, when the ^{17}O-excess is transferred via $O(^1D)$ to CO_2, it is lost from the O_x reservoirs; i.e., the transfer process represents a small leak of excess ^{17}O from O_2 to CO_2 (and finally to the large H_2O reservoir via isotope exchange in the troposphere). Over a time scale of about 1000 years (the exchange time of the atmospheric O_2 reservoir with the biosphere), this ^{17}O leak produces a measurable ^{17}O deficiency in atmospheric O_2. At equilibrium, the magnitude of this ^{17}O deficiency is controlled by the stratospheric leak and global biospheric productivity (Luz *et al.*, 1999). Measurements of $\delta^{17}O$ and $\delta^{18}O$ in atmospheric O_2 from air trapped in ice cores can thus used to estimate global productivity on large time scales (Blunier *et al.*, 2002). Measurements of ^{17}O in ancient evaporites and barites suggest that the negative $\Delta^{17}O$ value of atmospheric oxygen is also transmitted to sulfate under some

circumstances (Bao *et al.*, 2008), suggesting that this signal may be preserved in the geologic record for millions of years.

1.2.4.2 Sulfate

Following the development of a technique for the measurement of both $\delta^{17}O$ and $\delta^{18}O$ in sulfate (Savarino *et al.*, 2001), nonzero $\Delta^{17}O$ values in tropospheric sulfate were first reported by Lee *et al.* (2001) in rainwater and aerosol samples collected in La Jolla. They proposed that the ^{17}O-excess detected in sulfate stems from the aqueous-phase oxidation of sulfur dioxide (SO_2), which is the predominant anthropogenic sulfur-containing air pollutant. This oxidation can be performed directly by ozone, which results in a simple transfer of $\Delta^{17}O(O_3^*)$ to the product sulfate (Savarino *et al.*, 2000). However, the MIF signature can also be transferred to sulfate via oxidation by H_2O_2, which has been found to carry a $\Delta^{17}O$ value on the order of 0–2‰ (Savarino and Thiemens, 1999). All of the other precursors involved in sulfate production exhibit mass-dependent oxygen isotopic compositions ($\Delta^{17}O \approx 0$). Measurement of the MIF of sulfate therefore represents a means of investigating changes in the relative contribution of tropospheric aqueous (O_3 and H_2O_2) and gas-phase (OH) oxidation of atmospheric sulfur species. Furthermore, triple-oxygen isotope analysis of sulfate minerals in ancient sediments has revealed that the $\Delta^{17}O$ signature imparted to sulfate in the atmosphere is preserved over millions of years (Bao *et al.*, 2000). The $\Delta^{17}O$ of sulfate thus represents a potential proxy for the chemical composition and oxidation capacity of ancient atmospheres. The presence of relatively high concentrations of sulfate in polar snow and ice provides the possibility of extending atmospheric interpretations to the glacial/interglacial time scale, which could allow for a detailed examination of the relationship between climate and atmospheric oxidative capacity during rapid climate transitions. Alexander *et al.* (2002) measured the oxygen isotope composition of sulfate extracted from the Vostok, Antarctica ice core and report $\Delta^{17}O(SO_4^-)$ values between 1 - 5 ‰ over the course of one climatic cycle (~ 130 kyr). Maximum $\Delta^{17}O(SO_4^-)$ values were found to correspond with interglacial periods and *vice versa*, leading the authors of this study to conclude that the gas-phase oxidation of reduced atmospheric sulfur species was of greater relative importance during the last glacial as compared to the surrounding interglacial periods. Isotopic measurements of ice core sulfate by Savarino *et al.* (2003) were used to infer the stratospheric oxidation of SO_2 by ground-state oxygen during massive volcanic

eruptions. This unexpected pathway results in large $\Delta^{17}O(SO_4^-)$ values in the ice that are observed in conjunction with the high sulfate concentrations indicative of volcanic eruptions, which was attributed to a shutdown of stratospheric OH chemistry following the injection of volcanic emissions into the stratosphere. Several subsequent studies have also applied ice core $\Delta^{17}O(SO_4^-)$ measurements to investigations of atmospheric oxidative capacity at various time scales (Alexander *et al.*, 2004; Kunasek *et al.*, 2010; Sofen *et al.*, 2011). Further isotopic measurements of aerosol sulfate have demonstrated that $\Delta^{17}O$ provides an effective tracer of aqueous-phase oxidation pathways with potential for resolving complex sulfate production pathways in the atmosphere (Patris *et al.*, 2007; Alexander *et al.*, 2012; Hill-Falkenthal *et al.*, 2012).

1.2.4.3 Nitrous oxide

First simultaneous measurements of $\delta^{17}O$ and $\delta^{18}O$ in tropospheric N_2O revealed that this important trace gas possess a nonzero $\Delta^{17}O$ value, typically on the order of 0.9 ± 2‰. Röckmann *et al.* (2001) proposed a reaction mechanism to account for these observations in which the $\Delta^{17}O$ signature of ozone is first transferred to NO_2 via reaction with NO:

$$O_3 + NO \rightarrow NO_2 + O_2 \quad \text{(R1.33)}$$

followed by the transfer of ^{17}O-excess from NO_2 to N_2O via a NH_2 intermediate:

$$NH_3 + OH \rightarrow NH_2 + H_2O \quad \text{(R1.34)}$$

$$NH_2 + NO_2 \rightarrow N_2O + H_2O \quad \text{(R1.35)}$$

thus completing the transfer process from ozone to N_2O. Assuming a branching ratio of 0.60 for R1.35, Röckmann *et al.* (2001) found a strong agreement between atmospheric modeling predictions of the relative importance of the R1.35 pathway and a $\Delta^{17}O$ mass balance of measurements obtained for N_2O. From this analysis, they concluded that the R1.35 pathway was the only reaction needed to explain the $\Delta^{17}O$ values observed and thus proposed that oxygen isotopic measurements of N_2O could be used to investigate the variability of this N_2O production pathway. However, more recent measurements of the branching ratio for R1.35 have estimated contributions of only ~20% in terms of total N_2O production (Park and Lin, 1997). This indicates a smaller contribution of this source to the observed ^{17}O-excess in atmospheric N_2O than was previously estimated, suggesting the presence of additional $\Delta^{17}O$ transfer mechanisms accompanying unidentified N_2O production pathways. An identification

of these production mechanisms will represent an important contribution to our understanding of the atmospheric chemistry of N_2O, highlighting the role played by isotopic measurements in identifying and quantifying complex atmospheric processes that cannot be resolved through trace gas concentration measurements alone (McLinden *et al.*, 2003).

1.3 Isotope dynamics of atmospheric nitrate and its precursors

Reactive nitrogen oxides (NO and NO_2 = NO_x) exert a significant influence on the chemistry of the troposphere through the catalysis of photochemical ozone production and are closely coupled with air quality and atmospheric oxidative capacity (i.e., the lifetime of organic compounds from oxidation by radicals). NO_x is emitted to the troposphere or formed *in-situ* through several natural processes, including microbial activities in soils, conversion from inert nitrogen gas (N_2) by lightning, and downward transport from the stratosphere. However, the global tropospheric NO_x budget is currently dominated by anthropogenic activities, with fossil fuel combustion accounting for approximately 50 % of total emissions globally (Galloway *et al.*, 2003). In industrial regions, where sources of anthropogenic NO_x are abundant, high concentrations of surface ozone generated as a by-product of NO_2 photolysis represent a threat to public health and natural vegetation (Finlayson-Pitts and Pitts, 1997; Brunekreef and Holgate, 2002). Furthermore, the export of anthropogenic NO_x from industrialized continents can contribute to the global ozone budget, leading to enhancements in ozone concentration in the background troposphere and thus linking regional air pollution issues to global oxidative capacity (Lelieveld *et al.*, 2004; Cooper *et al.*, 2010). The quantification of NO_x emissions and the elucidation of its subsequent chemical transformation pathways are thus topics of considerable current interest, particularly in light of global atmospheric change (Monks *et al.*, 2009). However, despite the intense research effort dedicated to understanding the rates of the various pathways of the atmospheric NO_x cycle, several fundamental processes remain poorly constrained (Lerdau *et al.*, 2000; Brown *et al.*, 2006; Mollner *et al.*, 2010).

Nitrate, which is defined throughout this text as the sum of gaseous nitric acid (HNO_3) and particulate NO_3^-, is the major oxidation product of reactive nitrogen in

the atmosphere. Due to its exceptionally high solubility in water, nitrate is rapidly deposited upon formation onto surfaces and in water droplets, with a typical atmospheric lifetime from deposition of one or more days (Liang *et al.*, 1998). The deposition of atmospheric nitrate to natural ecosystems represents an environmentally significant material input pathway for two principal reasons. First, HNO_3 is a strong acid that can dramatically lower the pH of precipitation, which contributes to the acidification of soils and surface waters, a phenomenon with long-lasting ecological consequences (Likens *et al.*, 1996). Second, nitrogen is often the plant nutrient limiting biological production in both terrestrial and aquatic ecosystems, making nitrate deposition an important factor in ecological issues such as terrestrial carbon dynamics, surface water eutophication, and marine primary productivity (Holland *et al.*, 1997; Fenn *et al.*, 2003; Duce *et al.*, 2008). We will begin our discussion of the isotopic composition of atmospheric nitrate with a consideration of the basic atmospheric chemistry of NO_x.

1.3.1 The atmospheric reactive nitrogen (NO_x) cycle

1.3.1.1 Daytime chemistry

Figure 1.12 summarizes the essential features of the NO_x cycle, which terminates in the formation of a nitrate end-product. During the day, NO and NO_2 interconvert through the photochemical NO_x cycle, in which NO_2 undergoes photolysis to form NO (R1.19), generating excited oxygen atoms which may subsequently react with molecular oxygen and produce ozone (R1.9). The NO resulting from the R1.19 pathway reacts rapidly to reform NO_2, primarily through oxidation by ozone (Crutzen, 1970):

$$O_3 + NO \rightarrow NO_2 + O_2 \qquad \text{(R1.36)}$$

Cycling between NO and NO_2 occurs so rapidly that a steady-state is established during the day, known as the *photostationary state*. The relationship between ozone and NO_x concentrations at stationary state is given by:

$$[O_3] = \frac{j_{NO_2}[NO_2]}{k_{R1.36}[NO]} \qquad (1.31)$$

where j_{NO2} represents the photolysis rate coefficient for NO_2. In plain words, Equation 1.31 predicts that when the molar ratio of NO_2 ($\chi NO_2 = [NO_2]/[NO_x]$) increases, the

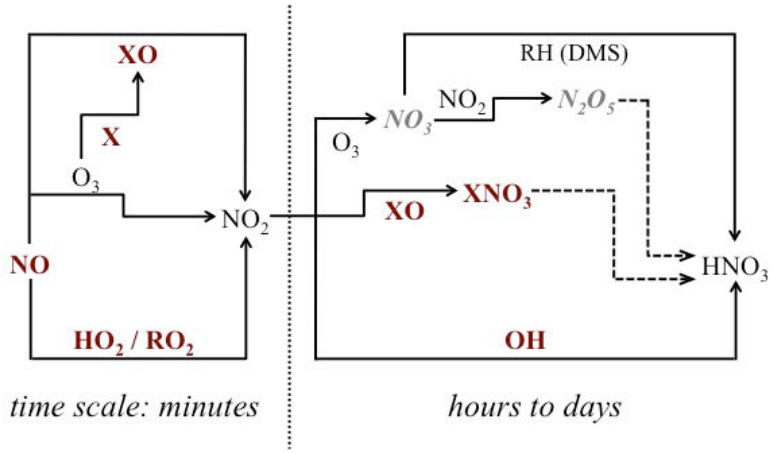

FIGURE 1.12 - Simplified NO_x cycle leading to the formation of nitrate in the atmosphere. Nitrate precursor gases associated with daytime and nighttime pathways are indicated by bold and italicized text, respectively. Dashed lines indicate heterogeneous surface reactions on atmospheric particles.

steady-state ozone concentration increases accordingly. However, as discussed in Section 1.2.1, the fate of the peroxy radicals can also have an effect on the propensity of the atmosphere to produce or to destroy ozone. Photolysis of NO_2 and the subsequent reaction of atmomic oxygen with O_2 (R1.9) is the only known mechanism for producing ozone in the troposphere. However, when the ozone and NO formed in these processes react to reform NO_2 through the R1.36 pathway, a null cycle is formed. In the presence of NO_x, the peroxy radicals (RO_2 = HO_2 and CH_3O_2) can catalyze the oxidation of NO to NO_2 (R1.18). This pathway results in net ozone formation because each time an RO_2 + NO reaction occurs, an additional ozone molecule is formed as the resulting NO_2 molecule photolyzes. This represents a "new" ozone molecule because the NO_2 formed from R1.18 does not destroy an ozone molecule in its formation via R1.36.

Clearly, there exists a delicate balance between photochemical ozone production and loss that is determined by HO_x and NO_x concentrations. **Figure 1.13** shows the results of a numerical simulation of the dependence of ozone production on NO_x concentration. There are three distinct regions in terms of net ozone production. In region A, where NO_x levels are relatively low, such as in the remote atmosphere, HO_2 reacts with ozone (R1.15), leading to net ozone destruction. As NO_x concentration increases, the participation of the R1.18 pathway results in increasing ozone production. The balance point where net production is equal to zero is often referred to as the *compensation point* and occurs at a critical concentration of NO_x. Above the compensation point, ozone production is greater than loss and therefore net

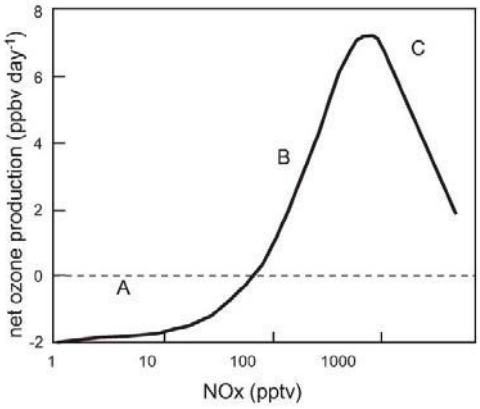

FIGURE 1.13 - Schematic representation of the dependence of the net ozone production (or destruction) on the concentration of NO_x. The magnitudes reflect clean free tropospheric condition (Monks, 2005).

production is positive and the system is forming ozone (region B). The *in-situ* formation rate for ozone in this region of the curve is given approximately the rate of the R1.18 reaction:

$$P_{O_3} = k_{R1.18}[RO_2][NO] \tag{1.32}$$

At a certain concentration of NO_x, the system reaches a maximum production rate for ozone and, while ozone production remains significantly larger than loss, the net production rate begins to decrease with increasing NO_x (region C). Until this maximum is reached, the system is said to be NO_x-limited with respect to the production of ozone. After this limit has been reached, the rate of the overall photochemical cycle is controlled by the CO + OH reaction (R1.3), which determines RO_2 production; in fact, as NO_x concentrations increase further into region C, the homogeneous OH + NO_2 termination reaction (R1.23) increases in importance, effectively terminating OH/HO_2 cycling and thereby decreasing the amount of ozone that can be formed.

1.3.1.2 Nighttime chemistry

While the vast majority of chemical processes in the atmosphere are initiated by sunlight, atmospheric chemistry does not cease during the nighttime. Nocturnal reactions tend to counteract the daytime photochemical production of ozone by removing NO_x and initiating the nocturnal oxidation of reactive VOCs, which can play an important role in the production of secondary pollutants. Nighttime reactions also play an important role in the atmospheric nitrate budget, particularly in high-latitude regions where they can be responsible for up to 75% of total nitrate production (Alexander *et al.*, 2009). In the troposphere, the main nighttime oxidant is

thought to be the nitrate radical (NO_3), which is formed by the relatively slow oxidation of NO_2 by ozone (Brown and Stutz, 2012):

$$O_3 + NO_2 \rightarrow NO_3 + O_2 \quad \text{(R1.37)}$$

The nitrate radical (NO_3) plays an important role in the chemistry of the nighttime troposphere, both as an oxidizing agent for a large number of organic species, and as a route for the removal of NO_x. The NO_3 radical absorbs strongly throughout the visible region, so that during the day it is photolyzed rapidly via two channels:

$$NO_3 + h\nu \rightarrow NO + O_2 \quad \text{(R1.38)}$$

$$NO_3 + h\nu \rightarrow NO_2 + O \quad \text{(R1.39)}$$

The lifetime of NO_3 from photolysis is on the order of five seconds for overhead sun and clear sky conditions (Allan *et al.*, 1999). The nitrate radical also reacts rapidly with NO:

$$NO_3 + NO \rightarrow 2NO_2 \quad \text{(R1.40)}$$

which can reach significant concentrations during the daytime; conversely, in the background troposphere where NO_x sources are low, NO concentrations should be near zero during the night due to rapid titration by ozone via R1.37. Under highly polluted conditions, it is possible for NO_3 to persist during the day (Brown *et al.*, 2005); however, under most atmospheric conditions, NO_3 has an exceedingly low lifetime during the day and thus reaches significant concentrations only during the night.

The nitrate radical is highly reactive towards certain VOCs, such as isoprene, a variety of butenes and monoterpenes, and reduced sulfur compounds, such as dimethyl sulfide (DMS). Depending on the chemical nature of the hydrocarbons present in the atmosphere, NO_3 + VOC chemistry can act to either recycle NO_x, thereby inhibiting the formation of nitrate aerosol, or form HNO_3:

$$NO_3 + RH \rightarrow HNO_3 + R \quad \text{(R1.41)}$$

In the case of NO_3 + DMS, which is the principal reaction of the R1.41 type, nitrate is formed at unit yield. The DMS sink from NO_3 oxidation can be even larger than the OH sink in the marine boundary layer (MBL), where R1.41 can be responsible for a large proportion of total nitrate production (Allan *et al.*, 1999). However, the fractional importance of this production channel can be highly variable in space and time (Osthoff *et al.*, 2009).

A key step in the nocturnal conversion of NO_x to nitrate is the heterogeneous hydrolysis of dinitrogen pentoxide (N_2O_5), which is closely coupled to NO_x and the

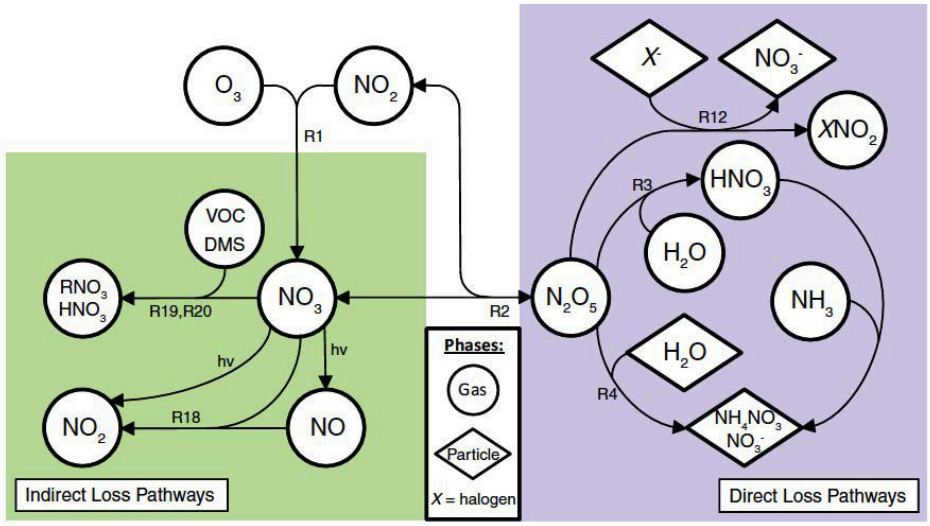

FIGURE 1.14 - Chemical mechanism for N_2O_5 formation and loss. X indicates halogen atoms such as chlorine and bromine that are commonly found in sea-salt aerosol. Circles denote gas-phase species, and diamonds denote species in particle phase (Chang *et al.*, 2011).

NO_3 radical through the following three-body reaction:

$$NO_3 + NO_2 + M \leftrightarrow N_2O_5 + M \quad \text{(R1.42)}$$

N_2O_5 is an important intermediate in the NO_x cycle that can hydrolyze to form HNO_3 through heterogeneous reactions on the surface of aerosol particles:

$$N_2O_5 + H_2O_{(liquid)} \rightarrow 2HNO_3 \quad \text{(R1.43)}$$

This N_2O_5 loss pathway represents a significant nocturnal sink of NO_x and a source of aerosol. However, N_2O_5 may act as only a temporary NO_x reservoir, eventually decomposing to reform NO_2 and NO_3 via R1.42 (**Figure 1.14**). The actual efficiency of N_2O_5 uptake and nitrate yield, which depends strongly on aerosol composition and meteorological conditions, remains an area of significant uncertainty (Brown *et al.*, 2004; Bertram and Thornton, 2009). Furthermore, the heterogeneous chemistry of N_2O_5 on chloride-containing aerosol, first identified in laboratory studies over two decades ago (Finlayson-Pitts *et al.*, 1989), has only recently been shown to efficiently release atomic chlorine radicals to the atmosphere (Osthoff *et al.*, 2008):

$$N_2O_5 + Cl^-_{(aq)} \rightarrow ClNO_2 + NO_3^-_{(aq)} \quad \text{(R1.44)}$$

Most previous studies of nocturnal NO_x transformations have assumed that N_2O_5 reactions on particles proceed solely through the hydrolysis channel to form two HNO_3 molecules. However, reaction with Cl^- may compete with N_2O_5 hydrolysis in the case of marine aerosols, with recent studies suggesting that this pathway represents a significant fraction of total N_2O_5 consumption in some polluted coastal

environments (Thornton *et al.*, 2010; Phillips *et al.*, 2012). This N_2O_5 loss mechanism has important implications for air quality because it results in the production of nitryl chloride ($ClNO_2$) and only one HNO_3 molecule, thereby decreasing the magnitude of the nocturnal NO_x sink from HNO_3 formation while also forming a reactive halogen species that may subsequently influence ozone chemistry (Sarwar *et al.*, 2012).

1.3.2 Isotopic composition of atmospheric nitrate

Nitrate stable isotope analysis is a powerful analytical tool for identifying sources of NO_x and quantifying and constraining the rates of the relevant NO_x removal mechanisms under various atmospheric conditions. The unique and distinctive ^{17}O-excess of ozone has been found to be a particularly useful isotopic fingerprint in studies of NO_x transformations. The $\Delta^{17}O$ signature of ozone is transferred to NO_x through oxidation reactions such that the $\Delta^{17}O$ of nitrate acts as a marker of the influence of ozone in its chemical formation. In this section, we will review the current state of knowledge concerning the factors that control the oxygen isotope composition of atmospheric nitrate. Particular attention will be given to the measurement and interpretation of the $\Delta^{17}O$ of nitrate and the ability of these measurements to increase our understanding of NO_x oxidation in the atmosphere.

1.3.2.1 Methods for nitrate isotope analysis

The initial approaches developed for isotopic analysis of nitrate were pyrolytic methods. The first technique to be employed used a mixture of potassium nitrate (KNO_3) salt and hydrogen cyanide, $Hg(CN)_2$, heated to 550 °C, with isotopic analysis being carried out on the product CO_2 after offline purification (Amberger and Schmidt, 1987). Similar offline methods were subsequently developed based on the reaction of KNO_3 or $AgNO_3$ with various C-bearing reducing reagents at 800 °C in sealed silica glass tubes (Revesz *et al.*, 1997; Silva *et al.*, 2000). This became the preferred method due to the toxicity of the cyanide and mercury compounds used in the original technique. However, three significant problems exist with the combustion techniques in terms of their applicability to the isotopic analysis of atmospheric nitrate: (i) the silicate in the quartz reaction vessels can exchange oxygen atoms to varying degrees with the product gases at 800 °C. This introduces analytical biases and high uncertainties in the data generated using this method (Revesz and Bohlke,

2002); (ii) the CO_2 and CO sample gases generated by the current combustion techniques are not suitable for the measurement of $\Delta^{17}O$ because of the isobaric interference of the ^{13}C at *m/z* 45 (i.e., $^{16}O^{13}C^{16}O$ and $^{16}O^{12}C^{17}O$ cannot be resolved); (iii) a rather large amount of nitrate sample (1 - 10 μmol) is required, which necessitates inefficient and time consuming purification steps in the analysis of environmental samples that contain low levels of nitrate. The two former limitations were addressed by Michalski *et al.* (2002), who developed a technique for the triple-oxygen isotope ($\delta^{17}O$ and $\delta^{18}O$) analysis of nitrate based on the thermal decomposition of $AgNO_3$ at 520 °C followed by analysis of the product O_2. The decreased temperature used in this method limited the amount of oxygen exchange, resulting in highly precise $\Delta^{17}O$ determination (± 0.3‰) for relatively large samples.

The size and purification limitations of the pyrolysis methods were largely overcome by the development of the bacterial denitrifier method. This technique is suitable for isotopic analysis of nanomolar quantities of nitrate and requires limited sample preparation. The bacterial denitrifier technique is based on the analysis of N_2O gas that is produced quantitatively from nitrate by denitrifying bacteria (Sigman *et al.*, 2001). The classical denitrification pathway consists of the following stepwise reduction of nitrate to N_2 gas:

$$NO_3^- \rightarrow NO_2^- \rightarrow NO \rightarrow N_2O \rightarrow N_2 \qquad \text{(R1.45)}$$

The bacterial reduction technique takes advantage of naturally occurring denitrifiers that lack an active N_2O reductase, the enzyme that catalyzes the reduction of N_2O to N_2. *Pseudomonas aureofaciens*, the most commonly used species, does not initiate exchange between nitrogen oxide intermediates and cellular water during R1.45 and has therefore been found suitable for use in determination of oxygen isotope ratios of nitrate (Casciotti *et al.*, 2002). However, because of the isobaric interference of $^{15}N^{16}O^{14}N$ at *m/z* 45, $\Delta^{17}O$ could not be determined until Kaiser *et al.* (2007) modified the technique by reacting the product N_2O over gold (Cliff and Thiemens, 1994) to produce N_2 and O_2 sample gases. This modification allows for the comprehensive isotopic determination of nitrate at typical precisions of 2.0‰, 0.5‰, and 0.5‰, for $\delta^{18}O$, $\Delta^{17}O$, and $\delta^{15}N$, respectively (Morin *et al.*, 2009).

1.3.2.2 Atmospheric observations

The first measurements of oxygen isotope ratios of nitrate in precipitation revealed large $\delta^{18}O$ enrichments of up to 75‰ relative to VSMOW (see Kendall *et al* (2007)

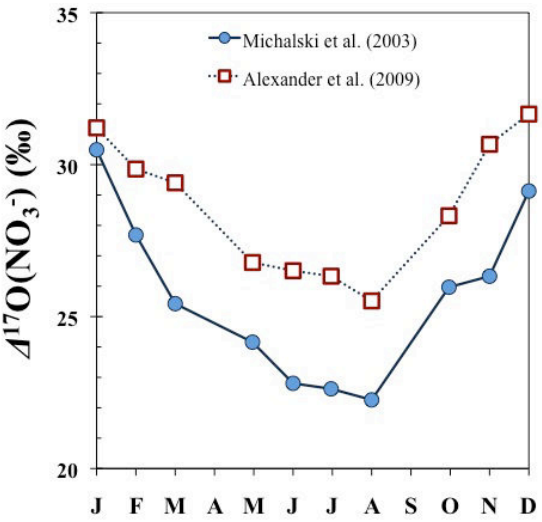

FIGURE 1.15 - Annual record of $\Delta^{17}O(NO_3^-)$ at La Jolla, California. Measurements conducted on nitrate aerosol samples by Michalski *et al.* (2003) are indicated by filled circles. Predictions obtained using the global 3-D atmospheric chemistry model GEOS-CHEM (open squares) are shown for comparison to the direct observations (Alexander *et al.*, 2009).

and references therein). The mass-independent nature of the oxygen isotope enrichments in atmospheric nitrate was later confirmed by Michalski *et al.* (2003), who collected

aerosol samples over a one-year period at La Jolla and determined the $\delta^{17}O$ and $\delta^{18}O$ values of nitrate using the $AgNO_3$ method (Michalski *et al.*, 2002). A clear seasonal trend in the $\Delta^{17}O$ of atmospheric nitrate was observed in this study, with values ranging from 23‰ during the summer and spring to over 30‰ in the winter months (**Figure 1.15**). This seasonal cycle was attributed to variations in the relative involvement of ozone oxidation chemistry during the conversion of NO_x to nitrate (see Section 1.2.1). Subsequent studies of $\Delta^{17}O(NO_3^-)$ in precipitation and aerosols from several mid-latitude locations showed similar ranges of values and confirmed the seasonal trend identified by Michalski *et al.* (2003); however, the observational dataset for mid-latitude and tropical regions remains quite small. Kaiser *et al.* (2007) measured $\Delta^{17}O(NO_3^-)$ values of 20 - 30‰ for precipitation collected in the eastern United States and the equatorial Pacific; Patris *et al.* (2007) reported values of 20 - 27‰ for aerosol samples collected in northern California; Morin *et al.* (2009) measured values of 20 - 35‰ for aerosol samples collected along a ship-borne latitudinal transect from 65 °S to 79 °N in the Atlantic Ocean.

Due to the interest in using isotopes in ice core nitrate as a paleo-atmospheric proxy for oxidation chemistry, a great number of isotopic measurements have been conducted on nitrate samples obtained from the polar atmosphere. Studies conducted

in both the Arctic (Morin *et al.*, 2007a; 2007b; 2008; 2012; Kunasek *et al.*, 2008) and Antarctic (Michalski *et al.*, 2005; McCabe *et al.*, 2007; Savarino *et al.*, 2007; Frey *et al.*, 2009) have revealed higher levels of ^{17}O-excess as compared to the studies at mid-latitudes, particularly during the winter months when $\Delta^{17}O(NO_3^-)$ values as high as 40‰ have been observed. Furthermore, the occurrence of continuous sunlight during the summer (polar day) and continuous darkness during the winter (polar night) has been found to induce pronounced seasonal differences in $\Delta^{17}O(NO_3^-)$ in the polar regions .

1.3.3 Δ^{17}O mass balance for nitrate

The seasonal and geographic trends observed in the Δ^{17}O of atmospheric nitrate provide a unique approach for tracing the spatiotemporal variability of chemical oxidation pathways involving gas-phase nitrate precursors. The theoretical framework commonly used in the interpretation of $\Delta^{17}O(NO_3^-)$ springs from the approach of Lyons (2001), who used a photochemical equilibrium model to quantify the transfer of the Δ^{17}O signal from ozone to species such as OH, H_2O, HO_2, and NO_x in both the troposphere and stratosphere. This pioneering work set the stage for the first modeling study of the isotopic composition of atmospheric nitrate by Michalski *et al.* (2003). In this approach, Δ^{17}O is interpreted using mass balance calculations that trace the origin of oxygen atoms transferred during the conversion of NO_x to nitrate. The implementation of Δ^{17}O into the mass balance equation follows from conservation of mass applied to the ^{17}O-excess: the key assumption behind these calculations is that sink reactions do not induce a specific non-mass dependent fractionation and that every source reaction induces the transfer of a given Δ^{17}O value to the newly produced nitrate. This rather simple method does not apply to isotopic enrichment (δ) values or isotopic fractionation would have to be taken into account for every reaction considered.

1.3.3.1 Δ^{17}O signatures of nitrate production pathways

In each atmospheric nitrate production channel, the main reactant is either NO_2 or a NO_x reservoir species derived from NO_2 (e.g., N_2O_5); therefore, the first step in determining the Δ^{17}O signature of each pathway is a quantitative assessment of the Δ^{17}O of NO_2. Due to the absence of direct observations, $\Delta^{17}O(NO_2)$ is typically

calculated based on assumptions regarding the $\Delta^{17}O$ value of ozone and the reaction dynamics involved in the conversion of NO to NO_2. In the photochemical steady state depicted on the left side of **Figure 1.12**, the $\Delta^{17}O$ of NO_2 in equilibrium with ozone and HO_2/RO_2 is given by the following formula:

$$\Delta^{17}O(NO_2) = \alpha \times \Delta^{17}O(O_3^*) \quad (1.33)$$

$\Delta^{17}O(O_3^*)$ represents the ^{17}O-excess transferred by ozone through bimolecular chemical reactions and α represents the fraction of the atmospheric NO_2 reservoir that has been produced through the $NO + O_3$ channel:

$$\alpha = \frac{k_{NO+O_3}[NO][O_3]}{k_{NO+O_3}[NO][O_3] + k_{NO+HO_2}[NO][HO_2] + k_{NO+RO_2}[NO][RO_2]} \quad (1.34)$$

As shown in Equation 1.33, the $\Delta^{17}O$ signature of NO_2 coupled to NO and ozone via the photostationary state can be determined at any given time and place provided that α and $\Delta^{17}O(O_3^*)$ are known. The value of α is purely a function of the activity of ozone relative to peroxy radicals (HO_2/RO_2), which are derived from O_2 and possess negligible ^{17}O-excess (Savarino and Thiemens, 1999). This parameter can be reasonably estimated using models of atmospheric photochemistry. For example, Michalski *et al.* (2003) modeled annual variations in α at La Jolla and obtained average values ranging from 0.85 during peak photochemical activity in the summer to near unity in the winter. Model calculations described by Röckmann *et al.* (2001) show that the global annual average turnover for the $NO + O_3$ reaction is approximately four times that of $NO + HO_2/RO_2$ pathways, suggesting an average α value of 0.80. The value of α is expected to reach unity during the night due to the rapid loss of HO_2/RO_2 in the absence of UV radiation, while photostationary cycling during the day results in α values less than 1.0 and as low as 0.2 in regions of maximum photochemical activity (Alexander *et al.*, 2009; Morin *et al.*, 2011).

By accounting for the origin of the oxygen atom transferred during the conversion of NO_2 to nitrate, the $\Delta^{17}O$ signature of the nitrate produced through different reaction mechanisms can be calculated. As previously discussed, NO_2 in the troposphere is converted to nitrate predominantly through the following processes:

$NO_2 + OH + M \rightarrow HNO_3 + M$ (R1.46)

$O_3 + NO_2 \rightarrow NO_3 + O_2$ (R1.47)

$NO_3 + DMS \rightarrow HNO_3 + products$ (R1.47b)

$NO_3 + NO_2 + M \leftrightarrow N_2O_5 + M$ (R1.48)

$N_2O_5 + H_2O_{(liquid)} \rightarrow 2HNO_{3\,(aq)}$ (R1.48b)

In order to predict the $\Delta^{17}O$ value of the nitrate produced through these processes using a simple isotope mass balance model, the isotopic composition of tropospheric O_3, H_2O, OH, and O_2 must be known. The $\delta^{17}O$ and $\delta^{18}O$ values of tropospheric H_2O can be assumed to possess a compact mass-dependent relationship ($\Delta^{17}O = 0$) (Zahn *et al.*, 2006). Furthermore, the OH radical participates in a rapid isotopic exchange with atmospheric water vapor and thus possesses negligible ^{17}O-excess under humidity and temperature conditions typical of most locations (Dubey *et al.*, 1997); therefore, the $\Delta^{17}O$ of the nitrate produced through the R1.46 channel is effectively diluted due to the addition of an oxygen atom with a $\Delta^{17}O$ equal to zero. The R1.47 reaction results in the transfer of an additional terminal oxygen atom from ozone to form a NO_3 radical with an increased $\Delta^{17}O$ value (Peìro-Garcìa and Nebot-Gil, 2003). In the R1.48 reaction, the bulk $\Delta^{17}O$ of the two HNO_3 molecules formed via N_2O_5 hydrolysis is ultimately diluted due to the incorporation of one oxygen atom inherited from water. Based on this reasoning, the specific $\Delta^{17}O$ signature induced by the R1-R3 channels can be computed as follows:

$$\Delta^{17}O(NO_3^-)_{R1.46} = \frac{2}{3}\alpha \times \Delta^{17}O(O_3^*) \quad (1.35)$$

$$\Delta^{17}O(NO_3^-)_{R1.47} = \frac{2}{3}\alpha \times \Delta^{17}O(O_3^*) + \frac{1}{3}\Delta^{17}O(O_3^*) \quad (1.36)$$

$$\Delta^{17}O(NO_3^-)_{R1.48} = \frac{1}{3}\alpha \times \Delta^{17}O(O_3^*) + \frac{1}{2}\left[\frac{2}{3}\alpha \times \Delta^{17}O(O_3^*) + \frac{1}{3}\Delta^{17}O(O_3^*)\right] \quad (1.37)$$

The bulk $\Delta^{17}O$ value of atmospheric nitrate can then be expressed as the sum of the $\Delta^{17}O$ signature of each channel multiplied by the fractional contribution from that channel in terms of total nitrate production:

$$\Delta^{17}O(NO_3^-) = \sum_i \frac{P_i}{P_{total}}\Delta^{17}O(NO_3^-)_i \quad (1.38)$$

where $\Delta^{17}O(NO_3^-)_i$ is the specific $\Delta^{17}O$ signature induced by the nitrate production channel P_i (R1.46 – R1.48).

From inspection of Equations 1.35 - 1.37, it is clear that $\Delta^{17}O(O_3^*)$ is a critical variable in the calculation of the $\Delta^{17}O(NO_3^-)_i$ values for the various nitrate production pathways. Due to the considerable amount of uncertainty regarding the $\Delta^{17}O$ value of tropospheric ozone and its potential spatial and temporal variability (see Section 1.2.3), in addition to the asymmetric distribution of ^{17}O-excess in the ozone molecule (see Section 1.2.2), choosing an appropriate value for $\Delta^{17}O(O_3^*)$ has always been a

matter of some debate. The $\Delta^{17}O$ value for bulk ozone is typically assumed to maintain an essentially constant value of 25 or 35 ‰, corresponding to $\Delta^{17}O(O_3^*)$ values of 38‰ and 53‰, respectively. Clearly, atmospheric $\Delta^{17}O(NO_3^-)$ measurements, which exhibit a natural variability of only ~10‰, cannot be useful in resolving atmospheric processes without quantitative constraints on $\Delta^{17}O(O_3^*)$ in the troposphere.

1.3.3.2 Modeling of $\Delta^{17}O(NO_3^-)$

Several model systems have been used to simulate atmospheric nitrate $\Delta^{17}O$ data. Atmospheric chemistry models are mostly driven by reaction kinetics: reaction rate constants (usually referred to as *k* values) and atmospheric concentration data are used to calculate the amount of nitrate produced by each major pathway (P_i). This output is then applied to Equation 1.38 in order to simulate $\Delta^{17}O(NO_3^-)$ dynamics. The first study utilized a box model for simulating nitrate production in La Jolla (Michalski *et al.*, 2003). There was reasonably good agreement between the observed $\Delta^{17}O(NO_3^-)$ observations and predicted values, but during the spring there were differences of up to 5‰, which was tentatively attributed to the model's inability to account for the transport of atmospheric nitrate from distant regions. However, the maximum $\Delta^{17}O(NO_3^-)$ values observed at La Jolla were largely consistent with the modeled shift from 50% homogeneous nitrate production (R1.46 and R1.47) in the spring to more than 90% production from N_2O_5 hydrolysis (R1.48) in the winter. This represented the first isotopic evidence of the dominant role played by nocturnal heterogeneous chemistry in nitrate production, which had long been expected from atmospheric modeling studies (Dentener and Crutzen, 1993).

In a subsequent study, Morin *et al.* (2008) measured the comprehensive isotopic composition of nitrate sampled at Alert, Canada (82.5°N) and used an atmospheric chemistry box model to compare the $\Delta^{17}O(NO_3^-)$ observations to modeled predictions for nitrate produced in winter and summer at middle (40 °N) and polar (80 °N) latitudes (**Figure 1.16**). For most of the year, the measured $\Delta^{17}O$ values were largely consistent with the model calculations; however, the samples collected during spring exhibited $\Delta^{17}O$ values as much as 10‰ higher than the model-calculated values. Morin *et al.* (2008) interpreted this disagreement between the measured and modeled values as a result of the participation of reactive bromine in the atmospheric NO_x cycle during the spring months. Bromine oxide (BrO) can reach high concentrations

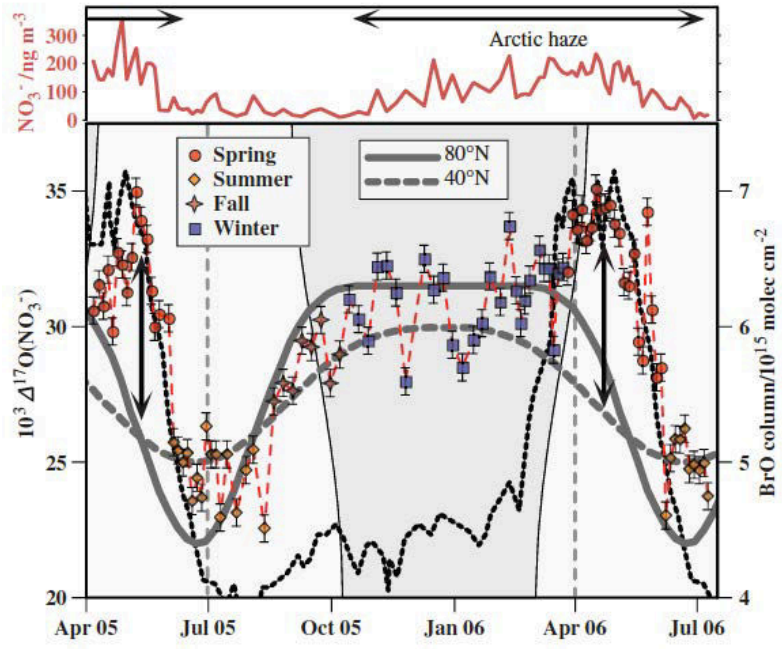

FIGURE 1.16 - Seasonal cycle of the concentration and $\Delta^{17}O$ of atmospheric nitrate from aerosol samples collected at Alert, Canada. The black dashed line represents a satellite-retrieved column of BrO north of 70°N. Thick broken and solid gray lines correspond to the $\Delta^{17}O$ value calculated for atmospheric nitrate formed at 40 °N and 80 °N, respectively. The black vertical arrows indicate the strong deviation from these seasonal cycles in spring, due to the interaction of BrO with snowpack-emitted NO_x. The vertical dotted lines indicate the periods of snowpack NO_x emissions from April to June (Morin *et al.*, 2008).

in the boundary layer during polar sunrise in association with "bromine explosions," an autocatalytic mechanism that enhances the release of gas-phase bromine from sea salt aerosols (Barrie *et al.*, 1988). BrO is produced through the reaction of Br with ozone, a pathway that plays an important role in the catalytic process responsible for ozone depletion events (ODEs) observed in the Arctic since the 1980s (Fan and Jacob, 1992):

$$Br + O_3 \rightarrow BrO + O_2 \qquad (R1.49)$$

The presence of reactive halogen radicals such as BrO in the boundary layer has a profound influence on the oxidative capacity of the atmosphere during Arctic springtime (Simpson *et al.*, 2007). In terms of the chemical budget of NO_x and the isotopic signature of nitrate, the impact of BrO can occur via two chemical mechanisms. First, BrO can oxidize NO to NO_2, a pathway that competes with the $NO + O_3$ and $NO + HO_2/RO_2$ reactions in terms of NO oxidation:

$$BrO + NO \rightarrow Br + NO_2 \qquad (R1.50)$$

For conditions typical of the Arctic boundary layer, 1 ppt of BrO has roughly the same oxidizing power as 2 - 4 ppb of ozone in terms of the NO oxidation (Atkinson *et al.*, 1997). This difference in reaction kinetics is accentuated during ODEs when the

ozone mixing ratio drops to only a few ppb and BrO levels can reach levels of over 10 ppt. Furthermore, an increasing body of evidence points towards reactive bromine chemistry as a major NO_x sink and source of nitrate via the production and subsequent hydrolysis of $BrNO_3$ (Vogt *et al.*, 1996; Sander *et al.*, 1999):

$$BrO + NO_2 + M \rightarrow BrNO_3 + M \quad \text{(R1.51)}$$

$$BrNO_3 + H_2O_{(liquid)} \rightarrow HNO_3 + HOBr \quad \text{(R1.52)}$$

The interaction of bromine in the NO_x cycle has important implications for the $\Delta^{17}O$ of atmospheric nitrate in polar regions. BrO is exclusively formed by R1.49, which proceeds through a direct transfer of a terminal oxygen atom from ozone to the BrO product (Zhang *et al.*, 1997). Therefore, it is expected that the $\Delta^{17}O$ of BrO is equal to $\Delta^{17}O(O_3^*)$. Experimental (Gane *et al.*, 2001) and theoretical (McNamara and Hillier, 2001) studies of $BrNO_3$ hydrolysis show that the oxygen atom initially associated with BrO combines with the N atom of NO_2 to form nitrate, thus transferring the isotopic signature of both BrO and NO_2. The specific $\Delta^{17}O$ signature induced by $BrNO_3$ hydrolysis can thus be expressed as follows (Morin *et al.*, 2007b):

$$\Delta^{17}O(NO_3^-)_{R1.52} = \frac{2}{3}\alpha \times \Delta^{17}O(O_3^*) + \frac{1}{3}\Delta^{17}O(O_3^*) \quad (1.39)$$

As can be seen from Equation 1.39, the $\Delta^{17}O$ value of nitrate produced via R1.52 will be significantly higher than that produced through the OH + NO_2 pathway (R1.46), which is typically expected to be the dominant formation channel during polar sunrise. Assuming $\Delta^{17}O(O_3^*) = 40‰$ and $\alpha = 0.80$, the $\Delta^{17}O$ signatures of the R1.46 and R1.52 channels are 21‰ and 35‰, respectively. The large difference in $\Delta^{17}O$ transfer between these two reactions was invoked by Morin *et al.* (2008) to explain the discrepancy between modeled and measured values at Alert (**Figure 1.16**), as the modeling treatment used in this study did not include bromine chemistry and only $BrNO_3$ hydrolysis is capable of producing $\Delta^{17}O(NO_3^-)$ values that are quantitatively consistent with the measurements. Therefore, the major conclusion of this study was that the hydrolysis of $BrNO_3$ represents the dominant source of nitrate in the Arctic troposphere during polar sunrise, an assertion that is in agreement with modeling studies (Calvert and Lindberg, 2003; Evans *et al.*, 2003). The study of Morin *et al.* (2008) provides an excellent example of the manner in which nitrate isotope analysis can be combined with traditional concentration measurements and numerical modeling to assess the relative activities of the different processes contributing to the NO_x cycle.

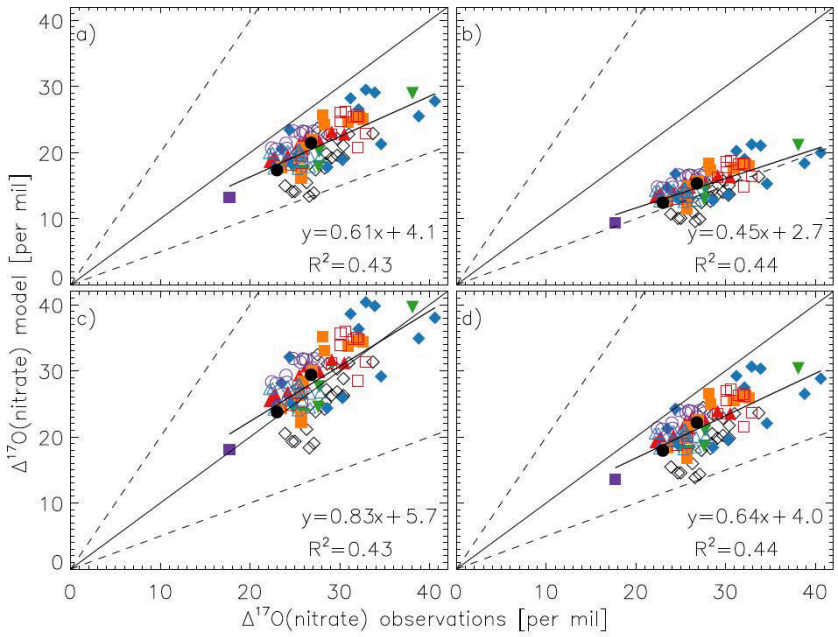

FIGURE 1.17 - Scatter plot of monthly-mean model calculations at the surface versus observations reported in the literature (see Section 1.2.2). Each panel uses different assumptions regarding $\Delta^{17}O(O_3^*)$, the ^{17}O-excess of ozone transferred via oxidations reactions in the atmosphere: 25‰ (a), 35‰ (b), 36‰ (c), and 48‰ (d). The linear least-squares regression (thick), y = x (solid), y = 2x, and y = 0.5x (dashed) lines are shown. Inset is the regression equation and r^2 values.

In a major development in the interpretation of the ^{17}O-excess of atmospheric nitrate, the $\Delta^{17}O(NO_3^-)$ tracer was recently implemented into the global 3-D chemical transport model GEOS-Chem by Alexander *et al.* (2009). This model uses the same fundamental mass balance approach described above, but the GEOS-Chem model includes a treatment of vertical and horizontal transport and incorporates spatial variations in surface fluxes of important primary pollutants such as NO_x and VOCs, which gives it a distinct advantage over the box model approach. However, as revealed in preliminary sensitivity studies, the unconstrained nature of $\Delta^{17}O(O_3^*)$ poses a major barrier to the robust interpretation of differences between measured and modeled $\Delta^{17}O(NO_3^-)$ values. Alexander *et al.* (2009) simulated nitrate $\Delta^{17}O$ dynamics using four different values of $\Delta^{17}O(O_3^*)$ (25‰, 35‰, 36‰, and 48‰) and compared the output to the existing literature data (**Figure 1.17**). The best agreement between measured and calculated $\Delta^{17}O(NO_3^-)$ values was found for the model simulation using 48‰ for $\Delta^{17}O(O_3^*)$, while other $\Delta^{17}O(O_3^*)$ values yielded predicted $\Delta^{17}O(NO_3^-)$ values that were 20 - 50% lower than the observations. However, as pointed out by Alexander *et al.* (2009), this is not unambiguous evidence for the true value of $\Delta^{17}O(O_3^*)$; for example, if $\Delta^{17}O(O_3^*)$ is in fact equal to 25‰, then the observation that $\Delta^{17}O(O_3^*)$ = 48‰ provides the best agreement between observed and modeled

$\Delta^{17}O(NO_3^-)$ values may indicate that the model systematically underestimates the mixing ratios of ozone or the relative importance of the nocturnal oxidation processes involving the NO_3 radical and N_2O_5 (Brown *et al.*, 2006; Osthoff *et al.*, 2009); conversely, it is possible that OH and/or peroxy radical concentrations or reaction kinetics are overestimated (Mollner *et al.*, 2010). The utility of $\Delta^{17}O(O_3^*)$ as a quantitative tracer of atmospheric chemistry is contingent upon a precise and accurate knowledge of its magnitude and the extent of its natural spatial and temporal variability, which is currently lacking (see Section 1.2.3). The atmospheric geochemistry community thus desperately needs reliable measurements of $\Delta^{17}O(O_3^*)$ in a variety of atmospheric environments in order to resolve such issues. Only at this cost may the transfer $\Delta^{17}O(O_3^*)$ be considered in a sound manner by larger-scale model implementations to simulate global and seasonal variations of $\Delta^{17}O(NO_3^-)$. Clearly, a better understanding of the seasonal and spatial features of $\Delta^{17}O(O_3^*)$ should be a priority of future research.

In addition to the uncertainty regarding the $\Delta^{17}O$ value transferred from ozone, the simulations described by Alexander *et al.* (2009) included no reactive halogen scheme, a reaction mechanism that has only recently been implemented into GEOS-Chem (Parrella *et al.*, 2012). As described above in regards to the Morin *et al.* (2009) study, bromine chemistry can induce high $\Delta^{17}O$ values in nitrate, thus leading to a disagreement between measurements and predictions based on modeling. Similar to Morin *et al.* (2007b, 2008), Alexander *et al.* (2009) observed large discrepancies between modeled values and observations in polar regions during spring and summer (up to 5‰ underestimate), which were hypothesized to result from the absence of reactive bromine chemistry in the model. It is worth noting that, due to the preponderance of studies conducted at polar sampling sites (see Section 1.2.2), these data seem to be over-represented in the model-measurement comparison shown in **Figure 1.17**, which could cause a bias when extrapolating interpretations based on the current observational dataset to the global scale.

The output of simulations conducted in GEOS-Chem using a $\Delta^{17}O(O_3^*)$ value of 48‰ are presented in **Figure 1.18**, which shows the average $\Delta^{17}O(NO_3^-)$ calculated for 0 - 200 meters above the surface during summer (June-July-August) and winter (December-January-February). Globally, $\Delta^{17}O(NO_3^-)$ values range from a low of ~7‰ up to a maximum of 41‰ and exhibit a seasonal variation similar to that observed by Michalski *et al.* (2003) and Morin *et al.* (2008). The largest values occur in the winter

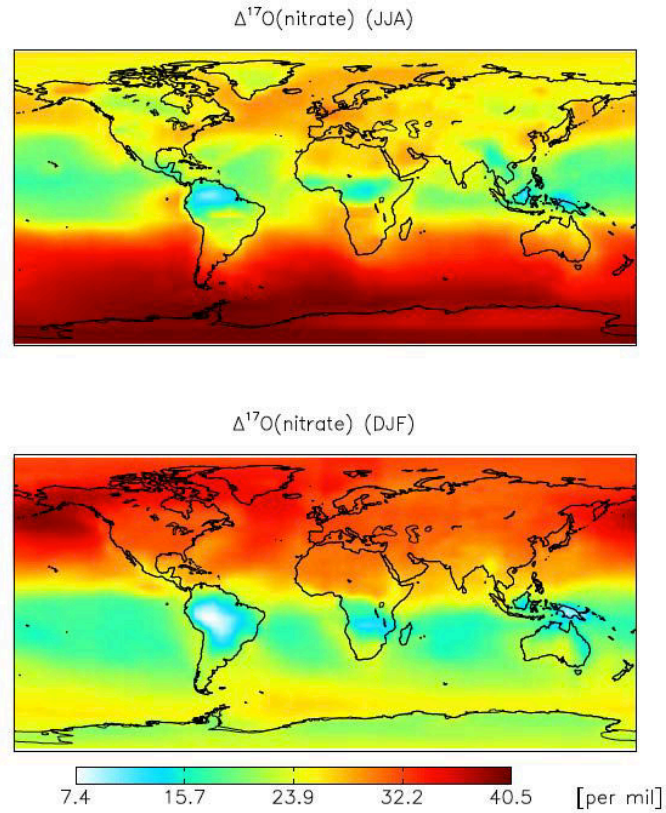

FIGURE 1.18 - June-July-August (top) and December-January-February (bottom) average $\Delta^{17}O(NO_3^-)$ values calculated by the global atmospheric chemistry model GEOS-Chem for 0–200m above the surface (Alexander *et al.*, 2009).

hemisphere high-latitudes. Alexander *et al.* (2009) demonstrated that these maximum values are attributable to the increased importance of ozone in nitrate formation via nocturnal oxidation processes (i.e., R1.47 and R1.48). The N_2O_5 hydrolysis pathway is limited by temperature due to the thermal decomposition of N_2O_5 to NO_2 and NO_3 (i.e., the R1.48 equilibrium favors N_2O_5 at cold temperatures). This reaction is therefore favored in the high latitude during winter when it is cold and dark and N_2O_5 possesses a longer lifetime against decomposition. The smallest modeled values of $\Delta^{17}O(O_3^*)$ occur in response to increased actinic flux in the summer hemisphere and in the tropics. This effect arises from the strong decrease in α that accompanies increased sunlight via increased production of peroxy radicals, as well as from the higher relative formation of nitrate via the OH + NO_2 pathway during periods of maximum photochemical radical production. The minimum values of ~7‰ are predicted for tropical forest region, where VOC emissions and actinic flux are high, resulting in minimum α values of ~0.1.

1.3.4 Nitrogen stable isotopes in the NO_x-nitrate system

The simultaneous measurement of the nitrogen isotopic composition ($^{15}N/^{14}N$) of nitrate can often complement and enhance the interpretation of $\Delta^{17}O(NO_3^-)$ measurements, which will be demonstrated several times in the chapters that follow. Variations in the $\delta^{15}N$ of atmospheric nitrate could plausibly be attributed to four different causes: (i) variations in the $\delta^{15}N$ value of the NO_x emission, or the "source signature;" (ii) partitioning of ^{15}N between NO and NO_2; (iii) isotopic fractionations associated with the conversion of NO_x to nitrate; or (iv) isotopic effects occurring during the transport of nitrate in the atmosphere (e.g., deposition, gas-particle partitioning of HNO_3, etc.) (Morin, 2008; Morin *et al.*, 2009). There remains a great deal of uncertainty regarding the potential quantitative impacts of these processes. Isotopic fractionations associated with the atmospheric NO_x cycle have been proposed, e.g., by Freyer (1991) and Freyer *et al.* (1993); however, there is very little experimental or observational evidence that supports these assertions. Isotopic fractionation during atmospheric transport is typically thought to be negligible due to the relatively short lifetime of nitrate against wet and dry deposition; therefore, it is often assumed in the literature that the $\delta^{15}N$ value of NO_x is conserved from source to sink and natural spatial and temporal variations in the $\delta^{15}N$ of atmospheric nitrate are thus typically attributed to NO_x source variability (Kendall *et al.*, 2007). In Chapter 4, we will see an example of an equilibrium isotope exchange process that can influence the distribution of $\delta^{15}N$ within the NO_x-nitrate system; however, in this introductory section, we will consider variations in $\delta^{15}N$ only as they relate to the nitrogen isotope composition of NO_x sources.

The framework commonly applied in the interpretation of atmospheric $\delta^{15}N(NO_3^-)$ values can be generalized as follows: anthropogenic NO_x emissions resulting from fuel combustion are enriched relative to atmospheric N_2. Therefore, positive $\delta^{15}N$ values in atmospheric nitrate are often taken to represent a combustion source signal (**Figure 1.19**). For example, Elliott *et al.* (2009) observed a strong spatial correlation between the $\delta^{15}N$ of nitrate in atmospheric dry deposition, which averaged 3.2‰, and the magnitude of NO_x emissions from stationary sources (e.g., power plants) in the eastern U.S.; in another study, Fang *et al* (2011) used $\delta^{15}N$ measurements of precipitation nitrate, which averaged 3.6‰ over a two-year period, to estimate the relative contributions of nitrate originating from fossil fuel NO_x emissions at an

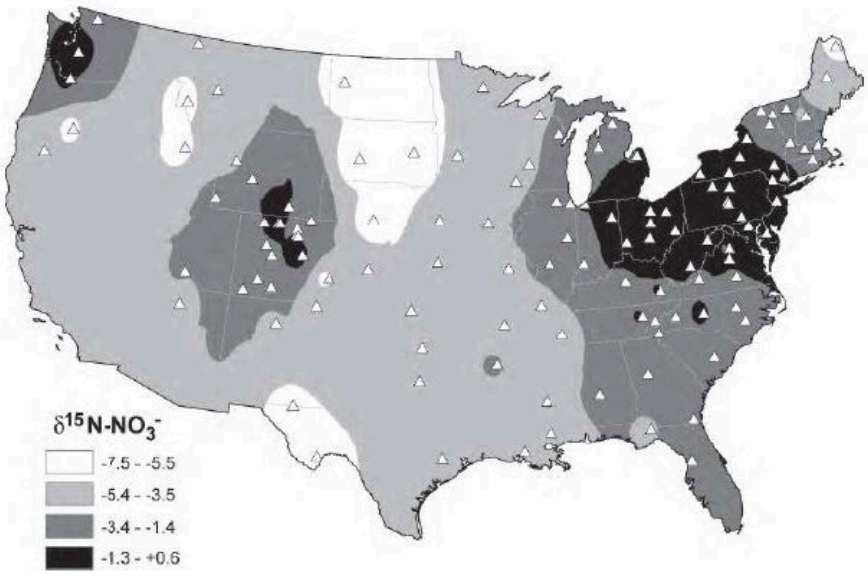

FIGURE 1.19 - Spatial variability in the average $\delta^{15}N(NO_3^-)$ of precipitation collected at National Atmospheric Deposition Program (NADP) sites in the USA in 2000. A strong correlation ($r^2 = 0.51$, $p < 0.001$) exists between precipitation $\delta^{15}N(NO_3^-)$ and NO_x emissions from power plants within 400 miles of individual NADP sites (Kendall *et al.*, 2007).

industrialized site in China. Lower atmospheric $\delta^{15}N(NO_3^-)$ values, such as those reported by Baker *et al.* (2007) and Morin *et al.* (2009) for the remote Atlantic MBL (-6 – 0 ‰), are generally assumed to indicate a mostly natural background NO_x source, such as emission from soils ($\delta^{15}N < -20$ ‰) (Freyer, 1991) or production during lighting strikes ($\delta^{15}N \sim 0$) (Hoering, 1957).

Despite the apparent simplicity of this approach, it should be noted that there exists some debate in the literature regarding the $\delta^{15}N$ value of fuel-derived NO_x emissions. There are two main classes of combustion-related NO_x emissions: "fuel" NO_x, which is produced directly through the release and subsequent oxidation of fuel-bound nitrogen, and "thermal" NO_x, which is produced via high-temperature oxidation of O_2 and N_2 gas in combustion air. These two classes of NO_x are known to possess different $\delta^{15}N$ signatures. The production of anthropogenic NO_x proceeds through both of these processes and their relative importance determines the $\delta^{15}N$ of the NO_x produced. Coal-fired energy production is well known to result in positive $\delta^{15}N(NO_x)$ values (Elliott *et al.*, 2007; Felix *et al.*, 2012); however, there is some indication that the $\delta^{15}N$ signature of NO_x derived from transport fuel combustion is negative and can induce negative $\delta^{15}N(NO_3^-)$ values in the atmosphere (Hastings *et al.*, 2003; 2009; Widory, 2007).

As can be seen from the preceding discussion, the $\delta^{15}N$ signatures of the various natural and anthropogenic NO_x sources typically exhibit overlapping ranges (e.g., thermal and fuel NO_x), often making $\delta^{15}N(NO_3^-)$ measurements difficult to rationalize within the common interpretive framework. However, the photolysis of snowpack nitrate in polar environments has been found to lead the formation of NO_x with a very unique nitrogen isotopic composition. The ^{15}N isotopic effect associated with snow photodenitrification is large, with a fractionation factor (ε) on the order of –54‰ in central Antarctica (Blunier *et al.*, 2005), leading to elevated $\delta^{15}N$ values in nitrate remaining in the snow and, as a consequence of mass conservation, depleted $\delta^{15}N$ values in the emitted species ($\delta^{15}N < -40‰$) (Frey *et al.*, 2009). Nitrate snow photochemistry in both the Greenland and Antarctic ice sheets (Honrath *et al.*, 1999; Davis *et al.*, 2001), results in strong fluxes of NO_x from the surface snow into the boundary layer where it has been shown to influence oxidation capacity via interaction in photochemical ozone production (Crawford *et al.*, 2001) and destruction cycles (Thomas *et al.*, 2012). The singular $\delta^{15}N$ source marker for snowpack NO_x emissions, when measured in conjunction with nitrate $\delta^{17}O$ and $\delta^{18}O$ values, has proven useful in evaluating the chemical connection between emissions of NO_x from the snowpack and the processes leading to the re-oxidation of these emissions in the polar atmosphere (Savarino *et al.*, 2007; Morin *et al.*, 2007a; 2008; 2012).

The strong ^{15}N fractionation associated with the photolysis of nitrate in snow has important implications for the interpretation of $\delta^{15}N(NO_3^-)$ measurements obtained from polar ice cores, particularly at low snow accumulation sites. Nitrate concentration profiles in ice cores have long been thought to preserve information regarding atmospheric NO_x source and sink variations and changes in the oxidative capacity of ancient atmospheres (Legrand *et al.*, 1988; Mayewski and Legrand, 1990; Dibb *et al.*, 1998; Legrand *et al.*, 1999). However, the interpretation of deep ice core nitrate records is not straightforward, as the photolysis and volatilization of nitrate in the snowpack results in the loss of nitrate mass and thus the amount of nitrate preserved in the ice may not directly reflect atmospheric concentrations of NO_x (Röthlisberger *et al.*, 2000; 2002). However, the stable isotope ratios of nitrate ($\delta^{17}O$, $\delta^{18}O$, $\delta^{15}N$) are also impacted by these processes, which allows for an assessment of the degree to which post-depositional loss and recycling has altered records of ice core nitrate (Freyer *et al.*, 1996; Jarvis *et al.*, 2008). Furthermore, ice core measurements of the ^{17}O-excess of nitrate have recently shown promise for

diagnosing past changes in atmospheric oxidation chemistry, as this unique isotopic signature is largely conserved during snowpack burial (Alexander *et al.*, 2004; McCabe *et al.*, 2005; Savarino *et al.*, 2007; Erbland, 2012). A major goal of Chapter 5 is to examine the atmospheric controls on the isotopic composition of nitrate preserved in polar ice, which will aid in our interpretation of past changes in ice nitrate and contribute to our understanding of present and future changes in the atmospheric NO_x cycle.

1.4 This thesis

In this introduction, an overview of the current state of knowledge regarding the anomalous isotopic composition of ozone and its propagation to nitrate in the atmosphere has been presented. The unique ^{17}O-excess signature of nitrate could greatly contribute to our quantitative understanding of the atmospheric reactive nitrogen (NO_x) cycle. However, there exist large uncertainties in our understanding of many key issues. Foremost, constraints on the isotopic composition of ozone are clearly necessary in order to derive quantitative information regarding atmospheric chemistry from $\Delta^{17}O$ measurements of nitrate. Furthermore, the atmospheric processes responsible for the transfer of $\Delta^{17}O$ to nitrate and their overall influence on nitrate isotopic composition on different spatial and temporal scales are not well understood. In this thesis, several questions related to these issues are addressed. The focus will be primarily on the following:

- Can the aqueous-phase reaction of ozone with nitrite (NO_2^-) be applied as a chemical probe for measuring $\Delta^{17}O(O_3)$ in ambient air?
- What is the transferrable $\Delta^{17}O$ signature of ozone in the troposphere and how does it vary over different spatial and temporal scales?
- Does the isotopic composition of nitrate exhibit diurnal variability analogous to its large-scale seasonal trend?
- How is the complex oxidation chemistry resulting from snow photo-denitrification reflected in the isotopic composition of nitrate in the surface snow and atmosphere of the Antarctic plateau?

The primary analytical tool used to address these questions was the bacterial denitrifier method, which allows for the comprehensive isotopic analysis of nitrate

(i.e., the simultaneous measurement of all its stable isotope ratios: $^{17}O/^{16}O$, $^{18}O/^{16}O$, and $^{15}N/^{14}N$). In this method, nitrate is converted via bacterial reduction to N_2O, which is then thermally decomposed to O_2 and N_2, followed by isotope ratio mass spectrometry (IRMS), as described by Kaiser *et al.* (2007) and Morin *et al.* (2009). This method was applied not only to the analysis of environmental nitrate samples (i.e., aerosol and snow), but also to the isotopic characterization of ozone via chemical conversion of its terminal oxygen atoms to nitrate. A large dataset of tropospheric $\Delta^{17}O(O_3)$ measurements is presented, including a full annual record from Grenoble, France (45 °N) and a ship-based latitudinal profile from 50 °S to 50 °N. This observational dataset represents a two-fold increase in the number of existing tropospheric $\Delta^{17}O(O_3)$ observations and a dramatic expansion in the global representation of this key isotopic entity. Additionally, two detailed case studies are presented in this thesis. These studies reveal novel and often unexpected aspects of the isotope dynamics of atmospheric nitrate, with potentially important implications for air quality modeling and the interpretation of isotopic information preserved in the polar ice core record.

Chapter 2: Measurement of the ^{17}O-excess ($\Delta^{17}O$) of tropospheric ozone using a nitrite-coated filter

In Chapter 2, we report observations that validate and inform the use of a nitrite-coated filter for determining the $\Delta^{17}O$ of the transferrable oxygen atom of tropospheric ozone via chemical trapping as nitrate. This method is inexpensive and easy to implement in nearly any environment; furthermore, it does not involve the cumbersome and logistically challenging collection technology utilized in prior studies of tropospheric ozone isotopes. However, despite the simplicity of the collection technique, several analytical obstacles are associated with this approach. Most significantly, the nitrite reagent used to trap ozone will invariably possess a certain level of background nitrate contamination, which must be accounted for in the calibration of samples. This involves not only a meticulous application of the "identical treatment principle," but also necessitates the combined measurement of the nitrogen isotopic composition ($\delta^{15}N$) of the nitrate formed on the sampling substrate, which provides a tracer for the efficacy of the calibration. The sample collection, post-treatment, analysis, and calibration/blank-correction procedures are described in

detail in this chapter. Other important method validation issues, such as ozone collection efficiency and sampling interferences are also addressed. Furthermore, the transfer function relating the $\Delta^{17}O$ of bulk ozone to that of the oxygen atom transferred to nitrate has been established through a series of tests using experimental ozone produced under various temperature and pressure regimes. The results obtained in these various preliminary studies indicate that, while it calls for great care in its use, the nitrite-coated filter method is sufficiently robust and reliable to be applied as a probe for assessing variations in the $\Delta^{17}O$ of tropospheric ozone.

Chapter 3: Quantitative constraints on the ^{17}O-excess ($\Delta^{17}O$) signature of surface ozone: Ambient measurements from 75°S to 50°N

In Chapter 3, we describe a systematic investigation of the spatial and temporal features of the $\Delta^{17}O$ of tropospheric ozone conducted using the methodological approach developed in Chapter 2. Measurements reported here include: (i) a full annual record from Grenoble, France (45 °N) (n = 71); (ii) a latitudinal record from 50 °S to 50 °N in the Atlantic Ocean (n = 30); and (iii) a four-week record from Dome C, Antarctica (75 °S) during polar summer (n = 28). The collection of samples over such a wide range of atmospheric settings (i.e., polluted urban, remote marine, polar) has allowed for a comprehensive assessment of the magnitude of natural variability in $\Delta^{17}O(O_3)$, specifically with regards to the hypothesis of its sensitivity to ozone production and loss mechanisms in various atmospheric contexts. The observational record described in this chapter, 139 samples in total, represents a dataset roughly the same size as that obtained using the cryogenic collection technique in the 1990s (Krankowsky *et al.*, 1995; Johnston and Thiemens, 1997). The cryogenic and nitrite-coated filter datasets are compared in terms of both $\delta^{18}O$ and $\Delta^{17}O$.

Chapter 4: Spatial and diurnal variability in nitrogen oxide chemistry as reflected in the isotopic composition of atmospheric nitrate: Results from the CalNex 2010 field study

Interpretations derived from nitrate isotope ratio measurements have been useful in the analysis of seasonal atmospheric trends in NO_x cycling. However, isotopic effects associated with atmospheric processes occurring on smaller temporal and spatial

scales (e.g., diurnal variations in atmospheric chemistry, meso-scale meteorological phenomena, etc.) are presently not well constrained. In Chapter 4, we present measurements of the size-resolved concentration and isotopic composition of atmospheric nitrate from samples collected onboard the R/V *Atlantis* during a cruise along the coast of California. This research cruise was organized as a component of the CalNex 2010 field study, a major multiagency campaign focusing on the atmospheric processes determining air quality over California and the eastern Pacific coastal region. One explicit goal of this campaign was to assess the importance of nocturnal oxidation pathways in determining the loss of NO_x, volatile organic carbon (VOC), and ozone. The processes and rates by which primary emissions are transformed within the atmosphere during the night is in an area of significant uncertainty and it is unclear to what extent current regional models accurately represent these processes and their effect on air quality. Aerosol sampling was conducted on a 12-hour frequency for much of the cruise, allowing for direct daytime/nighttime comparisons and providing an opportunity to extract quantitative information regarding the temporal evolution of nitrate stable isotope ratios. Furthermore, samples were collected under two distinct transport regimes, allowing for an evaluation of the differences in NO_x transformation pathways occurring in air masses of marine and continental origin. This study, to the best of our knowledge the first of its kind, represents a significant advance in our understanding of the factors controlling the isotopic composition of atmospheric nitrate.

Chapter 5: Nitrogen and oxygen isotope dynamics of nitrate in the surface snow and boundary layer of the East Antarctic plateau

Constraining the propagation of ozone's ^{17}O-excess signature within the NO_x cycle is critical in polar areas where there exists the possibility of extending atmospheric interpretations based on $\Delta^{17}O$ measurements to the glacial/interglacial time scale using deep ice core records of nitrate. However, the factors governing the isotopic composition of nitrate in the polar troposphere remain poorly understood, primarily due to the complex nature of the boundary layer photochemistry initiated during spring by NO_x emissions from the snowpack. Furthermore, significant uncertainty exists regarding the air-snow transfer of nitrate and the overall impact of post-depositional processes that alter the concentration and isotope ratios of nitrate both in

the atmosphere and in the snowpack. In Chapter 5, we describe the results of a field campaign organized to investigate these air/snow dynamics at Dome C, Antarctica, where we have measured the nitrogen ($\delta^{15}N$) and triple-oxygen ($\delta^{17}O$ and $\delta^{18}O$) isotope composition of nitrate year-round in both the atmosphere and in the snow "skin layer" (surface 3-4 mm) during 2009 - 2010. This dataset is further complimented by additional atmospheric nitrate samples conducted during November 2011 - January 2012 within the framework of the OPALE (Oxidant Production over Antarctic Land and its Export) project, which has provided an opportunity to combine nitrate isotopic observations with a wealth of meteorological and chemical data, including *in-situ* concentration measurements of the gas-phase precursors involved in nitrate production (NO_x, O_3, OH, HO_2, etc.). The primary goals of this study were: (i) to characterize the annual evolution of atmospheric nitrate concentration and isotopic composition at Dome C with regards to seasonal variations in NO_x sources and sinks; (ii) to establish the air-snow transfer function of nitrate stable isotope ratios and investigate the seasonal dynamics of the isotopic equilibrium at the air-snow interface; and (iii) to reconcile observations of $\Delta^{17}O$ for atmospheric nitrate at Dome C with quantitative predictions based on nitrate isotope mass balance and atmospheric chemistry parameters. Our results indicate a set of unique and highly complex isotopic dynamics, characterized by injections of stratospheric nitrate in the winter followed by the rapid photolytic recycling of nitrate at the air-snow interface in spring. The photoproducts of nitrate photolysis initiate a complex cycling of NO_x, HO_x, and O_x, which imparts an unexpectedly high level of ^{17}O-excess transfer to nitrate. Further information on the connection between snow photochemistry and nitrate production on the Antarctic plateau is critical to the development of ice-core proxies of paleo-oxidation chemistry based on the ^{17}O-excess of nitrate.

In the final chapter, we provide an overview of the results reported and highlight the key conclusions and implications. This thesis then closes with a consideration of the most significant gaps remaining in our understanding of the isotopic composition of ozone and its transfer to nitrate in the atmosphere.

Chapter 2

Measurement of the ^{17}O-excess (Δ^{17}O) of tropospheric ozone using a nitrite-coated filter

---

This chapter is based on:

Vicars, W. C., Bhattacharya, S. K., Erbland, J., and Savarino, J., **2012**. Measurement of the ^{17}O-excess (Δ^{17}O) of tropospheric ozone using a nitrite-coated filter. *Rapid Communications in Mass Spectrometry*, 26, 1219-1231.

Vicars, W. C. and Savarino, J., The role of combined ^{15}N/^{14}N measurements in the nitrite-coated filter method. *Rapid Communications in Mass Spectrometry* **(to be submitted)**.

Abstract

The ^{17}O-excess (Δ^{17}O) of tropospheric ozone (O_3) serves as a useful marker in studies of atmospheric oxidation pathways; however, due to the complexity and expense of currently available analytical techniques, no systematic sampling campaign has yet been undertaken and natural variations in $\Delta^{17}O(O_3)$ are therefore not well constrained. The nitrite (NO_2^-)-coated filter method is a new technique for ozone isotope analysis that employs the aqueous phase $NO_2^- + O_3 \rightarrow NO_3^- + O_2$ reaction to obtain quantitative information on ozone via the oxygen atom transfer to nitrate (NO_3^-). The triple-oxygen isotope analysis of the nitrate produced during this reaction, achieved in this study using the bacterial denitrifier method followed by continuous-flow isotope-ratio mass spectrometry (CF-IRMS), directly yields the Δ^{17}O value transferred from ozone. This isotope transfer process was investigated in a series of vacuum-line experiments, which were conducted by exposing coated filters to ozone of various known Δ^{17}O values and then determining the isotopic composition of the nitrate produced on the filter. The isotope transfer experiments reveal a strong linear correlation between the Δ^{17}O of the ozone produced and that of the oxygen atom

transferred to nitrate, with a slope of 1.55 for samples with bulk $\Delta^{17}O(O_3)$ values in the atmospheric range (20 - 40‰). This finding is in agreement with theoretical postulates that place the ^{17}O-excess on only the terminal oxygen atoms of ozone. Ambient measurements yield average $\Delta^{17}O(O_3)_{bulk}$ values in agreement with previous studies (23 ± 2‰). The nitrite-coated filter technique is a sufficiently robust, field deployable method for the determination of the triple-oxygen isotopic composition of tropospheric ozone. Further ambient measurements will undoubtedly lead to an improved quantitative view of natural $\Delta^{17}O(O_3)$ variation and transfer in the atmosphere.

2.1 Introduction

Ozone (O_3) is a key constituent of the troposphere, where it functions not only as an important greenhouse gas and anthropogenic pollutant, but also as a central participant in several important chemical processes. Most significantly, ozone and its photochemical counterpart, the hydroxyl radical (OH), largely determine the oxidizing capacity of the atmosphere and consequently the lifetimes and oxidation pathways of most reduced trace gases. Thus, through its interactions with other atmospheric species, ozone exerts a profound influence on the chemical composition of the troposphere (Monks, 2005).

Recently, there has been considerable interest in using oxygen isotopes found in various atmospheric compounds as an interpretive tool to quantify and constrain the rates of atmospheric processes (Brenninkmeijer *et al.*, 2003). The unique and distinctive ^{17}O-excess ($\Delta^{17}O$) of ozone, also referred to as the oxygen isotope "anomaly" of ozone, has proved to be a particularly useful isotopic fingerprint in such studies. The anomalous oxygen isotopic composition of ozone arises due to mass-independent fractionation (MIF) occurring during its formation in the atmosphere and results in isotopic enrichments that do not appear to scale with relative mass difference (Thiemens, 2006). For oxygen, this enrichment is defined as the excess in ^{17}O over what is expected based on the abundance of ^{18}O (we define this quantity in the present paper in its linearized form as follows: $\Delta^{17}O = \delta^{17}O - 0.52 \times \delta^{18}O$). The $\Delta^{17}O$ signature of ozone is transferred through oxidation reactions to other oxygen bearing compounds such that the $\Delta^{17}O$ of atmospheric species acts as a marker of the

influence of ozone in their chemical formation (Lyons, 2001). This isotopic fingerprint, although it is subject to dilution, cannot be removed or altered via subsequent mass-dependent fractionation processes and is thus conserved during atmospheric transport and processing (Mauersberger *et al.*, 2003). The ^{17}O-excess of ozone thus provides a useful tracer of atmospheric oxidation pathways and, since it's discovery in the early 1980s (Heidenreich and Thiemens, 1983; Thiemens and Heidenreich, 1983), numerous techniques have been developed in the field of isotope ratio mass spectrometry (IRMS) for the measurement of ^{17}O-excess in a wide range of atmospheric trace species. These developments have yielded valuable insight into the atmospheric chemistry of nitrate (Michalski *et al.*, 2003; Morin *et al.*, 2008), sulfate (Alexander *et al.*, 2002; Savarino *et al.*, 2003), CO_2 (Yung *et al.*, 1997; Boering *et al.*, 2004), N_2O (Röckmann *et al.*, 2001; Kaiser *et al.*, 2004), and carbonate (Shaheen *et al.*, 2010). Furthermore, variations in the Δ^{17}O of atmospherically-derived species preserved in ice cores and ancient sediments may serve as a useful proxies for paleo-oxidation chemistry, providing a means for the extension of these atmospheric interpretations into the past (Bao *et al.*, 2000; Alexander *et al.*, 2003; McCabe *et al.*, 2007).

Although there have been numerous tropospheric studies which report Δ^{17}O values for various oxygen bearing compounds carrying the anomalous isotopic signature inherited from ozone, there are presently very few published observations of Δ^{17}O for tropospheric ozone itself. Isotopic analysis of tropospheric ozone is particularly challenging due to its high volatility and low concentration (ppb level), as well as the high O_2/O_3 ratio found in the troposphere, which complicates the collection and isotopic analysis of ozone samples. To the best of our knowledge, only two studies report measurements of the comprehensive oxygen isotopic composition of ozone in the troposphere (Krankowsky *et al.*, 1995; Johnston and Thiemens, 1997). These initial studies featured fairly complex experimental designs and cumbersome sampling techniques based on the cryogenic trapping of ozone with liquid helium, followed directly by introduction into a mass spectrometer (Stehr *et al.*, 1996). The expense and logistical complexity of the cryogenic method has precluded any systematic sampling campaign, and potentially interesting field locations (e.g., marine, alpine and polar sites) have not been investigated. Furthermore, the data obtained using the cryogenic method may suffer from systematic errors due to

interference from atmospheric xenon, which condenses concurrently with ozone (Brenninkmeijer *et al.*, 2003; Mauersberger *et al.*, 2003; Morin *et al.*, 2007).

The paucity of information concerning the $\Delta^{17}O$ of tropospheric ozone remains a major barrier to the interpretation of $\Delta^{17}O$ measurements for other atmospheric species. For example, computational modeling of the ^{17}O-excess of nitrate could greatly contribute to our quantitative understanding of the atmospheric reactive nitrogen ($NO_x = NO + NO_2$) cycle, and there are several hundreds of $\Delta^{17}O(NO_3^-)$ measurements available in the literature for comparison to modeling results (see Alexander *et al.* (2009) and references therein). However, a quantitative interpretation of these measurements presently relies upon assumptions regarding the $\Delta^{17}O$ value of tropospheric ozone and its transfer function (Savarino *et al.*, 2008; Michalski and Bhattacharya, 2009); therefore, it has been difficult to truly evaluate the performance of the models due to an inability to distinguish between errors which arise from model biases and those due to potentially inappropriate assumptions regarding the isotopic composition of ozone. Because ozone is the predominant source of ^{17}O-excess in the troposphere, it is absolutely necessary to know the starting isotopic composition of its transferrable oxygen atom in order to extract quantitative information regarding oxidation pathways (Morin *et al.*, 2007; 2011). The same reasoning can be applied to the stratosphere, where ozone also transfers its ^{17}O-excess to other species, in particular to CO_2 (Thiemens *et al.*, 1995).

In this study, we present a new method for the collection and subsequent isotopic characterization of ozone using a simple, active air sampler with a nitrite-coated filter substrate in combination with the bacterial denitrifier/thermal decomposition method for the comprehensive isotopic analysis of nitrate via CF-IRMS (Kaiser *et al.*, 2007; Komatsu *et al.*, 2008). The collection technique used in this method does not involve the complex and expensive sampling technology utilized in prior studies of atmospheric ozone isotopes. The sampler is light, inexpensive, and easy to implement in nearly any sampling environment, providing researchers with the potential to investigate variations in ozone isotopes over a network of sites, even in remote or inaccessible areas (e.g., polar and alpine locations, stratosphere, etc.). Fundamental differences between the methods exist also in the quality of information collected. While the cryogenic methods are "bulk" methods, the filter method provides direct information on the isotopic composition of the oxygen atom of ozone transferred during oxidation reactions, $\Delta^{17}O(O_3^*)$, which is the variable most relevant to studies

of $\Delta^{17}O$ transfer in the atmosphere. Here we report observations that validate and inform the use of a nitrite-coated filter for determining the isotopic composition of the transferable oxygen atom of atmospheric ozone, as well as data for the first field measurements made using this method. Our results indicate that this technique is sufficiently robust and reliable to be applied to the routine analysis of stable isotope ratios of atmospheric ozone.

2.2 Experimental

2.2.1 Rationale

The ozone collection technique used in this study employs the aqueous phase nitrite (NO_2^-) oxidation reaction in which one oxygen atom is transferred from ozone to form nitrate:

$$NO_2^- + O_3 \rightarrow NO_3^- + O_2 \quad \text{(R2.1)}$$

The collection of ozone with nitrite-coated filter samplers is a technique that is well established in the literature and has been applied successfully in many previous studies using both active and passive sampler designs (Koutrakis *et al.*, 1993; Geyh *et al.*, 1997; Helaleh *et al.*, 2002; De Santis *et al.*, 2003; Adon *et al.*, 2010). For example, the method is commonly employed for routine indoor and outdoor monitoring by U.S. governmental agencies through use of commercial passive monitors, such as those produced by Ogawa & Co.™ (Pompano Beach, FL, USA) (Manning *et al.*, 1996; Krzyzanowski, 2004), or active samplers deployed at flow rates of 1.5 L min^{-1} (Method # ID-214) (OSHA, 1995). The nitrite-based oxidation reaction is very rapid, quickly goes to completion, and allows for the specific collection and measurement of ozone (Liu *et al.*, 2001). Previous studies have shown that the method yields concentration values that are in good agreement with those obtained using standard continuous ozone monitors; interferences from other atmospheric oxidants (e.g., O_2, NO_x, SO_x, HO_x, etc.) are typically thought to be negligible due to their lower concentration/reactivity relative to ozone, and have not been found to compromise the collection technique (Koutrakis *et al.*, 1993; OSHA, 1995).

By coupling the routine nitrite-coated filter method for ozone collection with recently developed CF-IRMS-based methods for the triple oxygen isotope analysis of nitrate (Sigman *et al.*, 2001; Casciotti *et al.*, 2002; Kaiser *et al.*, 2007), the ^{17}O-excess that is transferred from ozone in the $O_3 + NO_2^-$ reaction, denoted as $\Delta^{17}O(O_3^*)$ (Morin *et al.*, 2011), can be measured directly. The $\Delta^{17}O(O_3^*)$ value thus obtained is relevant to other bimolecular reactions incorporating in their products the same reactive oxygen atom of ozone (i.e., reactions involving a terminal atom transfer mechanism such as the reaction of ozone with NO, NO_2, or Br) (Zhang *et al.*, 1997; Peìro-Garcìa and Nebot-Gil, 2003; Savarino *et al.*, 2008; Berhanu *et al.*, 2012). It is therefore highly relevant to the study of the propagation of $\Delta^{17}O(O_3)$ via atmospheric oxidation chemistry.

2.2.2 Reagent preparation and filter coating procedure

The nitrite solution used to coat the filter sampling substrates (47 mm GF/A filters, Whatman™) was prepared following Koutrakis *et al.* (1993), with a composition of 0.1 mol L^{-1} $NaNO_2$, 0.05 mol L^{-1} K_2CO_3, and 0.1 mol L^{-1} glycerol. Solutions were prepared using reagents of the highest purity possible (typically ≥ 99%) and were diluted with UV-oxidized deionized water (18.2 MΩ resistivity, hereafter referred to as "MQ water") generated with a Milli-Q™ water purification system (Millipore™). GF/A filters were rinsed three times with MQ water and then dried for 10 - 15 minutes in a clean oven at 70 °C. The filters were then placed into individual pre-cleaned 47 mm PetriSlide™ containers (Millipore™) and coated with 1.0 mL of the coating solution (100 μmol of nitrite, over 100 times in excess of the amount needed to form sufficient nitrate on the filters). The coated filters were then placed back into the oven and allowed to dry at 70 °C for 10 - 15 minutes. During this time, the filter containers were kept slightly open to allow for evaporation. Once the filters had dried, they were immediately capped and the containers were covered in aluminum foil. Oven-drying the coated filters did not result in the accumulation of background nitrate and was found to be more efficient than drying at room temperature, which requires several hours of exposure time and thus represents a potential contamination pathway.

Nitrite on coated filters is slowly converted to nitrate even without exposure to ozone and previous studies have found that this conversion proceeds more rapidly when filters are stored at room temperature for long periods of time (e.g., > 30 days)

(OSHA, 1995). However, storing the filters frozen and in the dark can limit the production of background nitrate to an acceptable level (Koutrakis *et al.*, 1993; Geyh *et al.*, 1997); therefore, batches of coated filters were kept at -20 °C before and after sampling in their individual plastic containers, which were covered with aluminum foil. The effect of long-term storage on the stability of nitrite on the frozen coated filters was evaluated through analysis of the nitrate formed on blank filters in each batch, which were subjected to all of the same manipulations and storage conditions as samples. Additionally, a certain degree of nitrate accumulation resulting from exposure to ambient UV radiation was expected due to the photolability of nitrite ions in solution (Fischer and Warneck, 1996; Mack and Bolton, 1999). The impact of this effect was investigated in two experiments. First, four coated filters covered in aluminum foil were stored together with four uncovered filters in a vacuum-sealed glass desiccator and exposed to ambient light on a laboratory bench for a period of approximately two days (~12 hours of direct sunlight). Covered and uncovered filters were collected from the desiccator at regular intervals (6 - 12 hours) throughout this period to determine the impact of continuous light exposure, which was taken to be the difference in nitrate concentration between the covered and uncovered filters. In order to assess the impact of light exposure during sample collection, a series of ambient collections was conducted using two identical co-located samplers, one covered with aluminum foil to prevent exposing the coated filters to light, and the second left uncovered (see Section 2.2.5).

2.2.3 Preliminary tests of ozone sampling apparatus

Ozone collection was performed in all cases using a simple air sampler made of 1/4" Teflon™ (PFA) tubing connected to a standard vacuum pump (Welch™) with the nitrite-coated filters in an in-line PFA filter holder assembly (Savillex™). For all preliminary tests and subsequent ambient collections, the flow rate was maintained at approximately 2.5 - 3.0 L min^{-1}, somewhat higher than the flow rates used in previous studies using active samplers (OSHA, 1995; Geyh *et al.*, 1997). An increased flow rate could potentially shorten the contact time of ozone with nitrite and reduce ozone collection efficiency from that observed in earlier studies; however, at low ambient ozone concentrations (< 20 ppb), an increased flow rate is necessary for the collection of an adequate amount of nitrate for isotopic analysis via the denitrifier method when

the targeted sampling duration is in the range of 2 - 12 hours. In order to test the efficiency of ozone collection at the flow rate used in this study, preliminary tests were conducted by connecting the filter holder to a ozone calibration source (Model 306, 2B Technologies™) with approximately 50 cm of PFA tubing while measuring simultaneously the ozone mixing ratio downstream of the filter with a dual-beam ozone detector (Model 205, 2B Technologies™). Ozone mixing ratios generated for the preliminary tests varied between 30 and 150 ppb, concentrations spanning the range of those typically found in the troposphere. Tests were carried out at various mixing ratios and with both coated and uncoated filters to quantify the effect of the filter and sampler apparatus on the overall collection efficiency of the sampler. Reaction yield of the $O_3 + NO_2^-$ oxidation on the filter surface was taken to be the difference in collection efficiency between the tests with coated and uncoated filters.

2.2.4 Isotope transfer experiments

Studies of isotope transfer during the $O_3 + NO_2^-$ reaction on nitrite-coated filters were conducted in the dark and at room temperature in a custom-made vacuum line consisting of Pyrex™ glass components (see Savarino *et al.* (2008) and Berhanu *et al.* (2012) for full details). Ozone was produced via Tesla discharge in pure O_2 gas (99.9990%) obtained from a commercial tank supplied by Messer™. Temperature and oxygen pressure were manipulated during the individual experiments to obtain $\Delta^{17}O(O_3)_{bulk}$ values varying from approximately 7 to 40‰ (**Figure 2.1**). The general trend of $\Delta^{17}O(O_3)_{bulk}$ values produced using this technique was consistent with the known temperature and pressure dependencies of isotope effects during the ozone formation reaction (Thiemens and Jackson, 1988; 1990; Morton *et al.*, 1990; Janssen *et al.*, 2003). As a special case, one ozone sample with a mass-dependent isotopic composition (i.e., $\Delta^{17}O \approx 0$) was produced via electrolysis of acidified water (Bhattacharya *et al.*, 2009).

Discharge was carried out in a cylindrical glass trap, which was partially immersed in a Styrofoam™ balcony trap containing liquid nitrogen. After the experimental ozone was produced (typically 30 -120 μmol) and condensed at liquid nitrogen temperature (~77 K), the remaining oxygen was evacuated from the line until a pressure of 10 mTorr was obtained. Ozone was then brought into the gas phase by removing the glass trap from the Styrofoam™ balcony. After allowing time for the

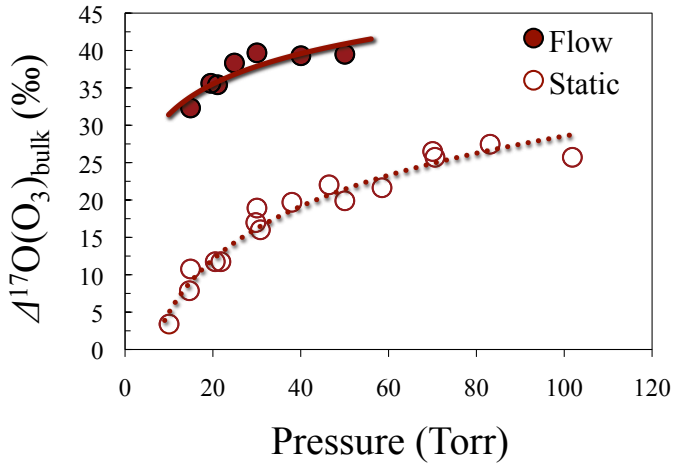

FIGURE 2.1 - The production of ozone with various $\Delta^{17}O(O_3)_{bulk}$ values was achieved by manipulating the pressure and temperature of ozone formation using static (liquid nitrogen temperature = 77 K) and flow (~298 K) systems. Static experiments were used to generate $\Delta^{17}O(O_3)_{bulk}$ values < 30‰ and flow experiments for $\Delta^{17}O(O_3)_{bulk}$ values of 30‰ - 40‰ (Savarino *et al.*, 2008; Berhanu *et al.*, 2012).

sample gas to equilibrate within the line, an aliquot of the experimental ozone was then collected using a molecular sieve trap held at liquid nitrogen temperature and analyzed via IRMS (see Section 2.2.8). To the portion of the ozone remaining in the vacuum line (typically the majority of the ozone produced), purified helium gas was added at a pressure of approximately 760 Torr. The combined gas was then pumped through a nitrite-coated filter assembly until only 10 Torr remained. The isotopic equality between the aliquot and the reacting portion of the ozone was verified in a separate experiment (Berhanu *et al.*, 2012). The isotopic composition of both the starting bulk ozone, denoted $\Delta^{17}O(O_3)_{bulk}$, and the resulting nitrate product were determined separately in order to quantify the transfer of the ^{17}O-excess of ozone to the nitrite-coated filter (see Section 2.2.8).

2.2.5 Ambient ozone collections

Tropospheric ozone samples were collected from the roof of our laboratory building in Grenoble, France (45˚N, 5˚E, 209 meters above mean sea level). The city of Grenoble is located in the Alps at the intersection of three valleys, with surrounding summits reaching 2000 to 3000 meters (Chaxel and Chollet, 2009). For the ambient collections, an open-faced filter holder assembly containing a Zefluor™ PTFE membrane pre-filter (Pall Corporation™) was used for the removal of atmospheric particulate matter upstream of the coated filter (**Figure 2.2**). Ozone mixing ratios were measured simultaneously with a standard continuous ozone monitor (Model O342M, Environnement S.A.™) during the period September-October 2011, allowing

FIGURE 2.2 - Photograph of the sampling apparatus in operation in Grenoble, France. The active ozone sampler consists of 1/4" PFA tubing connecting three main sampler components: (i) a standard low-volume vacuum pump (*bottom left*) equipped with a needle valve/flow meter (*top center*); (ii) a closed PFA filter holder assembly containing a nitrite-coated filter, covered in aluminum foil (*bottom center*); and (iii) an open-faced filter holder assembly containing a PTFE prefilter for the removal of particulate matter (*top right*).

for an estimation of collection efficiency for the ambient samples collected during this time (see below). In cases where an ozone monitor was unavailable, concentration data has been obtained from the local air quality monitoring agency (http://www.air-rhonealpes.fr) for comparison to the isotopic measurements presented here.

Three series of ambient collections will be discussed here. Each of these series is associated with a development in the underlying methodology or change in protocol; therefore, a comparison of the results obtained for these three different series of collections is useful in evaluating the performance of the method and its sensitivity to various controls. Series A samples (n = 9) were collected during the period 18 - 21 April 2011 in the dark and at room temperature. Many of these samples were collected at low sampling durations (1 - 2 hours, n = 5) in order to explore the diurnality of ozone isotopic composition, while other samples were collected over extended periods (12 - 24 hours, n = 3). Ozone concentration varied in the range of 40 - 50 ppb during this time, resulting in total sample sizes in the range of 90 - 900 ppb•hr. Series B samples (n = 24) were collected between 25 July and 12 August

2011, with total sample sizes ranging from 45 - 375 ppb•hr. For these collections, the sampling apparatus had been moved to a different location where it was subject to a high degree of light exposure on a laboratory workbench as in **Figure 2.2**. As will be demonstrated below, exposure to light during sample collection was observed to impact the isotopic results obtained for the Series B samples; therefore, Series C collections (n = 20) during the periods 6 - 9 September and 18 - 28 October 2011 were performed with the sampling apparatus covered in aluminum foil to prevent exposing the sample filters to ambient light. Seven of the Series C samples were collected in duplicate using two co-located samplers, one covered with aluminum foil and the second left uncovered to quantify the impact of light exposure in terms of nitrate blank accumulation. Ambient ozone concentrations were exceptionally low during September-October, often declining to less than 5 ppb for 10 - 12 hours per day, which resulted in relatively small sample sizes for many of the Series C collections (14 samples < 100 ppb•hr), despite the increased sampling durations employed during this time (8 - 30 hours).

For ambient collections, there is an increased potential for positive interferences, not only from oxidants other than ozone (e.g., O_2, SO_2, etc.) but also from other nitrogen-bearing atmospheric compounds. The use of a prefilter will exclude the vast majority of atmospheric nitrate, which exists predominantly in the particulate form; however, gaseous compounds not retained by the prefilter could possibly yield enhanced nitrate concentrations on the nitrite-coated substrate. For example, atmospheric nitrogen oxides ($NO + NO_2 = NO_x$) and their reservoir species (NO_y = NO_3, N_2O_5, HONO, etc.) could potentially react with the filter to form nitrate; additionally, gaseous nitric acid (HNO_3) is expected to be simultaneously collected on the alkaline filter. In any case, this would represent a dilution of the sample with nitrate not produced through the $O_3 + NO_2^-$ reaction. For typical tropospheric concentrations, positive interferences will probably represent less than 5% of the nitrate formed on the filter (Koutrakis *et al.*, 1993; OSHA, 1995); however, this has yet to be verified for active samplers deployed at flow rates as high as 3.0 L min^{-1}. In order to evaluate the effect of ambient atmospheric NO_x, NO_y, and gaseous HNO_3 on the accumulation of nitrate on the nitrite-coated filter, parallel collections were conducted using two identical active samplers, one equipped with a nitrite-coated filter and the other with an alkaline filter containing all of the coating reagents except for $NaNO_2$ (i.e., K_2CO_3 and glycerol). Nitrate concentration measurements for

extracts of the filters prepared without $NaNO_2$ are taken to indicate the quantitative impact of such interferences.

2.2.6 Sulfamic acid treatment

The bacterial denitrifier method, used in this study for the isotopic characterization of nitrate, is susceptible to interferences from nitrite, which is converted by bacterial cultures to N_2O along with the nitrate sample (Casciotti *et al.*, 2002; 2007). Due to the abundance of nitrite ion in extracts obtained from a nitrite-coated filter, the approach described in this study is dependent on the removal of excess nitrite from extract solutions prior to isotopic measurements (Granger *et al.*, 2006). For this purpose, sample filters and blanks were, after extraction in 18 mL of MQ water, treated with 1.0 mL of a 1.0 mol L^{-1} sulfamic acid (AcrosOrganics™) solution (Granger and Sigman, 2009). Sulfamic acid is a moderately strong acid ($pK_a \approx 1.3$) that reacts with nitrous acid ($pK_a = 3.4$) to yield N_2 gas and sulfuric acid:

$$HNO_2 + (H_2N)HSO_3 \rightarrow H_2SO_4 + N_2 + H_2O \qquad \text{(R2.2)}$$

After allowing sufficient time for the complete conversion of nitrite ion to N_2 gas (approximately 10-20 minutes), the extract solutions were neutralized with a corresponding addition of high-purity 1.0 mol L^{-1} NaOH. This step was necessary in order to bring the solutions into a pH range appropriate for nitrate isotope analysis via the bacterial denitrifier method (~ 7.2) (Sigman *et al.*, 2001).

2.2.7 Nitrate concentration analysis

After neutralization, extract solutions were filtered via centrifugation to remove particulates in preparation for sample analysis. Extract nitrate and nitrite concentrations were determined colorimetrically using a segmented-flow analyzer (QuAAtro, SEAL Analytical™). In this method, nitrate is quantitatively reduced to nitrite by passage through a column containing copperized cadmium. The resulting nitrite is then determined by diazotization with sulfanilamide dihydrochloride followed by detection of absorbance at 520 nm. This technique provides a measurement of both the nitrite resulting from nitrate reduction and the nitrite already present in the solution; nitrite alone is normally determined through the analysis of aliquots that have not been subjected to reduction by cadmium and nitrate is then

estimated by subtraction. Extract solutions treated with sulfamic acid are assumed to contain negligible nitrite; therefore, the colorimetric measurements reported here can be taken to represent only the nitrate extracted from the filter. The validity of this assumption was evaluated through analysis of residual nitrite in filter extracts, which was determined to be less than 0.1 μmol L^{-1} (< 2 nmol per filter).

Background contributions of nitrate from the filter and reagents were determined stepwise through analysis of unexposed coated filters, uncoated filters, and for each of the individual reagents used for filter coating and extraction. To account for the possible addition of nitrate background from the coating and extraction reagents (and also to control for the different absorbance properties of the filter extract matrix and pure water), the amount of nitrate formed on sample filters through reaction with ozone was determined by calibrating the sample extracts for each batch of coated filters to nitrate standards prepared using all of the same matrix reagents used in the filter extraction.

2.2.8 Isotopic measurements

2.2.8.1 Nitrate

Nitrate was prepared for comprehensive isotopic analysis (i.e., the simultaneous measurement of all its stable isotope ratios: $^{17}O/^{16}O$, $^{18}O/^{16}O$, and $^{15}N/^{14}N$) using the bacterial denitrifier method for the conversion of nitrate to nitrous oxide (N_2O) (Sigman *et al.*, 2001; Casciotti *et al.*, 2002) in combination with the thermal decomposition technique introduced by Kaiser *et al.* (2007) for the conversion of N_2O to O_2 and N_2 (Komatsu *et al.*, 2008; Morin *et al.*, 2009). In brief, denitrifying bacteria (*Pseudomonas aureofaciens*) obtained from the laboratory of Dr. Daniel Sigman (Princeton University) were cultured in nitrate-amended soy broth and incubated for five days in stoppered glass bottles. The bacterial cultures were then concentrated by centrifugation/resuspension and dispensed as 2 mL aliquots into 20 mL glass vials, which were capped with Teflon-backed silicone septa and crimp seals. To remove the N_2O produced from denitrification of the nitrate originally present in the soy broth and to ensure the anaerobic conditions necessary for bacterial nitrate reduction, each sealed vial was purged with helium for three hours. Approximately 50 - 100 nmol of sample nitrate, in addition to the nitrate blank associated with the coating reagent matrix (see below), was then injected into the purged vials and conversion of the

sample nitrate to N_2O was allowed to proceed overnight. The bacterial cultures were then deactivated using 0.5 mL of a 1.0 mol L^{-1} NaOH solution, which brings the sample to a pH > 12. The N_2O sample gas in the headspace of the vials was then purged with a purified helium carrier stream at ~10 mL min^{-1} and cryogenically trapped in a stainless-steel sample loop immersed in a liquid nitrogen bath. After 15 minutes of trapping, the N_2O sample gas was purged from the trap with a stream of helium and introduced into a gold furnace where it was thermally decomposed at 900 °C to O_2 and N_2 (Cliff and Thiemens, 1994; Kaiser *et al.*, 2007). Following separation via gas chromatography, the O_2 and N_2 sample gases were then directed into the ionization chamber of a Finnigan™ MAT253 isotope ratio mass spectrometer using a GasBench II™ on-line gas introduction system (Thermo-Fisher Scientific™). During the data acquisition run, the settings of the mass spectrometer were modified to measure nitrogen and oxygen isotope ratios sequentially (i.e., "peak-jumping"). A time lag of 60 seconds was used between the peaks corresponding to the O_2 and N_2 sample gases so that possible interferences arising from the tailing of the O_2 peak into the N_2 peak had no measurable effect on the data. Typical peak areas for a 100-nmol nitrate sample were on the order of 12.5 V s and 25 V s for O_2 and N_2, respectively.

All analytical steps were simultaneously performed on the nitrate isotopic standard reference materials (SRMs) USGS32, USGS34, and USGS35, which were obtained from the International Atomic Energy Agency (IAEA) (**Table 2.1**) (Böhlke *et al.*, 2003) (Böhlke *et al.*, 2003). Individual measurements for nitrate samples were normalized via linear calibration with concurrent measurements of the SRMs and their equimolar mixtures. **Figure 2.3** shows a typical example of calibration curves obtained for $\delta^{18}O$, $\Delta^{17}O$, and $\delta^{15}N$ (agreed standard values versus raw measured values) for a representative set of analyses. The slopes and intercepts of the linear correlations between expected and measured values were used to calibrate the raw isotopic measurements for the unknown samples in each batch. In accordance with the identical treatment principle (Werner and Brand, 2001), reference materials were prepared for isotopic analysis at an identical volume and concentration as samples (Sigman *et al.*, 2001; Casciotti *et al.*, 2002) and diluted with a background ("matrix") solution of filter coating reagents, which were found to carry a significant nitrate blank (see Section 2.3.2). This identical treatment allows for an automatic blank correction of the isotopic data when each batch of samples is calibrated using the nitrate SRMs. However, an implicit

TABLE 2.1 - Isotopic Data for Nitrate and Nitrite Reference Materials Used in This Study.

Material	ID	$\delta^{17}O_{VSMOW}$ (‰)	$\delta^{18}O_{VSMOW}$ (‰)	$\Delta^{17}O_{VSMOW}$ (‰)	$\delta^{15}N_{AIR}$ (‰)	Primary Reference
$NaNO_3$	USGS35	51.5[a]	57.5	21.6[b]	2.7	Böhlke *et al.*, 2003
KNO_3	USGS34	-14.8	-27.9	-0.3	-1.8	Böhlke *et al.*, 2003
KNO_3	USGS32	13.4[c]	25.7	≈ 0[c]	180	Böhlke *et al.*, 2003
$NaNO_2$	RSIL-N7373	-	4.5	-	-79.6	Casciotti *et al.*, 2007
$NaNO_2$	RSIL-N23	-	11.4	-	3.7	Casciotti *et al.*, 2007
$NaNO_2$	RSIL-N10219	-	88.5	-	2.8	Casciotti *et al.*, 2007

[a] Calculated from $\delta^{18}O$ and $\Delta^{17}O$ measurements by Böhlke *et al.* (2003)
[b] Determined by Michalski *et al.* (2002)
[c] Determined by Morin (2008)

assumption underlying this correction is that the relative proportions of blank and sample do not vary widely between individual ozone collections. In practice, any differences in blank content between samples and standards can degrade the calibration and decrease the precision of the method. For example, batches of filter samples that are subject to unanticipated blank accumulation or loss during sampling, handling, and storage, can be expected to produce varying proportions of blank and sample nitrate when extracted into solution. The calibration of such samples to SRMs prepared in an average matrix blank (i.e., nitrate blank expected from 100% recovery of coating reagents) would not be strictly valid, as variations in blank content will be associated with changes in the slopes and intercepts of the linear regressions used to calibrate the raw isotopic measurements (**Figure 2.3**). Therefore, unexpected variability in blank/sample mixing can compromise the efficacy of the calibration process and could result in erroneous conclusions regarding the isotopic composition of the ozone sampled. This effect could be particularly problematic for samples collected during field campaigns, which may be subject to increased contamination, extreme weather, and extended storage times at potentially elevated temperatures. In order to explore this blank variability effect and its impact on nitrate $\Delta^{17}O$ and $\delta^{15}N$ measurements, a recovery experiment was conducted using USGS35 and a synthetic nitrate blank, which was composed of 11% USGS32 and 89% USGS34 and thus possessed an isotopic composition similar to that observed for the actual filter blank ($\Delta^{17}O$ = -0.3‰, $\delta^{15}N$ = 18‰, see Section 2.3.4). USGS35-blank mixtures (n = 15) of

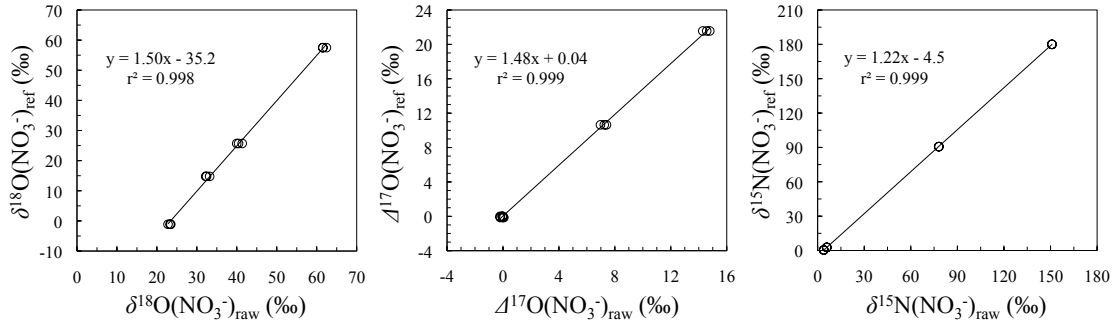

FIGURE 2.3 - Typical calibration plots for $\delta^{18}O$ (*left*), $\Delta^{17}O$ (*center*), and $\delta^{15}N$ (*right*) of nitrate (agreed values for the USGS standards from Böhlke *et al.* (2003) versus raw measured values).

identical volume and sample amount were prepared with synthetic blank levels ranging from 0 - 83% (17 - 100% USGS35) and analyzed using the method described above. The raw isotopic values for these USGS35 mixtures were normalized via calibration to a group of SRMs (n = 12) prepared at a 33% synthetic blank level in order to determine the quantitative impact of a varying blank composition in terms of the recovery of the accepted USGS35 $\Delta^{17}O$ values.

It is typically desirable to obtain a consistent final quantity of N_2O from both samples and standards in order to minimize uncertainties arising from the nonlinearities associated with IRMS (Werner and Brand, 2001). In the case of our experimental approach, the significance of this peak size consistency is enhanced due to the sample size dependence that has been observed in association with the N_2O thermal decomposition technique (Kaiser *et al.*, 2007). Furthermore, the efficacy of the automatic blank correction is also dependent on the comparison of samples and standards of identical sizes, which follows from the assumption that nitrate sample and blank are present at the same relative proportions in both the references and filter extracts (both volume and mass are normalized across all samples and standards). Therefore, special care was taken to equalize the peak sizes obtained via IRMS for all samples and standards in a given analytical run. Sample measurements for which the O_2 peak area differed by more than 5% from the peak areas corresponding to the USGS standards were not considered and subsequently re-measured. In practice, this process often involved measuring samples 2 - 3 times in an effort to match the O_2 peak size with that of the standards, thus allowing for the highest possible degree of comparability between samples and references. However, the Series A collections were not subjected to this rigorous peak matching process. These samples were

calibrated to SRMs with approximately 20 - 30% smaller peak sizes and are presented here to demonstrate the consequent impact on the isotopic results (see Section 2.3.5).

2.2.8.2 Ozone

Analyses of the bulk ozone from the isotope transfer experiments, $\Delta^{17}O(O_3)_{bulk}$, were conducted on the MAT253 in classic dual-inlet mode. Ozone samples produced in the vacuum line were converted to O_2 using a molecular sieve and injected into the MAT253 along with an oxygen reference gas. The inlet pressure was adjusted to obtain a signal level of 3.5 - 4.0 volts and eight isotope ratio pairs were obtained to determine the $\delta^{17}O$ and $\delta^{18}O$ values. The measured raw values were converted to enrichment values relative to the isotopic composition of the tank oxygen used for ozone production ($\delta^{17}O$ = 5.79‰ and $\delta^{18}O$ = 11.75‰ relative to VSMOW), which was determined previously (Bhattacharya *et al.*, 2008). The errors of ozone isotope ratio determination, including the various steps associated with the handling of ozone in the vacuum line, collection, and conversion to oxygen using the molecular sieve, are estimated to be 0.5‰ and 0.1‰ for $\delta^{17}O$ and $\delta^{18}O$, respectively (Berhanu *et al.*, 2012).

2.3 Results and discussion

2.3.1 Efficiency of ozone collection

Preliminary tests of collection efficiency conducted using a calibrated ozone source indicate an average yield (based on the mass of nitrate formed on the filter) of approximately 58 ± 5% at the flow rate used during this study. A linear regression of ozone mass throughput against sample nitrate in filter extracts (**Figure 2.4**) reveals a strong positive correlation (r = 0.99) with a slope of 0.66 (n = 13) for the preliminary tests. Collection efficiencies for the Series C ambient samples averaged 64 ± 10%, varying in the same range observed for the calibrated ozone source tests, but with a somewhat larger standard deviation. The greater scatter in the ambient data is perhaps a result of micro-scale variations in ozone concentration and meteorological conditions during ambient sampling; conversely, it could also indicate a quantitative impact from atmospheric oxidants other than ozone. However, the strong correlation

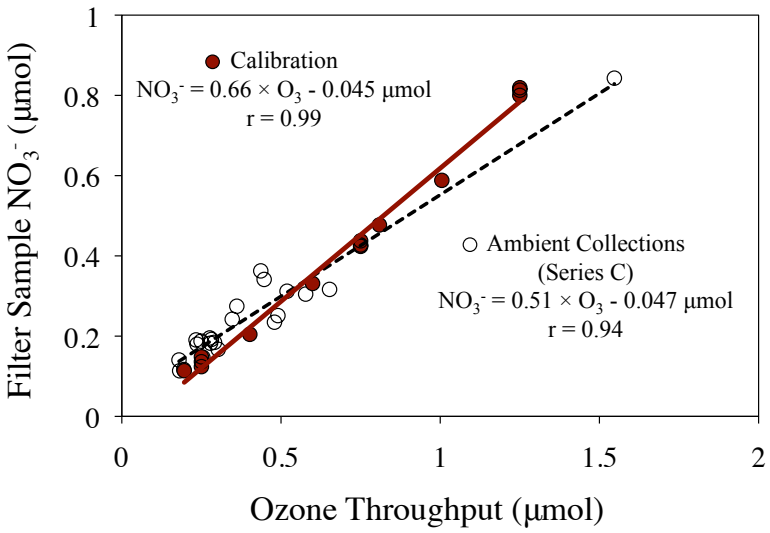

FIGURE 2.4 - Linear regressions of total ozone mass throughput against nitrate in coated filter extracts for the preliminary tests conducted with a calibrated ozone source and the Series C ambient collections. Ozone throughput for the field collections has been estimated based on ozone concentration measurements with the standard continuous monitor during the period of the Series C collections (September-October).

(r = 0.94) observed between ozone throughput and nitrate formation for the ambient collections indicates that this effect is likely to be quite small, even at the extremely low ozone levels (< 5 ppb) observed in Grenoble during the period of the Series C collections (September-October).

The yields observed for the calibration tests and ambient samples are lower than those typically reported for nitrite-coated filters in passive diffusive samplers or low-flow active designs (Koutrakis *et al.*, 1993; Geyh *et al.*, 1997; Helaleh *et al.*, 2002; De Santis *et al.*, 2003); however, they are in the same general range as the yields found for the cryogenic technique in the pioneering studies of ozone isotopic composition by Krankowsky *et al.* (1995) and Johnston and Thiemens (1997). Additional collection efficiency tests, conducted in an environmental chamber at -30 ˚C indicate a similar yield, suggesting that the method is appropriate for application to low-temperature environments (e.g., alpine and polar environments, stratosphere, etc.).

Destruction of ozone in the sampling line and filter holder (estimated from experiments conducted with an uncoated filter) was found to account for approximately 20% of the reduction in collection efficiency (**Figure 2.5a**), while approximately 5% was typically measured downstream of the nitrite-coated filter exposed to various ozone mixing ratios (**Figure 2.5b**). This leaves an additional loss (~ 15%) in our experiment that cannot be attributed to the sampling apparatus and filters via tests with an uncoated filter. If it is assumed that this unaccounted ozone

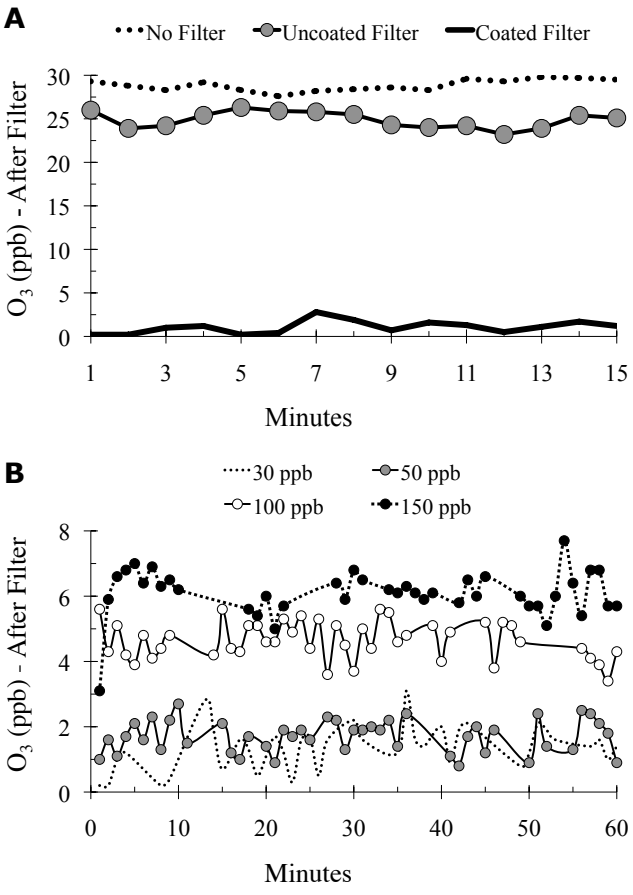

FIGURE 2.5 - **(a)** Results from 15-minute trials conducted by measuring the ozone mixing ratio (ppb) downstream of the filter holder with coated filters, uncoated filters, and the unloaded filter holder (no filter). All trials were conducted with a calibrated ozone source at a target ozone concentration of 30 ppb. **(b)** Results from 60-minute trials conducted by exposing nitrite-coated filters to various ozone mixing ratios while measuring ozone concentration downstream of the filter holder. The amount of ozone detected downstream corresponds to approximately 3 - 10% of ozone throughput.

also passes through the filter without reacting with nitrite then, by considering only the ozone that reaches the nitrite-coated filter, it can be estimated that the $O_3 + NO_2^-$ oxidation proceeds on the coated filter substrates with an average reaction yield of approximately 80% at the flow rate used in this study. It is conceivable that additional isotope effects will occur at reaction yields below 100%; however, an implicit assumption of this approach is that any such effects will operate in a mass-dependent fashion and will thus not impact the $\Delta^{17}O$ value of the sampled ozone. A reduction of flow rate would likely improve reaction efficiency by increasing the length of time in which ozone may react with nitrite within the filter matrix. However, a decrease in flow rate would require an accompanying increase in exposure time in order to collect enough mass for nitrate isotope measurements. An increase in exposure time would in turn decrease the time resolution of tropospheric ozone observations. These are considerations that must be balanced with regard to the particular goals of the study in question and are important topics for future research.

2.3.2 Nitrate blanks and interferences

The most significant nitrate blank was found to be associated with the $NaNO_2$ reagent used in the coating solution (**Table 2.2**). The Series A ambient collections were conducted using 99.99+% $NaNO_2$ (Sigma-Aldrich™, batch # 53696MJ), which was found to contribute approximately 7.27 μmol L^{-1} of background nitrate to the filter extract solution (140 nmol of nitrate per filter). Due to the relatively small sample size targeted for the ambient collections (~ 100 nmol), this was deemed to be an unacceptably high background level. Subsequent ambient collections, including the Series B and Series C samples described here, were conducted using a $NaNO_2$ reagent of a 99.999% purity (Sigma-Aldrich™, batch # MKBG2997V). This higher-purity reagent exhibited a much lower level of nitrate contamination, contributing only 2.24 μmol L^{-1} (45 nmol) per filter. The total nitrate blank attributable to the filter coating and extraction reagents (high-purity coating solution, sulfamic acid, NaOH) was determined to be 4.12 ± 0.41 μmol L^{-1} (82 ± 8 nmol for the 20 mL extract solutions).

In addition to the nitrate background originating from the coating and extraction reagents, several other possible sources of nitrate contamination and positive interference were also investigated (see Section 2.2.3). Of primary concern was the potential accumulation of nitrate blank on the sample filters due to exposure to light and high temperature during sample collection. The effect of temperature was evaluated through the analysis of coated filters that were covered in aluminum foil and stored at room temperature for 5 - 25 hours. These filters exhibited nitrate concentrations that were indistinguishable from those of blank filters from the same batch that were stored at -20 °C. However, the results of parallel ambient collections made using covered and uncovered sampling units suggest that light exposure is indeed a significant source of nitrate interference (**Table 2.2**). Uncovered filter samplers yielded nitrate extract concentrations that were, on average, 2.18 ± 1.33 μmol L^{-1} higher than co-located samplers covered with aluminum foil for samples collected during daylight hours (n = 7) (**Figure 2.6a**). When the total duration of exposure time is taken into account for each sample in the experiment, this corresponds to a nitrate accumulation rate of 0.56 ± 0.37 μmol L^{-1} hr^{-1} for daytime collections. This range is somewhat higher than the accumulation rate of 0.22 μmol L^{-1} hr^{-1} inferred from the experiment conducted with covered and uncovered coated filters exposed to ambient sunlight inside of a vacuum-sealed desiccator (**Figure**

TABLE 2.2 - Nitrate Blanks of Coating Reagents and Filters.

		Reagent conc. in extract soln. (mmol L^{-1})	NO_3^- contribution to filter extract (µmol L^{-1})
Coating solution	99.99% $NaNO_2$	50.0	7.27
	99.999% $NaNO_2$	50.0	2.24
	K_2CO_3	2.5	0.56
	Glycerol	5.5	0.54
Sulfamic acid		50	0.78
NaOH		45.8	< 0.1
Reagent Total		-	4.12[a]
Uncoated filter		-	0.10
Accumulation	Uncovered	-	0.56 ± 0.37[b]
	Covered	-	< 0.1
NO_y and HNO_3 interference		-	< 0.1[c]
Storage and handling		-	0.12[d]

[a] Includes the high-purity $NaNO_2$, K_2CO_3, glycerol, sulfamic acid, and NaOH
[b] Refers to the mean and standard deviation of the nitrate accumulation rate (µmol L^{-1} h^{-1}) inferred from the collections with uncovered and covered samplers
[c] Refers to the difference in filter nitrate accumulation between the parallel collections conducted using coated filters and filters containing all of the coating reagents except for $NaNO_2$
[d] This value has been obtained by calibrating nitrate concentration measurements for unexposed coated filters to standards prepared in the extract solution matrix and thus represents the nitrate blank above and beyond that associated with the reagents

2.6a). The larger magnitude of photo-induced nitrate accumulation observed for the ambient collections likely reflects the importance of trace species present in air, particularly the OH radical, H_2O, and O_2, that participate in aqueous nitrate production pathways involving the products of nitrite photolysis (Fischer and Warneck, 1996; Mark *et al.*, 1996; Mack and Bolton, 1999).

Parallel collections conducted using coated filters and filters containing all of the coating reagents except for $NaNO_2$ (see Section 2.2.5) indicate that the blank arising from positive interferences by atmospheric NO_y and HNO_3 is indistinguishable from the blank imparted by the uncoated filter itself (~0.10 µmol L^{-1}). The impact of storage and handling on the coated filters was also found to be relatively minor in terms of nitrate blank accumulation. Coated filter blanks stored at -20 °C for 2 - 6 weeks were found to have a nitrate background that was statistically indistinguishable from the reagent blank (average = 4.24 µmol L^{-1}, n = 10). Taken as a whole, these

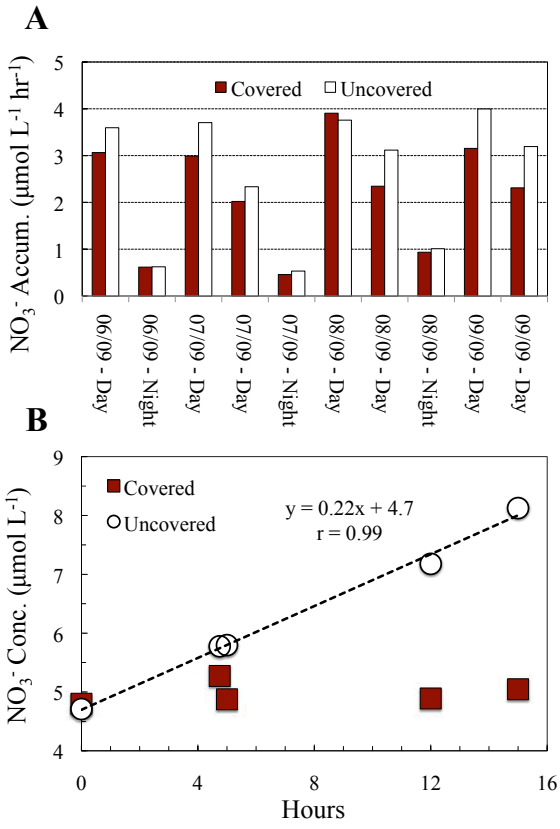

FIGURE 2.6 - **(a)** Reagent blank-corrected nitrate concentrations in filter extracts for the parallel ambient collections conducted using covered and uncovered sampling units (6 - 9 September). Concentrations are expressed as average nitrate accumulation rates (µmol L^{-1} hr^{-1}) over the total duration of each collection period. Average concentration differences between the samples collected with covered and uncovered samplers correspond to an average (± 1σ) nitrate blank accumulation rate of 0.56 ± 0.37 µmol L^{-1} hr^{-1} for daytime collections. **(b)** Uncorrected (total reagent blank and accumulated blank) nitrate concentrations in extracts of covered and uncovered coated filters exposed to direct sunlight in a desiccator. The nitrate accumulation rate inferred from this experiment is ~0.22 µmol L^{-1} hr^{-1} (i.e, the slope of the linear regression).

results suggest that, when the coated filters are protected from exposure to excessive amounts of light or direct sources of contamination, the majority of the nitrate blank present in the filter extract is originally present in the coating reagents.

2.3.3 Accuracy of isotopic measurements

2.3.3.1 Calibration curves for $\Delta^{17}O$

As noted previously, isotopic measurements of nitrate were normalized through comparison to isotopic standards (USGS32, USGS34, and USGS35), which were prepared in a background matrix of filter coating reagents and subjected to the same chemical processing (extraction with MQ water, sulfamic acid treatment, neutralization with NaOH, etc.) as sample filters (Werner and Brand, 2001). Due to the relatively high levels of nitrate blank present in the matrix solution (**Table 2.2**), this identical treatment represents the addition of a high N_2O blank in SRMs prepared for analysis via the denitrifier method. The quantitative impact of this blank is a function of the volume of filter extract that is injected with the bacteria; i.e., when

filter extract nitrate concentrations are low, a greater volume of sample must be injected with the bacterial denitirifiers; therefore, a larger proportion of the N_2O will originate from the nitrate blank present in the reagents. This suggests the possibility of an increased uncertainty of isotopic measurements when a relatively small amount of nitrate has been formed on the sample filters via oxidation by ozone and samples are calibrated to SRMs prepared in a large nitrate background. Extract solutions for the filter samples reported in this study had sample nitrate concentrations ranging from 5 - 200 μmol L^{-1} (not including the 4.12 μmol L^{-1} blank associated with the extract matrix), corresponding to necessary additions of 0.6 - 8.0 mL of sample for isotopic analysis at 40 - 125 nmol targets. These additions correspond to 2.5 - 33 nmol of blank.

Table 2.3 summarizes the calibration curves obtained for $\Delta^{17}O$ (agreed standard values vs. raw measured values) from measurements of various amounts (40 - 125 nmol) of the USGS references prepared in various volumes of extract matrix (i.e., various blank fraction levels). Each grouping of standards in **Table 2.3** refers to triplicate measurements USGS32, USGS35, equimolar mixtures of USGS35/34 and USGS32/34, and blanks prepared using the same concentrations of coating reagents that are found in the sample extracts (15 measurements in each grouping). The slopes and intercepts of these linear correlations were used to calibrate the raw isotopic data for samples processed within the same batch (i.e., samples sharing the same reagents and target volume), which corrects the samples for the nitrate blank present in the extract matrix. The total analytical uncertainty of the method for each batch of samples and reference materials is estimated as the reduced standard deviation of the residuals from the linear regression between the USGS reference materials and their expected values.

As anticipated, the slopes of these regression lines increase with increasing total matrix volume (i.e., increasing blank peak area), and decreasing standard mass, due to a dilution of the $\Delta^{17}O$ signal present in the sample with nitrate blank inherited from the reagents ($\Delta^{17}O \approx 0‰$). For the 100-nmol groups of standards prepared in the highest matrix volumes (7.5 - 8.5 mL), slopes increase by as much 50% over that observed for a pure water matrix. However, for total volumes of 6.0 mL or less, slopes were typically in the same range observed for water. An unexpected result is that the analytical uncertainty (standard deviation of the residuals) observed for each group of standards appears to be only weakly correlated with the blank fraction

TABLE 2.3 - Blank Measurements and $\Delta^{17}O$ Linear Regressions for Various Amounts of USGS32, USGS34, and USGS35 Standards Prepared in Various Total Matrix Volumes.

Matrix Type	Mass of Std. (nmol)	Total Matrix Vol. (mL)	Total Peak Area (V•s)	Blank Peak Area (V•s)	m^b	b^b	Std. Dev. of Residuals (‰)	Blank (%)
MQ water	100	2.4	15.7	0.3	1.5	0.00	0.45	2
Extract	40	6.0	6.5	2.9	2.4	0.08	0.50	45
Extract	40	7.5	7.2	3.4	2.6	0.00	0.75	48
Extract	50	6.0	7.6	2.9	2.2	-0.55	0.55	38
Extract	60	6.0	8.7	2.9	2.0	-0.49	0.42	33
Extract	70	6.0	9.6	2.9	1.9	-0.27	0.66	30
Extract	70	7.5	9.9	3.7	1.9	-0.20	0.52	37
Extract	70	7.5	10.0	3.4	2.0	0.08	0.71	34
Extract	80	5.9	11.4	2.6	1.7	-0.66	0.29	23
Extract	80	7.5	10.4	3.4	2.6	-0.74	0.80	33
Extract	85	7.5	11.2	3.7	1.7	-0.18	0.23	33
Extract	100	2.2	13.1	1.7	1.4	-0.15	0.31	13
Extract	100	2.3	12.4	1.3	1.8	-0.47	0.34	11
Extract	100	6.0	14.9	2.6	1.6	-0.49	0.44	17
Extract	100	6.0	12.7	3.2	2.1	-0.77	0.62	25
Extract	100	6.2	12.9	3.2	1.7	-0.34	0.36	25
Extract	100	7.5	12.1	3.4	2.3	-0.04	0.74	28
Extract	100	7.5	12.5	3.7	1.7	0.03	0.33	29
Extract	100	7.5	12.8	3.4	1.8	0.08	0.27	27
Extract	100	8.5	11.9	3.9	2.4	-1.21	0.58	33
Extract	125	6.0	16.5	2.6	1.5	-0.51	0.25	16
Extract	125	7.5	14.3	3.4	2.1	-0.14	0.75	24

[a] Each entry in the table refers to triplicate sets of measurements of (a) USGS32, (b) USGS35, (c) equimolar mixtures of USGS34/35, (d) equimolar mixtures of USGS34/32 and (e) a reagent matrix blank (n = 15).
[b] Refers to the slope (m) and y-intercept (b) of the linear regression between the raw $\Delta^{17}O$ values measured for the SRMs and their certified $\Delta^{17}O$ values (Bohlke *et al.*, 2003), where y = mx + b

present in the standards (r = 0.43). Uncertainty averaged 0.50 ± 0.18‰ for the 21 groups of standards shown in **Table 2.3**, and did not increase significantly with increasing total matrix volume or decreasing sample mass. For example, uncertainty averaged 0.59‰ for the seven 40 - 70 nmol groups of standards, only a small increase over that observed for the 80 - 125 nmol groups (0.45‰). This suggests that the variability in the isotopic measurements that can be attributed to the reagent nitrate background is only marginally increased over that induced by the varying performance of different bacterial cultures (Xue *et al.*, 2010). Therefore, we conclude that the quantitative impact of the nitrate blank can be adequately corrected through the normalization process described above for filter extracts with sample concentrations as low as 5 μmol L^{-1}. Nevertheless, the removal of this nitrate background in the $NaNO_2$ reagent should also be investigated in the future, either by finding a simple method for the elimination of nitrate contamination or by testing a brand of reagent with a higher purity.

2.3.3.2 USGS35 recovery experiment

While the $\Delta^{17}O$ calibration procedure described above can be expected to adequately control for the quantitative impact of a constant nitrate background, any differences in blank-sample mixing between ozone collections and standards can degrade the calibration and increase uncertainty as previously discussed. The impact of blank variability on nitrate $\Delta^{17}O$ and $\delta^{15}N$ measurements can be seen clearly in **Figure 2.7**, which presents the results of the USGS35 recovery experiment. The 15 USGS35/blank mixtures measured in this experiment were calibrated to a baseline blank level of 33%. Therefore, mixtures prepared at blank levels of 29 - 40% yielded calibrated $\Delta^{17}O$ values of 19.8 - 22.1‰, close to the certified value for USGS35 (21.6‰, **Table 2.1**). As anticipated, $\Delta^{17}O$ values decrease sharply with increasing blank levels due to the dilution of USGS35 by the synthetic blank with $\Delta^{17}O \approx 0$. As can be seen in **Figure 2.7**, this decrease in $\Delta^{17}O$ is accompanied by a corollary increase in the calibrated $\delta^{15}N$ values of the USGS35/blank mixtures. Similar to the case with $\Delta^{17}O$, this increase in $\delta^{15}N$ can be unambiguously attributed to the greater relative importance of the nitrate blank in determining the bulk isotopic composition of the mixture ($\delta^{15}N(NO_3^-)_{blank}$ = 18‰ as compared to 2.7‰ for USGS35). For mixtures prepared at synthetic blank levels lower than the 33% baseline, calibrated $\Delta^{17}O$ values increase significantly, reaching values as high as 32.1‰ for pure

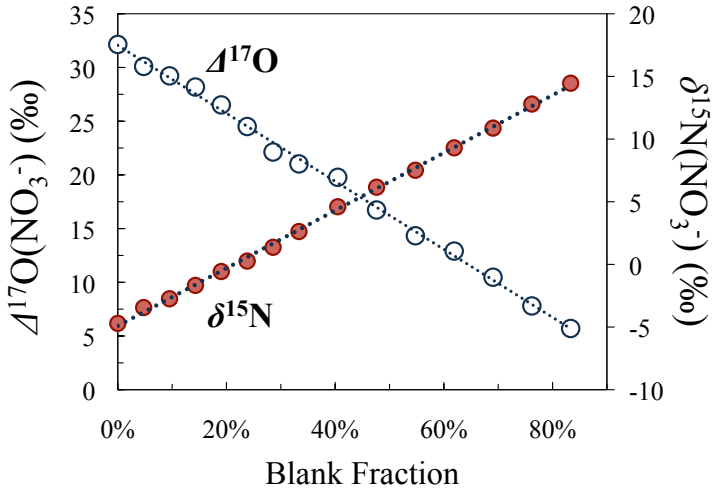

FIGURE 2.7 - The dependence of calibrated $\Delta^{17}O$ and $\delta^{15}N$ values on blank fraction for USGS35 standards mixed at varying proportions with a synthetic blank ($\Delta^{17}O$ = -0.3‰, $\delta^{15}N$ = 18‰) and calibrated to a baseline blank level of 33%.

USGS35, a 10‰ overestimate of its actual certified $\Delta^{17}O$ value. $\delta^{15}N$ values decrease in proportion with the increase in $\Delta^{17}O$ at low blank fractions and reach a minimum value of -4.7‰. A negative $\delta^{15}N$ value is a counterintuitive result considering that both USGS35 and the synthetic blank possess positive $\delta^{15}N$ values. However, it is important to keep in mind that these samples have been normalized via comparison to references prepared at a 33% blank level and have thus been overcorrected in the calibration process.

The dynamic shown in **Figure 2.7** indicates that unexpected variability in nitrate blank can act as a significant source of error when calibrating isotopic measurements for ambient ozone collections to standards prepared at a baseline blank level. However, the quantitative relationship that this effect produces between $\Delta^{17}O$ and $\delta^{15}N$ can provide a convenient means for correcting $\Delta^{17}O$ measurements of ambient samples. Because the nitrogen atom of the nitrite reagent is conserved during oxidation to nitrate, its $\delta^{15}N$ value (1.5‰, see Section 2.3.4) thus provides a source signature for nitrate produced from the $O_3 + NO_2^-$ reaction that contrasts sharply with the $\delta^{15}N$ value of the nitrate blank inherited from the reagents, which was found to vary in the range of 15 - 25‰. Linear regression analysis of $\delta^{15}N$ and $\Delta^{17}O$ for the USGS35/blank mixtures reveals a strong correlation between the two measurements ($\Delta^{17}O(NO_3^-) = -1.37 \times \delta^{15}N(NO_3^-) + 25.3$, r = 0.99, n = 15), suggesting that it provides a robust means for correcting inappropriately calibrated nitrate samples. Corrected

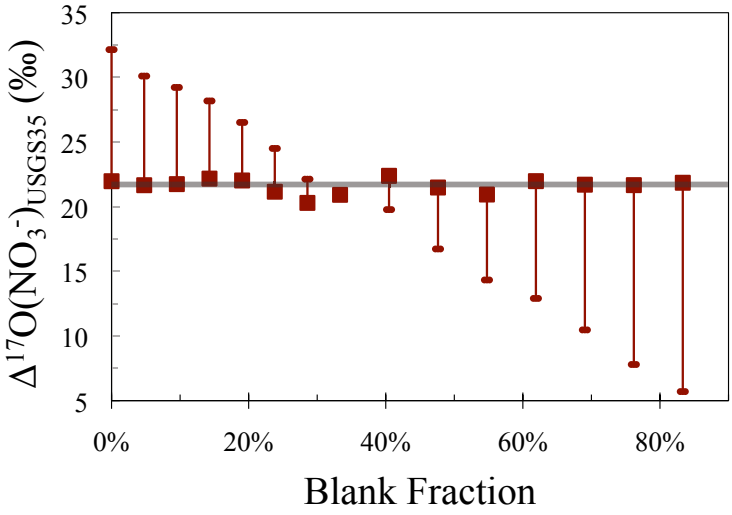

FIGURE 2.8 - $\Delta^{17}O(NO_3^-)$ measurements as a function of blank fraction for the USGS35/blank mixtures. The solid square symbols denote the corrected $\Delta^{17}O(NO_3^-)$ values obtained using Equation 2.1. The sizes of the symbols are equivalent to the standard deviation of the corrected values (± 0.6‰). The error bars denote the size of the correction in terms of the original $\Delta^{17}O(NO_3^-)$ values, which were calibrated to references prepared at a 33% blank level. The solid grey line represents the accepted $\Delta^{17}O$ value of USGS35 (21.6‰ relative to VSMOW).

$\Delta^{17}O$ values were calculated for the USGS35/blank mixtures using the empirical slope formed between $\delta^{15}N$ and $\Delta^{17}O$:

$$\Delta^{17}O_{USGS35} = \Delta^{17}O_{meas.} - \left[-1.37 \times \left(\delta^{15}N_{USGS35} - \delta^{15}N_{meas.}\right)\right] \quad (2.1)$$

The results of the $\delta^{15}N$-based correction are shown in **Figure 2.8**. The corrected $\Delta^{17}O$ values for the USGS35/blank mixtures average 21.6‰, in excellent agreement with the accepted value for USGS35, and vary within a remarkably narrow range (1σ = 0.6‰). Furthermore, the efficacy of the correction appears to be insensitive to the absolute difference in blank level between the standards and the USGS35 mixtures.

It should be noted that this approach to correcting $\Delta^{17}O$, when applied to nitrate formed on nitrite-coated filters via reaction with ozone, depends strongly on the assumption that kinetic isotope effects (KIEs) associated with the $O_3 + NO_2^-$ reaction do not enrich or deplete ^{15}N in the nitrate formed relative to the initial isotopic composition of the nitrite reagent. Observational accounts of isotope effects during the $O_3 + NO_2^-$ reaction are currently lacking in the literature. However, the atmospheric reaction of ozone with nitrogen dioxide (NO_2) is typically assumed to induce no partitioning ^{15}N (Freyer *et al.*, 1993; Hastings *et al.*, 2003). Furthermore, nitrogen isotope ratio measurements for the samples produced via reaction with laboratory ozone appear to validate this assumption. These samples yielded calibrated

δ^{15}N values of 2.8 ± 0.6‰, suggesting only a slight enrichment in ^{15}N over the nitrite reagent.

2.3.4 Isotope transfer during the $O_3 + NO_2^-$ reaction

The $NaNO_2$ reagent used to coat the filters was analyzed via the denitrifier method along with local $NaNO_2$ isotopic references described by Casciotti *et al.* (2007) (**Table 2.1)** and was found to possess δ^{18}O and δ^{15}N values of 16.7 ± 0.8‰ and 1.5 ± 0.2‰, respectively (n = 20). Although the RSIL $NaNO_2$ references do not have accepted δ^{17}O values, raw isotopic measurements of the $NaNO_2$ coating reagent suggest that it carries no ^{17}O-excess ($\Delta^{17}O_{raw}$ = -0.07‰ ± 0.22‰). Measured Δ^{17}O values for the filter sample nitrate are thus effectively diluted due to the presence of two oxygen atoms with $\Delta^{17}O \approx 0$‰, and the Δ^{17}O value of the oxygen atom transferred to form nitrate, $\Delta^{17}O(O_3^*)$, can be inferred by multiplying the calibrated $\Delta^{17}O(NO_3^-)$ values by three. Similarly, $\delta^{18}O(O_3^*)$ can be inferred using the same mass-balance approach:

$$\delta^{18}O(O_3^*) = 3\times\delta^{18}O(NO_3^-) - 2\times\left[\delta^{18}O(NaNO_2) = 16.7‰\right] \quad (2.2)$$

where $\delta^{18}O(NaNO_2)$ refers to δ^{18}O value of the nitrite trapping reagent.

The results of all isotope transfer experiments are summarized in **Figure 2.9a**, which shows the empirical relationship between the bulk oxygen anomalies of ozone generated via electrical discharge, denoted $\Delta^{17}O(O_3)_{bulk}$, and $\Delta^{17}O(O_3^*)$. Linear regression analysis reveals a strong correlation between these two variables ($\Delta^{17}O(O_3^*) = 1.28 \times \Delta^{17}O(O_3)_{bulk} + 7.6$‰, r = 0.97, n = 17), indicating that the anomalous oxygen signature of ozone is transferred to the filter in a quantitative and reproducible manner, despite the high blank level. Furthermore, the slope and intercept of the regression are very similar to those reported by Berhanu *et al.* (2012) for isotope transfer during the gas-phase $O_3 + NO_2$ reaction ($\Delta^{17}O(O_3^*) = 1.23 \times \Delta^{17}O(O_3)_{bulk} + 9.0$‰). These observations suggest that the nitrite-coated filter method is indeed an appropriate and reliable means for determining oxygen isotopic ratios of the transferable O-atom of ambient tropospheric ozone.

The observed relationship between $\Delta^{17}O(O_3)_{bulk}$ and $\Delta^{17}O(O_3^*)$ is in excellent agreement with theoretical postulates that place the ^{17}O-excess on only the terminal

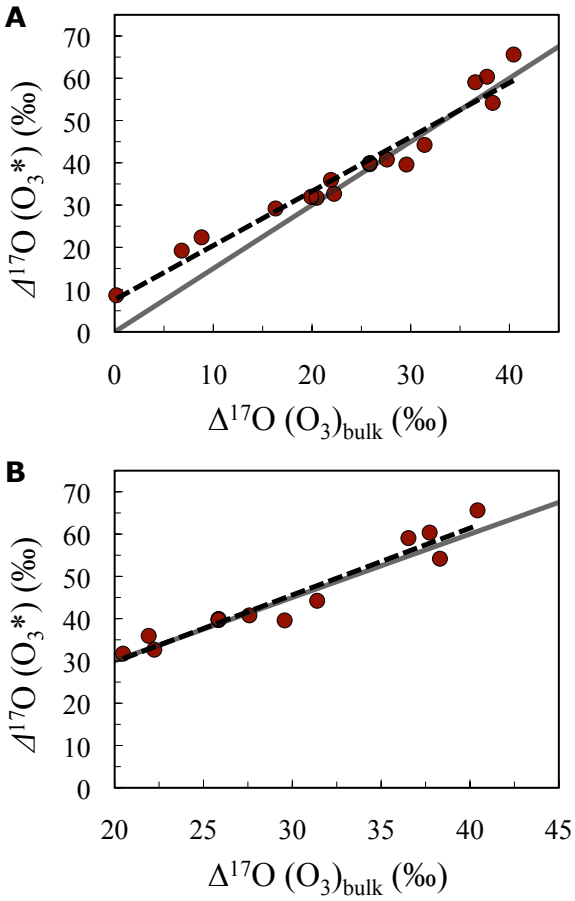

FIGURE 2.9 - Linear regressions of the bulk ^{17}O-excess of ozone, $\Delta^{17}O(O_3)_{bulk}$, produced in the isotope transfer experiments against $\Delta^{17}O(O_3^*)$, the ^{17}O-excess transferred to nitrate, for **(a)** all of the individual experiments ($\Delta^{17}O(O_3)_{bulk}$ = 0 - 40‰ range) and **(b)** for the expected atmospheric $\Delta^{17}O(O_3)_{bulk}$ range (20 - 40‰). The uncertainty of these measurements is estimated as the reduced standard deviation of the residuals from the linear regression between the measured reference materials (n= 12 for each batch) and their expected values (**Table 2.1**) and is represented approximately by the size of the symbols. The expected theoretical relationship of $\Delta^{17}O(O_3^*) = 1.5 \times \Delta^{17}O(O_3)_{bulk}$ is shown in each plot as a solid grey line.

oxygen atoms of ozone (Gellene, 1996; Gao and Marcus, 2001). Such arguments suggest that the $\Delta^{17}O$ value of the terminal oxygen atom is related to that of the bulk ozone molecule as follows:

$$\Delta^{17}O(O_3)_{terminal} = 1.5 \times \Delta^{17}O(O_3)_{bulk} \qquad (2.3)$$

For the $O_3 + NO_2^-$ transfer reaction, the participation of the terminal atom is energetically favored (Liu *et al.*, 2001) and $\Delta^{17}O(O_3)_{terminal}$ is therefore expected to be equal to $\Delta^{17}O(O_3^*)$. For the vacuum-line experiments in the $\Delta^{17}O(O_3)_{bulk}$ = 20 - 40‰ range (**Figure 2.9b**), the observed isotope transfer function is in very close agreement with the relationship predicted by Equation 2.3 ($\Delta^{17}O(O_3^*) = 1.55 \times \Delta^{17}O(O_3)_{bulk}$ + 0.7‰, r = 0.97, n = 12). This finding both lends credence to the theoretical basis of such arguments and indicates that the nitrite-coated filter method is sufficiently robust to be applied to the analysis of stable isotope ratios of tropospheric ozone. However, an intriguing point to note is the existence of a large positive intercept (7.6‰) in the regression line for the full range of $\Delta^{17}O(O_3)_{bulk}$ values and the divergence of the empirical slope from that expected by theory in the $\Delta^{17}O(O_3)_{bulk}$ = 0 - 10‰ range

(**Figure 2.9a**). This suggests that, at very low $\Delta^{17}O(O_3)_{bulk}$ values, the terminal position has a slightly larger ^{17}O-excess than expected based on the simple 3/2 rule of Equation 2.3. Recent studies have experimentally demonstrated that the ^{17}O-excess of ozone is indeed contained entirely in the terminal location (Bhattacharya *et al.*, 2008; Savarino *et al.*, 2008; Michalski and Bhattacharya, 2009); however, these studies consider only ozone with $\Delta^{17}O(O_3)_{bulk}$ values in the range of 10 to 30‰. Studies of the gas-phase reaction of ozone and nitric oxide (NO) conducted by Berhanu *et al.* (2012) show comparable deviations from the 3/2 rule in the 0 - 10‰ range, suggesting a variation in either the presumed internal isotope distribution of ozone or the relative involvement of the terminal oxygen atoms over the central position. This apparent deviation from theory may be related to the electrical discharge method of ozone production; i.e., the intramolecular distribution of oxygen isotopes in ozone generated via electrical discharge and/or electrolysis may differ somewhat from isotopic distributions observed in the atmosphere. Such differences between natural and laboratory-produced ozone are currently not well understood and are important topics for future research; however, these complex experimental issues are beyond the scope of this study. For our purposes, the correlation observed between the $\Delta^{17}O$ of the ozone produced and that of the nitrate formed can be simply taken to indicate that isotope transfer at the filter surface proceeds in a repeatable and linear fashion; however, this regression is not used as a means of calibrating measurements of $\Delta^{17}O(NO_3^-)$ to produce estimates for $\Delta^{17}O(O_3)_{bulk}$. In the analysis that follows, $\Delta^{17}O(NO_3^-)$ values for the ambient collections have been converted to $\Delta^{17}O(O_3)_{bulk}$ estimates by assuming a terminal atom transfer equal to 3/2 of the bulk ambient value; this theoretical relationship appears to be a good approximation for the $\Delta^{17}O(O_3)_{bulk}$ range expected under tropospheric/stratospheric temperature and pressure conditions (20 - 40‰, **Figure 2.9b**) (Krankowsky *et al.*, 1995; 2007; Johnston and Thiemens, 1997). The data has been presented this way to allow for the direct comparison of our measurements to those reported in the literature, which are exclusively measurements of bulk ozone; however, it should be kept in mind that $\Delta^{17}O(NO_3^-)$ and $\Delta^{17}O(O_3^*)$, equal to three times the measured $\Delta^{17}O(NO_3^-)$ value, are the only directly and unambiguously measured variables.

The total uncertainty of the method can be estimated for the isotope transfer experiments by comparing estimates of $\Delta^{17}O(O_3)_{bulk}$ (i.e., the calibrated $\Delta^{17}O(NO_3^-)$

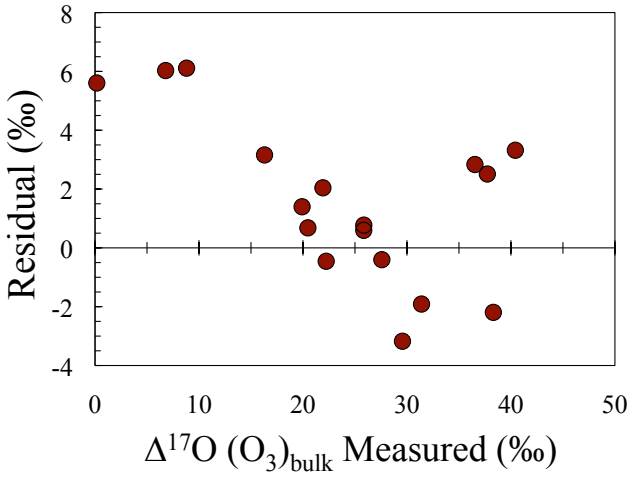

FIGURE 2.10 - Residuals between the inferred $\Delta^{17}O(O_3)_{bulk}$ values (i.e., two times the $\Delta^{17}O$ of the nitrate formed) and the actual $\Delta^{17}O(O_3)_{bulk}$ values for each isotope transfer experiment, plotted as a function of the actual $\Delta^{17}O(O_3)_{bulk}$.

values times two) with the actual $\Delta^{17}O(O_3)_{bulk}$ values obtained for the ozone produced in each experiment. The residuals between the inferred and measured values are shown in **Figure 2.10** and denote the total uncertainty of the technique, including: i) the analytical uncertainty inherent in the dual-inlet and continuous-flow IRMS measurements (**Table 2.3**), ii) the error arising from possible interferences or contamination of the experimental filters, and iii) the uncertainty caused by assuming a 3/2 relationship between $\Delta^{17}O(O_3)_{bulk}$ and $\Delta^{17}O(O_3^*)$. For the $\Delta^{17}O(O_3)_{bulk}$ = 0 - 10‰ range, residuals are relatively high (~6‰) as the assumption of a 3/2 rule appears to be invalid in this range. However, for the $\Delta^{17}O$ range of 10 - 40‰, inferred $\Delta^{17}O(O_3)_{bulk}$ values are much more similar to the $\Delta^{17}O(O_3)_{bulk}$ values measured for the experimental ozone. This is particularly true for the 20 - 30‰ range, where the residuals indicate an average overall uncertainty of ± 1.25‰ in terms of $\Delta^{17}O(O_3)_{bulk}$. This value is not appreciably higher than the analytical uncertainty of the isotopic measurements themselves, which averaged 0.50‰, but reached values as high as 0.80‰ (1.00‰ and 1.60‰ in terms of $\Delta^{17}O(O_3)_{bulk}$) as shown in **Table 2.3**. The mean absolute value of the residuals for the entire 10 - 40‰ range yields an uncertainty estimate of ± 1.71‰.

2.3.5 Isotopic composition of ambient samples

2.3.5.1 Sample nitrate

The oxygen triple-isotope composition of the nitrate extracted from ambient sample filters is summarized in **Figure 2.11a**. Samples from the three different series of

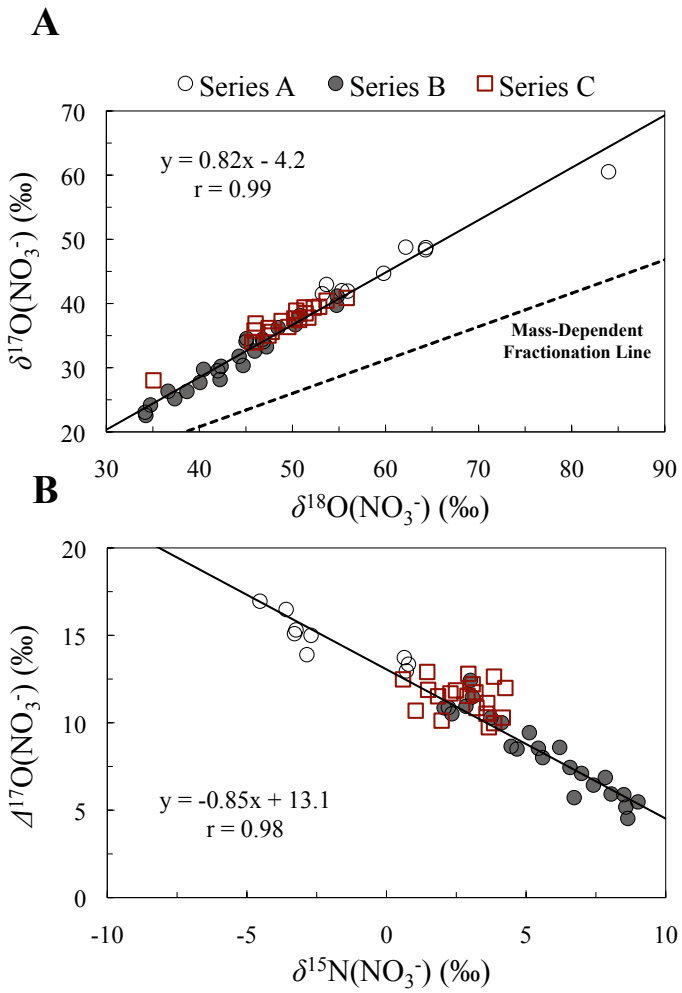

FIGURE 2.11 - **(a)** Oxygen three-isotope plot showing the mass-independent isotopic composition of the nitrate produced on the ambient sampling filters. **(b)** Correlation observed between $\delta^{15}N$ and $\Delta^{17}O$ for the nitrate in sample extracts for the Series A and Series B collections. The $\delta^{15}N$ of the nitrite reagent is approximately 1.5 ± 0.2‰. The Series C $\delta^{15}N$ values show no correlation with $\Delta^{17}O$.

TABLE 2.4 - Ozone Collection Efficiency and Nitrate Isotope Ratios for Series B Collections.

	n	Collection Efficiency[a] (%)	$\delta^{17}O(NO_3^-)$ (‰)	$\delta^{18}O(NO_3^-)$ (‰)	$\Delta^{17}O(NO_3^-)$ (‰)	$\delta^{15}N(NO_3^-)$ (‰)
Day[b]	15	100 ± 27	28.7 ± 4.6	40.9 ± 5.5	7.2 ± 1.9	6.6 ± 2.1
Night	4	60 ± 4	37.4 ± 3.0	49.8 ± 4.1	11.3 ± 0.8	2.7 ± 0.4
24-hr	5	80 ± 11	34 ± 1.8	47.1 ± 2.1	9.4 ± 0.8	4.7 ± 1.0

[a] Defined as the molar ratio of the blank-corrected nitrate mass recovered from filter extracts to the total ozone throughput. The overall collection efficiency of the sampling apparatus as determined with the calibrated ozone source (**Figure 2.4**) is 58 ± 5% for normal sampling conditions

[b] Day and night refer to samples collected between approximately 10:00 - 18:00 and 18:00 - 10:00, respectively

collections occupy distinct regions of the oxygen three-isotope plot. The Series A collections, whose isotope ratios were over-calibrated due to inadequate peak matching (i.e., SRM peak areas were 20 - 30% smaller than those corresponding to the samples, see Section 2.2.8), carry the highest enrichments, with $\delta^{17}O$ and $\delta^{18}O$ values of 46.6 ± 6.0‰ and 61.4 ± 9.5‰, respectively, corresponding to $\Delta^{17}O(NO_3^-)$ values of 14.8 ± 1.4‰. The Series B collections suffered from a large accumulation of nitrate blank due to light exposure, which is apparent in the large differences observed between the daytime and nighttime samples (**Table 2.4**). For Series B samples collected during the morning and afternoon, when the sampling apparatus was exposed to direct sunlight, the apparent collection efficiency of the sampler averaged 100 ± 27%. This range of recoveries is much larger and more variable than that observed for the preliminary tests conducted with a calibrated ozone source (58 ± 5%) or for the Series C collections (64 ± 10%) when the coated filters were protected from UV-exposure with aluminum foil (**Figure 2.4**). However, for the nighttime Series B collections, observed ozone recovery was 60 ± 4%, consistent with both Series C and the preliminary studies. The differences in recovery observed between the daytime and nighttime Series B collections correspond to an average photo-induced nitrate accumulation rate of 2.8 ± 1.8 μmol L^{-1} hr^{-1}. This rate is much higher than that inferred from the parallel collections using covered and uncovered samplers (0.56 ± 0.37 μmol L^{-1} hr^{-1}); however, the Series B collections were collected under particularly warm and clear-sky conditions in late July and early August, whereas the parallel tests were conducted during a relatively cool and overcast period in September. These considerable rates of background nitrate accumulation observed for the daytime Series B samples are associated with corresponding differences in nitrate isotope ratios. $\delta^{17}O$, $\delta^{18}O$, and $\Delta^{17}O$ are systematically lower for the daytime collections, while $\delta^{15}N$ is higher. This effect is integrated over the 24-hour collection periods; therefore, the 24-hour samples have collection efficiencies and isotope ratios that fall between those of the daytime and nighttime collections.

$\delta^{15}N(NO_3^-)$ values for the Series C collections varied within a relatively narrow range (2.8 ± 1.1‰) and exhibited no correlation with $\Delta^{17}O(NO_3^-)$. However, in the case of the Series A collections, the nitrate sample was observed to be significantly depleted in ^{15}N relative to the nitrite reagent ($\delta^{15}N$ = -2.0 ± 2.1) due to the overcorrection of these samples. Similarly, the Series B collections exhibit significantly increased $\delta^{15}N(NO_3^-)$ values (5.5 ± 2.3‰) due to the high level of blank

accumulation during these sampling periods (**Table 2.4**). In both cases, the $\delta^{15}N$ values observed for the nitrate samples are strongly correlated with their $\Delta^{17}O$ values (r = 0.98) (**Figure 2.11b**). This effect is largely consistent with the calibration dynamics described earlier with regards to the USGS35 recovery experiment (**Figure 2.7**). Taking the same approach used in that analysis, we have corrected the calibrated $\Delta^{17}O(NO_3^-)$ values for the Series A and Series B collections using the empirical slope between $\delta^{15}N$ and $\Delta^{17}O$ (**Figure 2.11b**) as in Equation 2.1. Because no correlations were observed among the nitrogen and oxygen isotope ratios of the Series C samples, these measurements have not been corrected.

2.3.5.2 $\Delta^{17}O$ of tropospheric ozone

$\Delta^{17}O$ values for the three series of ambient ozone collections are summarized in **Figure 2.12**. For the Series A and Series B collections, the difference between the $\delta^{15}N$-corrected values and the original calibrated values in terms of $\Delta^{17}O(O_3)_{bulk}$ are indicated by error bars. For the Series A collections, applied corrections are strongly correlated with total ozone throughput (**Figure 2.13a)**, suggesting that $\Delta^{17}O$ measurements of relatively small samples (< 150 ppb•hr) are highly sensitive to the calibration peak-matching routine described in Section 2.2.8. As anticipated, the correction sizes for the Series B collections are a strong function of the nitrate blank accumulation rate observed for the individual samples (**Figure 2.13b)**. For the Series B overnight collections, which exhibited collection efficiencies in the same range as established using the calibrated ozone source (**Figure 2.4**), the absolute correction sizes are rather small (2.0 ± 0.8‰). However, for the samples collected during daylight hours, corrections sizes average 8.7 ± 3.6‰, with a maximum correction of 12.8‰ applied to the sample with the largest inferred nitrate blank accumulation rate (5.9 μmol L^{-1} hr^{-1}). Because the Series C collections were obtained using the most refined version of the protocol (i.e., high-purity $NaNO_2$ reagent, protection from exposure to ambient radiation, meticulous peak matching with SRMs, etc.), they can be considered as an ideal case for comparison to the Series A and Series B collections. Isotopic results for the Series C collections are summarized in **Table 2.5**, while variations with respect to time are shown in **Figure 2.14** along with local ozone mixing ratio measured during the periods of sample collection.

The corrected $\Delta^{17}O(O_3)_{bulk}$ values are remarkably consistent between the three different collection series, with average ± 1σ values of 23.5 ± 1.8‰, 23.5 ± 1.5‰, and

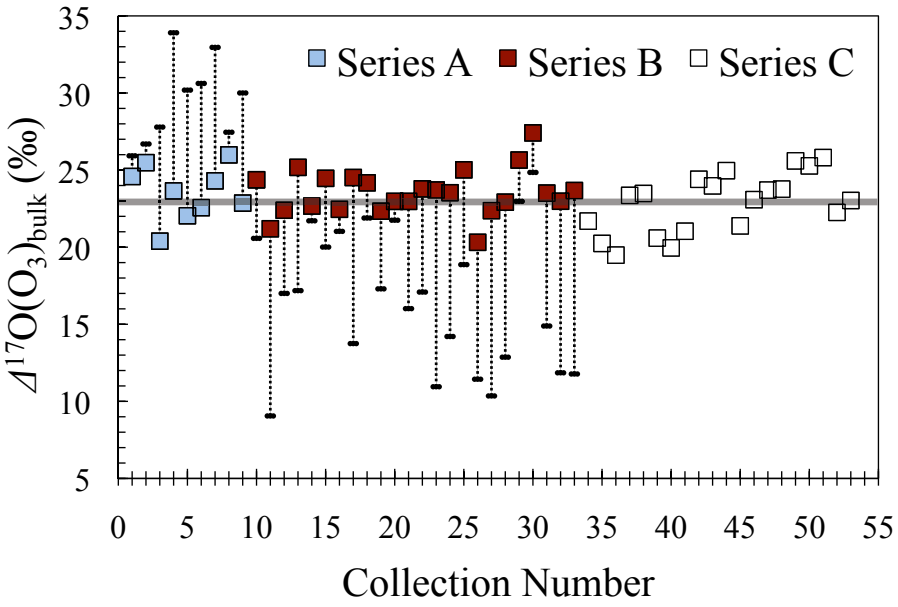

FIGURE 2.12 - $\Delta^{17}O(O_3)_{bulk}$ values for the three series of ambient collections: Series A (nr. 1 - 9), Series B (nr. 10 - 33), and Series C (nr. 34 - 53). The error bars represent the distance between the $\delta^{15}N$-corrected and uncorrected values for the Series A and Series B collections. The Series C collections have not been corrected. The average $\Delta^{17}O(O_3)_{bulk}$ value obtained for the Series C collections (23‰) is indicated by a solid grey line.

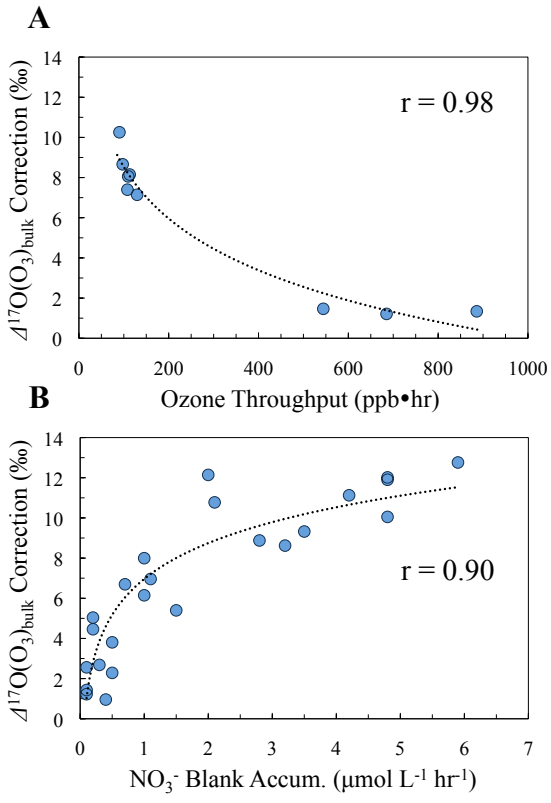

FIGURE 2.13 - Absolute differences between the $\delta^{15}N$-corrected values and the original calibrated values in terms of $\Delta^{17}O(O_3)_{bulk}$ for the **(a)** Series A and **(b)** Series B collections. The $\Delta^{17}O$ corrections for the Series A collections are shown as a function of total ozone sample size in ppb•hr. The corrections for the Series B samples are plotted against the calculated nitrate blank accumulation rate, which was inferred from the difference between the apparent collection efficiency for each Series B sample and the collection efficiency determined using a calibrated ozone source (58%) (**Figure 2.4**).

TABLE 2.5 - Oxygen Isotope Ratios for the Series C Ambient Ozone Samples.

Sample Collection Mid-point	Sample Duration (hr)	Ave. O_3 Conc. (ppb)	$\delta^{17}O$ (NO_3^-) (‰)	$\delta^{18}O$ (NO_3^-) (‰)	$\Delta^{17}O$ (NO_3^-) (‰)	$\delta^{18}O$ (O_3*) (‰)	$\Delta^{17}O$ $(O_3)_{bulk}$ (‰)	$\Delta^{17}O$ (O_3*) (‰)
06/09/11 15:02	5.9	16	37.8	51.7	10.8	121.8	21.7	32.5
07/09/11 02:04	15.8	4	34.0	45.7	10.1	103.7	20.2	30.4
07/09/11 12:34	4.7	11	28.0	35.1	9.7	71.9	19.5	29.2
07/09/11 16:36	3.1	20	38.5	51.4	11.7	120.9	23.4	35.0
08/09/11 02:21	16.1	4	37.3	48.8	11.7	113.2	23.5	35.2
08/09/11 12:28	3.8	14	35.0	47.4	10.3	108.9	20.6	30.9
09/09/11 01:25	16.7	7	34.0	46.0	10.0	104.7	20.0	29.9
09/09/11 12:02	4.1	15	36.3	49.6	10.5	115.3	21.0	31.5
18/10/11 14:15	8.0	10	39.4	52.3	12.2	123.6	24.4	36.6
19/10/11 13:16	8.4	5	39.5	52.9	12.0	125.3	24.0	36.0
20/10/11 01:33	15.9	5	40.4	53.7	12.5	127.7	25.0	37.4
20/10/11 13:04	6.9	14	35.6	47.8	10.7	110.0	21.4	32.1
21/10/11 01:00	16.7	8	36.2	47.4	11.5	109.0	23.1	34.6
21/10/11 12:14	5.5	8	40.9	55.8	11.9	134.2	23.7	35.6
24/10/11 16:01	2.3	28	35.8	45.9	11.9	104.4	23.8	35.6
25/10/11 01:58	17.4	20	39.4	51.3	12.8	120.6	25.6	38.4
25/10/11 13:58	6.2	7	38.9	50.4	12.6	117.9	25.3	37.9
26/10/11 01:29	16.6	7	36.9	46.0	12.9	104.8	25.8	38.7
26/10/11 21:56	24.1	6	37.4	50.7	11.1	118.8	22.3	33.4
28/10/11 01:35	30.9	3	37.7	50.2	11.5	117.3	23.0	34.5
Average	***11.5***	***10.5***	***36.9***	***49.0***	***11.4***	***113.7***	***22.9***	***34.3***
Std. Dev.	***7.8***	***6.7***	***2.9***	***4.3***	***1.0***	***13.0***	***1.9***	***2.9***

[a] Calculated using the mass balance in Equation 2.1. Estimates for $\delta^{18}O(O_3)_{bulk}$ can be obtained using the empirical relationships reported in Bhattacharya *et al.* (2008) and show a good agreement with the $\delta^{18}O(O_3)_{bulk}$ data reported by Krankowsky *et al.* (1995) and Johnston and Thiemens (1997) for the cryogenic method
[b] Values for $\Delta^{17}O(O_3)_{bulk}$ have been inferred by taking two times the measured $\Delta^{17}O(NO_3^-)$ for each sample
[c] Values for $\Delta^{17}O(O_3^*)$ have been inferred by taking three times the measured $\Delta^{17}O(NO_3^-)$ for each sample

22.9 ± 1.9‰ for the Series A, B, and C collections, respectively. This indicates that the $\delta^{15}N(NO_3^-)$ measurements for the ambient samples indeed serve as sensitive tracers for errors arising from isotope ratio normalization procedure and allow for a robust evaluation and correction of the ambient $\Delta^{17}O$ data. Furthermore, the $\Delta^{17}O(O_3)_{bulk}$ values obtained largely consistent with the range of values obtained previously with the cryogenic trapping technique: $\Delta^{17}O(O_3)_{bulk}$ = 25 ± 11‰ and 26 ± 5‰ for the Krankowsky *et al.* (1995) and Johnston and Thiemens (1997) studies, respectively. However, the magnitude of variability found in these landmark studies is conspicuously absent from our first nitrite-coated filter results. As pointed out by Morin *et al.* (2007), the considerable scatter in the ozone $\delta^{17}O$ and $\delta^{18}O$ values obtained with the cryogenic technique is likely the result of random error and therefore may not be representative of real variations in $\Delta^{17}O(O_3)$. Furthermore, the scale of variability observed in these studies is not quantitatively consistent with a theoretical assessment of $\Delta^{17}O(O_3)_{bulk}$ variability based on the known temperature and pressure dependencies of $\delta^{17}O$ and $\delta^{18}O$ enrichments associated with the ozone formation reaction (Thiemens and Jackson, 1988; 1990; Morton *et al.*, 1990; Janssen *et al.*, 2003). These observations suggest that it is perhaps more appropriate to consider the average values of the cryogenic measurements rather than the full range obtained. Brenninkmeijer *et al.* (2003) have critically evaluated the existing datasets obtained with the cryogenic technique and have inferred average $\Delta^{17}O(O_3)_{bulk}$ values of 24 ± 3‰ and 25 ± 2‰ from the Krankowsky *et al.* (1995) and Johnston and Thiemens (1997) studies, respectively, in excellent agreement with the measurements reported here, although somewhat lower than the 27 ± 5‰ average value recommended in the analysis of Morin *et al.* (2007). Given the possibility of small, undetected or underestimated systematic errors in both experimental approaches, the comparability of the $\Delta^{17}O$ data produced using the cryogenic and the nitrite-coated filter collection techniques is highly encouraging. Another satisfying result is the agreement between the cryogenic and nitrite-coated filter datasets in terms of $\delta^{18}O$. The $\delta^{18}O(NO_3^-)$ values measured for the Series C collections (49 ± 4‰) can be converted to $\delta^{18}O(O_3^*)$ using Equation 2.2, which results in estimates of 104 - 134‰, with the exception of one outlier (**Table 2.5**). The bulk and terminal $\delta^{18}O$ enrichments of ozone can be related using the empirical relationship obtained in experiments by

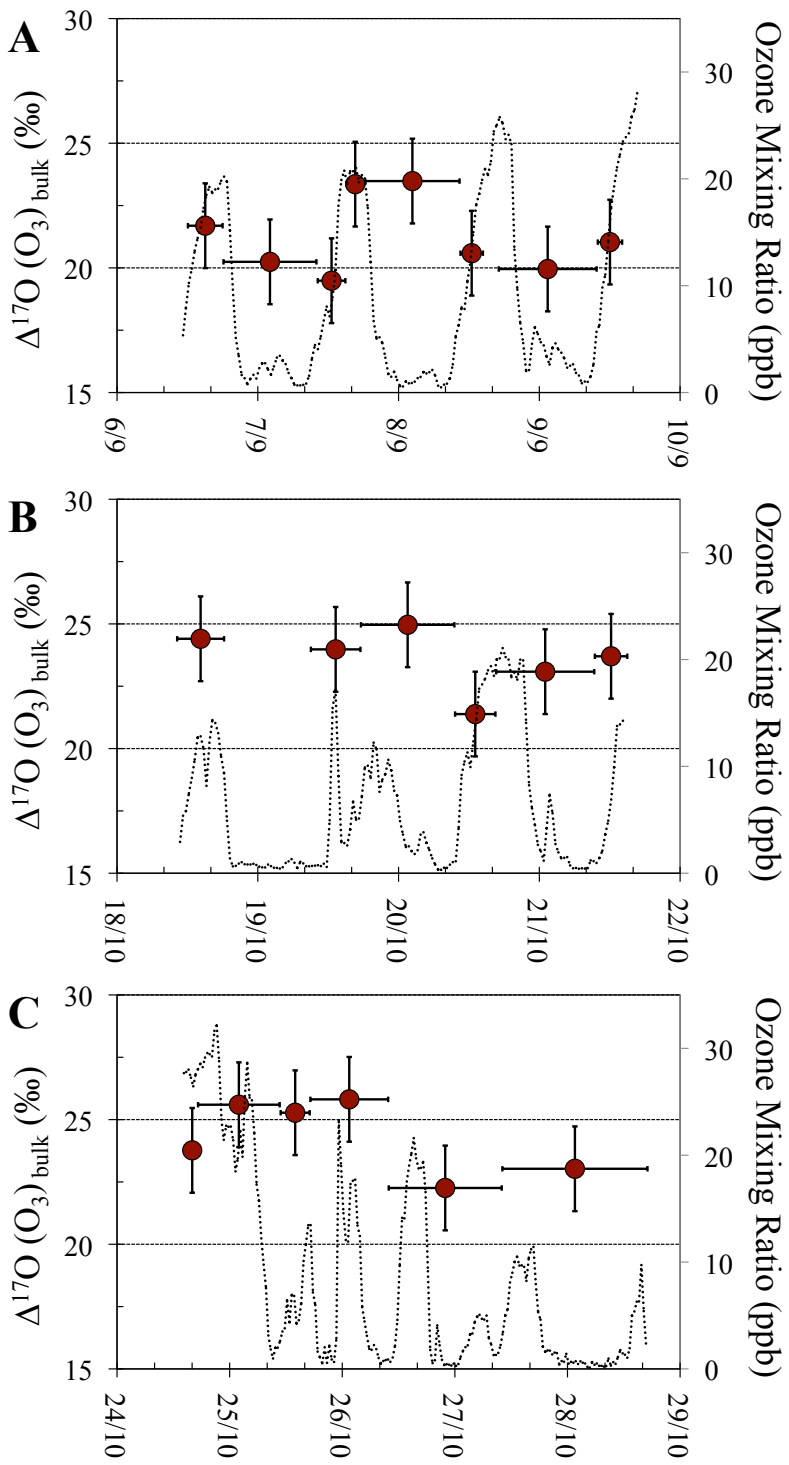

FIGURE 2.14 - Time-series for the Series C field collections on **(a)** 6 - 9 September, **(b)** 18 - 21 October, and **(c)** 24 - 28 October 2011. Inferred tropospheric $\Delta^{17}O(O_3)_{bulk}$ values (two times the $\Delta^{17}O(NO_3^-)$ measured for each ambient sample) are shown as solid circles (primary y-axis). Vertical error bars represent the total uncertainty estimated for the technique in the $\Delta^{17}O(O_3)_{bulk}$ = 10 - 40‰ range (± 1.7‰). Horizontal error bars represent the total duration of each sample collection period. Ambient ozone concentrations during the time of sample collection are shown as 30-minute averages connected by a smoothed dotted line (secondary y-axis).

Bhattacharya *et al.* (2008), which yields $\delta^{18}O(O_3)_{bulk}$ estimates of 103 ± 7‰. The $\delta^{18}O(O_3)_{bulk}$ values reported by Krankowsky *et al.* (1995) and Johnston and Thiemens (1997) average 91 ± 6‰ and 84 ± 7‰, respectively. However, the cryogenic isotope ratio measurements were reported with respect to air O_2, which is +23.5‰ relative to VSMOW (Kroopnick and Craig, 1972). Expressed on the VSMOW scale, the cryogenic $\delta^{18}O(O_3)_{bulk}$ measurements average 117 ± 6‰ and 109 ± 7‰ for the Krankowsky *et al.* (1995) and Johnston and Thiemens (1997) datasets, respectively, in favorable comparison with the $\delta^{18}O(O_3)_{bulk}$ values inferred here. This indicates that the nitrite-coated filter method may serve as a robust means for assessing $\delta^{18}O$ variations in tropospheric ozone in addition to $\Delta^{17}O$.

Although the $\Delta^{17}O(O_3)_{bulk}$ values obtained in this study are largely consistent with the tropospheric observations reported in the literature, they are somewhat lower than the value anticipated based on the experimental temperature and pressure dependency data (Thiemens and Jackson, 1988; 1990; Morton *et al.*, 1990; Janssen *et al.*, 2003). For average surface pressure and temperature conditions, the laboratory studies predict average enrichments for tropospheric ozone of $\delta^{17}O(O_3)_{bulk}$ = 85 ± 6‰ and $\delta^{18}O(O_3)_{bulk}$ = 101 ± 6‰ (relative to VSMOW), which corresponds to an average $\Delta^{17}O(O_3)_{bulk}$ value of 32.4‰ (e.g., see Brenninkmeijer *et al.* (2003) and references therein). This expected value is 9‰ higher than the average value found here (although it is interesting to note that, perhaps coincidentally, the average $\delta^{18}O(O_3)_{bulk}$ value estimated for the measurements described here (103 ± 7‰) is in almost perfect harmony with the predictions based on the experimental data). It is therefore important to evaluate the potential impact of sampling interferences. While interferences from atmospheric NO_y and HNO_3 were found to be negligible (**Table 2.2**), there also exists the possibility of positive interferences from weak atmospheric oxidants, such as O_2. It is reasonable to assume that such interferences are more likely to have a significant quantitative impact on the nitrite-coated filter collection technique when ambient ozone mixing ratios are low, such as was the case in this study. In **Figure 2.15**, corrected $\Delta^{17}O(O_3)_{bulk}$ values for the samples obtained during the three collection series are shown as a function of the average ozone concentration observed during the sampling period (**Figure 2.15a**) and as a function of total sample size (**Figure 2.15b**). The lowest $\Delta^{17}O(O_3)_{bulk}$ values (20 - 21‰) are clearly associated with ambient ozone concentrations lower than 20 ppb. These low values are further associated with low total sample sizes (< 150 ppb•hr). Conversely, for samples that

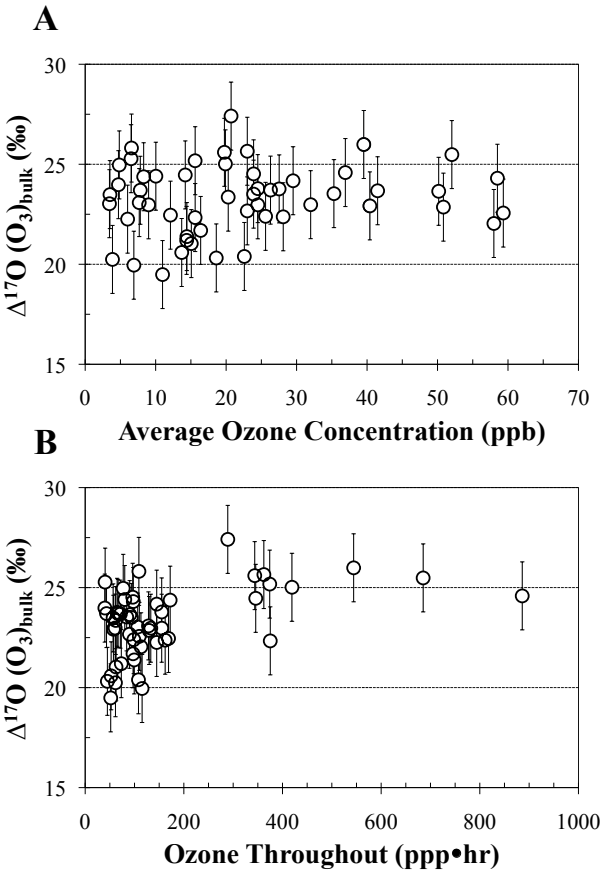

FIGURE 2.15 - Corrected $\Delta^{17}O(O_3)_{bulk}$ values for the 53 ambient collections discussed in this study (Series C samples have not been corrected) plotted against **(a)** the average ozone concentration observed during collection and **(b)** total ozone throughput (ppb•hr). Vertical error bars represent the total uncertainty estimated for the technique in the $\Delta^{17}O(O_3)_{bulk}$ = 10 - 40‰ range (± 1.7‰).

were collected at ambient concentrations > 20 ppb for durations corresponding to total sample sizes > 150 ppb, $\Delta^{17}O(O_3)_{bulk}$ = 24.9 ± 1.5‰. These observations seem to signify an increased impact of interferences for samples collected during periods of low ozone concentration. Assuming that the interfering oxidant in question transfers a $\Delta^{17}O$ equal to zero, the quantitative impact of these interferences can be estimated in terms of $\Delta^{17}O(O_3)$ by simple mass-balance:

$$\Delta^{17}O(O_3)_{actual} = \frac{\Delta^{17}O(O_3)_{measured}}{f}$$

(2.4)

where f is the fraction of nitrate on the sample filter produced through the $O_3 + NO_2^-$ reaction. The strong correlation (r = 0.94) found between ozone throughput and nitrate formation for the ambient collections (**Figure 2.4**) indicates that the impact of interferences was relatively small (i.e., the vast majority of nitrate formation on the ambient sample filters can be attributed to reaction with ozone). Furthermore, the absence of large variations in $\Delta^{17}O(O_3)$ between periods of high and low ozone

concentration during the Series C collection period (**Figure 2.14**) is further evidence that the impact of interferences from oxidants other than ozone was likely negligible. If an average of 5% of the nitrate formed on the ambient collection filters is assumed to be attributable to such interferences ($f = 0.95$), we estimate a negative interference of 1.2‰ in terms of the mean $\Delta^{17}O(O_3)_{bulk}$ value found in this study, consistent with the difference in $\Delta^{17}O(O_3)_{bulk}$ observed between periods of low and high ozone concentrations. This is a relatively small error that is within the uncertainty reported for the technique (± 1.7‰); however, it should be noted that this is a directional effect that will always act to reduce the inferred $\Delta^{17}O(O_3)_{bulk}$ values. The participation of atmospheric oxidants possessing positive $\Delta^{17}O$ values (e.g., NO_x) would result in a smaller quantitative impact in terms of inferred $\Delta^{17}O(O_3)_{bulk}$. An assessment of the magnitude and variability of this effect under various sampling conditions is a key goal for future research.

An interesting point to note is that the standard deviation of all ambient $\Delta^{17}O(O_3)_{bulk}$ measurements (1.8‰) is close to the total uncertainty estimated above (1.7‰), indicating that the observed variations from the mean are not significant. This is an important result and one with implications for the use of ozone isotope transfer processes to quantify and constrain the rates of atmospheric processes. Most current approaches in the study of the ^{17}O-excess, both in the atmosphere and for geological materials (Böhlke *et al.*, 1997; Bao *et al.*, 2000), assume that $\Delta^{17}O(O_3)_{bulk}$ does not vary, either spatially, seasonally, or diurnally. Our observations would seem to lend credence to this assumption, at least in the case of diurnal variations. However, while significant variations are absent at the spatial and temporal scale of this study, it is not possible to conclude from these preliminary results that $\Delta^{17}O(O_3)_{bulk}$ does not vary on shorter (e.g., hourly) or longer (e.g., seasonal) frequencies. Furthermore, potential variations with latitude or altitude can certainly not be ruled out. Clearly, a more complete understanding of the nature and scale of variability in tropospheric $\Delta^{17}O(O_3)_{bulk}$ will require a great number of observations in different contexts and environments. Using the method described here, we can now investigate the potential seasonal, diurnal, and spatial features of ozone's ^{17}O-excess and also search for processes to explain these variations. Future research using the nitrite-coated filter method will thus undoubtedly lead to a more robust theoretical framework for interpreting natural $\Delta^{17}O$ variation and transfer in the atmosphere.

2.4 Conclusions and recommendations

The nitrite-coated filter method, a fusion of a previously existing technique for ozone concentration measurement and the bacterial denitrifier/thermal decomposition method, has been applied for the first time to the triple-oxygen isotopic characterization of tropospheric ozone. This method offers several advantages over previous techniques (Krankowsky *et al.*, 1995; Johnston and Thiemens, 1997): i) ozone collection involves simple technologies that can be implemented nearly anywhere (e.g., alpine and polar environments, remote ocean, stratosphere, etc.), ii) due to a relatively high flow rate and low sample size requirement, samples can be collected at a high frequency allowing for greater time resolution, iii) the method is not susceptible to a systematically low collection efficiency or interferences from other compounds, and iv) the method provides a direct isotopic measurement of the O-atom of ozone that is transferred during oxidation reactions, rather than a bulk isotopic measurement.

The results obtained in this study indicate that the coated-filter collection technique is a sufficiently robust and reliable method for routine application. Studies of ^{17}O-excess transfer show a strong linear correlation between $\Delta^{17}O(O_3)_{bulk}$ and the $\Delta^{17}O$ value of the nitrate formed on the filter, suggesting that isotope transfer at the filter surface proceeds in a repeatable and linear fashion. The transfer function found in these studies is in close agreement with previous investigations of the ozone/nitrite reaction and provides further substantiation of theoretical postulates that place the ^{17}O-excess on only the terminal oxygen atoms of ozone. First measurements of ambient tropospheric $\Delta^{17}O(O_3)$ are in good agreement with data obtained using the cryogenic technique. Significant variations in $\Delta^{17}O(O_3)$ were not observed at the time scale of this study; however, a true evaluation of $\Delta^{17}O(O_3)$ variability will require a systematic sampling approach on a wide range of spatial and temporal scales.

While this method is relatively straightforward, it nevertheless calls for great care in its use. Primarily, caution must be taken in the use of reagents for the normalization of nitrate concentration and isotopic data. Because the reagent nitrate blank (resulting mostly from the relatively high blank associated with $NaNO_2$ reagent) is large and may vary between batches of reagents, it is absolutely necessary that samples and standard references are processed in batches; i.e., groups of filter samples sharing the

same coating date, storage and transport conditions, etc., must be normalized to standards prepared with the same reagents used to coat the filters from that batch. Additionally, coated filters should be protected at all times from excessive exposure to light, which was found to lead to an accumulation of nitrate background that interfered with isotopic measurements. The $\delta^{15}N$ of the nitrate formed on the sample filters, which should be equal to the $\delta^{15}N$ signature of the $NaNO_2$ coating reagent, acts as a sensitive indicator of the accuracy of the $\Delta^{17}O$ calibration. Samples with enhanced blank levels (i.e., increased blank to sample ratio) exhibit systematically higher $\delta^{15}N$ and lower $\Delta^{17}O$ values and *vice versa*. The strong anticorrelation observed between these two variables provides a means for correcting the measured $\Delta^{17}O$ values. Therefore, $\delta^{15}N$ should always be measured in parallel with $\delta^{17}O$ and $\delta^{18}O$.

Chapter 3

Quantitative constraints on the ^{17}O-excess (Δ^{17}O) signature of surface ozone: Ambient measurements from 75°S to 50°N

This chapter is based on:

Vicars, W. C. and Savarino, J., Quantitative constraints on the ^{17}O-excess (Δ^{17}O) signature of surface ozone: Ambient measurements from 75°S to 50°N. *Geophysical Research Letters* **(to be submitted)**.

Abstract

The unique and distinctive ^{17}O-excess (Δ^{17}O) of ozone (O_3) serves as a valuable tracer for oxidative processes in both modern and ancient atmospheres; however, due to the inherent complexity of extracting ozone from ambient air, the existing observational dataset for ozone isotopic composition remains quite small. Recent analytical developments have provided a robust and reliable means for determining the transferrable Δ^{17}O of ozone (Chapter 2). We have employed this new methodology in a systematic investigation of the spatial and seasonal features of $\Delta^{17}O(O_3)$ in three separate field campaigns: (i) a weekly sampling effort at our laboratory in Grenoble, France (45 °N) throughout 2012 (n = 71); (ii) a four-week campaign onboard the Research Vessel (R/V) *Polarstern* along a latitudinal transect from 50 °S to 50 °N in the Atlantic Ocean (n = 30); and (iii) a daily sampling campaign on the Antarctic plateau (Dome C, 75 °S) during a four-week period in polar summer (n = 28). The ^{17}O-excess of bulk ozone, denoted $\Delta^{17}O(O_3)_{bulk}$, exhibited average (± 1σ) values of 26.2 ± 1.3‰, 25.9 ± 1.1‰, and 22.4 ± 1.7‰ for the Grenoble, R/V *Polarstern*, and Dome C collections, respectively. This range of values is in excellent quantitative agreement with the two previous studies of ozone triple-isotope composition, which have yielded average $\Delta^{17}O(O_3)_{bulk}$ values of 25.4 ± 9.0‰ (n = 89); however, the

magnitude of variability detected in the present study is much smaller than that formerly reported. In fact, the standard deviation of $\Delta^{17}O(O_3)_{bulk}$ in each dataset is consistent with the precision previously estimated for the filter technique (1.7‰), indicating a low level of natural spatial and temporal variability in the ^{17}O-excess of surface ozone. For instance, no clear temporal pattern in $\Delta^{17}O(O_3)$ is evident in the annual record from Grenoble despite dramatic seasonal variability in meteorological conditions and ozone and atmospheric reactive nitrogen concentrations. However, a small but statistically significant difference is distinguishable in the R/V *Polarstern* record when comparing samples collected in the Southern and Northern Hemispheres, which possessed average values of 25.3 ± 1.0‰ and 26.6 ± 0.7‰, respectively. The implications of these results are discussed in the context of the tropospheric ozone budget and the use of oxygen isotope ratios of secondary atmospheric species to derive information regarding oxidation pathways from modern and paleo-atmospheres.

3.1 Introduction

Stable isotope variations in atmospheric compounds are novel indicators of important earth system processes, often acting as source markers for trace gases and aerosols and providing both qualitative and quantitative constraints on the chemical and physical pathways that determine their fate. Isotope ratio measurements offer direct insight into the nature and magnitude of the fluxes associated with different processes, thus providing unique information regarding phenomena that are often difficult to quantify from concentration measurements alone. Stable isotope analysis has been particularly useful in the development of global trace gas budgets, a tool that has important applications in global change research. Furthermore, kinetic isotope effects (KIEs) associated with the removal of trace gases (e.g., reaction with OH, photolysis, etc.) provide a means for identifying and evaluating chemical reactions occurring in the atmosphere (Johnson *et al.*, 2002).

Research within the atmospheric isotope community in recent years has become increasingly focused on ozone (O_3). The reason for this is partly historical: the gas-phase ozone formation reaction exhibits a large and unique non-mass dependent KIE that endows ozone with a distinctive excess of ^{17}O over that expected based on the

abundance of ^{18}O (we define this quantity in the present paper in its simplified linearized form as follows: $\Delta^{17}O = \delta^{17}O - 0.52 * \delta^{18}O$) (Miller, 2002; Kaiser, 2009). This "anomalous" isotopic signature was immediately recognized upon its identification in the early 1980's as a breakthrough discovery of a previously unknown process occurring in the atmosphere. An understanding of this puzzling isotope effect has been the driving force behind a broad range of experimental and theoretical developments in physical chemistry, reviewed extensively by Thiemens (1999; 2006), Weston (1999), Brenninkmeijer *et al.* (2003), and Mauersberger *et al.* (2003).

The second reason for the intense research focus on ozone isotopic composition arises from the fundamental role played by ozone in atmospheric chemistry. In conjunction with its photochemical counterpart the hydroxyl radical (OH), ozone is central to the chemistry of the troposphere and is closely coupled to the oxidative cycles of most atmospheric trace species (Monks, 2005). The distinctive $\Delta^{17}O$ signature of ozone is propagated throughout the atmosphere via oxidation reactions (Lyons, 2001) and has now been detected in a broad range of atmospheric gas and aerosol species, including CO_2, N_2O, sulfate, nitrate, and carbonate (**Figure 3.1**) (Thiemens *et al.*, 1995; Röckmann *et al.*, 2001; Lee *et al.*, 2001; Michalski *et al.*, 2003; Shaheen *et al.*, 2010). The $\Delta^{17}O$ fingerprint is resistant to degradation through traditional mass-dependent fractionation and is thus conserved during atmospheric transport and processing; therefore, once a compound has inherited $\Delta^{17}O$ from ozone, it is permanently labeled with this signature. The $\Delta^{17}O$ of ozone thus provides a powerful research tool in studies of atmospheric oxidation pathways with several emerging applications. Particularly encouraging developments have been made in the study of the oxygen isotope dynamics of atmospheric nitrate (Morin *et al.*, 2007; 2011; Alexander *et al.*, 2009), an important secondary species resulting from reactions involving atmospheric reactive nitrogen species ($NO + NO_2 = NO_x$). Ozone also transfers its ^{17}O-excess to sulfate via aqueous phase atmospheric reactions, a signature that is preserved in ancient sediments, representing a potential proxy for the composition of ancient atmospheres (Bao *et al.*, 2000; 2008; Savarino *et al.*, 2000). Furthermore, due to the relatively high concentrations of nitrate and sulfate preserved in polar snow and ice, there also exists the possibility of extending these interpretations to the glacial/interglacial time scale through ice core analysis (Savarino *et al.*, 2003; Alexander *et al.*, 2004; Hastings *et al.*, 2005).

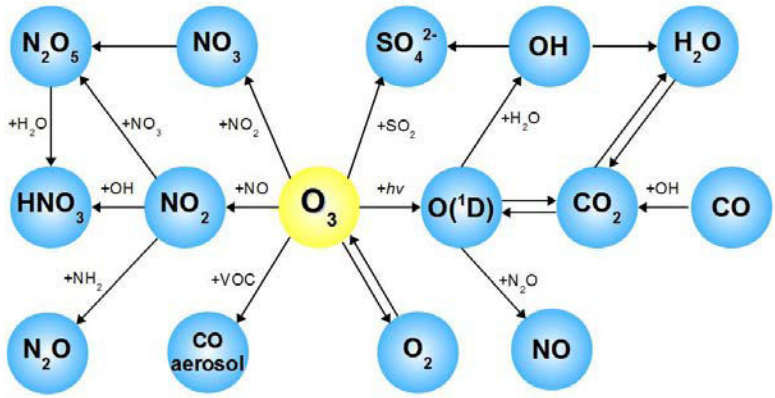

FIGURE 3.1 - The propagation of ozone's anomalous $\Delta^{17}O$ signature via chemical and isotope transfer reactions in the atmosphere.

The utility of $\Delta^{17}O(O_3)$ as a quantitative tracer of atmospheric chemistry is contingent upon a precise and accurate knowledge of its magnitude and the extent of its natural spatial and temporal variability. However, due to the inherent complexity of extracting ozone from surface air, the observational record for tropospheric $\Delta^{17}O(O_3)$ remains quite small, despite the effort that has been devoted to the study of the various oxygen bearing atmospheric trace species carrying the isotopic signature inherited from ozone. Until recently, only two studies reported measurements of the triple-isotope composition of ozone collected from the troposphere (Krankowsky *et al.*, 1995; Johnston and Thiemens, 1997). These landmark investigations were performed using a cryosampling technique in which ozone is trapped using liquid helium and subsequently converted to molecular oxygen for isotopic analysis. Krankowsky *et al.* (1995) collected and analyzed 47 ozone samples from ambient air outside of the German city of Heidelberg and found (mean ± 1σ) $\delta^{17}O$ and $\delta^{18}O$ values of 72 ± 11‰ and 91 ± 6‰ (relative to air O_2), respectively. In a subsequent study using the cryogenic method, Johnston and Thiemens (1997) analyzed a total of 42 samples collected from three sites in the U.S. Southwest and found $\delta^{17}O = 70 \pm 7‰$ and $\delta^{18}O = 84 \pm 7‰$. The $\Delta^{17}O$ of ozone, which can be readily calculated from the individual δ measurements reported, compare quite well for these two datasets in terms of average value: 25 ± 11‰ and 26 ± 5‰ for the Krankowsky *et al.* (1995) and Johnston and Thiemens (1997) studies, respectively. However, the magnitude of variability in $\Delta^{17}O(O_3)$ observed in the cryogenic data greatly exceeds the expected quantitative effects from variations in the pressure and temperature of ozone

formation, indicating a likelihood of random errors, possibly associated with low collection efficiency and interference from xenon (Mauersberger *et al.*, 2003). Furthermore, while the two datasets appear to be internally coherent when comparing average $\Delta^{17}O(O_3)$ values, the averages observed (i.e., 25 - 26‰) are not quantitatively consistent with the $\Delta^{17}O(O_3)$ value predicted from the measured temperature and pressure dependencies for the ozone formation reaction, which is on the order of 32‰ for average surface conditions (e.g., see Brenninkmeijer *et al.* (2003) and references therein). This discrepancy between predicted and observed tropospheric $\Delta^{17}O(O_3)$ may arise from the analytical deficiencies of the cryogenic trapping method; however, uncertainty also exists in the extrapolation of the laboratory data to ambient conditions, which is presently speculative as no experimental data for the impact of ozone formation temperature on $\Delta^{17}O(O_3)$ exists for the surface pressure regime. Therefore, doubt persists regarding the value of the field measurements and the true quantity of $\Delta^{17}O(O_3)$ in the troposphere (Morin *et al.*, 2007; 2011; Alexander *et al.*, 2009; Michalski and Bhattacharya, 2009).

The $\Delta^{17}O$ of ozone in the troposphere, should it be found to exhibit systematic variability, may also convey quantitative information regarding the balance between ozone production and loss in different atmospheric environments. In the study of Krankowsky *et al.* (1995), no correlation was found between the $\delta^{17}O$ and $\delta^{18}O$ values of ozone, suggesting that the large degree of variability observed for $\Delta^{17}O$ is an artifact resulting from statistical scatter of the individual δ measurements, particularly $\delta^{17}O$. These results are therefore not inconsistent with the hypothesis that the tropospheric value of $\Delta^{17}O(O_3)$ is constant. However, the data of Johnston and Thiemens (1997) reveal a systematic variability in the relationship between $\delta^{17}O$ and $\delta^{18}O$, with data from three different sites aligning on different slopes in a three-isotope plot. The authors of this study concluded that the observed variability resulted from differences in ozone transformation pathways between the three sites and suggested that measurements of the triple-isotope composition of ozone could therefore be useful in constraining the tropospheric ozone budget. This conclusion that was later questioned by Brenninkmeijer *et al.* (2003), who argued that the differences in slope were not statistically significance considering the precision of the technique and suggested that they were most likely related to analytical bias.

To summarize, field measurements of ozone isotopic composition are urgently needed to: (i) provide quantitative constraints for models of $\Delta^{17}O$ propagation in the

atmosphere and substantiate previous interpretations based on assumptions regarding the quantity of $\Delta^{17}O(O_3)$; (ii) supply an observational dataset for testing predictions based on experimental data and theoretical models of ozone isotope chemistry; and (iii) investigate the natural variability of $\Delta^{17}O(O_3)$ as it relates to the tropospheric ozone budget in different locations under various atmospheric contexts. In order to address this need, we have developed a new technique for $\Delta^{17}O(O_3)$ analysis that employs a chemical ozone trapping mechanism, thus circumventing the need for liquid helium, which is the principal drawback of the cryogenic technique that has thus far limited its application. Preliminary ambient measurements using this method, described in Chapter 2, yielded an average bulk $\Delta^{17}O(O_3)$ value of approximately 23 ± 2‰ for 19 samples collected during autumn in Grenoble, France. This range is in reasonably good agreement with the average values inferred from the cryogenic data; more interesting is the low standard deviation observed for $\Delta^{17}O(O_3)$ in this study, which seems to suggest a low level of natural variability. However, lacking a detailed record of observations from other locations, it has until now been impossible to draw any conclusions regarding the quantity of $\Delta^{17}O(O_3)$ or its spatial and temporal variability in the troposphere.

Here we present the results of a systematic investigation of the spatial and seasonal features of tropospheric $\Delta^{17}O(O_3)$. Measurements reported here include: (i) a full annual record from Grenoble, France (45 °N) (n = 71); (ii) a latitudinal record from 50 °S to 50 °N in the Atlantic Ocean (n = 30); and (iii) a four-week record from Dome C, Antarctica (75 °S) during polar summer (n = 28). This observational dataset represents a two-fold increase in the number of existing tropospheric observations and a dramatic expansion in the global representation of $\Delta^{17}O(O_3)$.

3.2 Experimental

The nitrite-coated filter technique for ozone $\Delta^{17}O$ analysis has been described in detail in Chapter 2, which introduced the methodological rationale and addressed important analytical issues such as collection efficiency, isotope transfer, blanks and interferences, and sample normalization. The focus of the present report is the application of the method to the ambient troposphere and an interpretation of results obtained in different environmental contexts. Therefore, the description of the

analytical approach will be only cursory. The reader is referred to Chapter 2 for full details of the methodology.

The principal of ozone collection underlying this method is the filter-based trapping of ozone via aqueous phase reaction with nitrite, which acts as a chemical probe for the terminal oxygen atom of the ozone molecule:

$$NO_2^- + O_3 \rightarrow NO_3^- + O_2 \quad \text{(R3.1)}$$

The collection of ozone with nitrite-coated filters is a well-established technique for the determination of ozone mass concentration (Koutrakis *et al.*, 1993; Geyh *et al.*, 1997; Krzyzanowski, 2004; Adon *et al.*, 2010). By coupling this routine ozone measurement technique with recent analytical developments in the $\Delta^{17}O$ analysis of nanomole quantities of nitrate (Sigman *et al.*, 2001; Casciotti *et al.*, 2002; Kaiser *et al.*, 2007; McIlvin and Casciotti, 2011), the ^{17}O-excess transferred by ozone through bimolecular chemical reactions, denoted $\Delta^{17}O(O_3^*)$, can be inferred from the oxygen isotopic composition of the nitrate produced via R1 within the coated filter matrix (Michalski and Bhattacharya, 2009).

3.2.1 Sample collection

Ambient ozone collections were performed in all cases using an active air sampler consisting of 1/4" Teflon™ (PFA) tubing connecting three main sampler components: (i) a standard low-volume vacuum pump equipped with a volume counter and needle valve (or flow meter) for flow rate regulation; (ii) a closed PFA filter holder assembly containing a pre-coated 47 mm glass fiber sampling substrate (Whatman™, GF/A type); and (iii) an open-faced filter holder assembly containing a Zefluor™ PTFE membrane pre-filter for the removal of particulate species upstream of the coated filter. Glass fiber sampling substrates were coated prior to sample collection with 1 mL of a nitrite-based ozone trapping solution (0.1 mol L^{-1} $NaNO_2$, 0.05 mol L^{-1} K_2CO_3, 0.1 mol L^{-1} glycerol), allowed to dry at 75 °C for approximately 10 min, and then stored frozen and in the dark in individual plastic PetriSlide™ containers (Millipore™). Samples were collected by loading pre-coated filters into the sampling filter holder, which was then connected to the prefilter (upstream) and needle valve/pump (downstream) and covered in aluminum foil to limit light exposure. Air was then pumped through the sampling system at a target flow rate of 3 L min^{-1} for durations ranging from 2 - 30 hours. After sample collection, filters were returned to

their containers, which were covered in aluminum foil and stored at -20 °C before processing and analysis. The stability of nitrite on the coated filters during storage was evaluated through analysis of the nitrate formed on blank filters in each batch, which were subjected to all of the same manipulations and storage conditions as samples.

3.2.1.1 Grenoble, France

The city of Grenoble (45.2 °N, 5.8 °E, 209 m above mean sea level) is located in the French Alps at the Y-shaped confluence of three deep mountain valleys, with surrounding summits reaching 2000 to 3000 m. Due to strong emissions of NO_x and volatile organic compounds (VOCs) from industrial emissions and road traffic, the Grenoble region is often subject to high ozone levels, particularly during the summer when concentration can exceed 24-hour averages of 40 ppb and reach values higher than 100 ppb on warm afternoons (Chaxel and Chollet, 2009). During the late fall and winter, stable thermal inversions develop over the valley leading to a reduction in the vertical exchange of low-level air, effectively trapping urban emissions at the surface (Couach *et al.*, 2003). Ozone concentrations are often reduced to 24-hour average values of less than 5 ppb during these periods via titration by NO (Zhang *et al.*, 2004), which can reach daily average concentrations as high as 90 ppb during October - February. Average hourly concentrations of ozone, NO, NO_2, and SO_2 were obtained from the local air quality monitoring agency (http://www.air-rhonealpes.fr) for comparison to the isotopic results obtained for the Grenoble samples. 24-hour average values for ozone, NO_x, and NO_2 molar ratio ($\chi NO_2 = NO_2/NO_x$) throughout 2012 are presented in **Figure 3.2**.

Coated filter samples were collected from the roof of our laboratory building (LGGE) in Grenoble on a weekly basis from 6 January 2012 - 17 December 2012 (n = 71). In accordance with the methodological recommendations in Chapter 2, ozone concentrations were monitored during sample collection and the total collection time for each individual sample was adjusted to ensure the collection of at least 0.5 - 1.0 μmol of nitrate on each filter. In terms of ozone mixing ratio, this minimum sample size correlates to 150 - 200 ppb•hr, which was typically exceeded within 12 - 24 hours of sampling time. However, during periods of exceptionally low ozone concentrations (< 5 ppb) in the late fall and winter, several samples were collected below this threshold (n = 19); additionally, five 2 - 6-hour intensive filter collections

during July ozone maxima also fell below the 150 ppb•hr minimum sample intensity. Results for the samples smaller than 150 ppb•hr will be considered in the following discussion; however, they are typically segregated for comparison to larger samples.

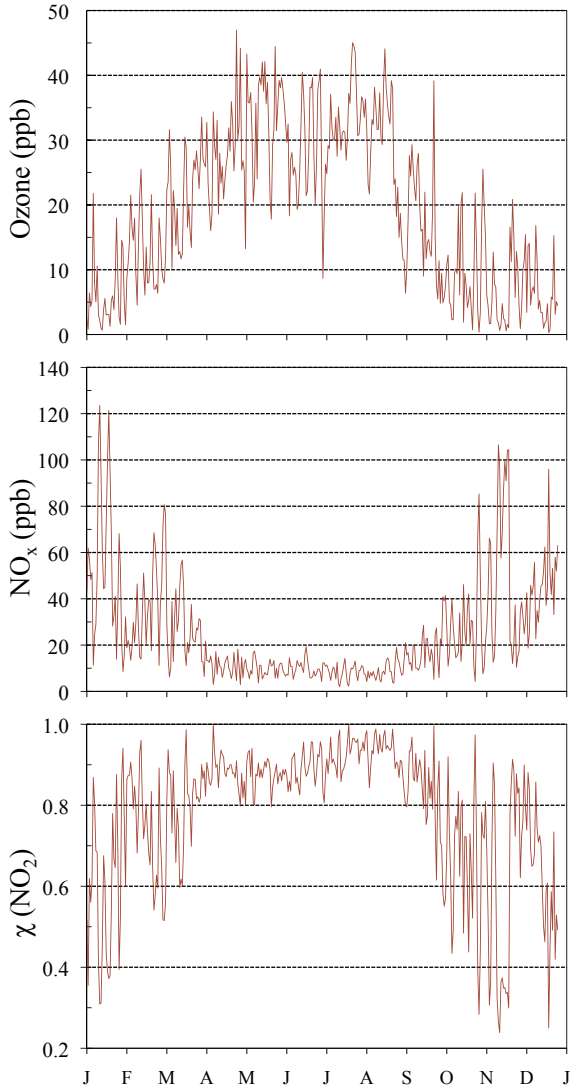

FIGURE 3.2 - 24-hour average mixing ratios of ozone (top) and NO_x (center) in Grenoble during the 2012 filter sampling campaign. The NO_2 molar ratio ($\chi NO_2 = NO_2/NO_x$) is shown in the bottom panel. Data has been obtained from the local air quality monitoring agency (http://www.air-rhonealpes.fr).

3.2.1.2 R/V Polarstern

Samples were obtained during an Atlantic transfer cruise of the Research Vessel (R/V) *Polarstern* between Punta Arenas, Chile (53.2 °S, 70.9 °W) and Bremerhaven, Germany (53.5 °N, 8.6 °E) (cruise ANT XXVIII/5 from 12 April to 14 May 2012) (**Figure 3.3)**. During its voyage across the equatorial Atlantic to Europe, the R/V *Polarstern* was exposed to a broad gradient of atmospheric conditions, including wide

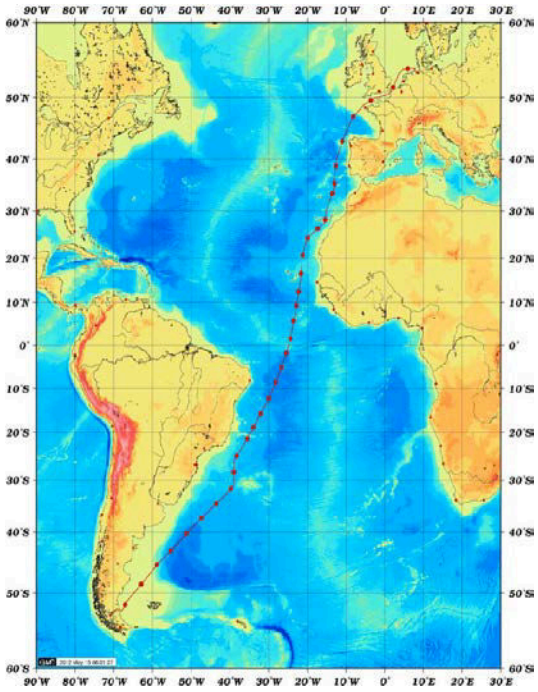

FIGURE 3.3 - Ship track of the ANT XXVIII/5 cruise of the R/V *Polarstern*.

variability in actinic flux (i.e., the amount of light available for photochemical reactions) and water vapor content. Furthermore, air masses of diverse origins were encountered along this transect, including remote marine air masses from the Southern Atlantic Ocean, which are largely representative of the unpolluted marine boundary layer (MBL), and continental North African and European air masses, which are strongly impacted by anthropogenic emissions (Virkkula *et al.*, 2006a; 2006b; Morin *et al.*, 2009). The abundances of atmospheric trace species, such as NO_x and VOCs, are thus expected to have varied significantly during the cruise as well (Monks *et al.*, 2000; van der A *et al.*, 2008; Lee *et al.*, 2009). This conjunction of atmospheric settings provided a unique opportunity to investigate the scale of natural variability in $\Delta^{17}O(O_3)$ and to test the hypothesis of its sensitivity to ozone production and loss processes under various atmospheric contexts (Johnston and Thiemens, 1997; Brenninkmeijer *et al.*, 2003).

The sampling apparatus was installed inside of a climate-controlled instrument container on the R/V *Polarstern* with the sampler inlet / prefilter affixed to the container's exterior at a height of approximately 20 m above sea level. Ozone mixing ratio was measured throughout the cruise using a standard UV-absorption monitor (Model 205, 2B Technologies™) beginning 16 April, while meteorological data (e.g., air temperature, relative humidity, wind speed and direction, etc.) were provided by

FIGURE 3.4 - The sampling shelter "Astro Tent" at Dome C, Antarctica during the OPALE field campaign.

the onboard weather station. Filter sampling was conducted on a continuous basis and a total of 30 samples were obtained. Individual filter samples were typically collected over 24-hour periods (n = 22); however, several samples were collected at lower durations (~ 12 hrs) during ozone concentration maxima observed in the northern latitudes (n = 8). All samples collected onboard R/V *Polarstern* were in the range of 300 - 700 ppb•hr. After sample collection, filters were stored onboard at -20 °C and then transported to the LGGE for processing and analysis.

3.2.1.3 Dome C, Antarctica

Filter samples were collected at Dome C (75.1°S, 123.3°E), a high-elevation site located 3,233 meters above mean sea level on the Antarctic plateau. Sampling was conducted within the framework of the OPALE (Oxidant Production over Antarctic Land and its Export) 2011 - 2012 field campaign, a major collaborative study focusing on boundary layer chemistry over Antarctica (Preunkert *et al.*, 2012). Reagent preparation and filter coating was conducted on-site using MQ water purified from the local supply. 24-hour filter samples were collected continuously from a climate-controlled shelter (**Figure 3.4)** during the period 10 December 2011 - 14 January 2012 and a total of 28 samples were obtained, each sample in the range of 300 - 800 ppb•hr. Ozone was measured at one-minute intervals during this campaign using a standard UV-absorption technique with a detection limit of ~ 1 ppb, while NO_x concentrations were determined via ozone-induced chemiluminescence with detection limits of approximately 2 ppt and 6 ppt for NO and NO_2, respectively. Meteorological data were obtained from the Dome C weather station. Samples were

processed immediately after collection using local MQ water (see following section) and the unfiltered extract solutions were then shipped frozen to the LGGE for analysis.

2.2 Sample extraction and isotopic analysis

The nitrite-coated filter samples were extracted in 18 mL of UV-oxidized deionized water (18.2 MΩ resistivity). In order to remove the excess nitrite reagent from the sample extracts, the solutions were treated with 1 mL of a 1 mol L^{-1} sulfamic acid solution and then neutralized with a corresponding addition of high-purity sodium hydroxide (Granger and Sigman, 2009). Extract solutions were then filtered via centrifugation using Millipore Centricon™ assemblies.

Nitrate extracted from the sampling filters was prepared for isotopic analysis via conversion to N_2O using the bacterial denitrifier method (Sigman *et al.*, 2001; Casciotti *et al.*, 2002; Kaiser *et al.*, 2007; McIlvin and Casciotti, 2011). The comprehensive isotopic composition of N_2O was subsequently measured, following thermal decomposition to O_2 and N_2, on a Finnigan™ MAT253 isotope ratio mass spectrometer, which was equipped with a GasBench II™ on-line gas introduction system and coupled to an in-house built nitrate interface (Komatsu *et al.*, 2008; Morin *et al.*, 2009). Individual $\delta^{17}O$, $\delta^{18}O$, $\Delta^{7}O$, and $\delta^{15}N$ measurements were normalized via linear calibration with concurrent measurements of isotopic standards (USGS32, USGS34, and USGS35), which were prepared in a background matrix of filter coating reagents and subjected to the same chemical processing as sample filters (Werner and Brand, 2001). The details of our analytical procedure are described thoroughly in Chapter 2 and will not be treated further here.

3.3 Results

3.3.1 Isotopic composition of nitrate in filter extracts

The average (± 1σ) $\delta^{17}O$, $\delta^{18}O$, $\Delta^{7}O$, and $\delta^{15}N$ values obtained for nitrate extracted from the ambient filter samples are summarized in **Table 3.1**, while the triple-oxygen isotope composition of the samples are shown in a three-isotope plot in **Figure 3.5**.

TABLE 3.1 - Isotopic Composition of Nitrate in Filter Extracts.

Campaign	*n*	$\delta^{17}O(NO_3^-)$ (‰)	$\delta^{18}O(NO_3^-)$ (‰)	$\Delta^{17}O(NO_3^-)$ (‰)	$\delta^{15}N(NO_3^-)$ (‰)
Grenoble < 150 ppb•hr	24	43.8 ± 4.1	57.7 ± 5.7	13.5 ± 1.4	0.3 ± 1.3
Grenoble > 150 ppb•hr	47	40.8 ± 2.5	53.2 ± 4.0	13.1 ± 0.7	2.0 ± 1.0
R/V *Polarstern*	30	41.9 ± 4.9	55.4 ± 6.9	12.9 ± 1.3	0.9 ± 4.9
Dome C	28	25.8 ± 5.4	27.9 ± 7.8	11.3 ± 1.4	1.1 ± 4.2

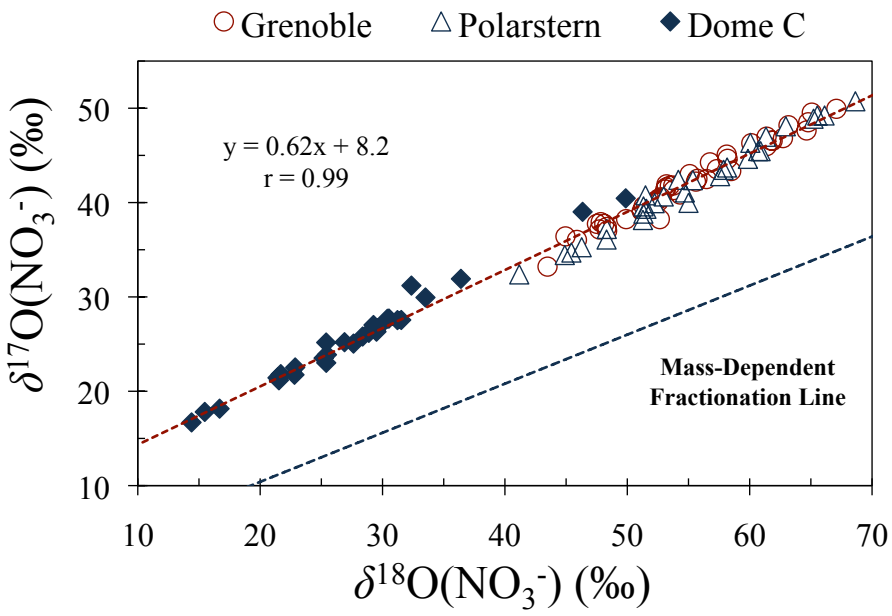

FIGURE 3.5 - Oxygen three-isotope plot showing the mass-independent isotopic composition of the nitrate produced on the ambient sampling filters from Grenoble, R/V *Polarstern*, and Dome C campaigns. The mass-dependent fractionation line in defined as $\delta^{17}O = 0.52 \times \delta^{18}O$.

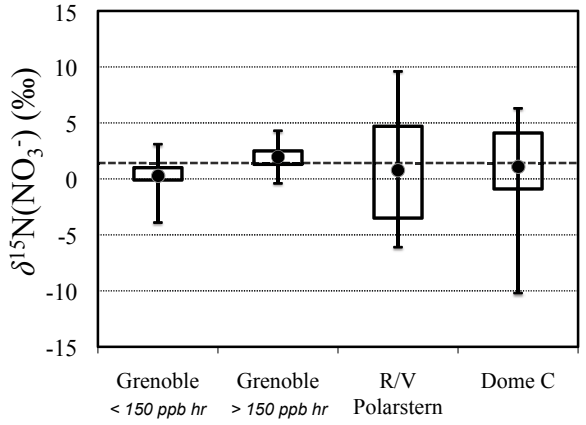

FIGURE 3.6 - δ^{15}N measurements for the nitrite-coated filter samples presented in this study. The box plot indicates the interquartile range (box) and the median (line), maximum, and minimum values. The mean value is denoted by a black circle. The δ^{15}N of the nitrite coating reagent is denoted by a broken grey line.

Oxygen isotope enrichments are largely consistent for the Grenoble and R/V *Polarstern* records, with both sets of samples exhibiting average δ^{17}O and δ^{18}O values of approximately 40‰ and 50‰, respectively, in favorable comparison with previous measurements in Grenoble during September-October 2011 (see Chapter 2). However, nitrate in the Dome C sample extracts consistently exhibited δ^{17}O and δ^{18}O values much smaller than those obtained in any previous nitrite-coated filter measurements, with only two samples falling within the range observed for the Grenoble and R/V *Polarstern* samples. The δ^{18}O values measured for the Dome C samples were in some cases even depleted relative to the nitrite reagent used for ozone collection, which possessed an average δ^{18}O of 16.7 ± 0.8‰.

Average $\delta^{15}N(NO_3^-)$ values for the three datasets are on the order of 1 - 2‰, consistent with the δ^{15}N signature of the nitrite collection reagent (1.5 ± 0.2‰). However, while the samples collected in Grenoble possessed $\delta^{15}N(NO_3^-)$ values that varied within a relatively narrow range (± 1‰), similar to the Series C collections presented in Chapter 2, the R/V *Polarstern* and Dome C collections exhibited significant variability in terms of δ^{15}N, with values ranging between -10 and 10‰ (**Figure 3.6**). This variability in δ^{15}N was clearly associated with co-variations in the oxygen isotope ratios of nitrate, particularly Δ^{17}O (**Figure 3.7**), which was significantly correlated with δ^{15}N in both the R/V *Polarstern* and Dome C datasets (**Table 3.2**). The negative linear relationships formed between $\delta^{15}N(NO_3^-)$ and the oxygen isotope ratios of nitrate are highly consistent for these two records, with almost identical slopes for δ^{17}O, δ^{18}O, and Δ^{17}O. These correlations are largely analogous to those observed for the Series A and Series B samples discussed in

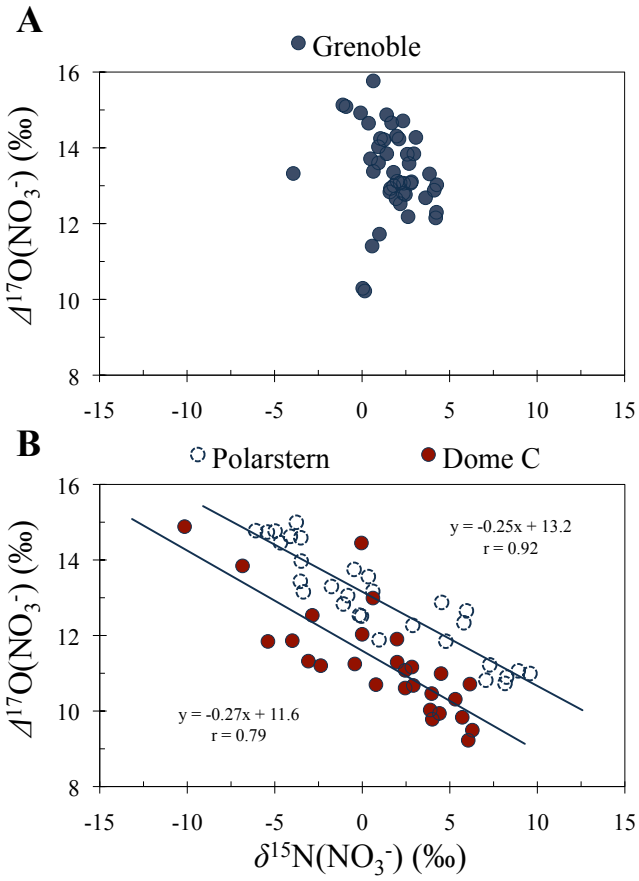

FIGURE 3.7 - $\Delta^{17}O$ as a function of $\delta^{15}N$ for the nitrate in sample extracts from the **(a)** Grenoble and **(b)** R/V *Polarstern* and Dome C campaigns. The $\delta^{15}N$ of the nitrite reagent used in field collections is 1.5 ± 0.2‰.

Chapter 2 and signify an inadequate isotopic calibration of the ambient collections arising from variability in the quantity of blank nitrate in the filter extracts (i.e., negative $\delta^{15}N$ values are indicative of an overcorrection of the isotopic results, while values greater than 1.5‰ indicate an under-correction). Analysis of procedural blanks from the three field campaigns (**Table 3.3**) suggest that the R/V *Polarstern* filters were subject to a high and variable blank accumulation, while the blanks from the Grenoble and Dome C filter batches exhibited concentrations consistent with the average reagent blank contribution determined in Chapter 1 (4.12 µmol L^{-1}). This additional blank accumulation represents a dilution of the $\Delta^{7}O$ signal via addition of mass-dependent nitrate and it is also associated with a considerable enrichment in ^{15}N over that of the nitrate background originally present in the coating matrix. The $\delta^{15}N$ of the nitrate present in R/V *Polarstern* filter blanks averaged ~ 28‰, while the coating matrix blank has been observed to range between 16 - 22‰ over repeated analyses, consistent with the filter blank $\delta^{15}N$ measurements for the Grenoble and Dome C campaigns. The cause of this blank accumulation in the R/V *Polarstern* filter

TABLE 3.2 - Linear Regressions Between $\delta^{15}N$ and Oxygen Isotope Ratios of Nitrate.

	$\delta^{17}O(NO_3^-)$			$\delta^{18}O(NO_3^-)$			$\Delta^{17}O(NO_3^-)$		
Campaign	***m***[a]	***b***	***r***	***m***	***b***	***r***	***m***	***b***	***r***
Grenoble < 150 ppb•hr	0.03	-0.91	0.09	0.03	-1.56	0.14	0.00	0.38	0.00
Grenoble > 150 ppb•hr	-0.15	8.31	-0.38	-0.11	8.06	-0.43	-0.12	3.59	-0.08
R/V *Polarstern*	-0.86	42.6	0.85	-1.13	56.2	0.79	-0.25	13.2	0.92
Dome C	-0.89	26.8	0.69	-1.17	29.2	0.64	-0.27	11.6	0.79

[a] y = mx + b

TABLE 3.3 - Concentrations and $\delta^{15}N$ Values of Nitrate in Coated Filter Blanks.

		Nitrate Concentration	$\delta^{15}N(NO_3^-)$
	n	**(μmol L^{-1})**	**(‰)**
Grenoble	11	4.6 ± 0.3	17.2 ± 0.7
R/V *Polarstern*	9	12.0 ± 2.9	27.9 ± 1.5
Dome C	6	5.1 ± 0.7	18.6 ± 1.3
Reagent Blank[a]	31	4.12 ± 0.41	18.6 ± 2.2

batch is not immediately clear as the filters were protected from light exposure during sampling and stored frozen and in the dark while onboard (see Chapter 2). However, it seems likely that the higher blanks are associated with the transport of the filters, which may have experienced freeze/thaw cycles *en route*.

Considering that the R/V *Polarstern* filter batch appears to have been subjected to a consistently large blank accumulation (12 μmol L^{-1}), it is counterintuitive that a considerable number of these samples have been overcorrected via calibration to USGS standards prepared at baseline blank level (4 μmol L^{-1}) and thus possess negative $\delta^{15}N$ values (**Figure 3.6**). This observation suggests that, while the procedural blanks exhibited nitrate concentrations that were significantly increased over that of the filter coating matrix, some sample filters actually possessed a nitrate blank lower than this baseline. In other words, the coated filters appear to have lost

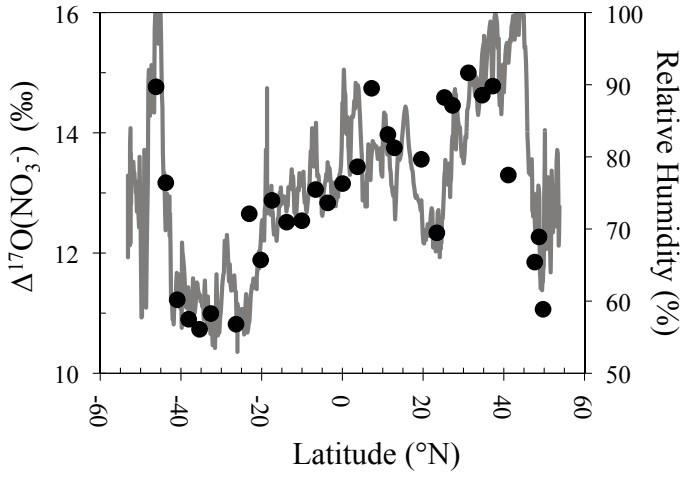

FIGURE 3.8 - Co-variations of $\Delta^{17}O(NO_3^-)$ (black circles) and relative humidity (one-hour averages, solid grey line) during the cruise on R/V *Polarstern*.

blank nitrate during the course of sample collection in many cases. This unexpected result can be understood by considering the effect of relative humidity, which was strongly correlated with both the nitrogen and oxygen isotope ratios of nitrate for the samples collected onboard R/V *Polarstern*, with r = 0.78, 0.73, 0.83, and 0.85 for $\delta^{17}O$, $\delta^{18}O$, $\Delta^{17}O$, and $\delta^{15}N$, respectively (**Figure 3.8**). During periods of increased relative humidity (> 80%) and precipitation, it seems possible that the sampling filters became saturated with water, which leached the coating reagents from the filter and onto the surface of the filter holder grid. This loss of reagent equally represents a loss of the background nitrate contamination associated with the coating solution, which results in the overcorrection of these samples when calibrated to isotopic reference materials prepared at a nitrate blank level that assumes 100% recovery of the coating reagents applied to the sampling filters. $\delta^{15}N$ values for samples collected during periods of relatively low relative humidity were consistently enriched over the value of the nitrite reagent, suggesting that these samples had been under-calibrated due to the accumulation of nitrate as inferred from the analysis of the R/V *Polarstern* filter blanks. Therefore, the R/V *Polarstern* samples were both over- and under-corrected with respect to the baseline reagent blank level depending on the degree of relative humidity during the period of sample collection.

Using the same approach developed in Chapter 2, the calibrated oxygen isotope ratios for the R/V *Polarstern* and Dome C samples have been corrected for calibration bias based on the difference between the $\delta^{15}N$ measured for the sample and that of the nitrite reagent used to coat the filters:

$$\Delta^{17}O_{correct.} = \Delta^{17}O_{meas.} - m \times \left(\delta^{15}N_{reagent} - \delta^{15}N_{meas.}\right) \quad (3.1)$$

TABLE 3.4 - δ^{15}N-Corrected Oxygen Isotope Ratios of Nitrate.

Campaign	*n*	$\delta^{17}O(NO_3^-)$ (‰)	$\delta^{18}O(NO_3^-)$ (‰)	$\Delta^{17}O(NO_3^-)$ (‰)
R/V *Polarstern*	30	41.3 ± 2.6	54.5 ± 4.3	12.7 ± 0.5
Dome C	28	25.4 ± 3.9	27.4 ± 6.0	11.2 ± 0.9

where *m* is the empirical slope formed between δ^{15}N and δ^{17}O, δ^{18}O, or Δ^{17}O (**Table 3.2**), and $\delta^{15}N_{reagent}$ is 1.5‰ for the $NaNO_2$ used in this study. This correction results in little or no change to the nitrate oxygen isotope ratios in terms of average value but reduces significantly the degree of variability in the data (**Table 3.4**). For example, the average (± 1σ) $\Delta^{17}O(NO_3^-)$ values for the R/V *Polarstern* and Dome C records are corrected from 12.9 ± 1.3‰ to 12.7 ± 0.5‰ and from 11.3 ± 1.4‰ to 11.2 ± 0.9‰, respectively. Because no significant correlations were found among the nitrogen and oxygen isotope ratios of the Grenoble samples, these measurements have not been corrected.

3.3.2 Isotopic composition of ozone

The δ^{18}O and Δ^{17}O values of the oxygen atoms transferred from ozone to nitrate through the $O_3 + NO_2^-$ reaction (i.e., $\delta^{18}O(O_3^*)$ and $\Delta^{17}O(O_3^*)$) are effectively diluted in the nitrate product due to the presence of two oxygen atoms inherited from the nitrite reagent ($\delta^{18}O(NaNO_2)$ = 16.7‰, $\Delta^{17}O(NaNO_2) \approx 0$). The δ^{18}O and Δ^{17}O values transferred to nitrite can be inferred by simple mass-balance:

$$\delta^x O(O_3^*) = 3 \times \delta^x O(NO_3^-) - 2 \times \delta^x O(NaNO_2) \quad (3.2)$$

The transferrable δ^{18}O and Δ^{17}O values obtained using Equation 3.2 are highly relevant for studies of the propagation of ozone's isotopic composition via atmospheric reactions (**Figure 3.9**). Indeed, considering the isotopic and chemical asymmetry of the ozone molecule, $\delta^{18}O(O_3^*)$ and $\Delta^{17}O(O_3^*)$ are undoubtedly more suitable measures of ozone's isotopic source strength in the atmosphere (Janssen, 2005; Morin *et al.*, 2011). However, previous tropospheric measurements (i.e., the cryogenic collection technique) were of bulk ozone isotopic enrichments; therefore, comparison of the results obtained using the nitrite-coated filter method to those

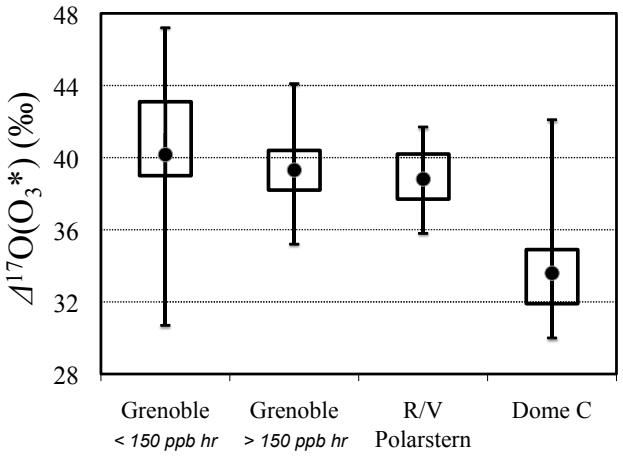

FIGURE 3.9 - $\Delta^{17}O(O_3^*)$ values for the nitrite-coated filter samples presented in this study. The box plot indicates the interquartile range (box) and the median (line), maximum, and minimum values. The mean value is denoted by a black circle.

reported in the literature involves expressing the measured $\delta^{18}O(O_3^*)$ and $\Delta^{17}O(O_3^*)$ values in terms of the bulk ozone molecule. This transformation requires knowledge of the intramolecular distribution of oxygen isotopes in ozone, specifically the relationship between the bulk $\delta^{18}O$ and $\Delta^{17}O$ values and those of the terminal oxygen atoms, which are preferentially transferred during the $O_3 + NO_2^-$ reaction (Liu *et al.*, 2001). The distribution of ^{17}O and ^{18}O among the central and terminal atoms of ozone has been previously investigated in laboratory experiments that have exploited chemical reactions in which ozone transfers a terminal oxygen atom to form a stable product. This technique was first applied to the oxidation reaction of ozone and silver (Bhattacharya *et al.*, 2008). In a subsequent experiment, Michalski and Bhattacharya (2009) utilized the aqueous-phase $O_3 + NO_2^-$ transfer, the same reaction underlying the nitrite-coated filter method. In both of these experiments, the relationship observed between the $\Delta^{17}O$ of bulk ozone and that of the atom transferred during the reaction suggests that the non-zero $\Delta^{17}O$ of ozone resides only, or predominantly, in molecules of the type OOQ (asymmetric) and not in the type OQO (symmetric), thus:

$$\Delta^{17}O(O_3)_{terminal} \approx 1.5 \times \Delta^{17}O(O_3)_{bulk} \quad (3.4)$$

This observation is largely consistent with the symmetry-based theoretical model of Gao and Marcus (2001) as well as spectroscopic evaluations of the positional dependence of ^{17}O and ^{18}O enrichments in ozone (Janssen *et al.*, 2001; Janssen and Tuzson, 2006). Results of the vacuum-line experiments presented in Chapter 2 suggest that isotope transfer from ozone to nitrite on the coated filters generally

TABLE 3.5 - Isotopic Composition of Ozone.

Campaign	*n*	$\delta^{18}O(O_3^*)$ (‰)	$\delta^{18}O(O_3)_{bulk}$ (‰)	$\Delta^{17}O(O_3^*)$ (‰)	$\Delta^{17}O(O_3)_{bulk}$ (‰)
Grenoble < 150 ppb•hr	24	139.9 ± 17.1	122.4 ± 13.8	40.5 ± 4.2	27.0 ± 2.8
Grenoble > 150 ppb•hr	47	126.3 ± 11.9	111.4 ± 9.6	39.3 ± 2.0	26.2 ± 1.3
R/V *Polarstern*	30	130.4 ± 12.9	114.8 ± 10.4	38.8 ± 1.6	25.9 ± 1.1
Dome C	28	48.9 ± 18.1	50.4 ± 14.1	33.6 ± 2.6	22.4 ± 1.7

conforms to the relationship shown in Equation 3.4 (i.e., $\Delta^{17}O(O_3^*) = 1.5 \times \Delta^{17}O(O_3)_{bulk}$). Therefore, $\Delta^{17}O(O_3)_{bulk}$ values have been inferred for the Grenoble, R/V *Polarstern*, and Dome C as twice the $\Delta^{17}O$ value measured for nitrate (**Table 3.5**).

The empirical relationship linking bulk and terminal ^{18}O enrichments reported by Michalski and Bhattacharya (2009) is a simple linear function:

$$\delta^{18}O(O_3)_{terminal} \approx 1.26 \times \delta^{18}O(O_3)_{bulk} - 13.5‰ \quad (3.5)$$

$\delta^{18}O(O_3)_{bulk}$ estimates obtained using Equation 3.5 are highly compatible (± 0.3%) with those calculated using a best-fit line of the experimental data of Bhattachrya *et al.* (2008). $\delta^{18}O(O_3)_{bulk}$ values computed for the samples collected during Grenoble, R/V *Polarstern*, and Dome C campaigns are shown in **Table 3.5**.

3.4 Discussion

3.4.1 Comparison to "cryogenic" measurements

For intercomparison of the data reported for the two previous isotopic studies of tropospheric ozone, the three-isotope plots of Krankowsky *et al.* (1995) have been digitized in order to obtain the individual $\delta^{17}O$ and $\delta^{18}O$ values for the 47 measurements reported therein and $\Delta^{17}O$ has been calculated using the linearized definition ($\Delta^{17}O = \delta^{17}O - 0.52 \times \delta^{18}O$). Measurements obtained at three different sites (La Jolla, Pasadena, and White Sands) by Johnston and Thiemens (1997) have been merged and averaged together, despite the emphasis that the authors of this study placed on the variability observed between the sites. Contrary to the analysis of

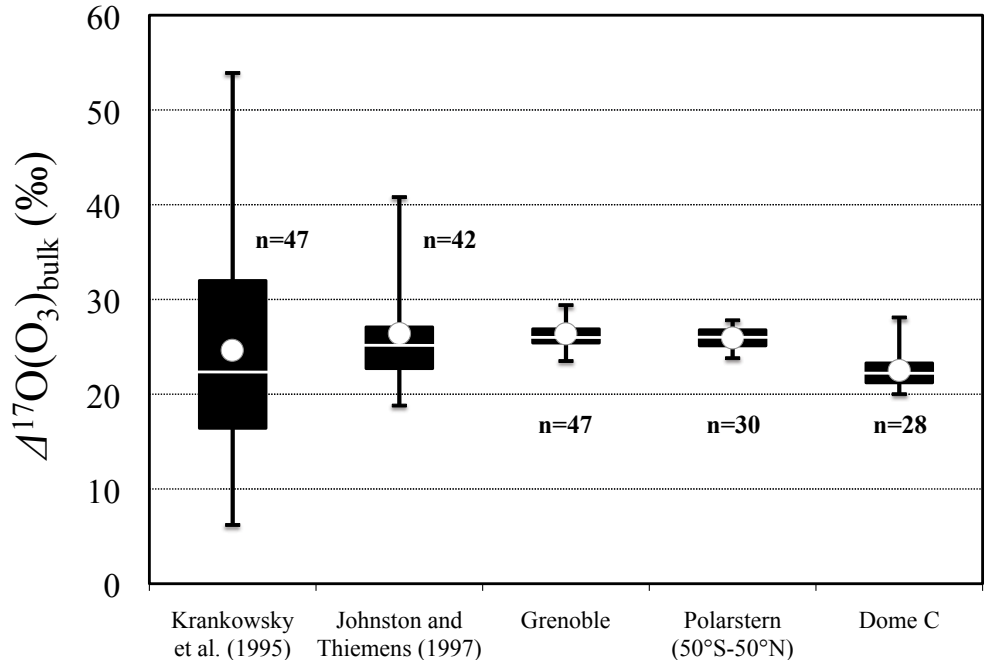

FIGURE 3.10 - $\Delta^{17}O(O_3)_{bulk}$ measurements obtained with the cryogenic collection method and those reported here. The box plot indicates the interquartile range (box) and the median (line), maximum, and minimum values. The mean value is denoted by a white circle. Only samples larger than 150 ppb•hr are included in the Grenoble dataset.

Brenninkmeijer *et al.* (2003), standard deviations from the mean $\delta^{17}O$ and $\delta^{18}O$ values reported in these studies are considered rather than errors of the mean.

$\Delta^{17}O(O_3)_{bulk}$ measurements obtained with the cryogenic technique and those inferred from the samples described in this study are presented in **Figure 3.10**. In terms of average value, the comparison between the cryogenic and nitrite-coated filter measurements is very favorable: 24.7 ± 11.4‰ and 26.2 ± 5‰ for the Krankowsky et al. (1995) and Johnston and Thiemens (1997) studies, respectively, as compared to 26.2 ± 1.3‰ for Grenoble (> 150 ppb•hr samples only) and 25.9 ± 1.1‰ for the R/V *Polarstern* campaign. Considering the vast methodological differences between the two approaches (i.e., wet chemistry vs. cryogenic trapping, terminal atom vs. bulk ozone, denitrifier method vs. direct conversion of ozone to O_2, etc.), the agreement observed in the data is very encouraging. However, the most striking point of the comparison is the sharply decreased level of variability observed in the nitrite-coated filter data. Considering that the measurement technique carries an uncertainty on the order of ±1.7‰ (see Chapter 2), the standard deviations observed for the three field campaigns are remarkably low, approaching the precision of the bacterial denitrifier method itself (~0.5‰ in terms of the $\Delta^{17}O(NO_3^-)$ measurement). This observation indicates a low level of natural variability in the $\Delta^{17}O$ of surface ozone and suggests

that the large variations in the cryogenic measurements are indeed an artifact associated with the collection technique rather than an indication of actual variations in $\Delta^{17}O(O_3)$, as pointed out by several previous authors (Brenninkmeijer *et al.*, 2003; Mauersberger *et al.*, 2003; Morin *et al.*, 2007). Furthermore, the absence of large variations in $\Delta^{17}O(O_3)$ in the troposphere is largely consistent with the following theoretical considerations: (i) the only factor widely accepted to influence the isotopic composition of ozone in the atmosphere is the isotope effect associated with the formation reaction (Thiemens and Heidenreich, 1983). Cycling within the O_x reservoir proceeds rapidly compared to source or sink reactions for the odd oxygen species and, consequently, the reaction pathways capable of producing significant isotope fractionation in ozone are limited (Houston *et al.*, 1996; Johnston and Thiemens, 1997); (ii) atmospheric destruction processes that may induce variability in the isotopic composition of ozone (e.g., photodissociation) proceed in a strictly mass-dependent fashion (Bhattacharya and Thiemens, 1988; Wen and Thiemens, 1991; 1993; Chakraborty, 2003; Ndengue *et al.*, 2012a; 2012b) and should therefore leave the $\Delta^{17}O$ signal intact. However, it should be noted that there is some debate regarding the fractionation effects associated with UV-photolysis and surface-induced dissociation (Chakraborty and Bhattacharya, 2003a; 2003b; 2003c; Janssen, 2003; Cole and Boering, 2006); (iii) the experimentally determined dependency of $\Delta^{17}O(O_3)$ on the pressure of ozone formation suggests a relatively small decrease of only ~ 2‰ for an increase in pressure from 500 to 760 Torr (0.7 to 1.0 atm) (Morton *et al.*, 1990; Thiemens and Jackson, 1990); (iii) temperature dependency studies suggest an increase in $\Delta^{17}O$ of only ~ 5‰ for an increase in ozone formation temperature from 260 to 320 K (Morton *et al.*, 1990; Janssen *et al.*, 2003) (see Section 1.2.2 for a full derivation of an equation[1] relating the $\Delta^{17}O$ of ozone to the temperature and pressure of formation). For these reasons, it is often assumed that $\Delta^{17}O(O_3)_{bulk}$ in the troposphere exhibits no more than a 1 - 2‰ level of variability under standard surface conditions and, consequently, this variable is often taken to be constant in the numerical modeling of $\Delta^{17}O$ propagation in the atmosphere (Lyons, 2001; Zahn *et al.*, 2006; Morin *et al.*, 2007; 2011; Alexander *et al.*, 2009; Gromov *et al.*, 2010) and in the interpretation of $\Delta^{17}O$ measurements for atmospherically-derived trace species preserved in sediment and polar ice records (Luz *et al.*, 1999; Bao *et al.*, 2000; 2008;

[1] $\Delta^{17}O(O_3) = \left(78.8 \times P(Torr)^{-0.122}\right) + 0.06 \times \left(T(K) - 321\right)$

Blunier *et al.*, 2002; Michalski *et al.*, 2004). The results presented in this study thus provide a satisfying substantiation of a key assumption in atmospheric geochemistry, validating several past interpretations.

The Dome C sample measurements correspond to an average $\Delta^{17}O(O_3)_{bulk}$ of 22.4 ± 1.7‰, approximately 3 - 4‰ lower than the measurements from extra-polar locations (**Figure 3.10**). Given that the average surface temperature at Dome C was on the order of -30 °C during the sampling campaign, the reduced $\Delta^{17}O(O_3)_{bulk}$ values would appear to be consistent with the temperature dependency studies, which predict a $\Delta^{17}O(O_3)_{bulk}$ value approximately 3 - 4‰ lower for ozone formed at -30 °C relative to 0 - 30 °C. However, the reduced surface pressure at Dome C (December-January average ≈ 484 Torr) as compared to the extra-polar sites would suggest an opposite and nearly equal difference, effectively canceling the quantitative effect of temperature. For temperature and pressures typical of conditions during the tropospheric measurements, the $\Delta^{17}O(O_3)_{bulk}$ value calculated for Dome C is only ~ 1.5‰ lower than that calculated for the equatorial Atlantic.

In addition to the strong agreement between the cryogenic and filter method $\Delta^{17}O(O_3)_{bulk}$ values, these two observational datasets are equally consistent in terms of $\delta^{18}O(O_3)_{bulk}$ when considering the extra-polar sites (**Figure 3.11**). Isotopic measurements of tropospheric ozone obtained with the cryogenic method were originally reported relative to atmospheric O_2, which is enriched by 23.5‰ in $\delta^{18}O$ relative to VSMOW (Kroopnick and Craig, 1972). When converted to the VSMOW scale,[2] the average (± 1σ) $\delta^{18}O(O_3)_{bulk}$ measurements of Krankowsky *et al.* (1995) and Johnston and Thiemens (1997) are 117 ± 6‰ and 109 ± 7‰, respectively, in excellent agreement with the average values obtained for the Grenoble and R/V *Polarstern* campaigns, which are 111.4 ± 9.6‰ and 114.8 ± 10.4‰, respectively. Furthermore, this range of $\delta^{18}O(O_3)_{bulk}$ values is comparable to that derived from the experimental temperature and pressure dependency studies for typical surface conditions (~ 100 - 110‰, relative to VSMOW). This is a surprising and encouraging result considering that the nitrite-coated filter method was originally expected to be unsuitable for the measurement of $\delta^{18}O$ due to potential mass-dependent fractionation effects associated with the collection technique (e.g., due to the ca. 60% collection efficiency, etc., see Chapter 2). The results presented here would seem to suggest otherwise; however, the

[2] $\delta^{18}O(O_3)_{VSMOW} = \delta^{18}O(O_3)_{air-O_2} + \delta^{18}O(air-O_2)_{VSMOW} + \left[\delta^{18}O(O_3)_{air-O_2} \times \delta^{18}O(air-O_2)_{VSMOW}\right]$

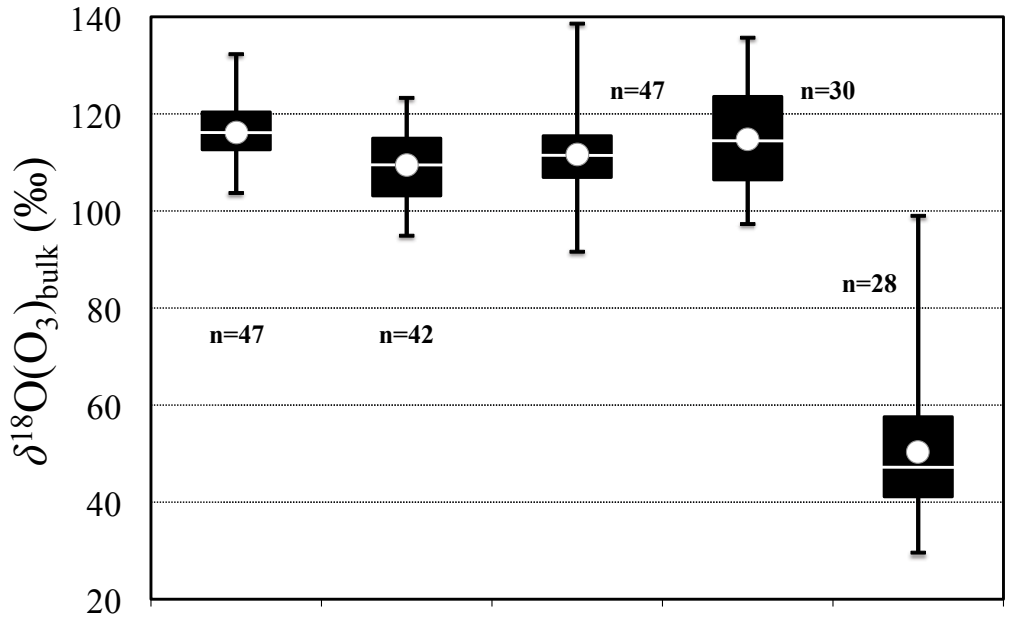

FIGURE 3.11 - $\delta^{18}O(O_3)_{bulk}$ measurements obtained with the cryogenic collection method and those reported here. The box plot indicates the interquartile range (box) and the median (line), maximum, and minimum values. The mean value is denoted by a white circle.

observed level of variability in $\delta^{18}O(O_3)_{bulk}$ for the Grenoble and R/V *Polarstern* campaigns is somewhat higher relative to the cryogenic measurements. Furthermore, considering that the experimental data would predict a decrease in $\delta^{18}O$ of only ~ 30‰ for a 60 K decrease in temperature, the very low $\delta^{18}O(O_3)_{bulk}$ values calculated for the Dome C samples are not quantitatively consistent with a temperature effect. Indeed, in light of the previous laboratory and field studies, it would seem that the Dome C $\delta^{18}O(O_3)_{bulk}$ estimates are almost certainly biased. The reduced values $\delta^{18}O$ measured for the Dome C samples suggest a possible impact of isotopic exchange between the nitrite reagent and water within the filter matrix (Bunton *et al.*, 1955; Bunton *et al.*, 1959). While nitrate is relatively stable with respect to exchange with water, the oxygen atoms of nitrite are more labile (Böhlke *et al.*, 2003). Isotopic exchange has the potential to alter the distributions of oxygen isotopes in the nitrite reagent by promoting equilibration with the water used in the preparation of the filters (ε = +15‰) (Casciotti et al., 2007), thus affecting the apparent (i.e., measured) $\delta^{17}O$ and $\delta^{18}O$ values of the nitrate produced via $O_3 + NO_2^-$. The alkaline nature of the coating solution matrix (pH ≈ 11) should largely limit the extent of this exchange, which occurs exclusively between water and nitrous acid (HNO_2, $K_a = 5.1 \times 10^{-4}$); furthermore, storage at -20 °C has been found to ensure the long-term stability of

nitrite isotopologues in solution (McIlvin and Altabet, 2005; Böhlke *et al.*, 2007; Casciotti *et al.*, 2007). However, should some degree of exchange occur between water and the nitrite reagent, it is reasonable to assume that this effect would be more pronounced for filters coated and extracted at Dome C, where the $\delta^{18}O$ of meteoric water is on the order of -50‰, as compared to western European sites (i.e., Grenoble), where $\delta^{18}O(H_2O) > -10‰$ (Bowen and Wilkinson, 2002; Landais *et al.*, 2008). Furthermore, the enrichment factor associated with this effect is known to decrease with temperature (Böhlke *et al.*, 2003), which could potentially amplify its impact for samples collected in polar environments. The impact of isotopic exchange with water during sample collection should be investigated in future experiments by determining the oxygen isotopic composition of nitrite in blank filters prepared using waters with various $\delta^{18}O$ enrichments. If this impact can be quantified, controlled, or eliminated entirely by increasing the pH of the coating solution, then the nitrite-coated filter method could perhaps be applied to the detection of $\delta^{18}O(O_3)_{bulk}$ variations in the atmosphere.

3.4.2 Annual $\Delta^{17}O(O_3)$ record from Grenoble, France

3.4.2.1 Sample size dependence

The $\Delta^{17}O(O_3)_{bulk}$ values for the Grenoble samples are shown in **Figure 3.12** as a function of ambient ozone concentration and sample size (ozone throughput = ppb•hr). Contrary to the measurements described in Chapter 2, the Grenoble 2012 measurements suggest that the nitrite-coated filter method returns relatively consistent results over a wide range of concentrations, although two samples collected in January under extremely at < 5 ppb ozone returned the lowest $\Delta^{17}O(O_3)_{bulk}$ values (≈ 20‰). However, unlike the Grenoble 2011 samples, which possessed sizes almost exclusively < 200 ppb•hr, the Grenoble 2012 samples were typically much larger, with sizes spanning a relatively wide range from 50 - 1100 ppb•hr (the two anomalously low January values are for samples in the 50 - 75 ppb•hr range). A very clear trend is present when comparing the 2012 $\Delta^{17}O(O_3)_{bulk}$ values to the size of the individual collections, with the vast majority of variability in the measurements associated with samples < 150 ppb•hr. This observation could be attributable to high-frequency variations in the $\Delta^{17}O$ of ozone that are only detectable over relatively limited time periods, as the < 150 ppb•hr samples often correspond to short collection

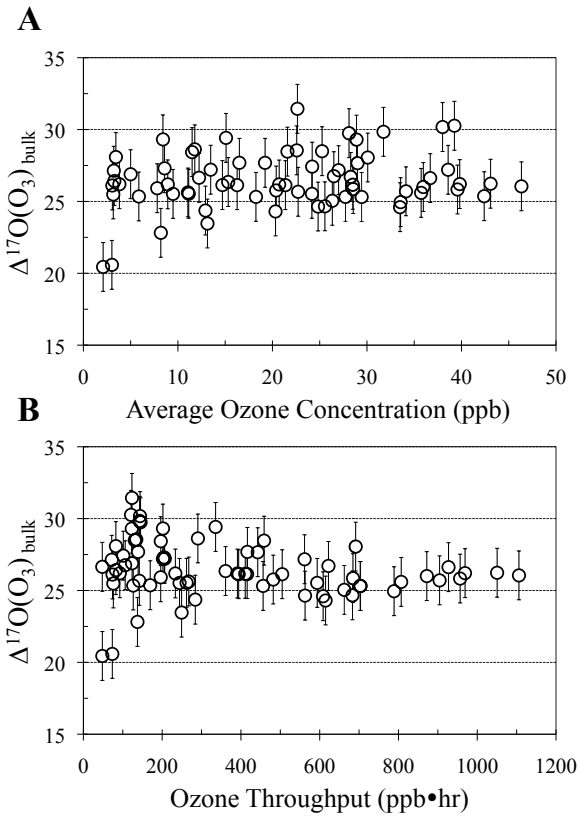

FIGURE 3.12 - $\Delta^{17}O(O_3)_{bulk}$ values for the 71 ambient collections in Grenoble during 2012 plotted against **(a)** the average ozone concentration observed during collection and **(b)** total ozone throughput (ppb•hr = sample size). Vertical error bars represent the total uncertainty estimated for the technique in the $\Delta^{17}O(O_3)_{bulk}$ = 10 - 40‰ range (± 1.7‰).

periods; however, subdiurnal collections conducted in July with sample sizes < 150 ppb•hr consistently yielded $\Delta^{17}O(O_3)_{bulk}$ values that were higher than those obtained from the analysis of simultaneous 24-hr collections. This suggests that the size-dependent variability observed in the data is associated with the increased uncertainty involved in the calibration of small samples (see Chapter 2), rather than an indication of actual diurnal variations in the $\Delta^{17}O$ of tropospheric ozone. The results obtained for 2012 thus confirm that the method is sensitive to a minimum sample size of approximately 150 - 200 ppb•hr, which was speculated in Chapter 2. The 2012 Grenoble samples with sizes < 150 ppb•hr (n = 24) will therefore not be considered in what remains of this discussion. Furthermore, it seems that the Grenoble 2011 data from Chapter 2 (i.e., the Series C collections) should also be rejected as only one of these samples was collected at a throughput >150 ppb•hr (note in **Table 2.5** that this sample possessed a $\Delta^{17}O(O_3)_{bulk}$ value of 25.6‰, in agreement with the average value obtained for the 2012 samples).

3.4.2.1 Seasonal uniformity of $\Delta^{17}O(O_3)$

A time-series showing the $\Delta^{17}O(O_3)_{bulk}$ measurements for samples collected in Grenoble during 2012 is presented in **Figure 3.13**. The annual record is remarkably featureless with the exception of one broad peak during the winter-spring transition, when $\Delta^{17}O(O_3)_{bulk}$ averaged 28 ± 2‰ over the course of seven consecutive collections (13 February - 26 March). The stability of the $\Delta^{17}O$ signature throughout the year is particularly remarkable considering the large seasonal variability observed in the concentrations of ozone and NO_x (**Figure 3.2**). In the study of Johnston and Thiemens (1997), systematic spatial variability was detected in the ^{17}O-excess of ozone, with $\delta^{17}O$ and $\delta^{18}O$ measurements from three different sites aligning on different slopes in a three-isotope plot. Because the magnitude of the diurnally averaged trend in ozone concentration was observed to decrease with increasing $\Delta^{17}O$ (i.e., Pasadena > La Jolla > White Sands), Johnston and Thiemens (1997) suggested that the degree of photochemical control on the local ozone budget was a potential determining factor for ^{17}O-excess in tropospheric ozone. The uniformity of the $\Delta^{17}O$ signal observed throughout the year in Grenoble, as well as its comparability to the data obtained for the remote Atlantic MBL, is not consistent with these conclusions. Indeed, considering the large differences in photochemical ozone balance between polluted urban sites and the relatively unimpacted Atlantic MBL (Sillman, 1999; Monks *et al.*, 2000), the temporal and spatial consistency observed in this study suggests that $\Delta^{17}O(O_3)$ is insensitive to such local controls. This finding represents an important substantiation of the basic interpretive framework typically applied to $\Delta^{17}O$ measurements in atmospheric trace species, such as nitrate and sulfate, which is centered around seasonal fluctuations in atmospheric oxidation mechanisms rather than seasonal variability in the $\Delta^{17}O$ of ozone itself (Michalski *et al.*, 2003; Morin *et al.*, 2007; 2008; 2009; 2011; Alexander *et al.*, 2009; 2012; Hill-Falkenthal *et al.*, 2012; Savarino *et al.*, 2013).

The presence of successive peak values in February-March is difficult to assess. Firstly, the $\Delta^{17}O(O_3)_{bulk}$ values inferred for these samples are only 2 - 3‰ greater than the annual mean, a modest increase when considering the ± 1.7‰ uncertainty associated with the analytical technique. Therefore, two interpretations of these peak values are possible: either they are "real" or purely a consequence of measurement artifacts. Given that this apparent increase in $\Delta^{17}O(O_3)_{bulk}$ is consistent over the course of several individual collections, it seems unlikely that it could be attributable to an

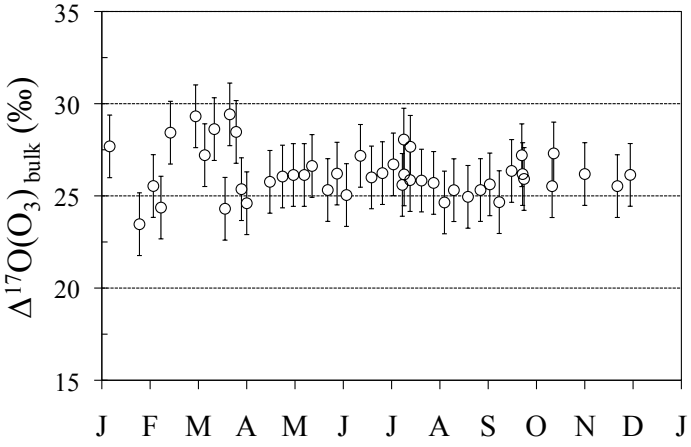

FIGURE 3.13 - Annual record of $\Delta^{17}O(O_3)_{bulk}$ from Grenoble (2012). Only samples > 150 ppb•hr are shown. Vertical error bars represent the total uncertainty estimated for the technique in the $\Delta^{17}O(O_3)_{bulk}$ = 10 - 40‰ range (± 1.7‰).

analytical bias, unless this bias was itself seasonal. Furthermore, it is intriguing that these peak values seem to occur in conjunction with the spring ozone maximum, a well-known phenomenon that is observed at many background surface measurement stations in the Northern Hemisphere, typically during the period March-May (Monks, 2000). A comparison of the seasonal cycles of surface ozone mixing ratios with those of cross-tropopause fluxes of ozone has often led to the conclusion that these enhanced surface concentrations are related to stratosphere-troposphere exchange (Beekmann *et al.*, 1994; VanHaver *et al.*, 1996; Austin and Follows, 1991). Other authors have emphasized the role of photochemical production within the free troposphere, which leads to an accumulation of ozone at high altitudes (5 - 6 km) during the winter-spring transition (Roelofs and Lelieveld, 1997; Stohl *et al.*, 2003; Zanis *et al.*, 2007). Ozone formed in the stratosphere and high troposphere is expected to possess a larger excess ^{17}O enrichment relative to ozone formed at the surface due to the reduced pressure at altitude. For example, measurements of the isotopic composition of ozone collected at an altitude range of 25 to 35 km over Aire-sur-l'Adour, France (44°N), have yielded average $\Delta^{17}O(O_3)_{bulk}$ values of 35 ± 4‰ (Krankowsky *et al.*, 2007), significantly higher than the average 26 ± 1‰ values obtained for the surface measurements at Grenoble. The February-March peaks could therefore be attributable to the greater relative importance of stratospheric/free tropospheric inputs in determining the surface ozone concentration during this time of the year. However, when considering the potential for atmospheric transport to impact the $\Delta^{17}O$ of ozone in a given location, it is important to distinguish between the chemical and isotopic lifetimes of the ozone molecule (Johnston and Thiemens, 1997; Houston *et al.*, 1996). The photolytic cycling of ozone leads ultimately to a null cycle,

as the dominant fate of the ground-state O atom produced from ozone photolysis is to recombine with O_2. However, this rapid cycling results in the continuous reformation of isotopically "new" ozone molecules that possess an isotopic composition that depends only on local temperature and pressure, which determine the isotope enrichments associated with the formation reaction. Therefore, while the chemical lifetime of ozone is on the order of weeks to months, the isotopic lifetime is determined by the absolute ozone photolysis frequency, $j(O^3P)$. For Grenoble, $j(O^3P)$ is typically on the of 5×10^{-4} s^{-1} during the morning and afternoon, corresponding to an isotopic lifetime against photolysis of approximately 30 minutes. At night, in the absence of photolytic cycling, the isotopic lifetime of ozone is extended. However, due to the high NO_x concentrations in Grenoble, the lifetime of ozone against the NO + O_3 reaction is less than one hour throughout the year, and often less than one minute during the fall and winter. Therefore, it is unlikely that the isotopic composition of the ozone sampled in Grenoble would convey information regarding transport. Thus, while the peak $\Delta^{17}O(O_3)_{bulk}$ values in February-March are intriguing, their significance is unclear.

3.4.3 $\Delta^{17}O(O_3)$ from 50°S to 50°N in the Atlantic MBL

Similar to the annual record from Grenoble, the latitudinal record obtained from the samples collected onboard the R/V *Polarstern* reveals very little variability in $\Delta^{17}O$. In terms of bulk ozone, the $\Delta^{17}O$ values obtained for these 30 samples range between 24 and 28‰, with a standard deviation of 1.1‰. Nevertheless, a small but statistically significant ($p < 0.05$) difference is apparent when comparing samples collected in the Southern and Northern Hemispheres, which possessed $\Delta^{17}O(O_3)_{bulk}$ values of 25.3 ± 1.0‰ (n = 16) and 26.6 ± 0.7‰ (n = 14), respectively. This hemispheric asymmetry in the ^{17}O-excess of ozone is particularly evident for the samples collected 30 degrees north and south of the intertopical convergence zone (ITCZ, located at approximately 3.5 °N during the April-May 2012 cruise) (**Figure 3.14**). The ITCZ is an important meteorological boundary that separates the southern and northern equatorial atmospheres in terms of chemical composition and oxidation capacity (Thompson *et al.*, 2003). The northward crossing of the ITCZ during the R/V *Polarstern* cruise was associated with a twofold increase in ozone mixing ratio and a simultaneous 2‰ increase in average $\Delta^{17}O(O_3)_{bulk}$ values. Due to the kinetic considerations discussed

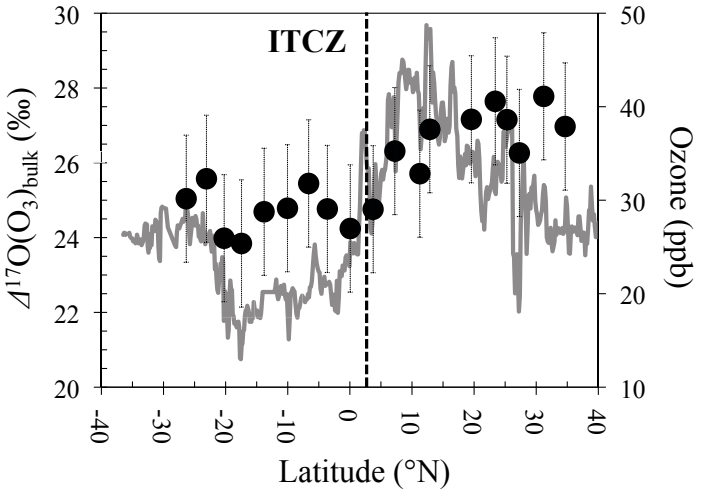

FIGURE 3.14 - $\Delta^{17}O(O_3)_{bulk}$ measurements for samples collected 30 degrees north and south of the intertropical convergence zone (ITCZ). The ambient ozone mixing ratio is indicated by a solid grey line (secondary y-axis).

above, it is difficult to conceive of a process that would produce such a trend in the $\Delta^{17}O$ of ozone without invoking the temperature or pressure of the ozone formation reaction. Local pressure and temperature varied within a narrow range during the cruise on R/V *Polarstern*; therefore, a formation-based explanation for the increased $\Delta^{17}O$ values observed north of the ITCZ must also invoke long-range transport or subsidence from high altitudes, which should not have a quantitative impact on the isotopic composition of ozone at the surface due to the rapidity of photochemical O_x cycling. Mass-dependent isotopic fractionation is associated with these null cycles; however, these processes should not impact the $\Delta^{17}O$ of the remaining ozone reservoir (Chakraborty, 2003; Cole and Boering, 2006; Ndengue *et al.*, 2012b). The trend observed in the R/V *Polarstern* record is interesting and it may indicate the existence of an unidentified process influencing the isotopic composition of ozone. However, given the rather marginal difference observed between the Southern and Northern Hemisphere sample and the relatively high uncertainty involved in the measurements, the evidence for such a process is not unambiguous.

3.5 Summary and conclusions

The nitrite-coated filter method has been applied in a systematic investigation of the isotopic composition of ambient surface ozone in three sampling campaigns. The results of theses measurements indicate that the ^{17}O-excess of ozone, an important isotopic marker of atmospheric oxidation mechanisms, is spatially and seasonally

homogeneous within the analytical uncertainty of the technique (± 1.7‰). This finding is contrary to that of Johnston and Thiemens (1997), who detected a systematic variability in $\Delta^{17}O(O_3)$ that was attributed to the inetensity of local photochemical cycling among three different sites. $\Delta^{17}O(O_3)$ measurements from Grenoble (45 °N) reveal very little variability on an annual basis despite strong seasonal fluctuations in atmospheric composition; furthermore, the samples obtained at this highly impacted urban site yield $\Delta^{17}O(O_3)$ values consistent with those collected in the remote Atlantic MBL between 50 °S and 50 °N. These observations suggest that measurements of $\Delta^{17}O(O_3)$ using the nitrite-coated filter method are unlikely to provide relevant information regarding the tropospheric ozone budget. However, as discussed at length in Chapter 2, the observational record compiled in this study represents an invaluable constraint on the transferrable ^{17}O-excess of tropospheric ozone.

In terms of the bulk ozone $\Delta^{17}O$ value ($\Delta^{17}O(O_3)_{bulk}$), the measurements obtained with the nitrite-coated filter method are in strong quantitative agreement with the cryogenic measurements of Krankowsky et al. (1995) and Johnston and Thiemens (1997). Furthermore, the two techniques have yielded comparable $\delta^{18}O(O_3)_{bulk}$ enrichments (100 - 120‰, relative to VSMOW), which are in broad agreement with the values predicted from laboratory studies. Therefore, it is possible that the nitrite-coated filter technique may also serve as an analytical approach for the measurement of $\delta^{17}O$ and $\delta^{18}O$. However, samples collected from Dome C, Antarctica indicate that isotopic exchange between the nitrite collection reagent and water may limit the precision of this application. Future studies should seek to quantify the impact of this exchange, particularly with regard to the $\delta^{18}O$ enrichment of both the water used in the preparation of the filter coating solution and the water vapor present at the sampling location.

The finding of an average $\Delta^{17}O(O_3^*)$ value of ~39‰ is a result with important implications for the interpretation of ^{17}O-excess in the atmosphere. In many cases, $\Delta^{17}O$ measurements for species such as nitrate and sulfate provide information regarding chemical transformation processes in the atmosphere; however, the quantification of isotope transfer in these processes typically involves assumptions regarding the value of $\Delta^{17}O(O_3^*)$. Modeling studies that seek to simulate the propagation of $\Delta^{17}O$ in the atmosphere typically assume a $\Delta^{17}O(O_3)_{bulk}$ of 25 - 35‰ (Morin *et al.*, 2011). In some cases, isotope transfers during reactions involving ozone

have been assumed to be similar to the $\Delta^{17}O(O_3^*) \approx 1.5 \times \Delta^{17}O(O_3)_{bulk}$ transfer mechanism found in this study for the aqueous-phase ozone/nitrite reaction; in other cases, transfer is assumed to be statistical (i.e., equality between transferrable and bulk $\Delta^{17}O$). For example, modeling studies conducted by Alexander *et al.* (2009) using the global 3-D atmospheric chemistry model GEOS-Chem found the best agreement between the modeled $\Delta^{17}O(NO_3^-)$ values and existing observations when $\Delta^{17}O(O_3)_{bulk}$ was assumed to be 35‰ and $\Delta^{17}O(O_3^*)$ was calculated to be ~48‰ based on the transfer function reported by Savarino *et al.* (2008). This value is significantly higher than the ambient measurements reported here, suggesting a discrepancy between our results and expectations based on the analysis of Alexander *et al.* (2009). However, the average $\Delta^{17}O(O_3^*)$ obtained here is largely consistent with the 35 - 40‰ range assumed in several previous studies (Lyons, 2001; Michalski *et al.*, 2003; 2004; Zahn *et al.*, 2006; Morin *et al.*, 2007; 2008; Savarino *et al.*, 2007). Based on our measurements, we conclude that the quantitative interpretations of these studies can be considered largely valid. The consistent use of a $\Delta^{17}O(O_3^*)$ value of 39 ± 3‰ in modeling studies should aid in the further application of this tracer in studies of atmospheric oxidation pathways.

Chapter 4

Spatial and diurnal variability in reactive nitrogen oxide chemistry as reflected in the isotopic composition of atmospheric nitrate: Results from the CalNex 2010 field study

---

This chapter is based on:

Vicars, W. C., Morin, S., Savarino, J., Wagner, N. L., Erbland, J., Vince, E., Martins, J. M. F., Lerner, B. M., Williams, E. J., and Brown, S. S., Spatial and diurnal variability in reactive nitrogen oxide chemistry as reflected in the isotopic composition of atmospheric nitrate: Results from the CalNex 2010 field study. *Journal of Geophysical Research-Atmospheres* **(in review)**.

Abstract

The comprehensive isotopic composition of atmospheric nitrate (i.e., $\delta^{17}O$, $\delta^{18}O$, and $\delta^{15}N$) can convey valuable information regarding reactive nitrogen oxide ($NO_x = NO_2$ and NO) sources, cycling, and removal pathways; however, interpretations derived from nitrate isotope ratio measurements have thus far been useful primarily in the analysis of annual or seasonal atmospheric trends, while isotopic effects associated with faster atmospheric processes (e.g., diurnal variations, meso-scale meteorological phenomena) are presently not well constrained. In order to assess the impact of temporal variability in atmospheric chemistry on nitrate stable isotope ratios, we have measured the size-resolved concentration and isotopic composition of atmospheric nitrate at a diurnal/semidiurnal resolution onboard the R/V *Atlantis* during a cruise along the coast of California. This campaign was a major component of the CalNex 2010 field study and consisted of two distinct cruises in the South Coast and San Francisco Bay regions from 14 - 31 May and 1 - 7 June, respectively. Significant differences in air mass origin and atmospheric chemistry were observed for these two

regions with corresponding differences in the concentration and isotopic composition of nitrate. Measurements of the ^{17}O-excess ($\Delta^{17}O = \delta^{17}O - 0.52 * \delta^{18}O$) of nitrate suggest that nocturnal processes involving the nitrate radical play an important role in terms of NO_x sinks in the South Coast region, where atmospheric nitrate concentrations were elevated due to the influence of continental outflow and $\Delta^{17}O(NO_3^-)$ averaged 25.3 ± 1.6‰; conversely, $\Delta^{17}O(NO_3^-)$ averaged 22.3 ± 1.8‰ in the San Francisco Bay region suggesting that the daytime OH + NO_2 reaction is a relatively more significant NO_x loss mechanism in the predominantly marine air masses sampled in this area. A strong diurnal signal was observed for both the $\delta^{15}N$ and $\Delta^{17}O$ of atmospheric nitrate. In the case of $\Delta^{17}O$, this diurnal pattern can be interpreted quantitatively as a result of the relative involvement of ozone in daytime and nighttime NO_x cycling. For $\delta^{15}N(NO_3^-)$, which ranged between -6.2 and 8.0‰ during the campaign with an average value of 0.0 ± 3.2‰, the diurnal pattern suggests that isotopic fractionation processes associated with the photolytic cycling of NO_x exert primary control on $\delta^{15}N(NO_3^-)$. This is a surprising and significant result considering the long standing debate over the relative importance of NO_x sources, ^{15}N partitioning within NO_x, and the effect of atmospheric transport in determining temporal variations in the $\delta^{15}N$ of atmospheric nitrate. These findings represent a significant advancement in our understanding of the factors controlling the isotopic composition of atmospheric nitrate, with important implications for air quality modeling.

4.1 Introduction

Reactive nitrogen oxides (NO and $NO_2 = NO_x$) exert a significant influence on the chemistry of the troposphere through the catalysis of photochemical ozone production and are closely coupled with air quality and atmospheric oxidative capacity (i.e., the lifetime of organic compounds from oxidation by radicals) (Sillman, 1999; Monks, 2005). The quantification of NO_x emissions and the elucidation of its subsequent chemical transformation pathways are thus topics of considerable current interest (Ryerson *et al.*, 2012). NO_x is emitted to the troposphere or formed *in-situ* through several natural processes, including microbial activities in soils, conversion from inert nitrogen gas (N_2) by lightning, and downward transport from the stratosphere.

However, the global tropospheric NO_x budget is currently dominated by anthropogenic activities with fossil fuel combustion accounting for approximately 50% of total emissions globally (Galloway *et al.*, 2003; Seinfeld and Pandis, 2006).

Nitrate, defined in the present study as the sum of gaseous nitric acid (HNO_3) and particulate NO_3^-, is the major oxidation product of NO_x in the atmosphere. Due to its exceptionally high solubility in water, nitrate is rapidly deposited upon formation onto surfaces and in water droplets. These dry and wet deposition processes represent environmentally significant material input pathways and have been intensively studied with regards to their role in the eutrophication of aquatic ecosystems and the acidification of soils and surface waters (Likens *et al.*, 1996; Holland *et al.*, 1997; Fenn *et al.*, 2003). Some recent studies of nitrate deposition have focused on the extraction of quantitative information regarding NO_x sources and cycling in the troposphere (Elliott *et al.*, 2007; Costa *et al.*, 2011); because nitrate is one of the most abundant ions present in polar ice and snow, there also exists the possibility of extending these atmospheric interpretations based on nitrate into the past using ice cores (Morin *et al.*, 2008; Hastings *et al.*, 2009).

Figure 4.1 summarizes the essential features of the NO_x cycle leading to nitrate formation in the atmosphere. During the day, NO and NO_2 interconvert through the photochemical NO_x cycle, in which NO_2 undergoes photolysis to form NO (R4.1), generating excited oxygen atoms which may subsequently react with molecular oxygen and produce ozone (R4.2) (Crutzen, 1970):

$$NO_2 + h\nu \rightarrow NO + O \quad \text{(R4.1)}$$

$$O + O_2 + M \rightarrow O_3 + M \quad \text{(R4.2)}$$

$$O_3 + NO \rightarrow NO_2 + O_2 \quad \text{(R4.3)}$$

$$HO_2 + NO \rightarrow NO_2 + OH \quad \text{(R4.4a)}$$

$$RO_2 + NO \rightarrow NO_2 + RO \quad \text{(R4.4b)}$$

$$XO + NO \rightarrow NO_2 + X \quad \text{(R4.5)}$$

The NO resulting from the R4.1 pathway reacts rapidly to reform NO_2, primarily through oxidation by ozone (R4.3) or peroxy radicals, HO_2/RO_2 (R4.4), although reactive halogen oxides (e.g., BrO) may also participate in NO oxidation in some cases (R4.5) (Sander *et al.*, 2003). Cycling between NO and NO_2 occurs so rapidly that a steady-state is established during the day ("photostationary state"); conversely, the processes leading to the conversion of NO_2 to nitrate operate on time scales at least three orders of magnitude longer (Atkinson *et al.*, 1997). NO_2 is oxidized

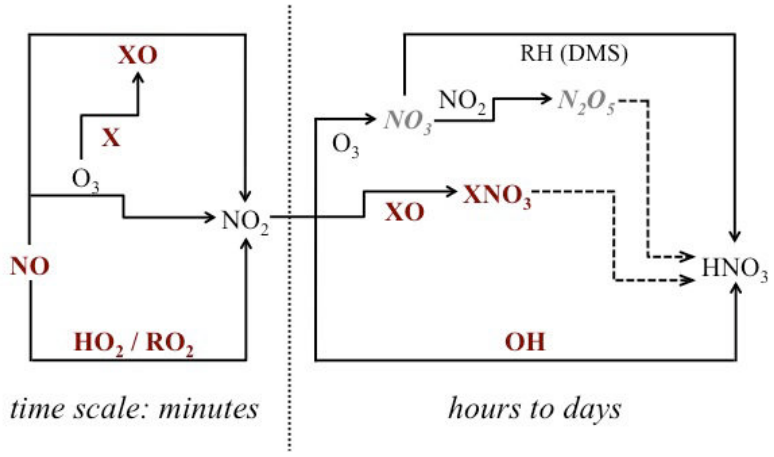

FIGURE 4.1 - Simplified NO_x cycle leading to the formation of nitrate in the atmosphere. Nitrate precursor gases associated with daytime and nighttime pathways are indicated by bold and italicized text, respectively. Dashed lines indicate heterogeneous surface reactions on atmospheric particles.

primarily by ozone (R4.6) or the hydroxyl radical (OH) (R4.7). Halogen oxides (e.g., BrO) are also thought to play a role in NO_2 oxidation, which can lead to nitrate formation through the hydrolysis of XNO_3 intermediates (R4.8) (Sander *et al.*, 1999; Savarino *et al.*, 2013). However, the R4.5 and R4.8 pathways are typically difficult to assess due to a lack of observational constraints on halogen activity in the ambient troposphere (Alexander *et al.*, 2009; Parrella *et al.*, 2012).

$$NO_2 + O_3 \rightarrow NO_3 + O_2 \quad \text{(R4.6)}$$

$$NO_2 + OH + M \rightarrow HNO_3 + M \quad \text{(R4.7)}$$

$$NO_2 + XO + M \rightarrow XNO_3 + M \quad \text{(R4.8a)}$$

$$XNO_3 + H_2O_{(liquid)} \rightarrow HOX + HNO_{3\,(aq)} \quad \text{(R4.8b)}$$

The nitrate radical (NO_3), the product of the R4.6 reaction, has an exceedingly low lifetime from photolysis and reaches significant concentrations only during the night; therefore, reaction with OH (R4.7) is the principal nitrate production channel operating during daylight hours. During the night, the NO_3 radical is converted to nitrate through reactions with hydrocarbons (RH), principally dimethyl sulfide (DMS) in marine or coastal regions (Stark *et al.*, 2007), and with NO_2 to produce dinitrogen pentoxide (N_2O_5):

$$NO_3 + RH\ (DMS) \rightarrow HNO_3 + products \quad \text{(R4.9)}$$

$$NO_3 + NO_2 \leftrightarrow N_2O_5 \quad \text{(R4.10a)}$$

$$N_2O_5 + H_2O_{(liquid)} \rightarrow 2HNO_{3\,(aq)} \quad \text{(R4.10b)}$$

N_2O_5 is an important intermediate in the NO_x cycle that can hydrolyze to form HNO_3 through heterogeneous reactions on the surface of aerosol particles (R4.10b), thereby

acting as a nocturnal sink of NO_x. However, N_2O_5 may act as only a temporary NO_x reservoir, eventually decomposing to reform NO_2 and NO_3, and the actual efficiency of N_2O_5 uptake and nitrate yield remains an area of significant uncertainty (Bertram and Thornton, 2009; Chang *et al.*, 2011). The nitrate formed through the R4.7 - R4.10 pathways is ultimately removed from the atmosphere through deposition, with an atmospheric lifetime typically on the order of one day to one week (Liang *et al.*, 1998; Finlayson-Pitts and Pitts, 2000).

Recently, there has been considerable interest in the use of nitrate stable isotope ratios as interpretive tools to identify sources of NO_x and to quantify and constrain the relative rates of NO_x removal mechanisms (i.e., the reactions leading to nitrate formation: R4.7, R4.8, R4.9, and R4.10) (Michalski *et al.*, 2003; Morin *et al.*, 2007). Stable isotope measurements for nitrate are reported as isotopic enrichments (δ) relative to a standard reference material:

$$\delta = \frac{R_{sample}}{R_{reference}} - 1 \tag{4.1}$$

where R represents the elemental $^{17}O/^{16}O$, $^{18}O/^{16}O$, or $^{15}N/^{14}N$ ratio in the sample and reference material, respectively. The reference used for oxygen isotope analysis is Vienna Standard Mean Ocean Water (VSMOW) and the reference for nitrogen is atmospheric N_2. For practical reasons, δ values are typically reported in per mill (‰), as variations in isotopic ratios for natural samples occur within a very narrow range.

While nitrogen isotope ratios ($\delta^{15}N$) of nitrate are typically thought to convey information regarding NO_x sources (Russell *et al.*, 1998; Hastings *et al.*, 2003; Elliott *et al.*, 2007; 2009; Morin *et al.*, 2009), oxygen isotopic composition is usually interpreted in terms of the relative activities of different NO_x oxidation pathways (Michalski *et al.*, 2003; Alexander *et al.*, 2009; Morin *et al.*, 2011). The unique and distinctive ^{17}O-excess ($\Delta^{17}O$) of ozone (O_3) has been found to be a particularly useful isotopic fingerprint in studies of NO_x transformations. Ozone's anomalous oxygen isotopic composition arises due to non-mass dependent fractionation during its formation in the atmosphere and results in an excess of ^{17}O over what is expected based on the abundance of ^{18}O (we define this quantity in the present paper in its linearized form as follows: $\Delta^{17}O = \delta^{17}O - 0.52 \times \delta^{18}O$) (Thiemens, 1999). The $\Delta^{17}O$ signature of ozone is transferred to NO_x through oxidation reactions such that the $\Delta^{17}O$ of nitrate acts as a marker of the influence of ozone in its chemical formation

(i.e., NO_x transformation pathway). This isotopic fingerprint, although it is subject to dilution, cannot be removed or altered via subsequent mass-dependent fractionation processes and is thus conserved during atmospheric transport and processing (Brenninkmeijer *et al.*, 2003).

The oxidative cycle shown in **Figure 4.1** results in varying degrees of $\Delta^{17}O$ transfer depending on the relative importance of the different oxidants involved in nitrate production. Nighttime reactions involving the NO_3 radical lead to the formation of a nitrate product with a relatively high $\Delta^{17}O$ inherited from ozone; conversely, the daytime production of nitrate leads to a lesser $\Delta^{17}O$ transfer as the photochemically produced radicals (OH, HO_2, RO_2) involved in the NO_x cycle posses negligible ^{17}O-excess (Lyons, 2001; Röckmann *et al.*, 2001; Michalski *et al.*, 2003). This disproportionality in isotope transfer provides a unique approach for tracing the chemical oxidation of gas-phase nitrate precursors, a technique that has been particularly effective in studies of NO_x cycling in the polar atmosphere where the occurrence of continuous sunlight during the summer (polar day) and continuous darkness during the winter (polar night) leads to pronounced seasonal differences in atmospheric chemistry (Michalski *et al.*, 2005; McCabe *et al.*, 2007; Savarino *et al.*, 2007; Morin *et al.*, 2008; 2012; Frey *et al.*, 2009; Erbland *et al.*, 2013). $\Delta^{17}O(NO_3^-)$ measurements have also allowed for the analysis of seasonal variations in NO_x transformation dynamics occurring in the mid-latitude and tropical troposphere (Hastings *et al.*, 2003; Michalski *et al.*, 2003; Morin *et al.*, 2009). However, while interpretations derived from nitrate isotope ratios have proven useful in the analysis of annual and seasonal atmospheric trends, any potential isotopic effects associated with more rapid changes in atmospheric chemistry (e.g., diurnal variations) are presently not well documented. Diurnal fluctuations in $\Delta^{17}O(NO_3^-)$, which should be present only when the atmospheric lifetime of nitrate is sufficiently low to allow for their development, are expected to reflect the relative activities of nighttime and daytime nitrate production pathways (Morin *et al.*, 2011). The $\Delta^{17}O$ of atmospheric nitrate may thus provide a tracer for the magnitude of the nocturnal NO_x sink in different atmospheric contexts. This could be a particularly useful tool, as the role played by nocturnal oxidation pathways in the transformation and removal of NO_x emissions is an area of significant uncertainty and it is unclear to what extent current regional models accurately represent these processes and their impact on air quality (Brown *et*

al., 2004; 2006; Brown and Stutz, 2012). However, the sensitivity of $\Delta^{17}O(NO_3^-)$ to diurnal variations in NO_x oxidation pathways has yet to be established in field studies.

In this study, measurements of the mass concentration and isotopic composition of atmospheric nitrate are reported for size-segregated aerosol samples collected during a research cruise along the coast of California. This cruise was organized as a component of the CalNex 2010 field study, a major multiagency campaign focusing on the atmospheric processes determining air quality over California and the eastern Pacific coastal region (Ryerson *et al.*, 2012). Aerosol sampling was conducted on a 12-hour frequency for much of the cruise, allowing for direct daytime/nighttime comparisons and providing an opportunity to extract quantitative information regarding the temporal evolution of nitrate stable isotope ratios. Furthermore, samples were collected under two distinct transport regimes, allowing for an evaluation of the differences in NO_x transformation pathways occurring in air masses of marine and continental origin. This study, to the best of our knowledge the first of its kind, represents a significant advance in our understanding of the factors controlling the isotopic composition of atmospheric nitrate, with potentially important implications for air quality modeling.

4.2 Methods

4.2.1 High-volume air sampling

Sampling was conducted onboard the research vessel (R/V) *Atlantis* during a cruise along the coast of California (32.8° N – 38.6° N) throughout the period 14 May – 7 June 2010 (**Figure 4.2**) (see *Ryerson et al.* (2012) for details of the CalNex 2010 campaign). Atmospheric aerosol samples were collected onboard the R/V *Atlantis* using a high-volume air sampler (HVAS), which was operated at various sampling durations ranging from 2 to 22 hours. The HVAS draws air at a flow rate of 1.1 m^3 min^{-1} through a four-stage cascade impactor (Tisch Series 230), which is loaded with pre-cleaned slotted glass fiber (GF) filters (Tisch TE-230GF, 12.7 × 17.8 cm) and a larger GF backup filter (Whatman GF/A, 20.3 × 25.4 cm). The cascade impactor aerodynamically fractionates particles into five size classes with cuts at 7.2, 3.0, 1.5, 0.95, and 0.49 μm aerodynamic diameter (D_a). In order to ensure an amount of nitrate

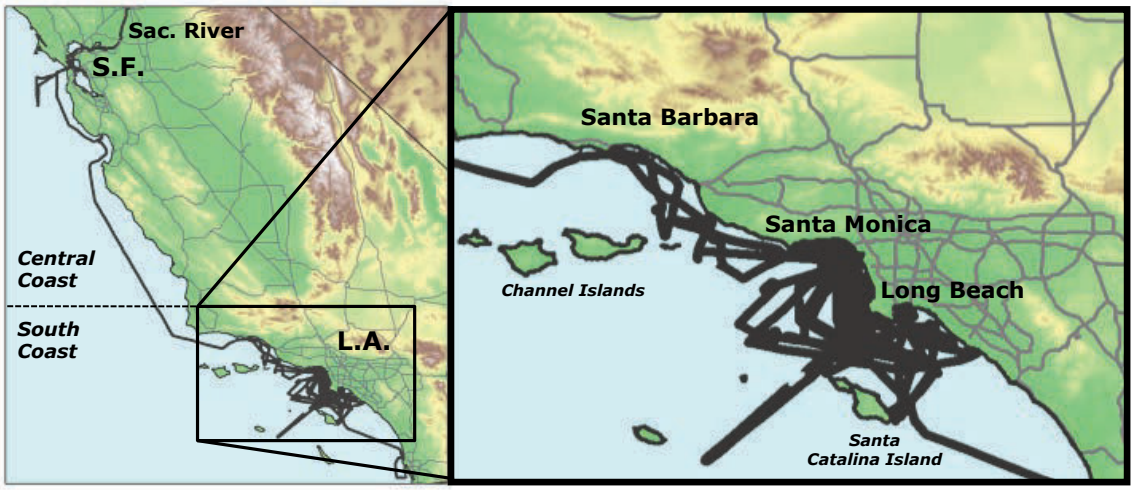

FIGURE 4.2 - Map of California showing the cruise track (black lines) of the R/V *Atlantis* in relation to the geographical features discussed in the text.

sample sufficient for isotopic analysis (approximately 100 nmol) in each extract solution, the filters of the first three stages and those of the last two stages were combined into two separate samples, one comprised of the total supermicron ("coarse fraction," $D_a > 0.95$ μm) particle fraction and the other containing all submicron ("fine fraction," $D_a < 0.95$ μm) particles.

The exact nature of the nitrate species collected during sampling using GF filters has always been an area of some debate (for example, see Yeatman *et al.* (2001) and references therein) due primarily to: i) the likelihood of gaseous HNO_3 adsorption onto the aerosol particles already captured within the filter material and ii) the disassociation and subsequent evaporative loss of NH_4NO_3. In this study, we have assumed that the HVAS filters quantitatively collect both particulate bound nitrate and gaseous HNO_3, which is likely considering the high sea-salt content of the marine boundary layer (MBL) (Prospero and Savoie, 1989). This approach is identical to that adopted by Morin *et al.* (2009) in a previous sampling campaign using the HVAS in the Atlantic MBL; furthermore, it is consistent with most previous studies of atmospheric nitrate isotopes at coastal sites (Michalski *et al.*, 2003; Morin *et al.*, 2007; Patris *et al.*, 2007; Savarino *et al.*, 2007), thus insuring that the results obtained here are intercomparable with those reported in the literature.

A total of 63 sets of coarse and fine aerosol samples were collected during the cruise. The first 27 sets of samples, obtained during the period 14 May - 27 May in the South Coast region (**Figure 4.2**), were collected on a diurnal frequency, from

approximately 08:00 - 19:00 and 19:00 - 08:00 Pacific Standard Time (PST) for daytime and nighttime collections, respectively. Sampling durations were allowed to vary in the range of 3 - 22 hours for the subsequent collection periods in the South Coast region during the period 28 May - 31 May (n = 12). For the remainder of the cruise (1 - 7 June), the R/V *Atlantis* transited through the San Francisco Bay and the Sacramento River (Central Coast) where an additional 24 sets of HVAS samples were collected with sampling durations in the range of 2 - 12 hours. In addition to the aerosol samples, 7 sets of operational blanks were collected at regular intervals throughout the cruise. Blank filters were subjected to all of the same storage, handling, and analytical procedures as field samples. After sampling, the filters were folded, placed into plastic bags, and stored in a freezer at -20 °C. Samples were then transported frozen to Grenoble for further processing.

4.2.2 Nitrate extraction and chemical analysis

Aerosol filter samples were extracted in 40 mL of UV-oxidized deionized water (18.2 MΩ resistivity) via centrifugation using Millipore Centricon™ filter units. Extract nitrate concentrations were then determined colorimetrically using a segmented-flow analyzer (QuAAtro™, SEAL Analytical). In this technique, nitrate was quantitatively reduced to nitrite by passage through a column containing copperized cadmium. The resulting nitrite was then determined by diazotization with sulfanilamide dihydrochloride followed by detection of absorbance at 520 nm. Samples were calibrated against nitrate standards obtained from the National Institute of Standards and Technology. Atmospheric nitrate concentrations were calculated as the quotient of nitrate filter loading and the total volume of air pumped through the filter at standard temperature and pressure. The nitrate contribution from blank filters was almost always found to be negligible (< 5 % of sample nitrate concentration for all samples with isotopic values reported in this study).

4.2.3 Isotopic analysis

Isotope ratios of NO_3^- ($^{17}O/^{16}O$, $^{18}O/^{16}O$, and $^{15}N/^{14}N$) were measured on a Finnigan™ MAT253 isotope ratio mass spectrometer (IRMS), which was equipped with a GasBench II™ on-line gas introduction system and coupled to an in-house built

nitrate interface. Nitrate in the PM filter extracts was prepared for isotopic analysis by conversion to N_2O via the bacterial denitrifier method (Sigman *et al.*, 2001; Casciotti *et al.*, 2002; Kaiser *et al.*, 2007). The details of our analytical procedure have been described thoroughly in Chapter 2 and elsewhere in the literature (for example, by Komatsu *et al.* (2008) and Morin *et al.* (2009)) and will be only briefly outlined here.

Denitrifying bacteria (*Pseudomonas aureofaciens*) were cultured in nitrate-amended soy broth and incubated for 5 days in stoppered glass bottles. Bacterial cultures, after concentration by centrifugation and resuspension, were dispensed as 2 mL aliquots into 20 mL glass vials, which were then crimped and purged with helium for 3 hours. Approximately 100 nmol of sample nitrate was then injected into the purged vials and the conversion of nitrate to nitrous oxide (N_2O) via bacterial denitrification was allowed to proceed overnight. The N_2O produced via denitrification was then cryofocused in a liquid nitrogen trap and introduced into a gold furnace where it was thermally decomposed at 900 °C to O_2 and N_2. Following separation via gas chromatography, the O_2 and N_2 sample gases were directed into the ionization chamber of the IRMS. All analytical steps were simultaneously performed on 100 nmol of nitrate isotopic standards and their equimolar mixtures (International Atomic Energy Agency USGS32, USGS34, and USGS35) (see Chapter 2). Individual analyses were normalized through comparison with these three nitrate reference materials. The overall accuracy of the method is estimated as the reduced standard deviation of the residuals from the linear regression between the measured reference materials and their expected values. For the results described here, the highest uncertainty values obtained for $\delta^{18}O$, $\Delta^{17}O$, and $\delta^{15}N$ were 2.0‰, 0.43‰, and 0.46‰, respectively.

4.2.4 Complementary Data

In order to establish the dominant routes of atmospheric transport during the cruise, air mass back trajectory (AMBT) analysis was conducted using the NOAA HYSPLIT (HYbrid Single-Particle Lagrangian Integrated Trajectory) model (Draxier and Hess, 1998). A five-day AMBT was computed for each sampling midpoint at an arriving altitude of 100 meters above sea level. The position of arrival for each AMBT was set to match the geographical location of the ship at the midpoint of each sampling period.

In addition to the HVAS, the R/V *Atlantis* also carried an assortment of instrumentation for *in-situ* measurements of trace gases (e.g., O_3 and NO_x), spectrally resolved irradiance (e.g., $j(O^1D)$ and $j(NO_2)$ the photolysis rate coefficients of ozone and NO_2, respectively), and meteorological variables (e.g., temperature, wind speed, relative humidity, etc.) (Ryerson *et al.*, 2012). One-minute average NO_x concentrations were determined via ozone-induced chemiluminescence/LED photolysis with a reported uncertainty of ± 4% and ± 11% for NO and NO_2, respectively (Lerner *et al.*, 2009). Ozone was measured continuously using a standard UV-absorption technique with a reported uncertainty of ± 2% (Williams *et al.*, 2006). Additionally, *in-situ* measurements of N_2O_5 were obtained via Cavity Ring-Down Spectroscopy (CaRDS). The CaRDS instrument detects N_2O_5 by thermal conversion to NO_3 followed by detection of absorbance at 662 nm. N_2O_5 was measured at one-minute sampling durations throughout the cruise with a reported uncertainty of ± 10% (Wagner *et al.*, 2011).

4.3 Results

The following section presents time-series of the concentration and stable isotope ratios of atmospheric nitrate collected throughout the R/V *Atlantis* cruise. This approach in displaying the results has been adopted in order to emphasize the diurnal variations observed. However, it should be kept in mind that these are not strictly temporal variations due to the movement of the ship. Nevertheless, these spatial variations were limited within the two major regions of sampling (South Coast and Central Coast, **Figure 4.2**); therefore, we have presented our measurements as a function of time but have made an effort to differentiate between the two regions, which were found to have distinct characteristics in terms of air mass history, gas-phase chemistry, and nitrate concentration and isotopic composition. Results for atmospheric nitrate are first presented in their raw size-segregated form in order to highlight variations observed as a function of aerosol size. Subsequently, results are presented in bulk form by mass-weighting the results obtained for the different size fractions, which have been summarized in **Table 4.1** (end of text). This has been done to allow for the direct comparison of our data to previous measurements of nitrate

isotopic composition, which have typically been performed on bulk aerosol samples (Michalski *et al.*, 2003; Morin *et al.*, 2007; 2008; Savarino *et al.*, 2007).

4.3.1 Atmospheric nitrate concentration and complementary data

Variations in the concentration of atmospheric nitrate in the coarse (D_a > 1 μm) and fine (D_a < 1 μm) PM fractions are shown in **Figure 4.3**. Nitrate concentrations varied over a wide range during the cruise, with bulk values as high as 5 μg m^{-3} measured in the Santa Monica Bay (15 - 16 May and 30 - 31 May) and values as low as 150 ng m^{-3} in the San Francisco Bay area. In agreement with previous studies of nitrate particle size distributions in the MBL (Yeatman *et al.*, 2001; Virkkula *et al.*, 2006; Arnold and Luke, 2007; Morin *et al.*, 2009), nitrate was consistently enriched in the coarse fraction, with mean (± 1σ) atmospheric concentrations of 1282 ± 1204 ng m^{-3} and 366 ± 434 ng m^{-3} for the coarse and fine PM fractions, respectively. The proportion of nitrate in the fine particle fraction varied in the range of 5 - 67% throughout the cruise, with a mean value of 27 ± 17%.

Clear differences in atmospheric nitrate concentration were observed between the South and Central Coast portions of the campaign. For the Central Coast, total atmospheric nitrate averaged 525 ± 321 ng m^{-3}, a range of values that is typical of the Pacific coastal MBL in areas not directly impacted by anthropogenic emissions (Malm *et al.*, 2004; Patris *et al.*, 2007). Conversely, the South Coast region was characterized by elevated concentration, with an average of 2388 ± 1438 ng m^{-3}. This observation can be unambiguously attributed to differences in atmospheric transport pathways between the two regions: the results of five-day AMBT runs (**Figure 4.4**) indicate that the air masses reaching the South Coast region frequently arrived from a northerly or northeasterly direction, often passing over the Los Angeles metropolitan area en route (**Figure 4.4a**). These air masses typically transport large quantities of anthropogenic aerosol due to the influence of urban emissions in the South Coast air basin (CARB, 2009). Samples obtained in the Central Coast region were collected from marine air masses arriving almost exclusively from a westerly or southwesterly direction (**Figure 4.4b**). The impact of air mass history is evident not only in the concentration of atmospheric nitrate but also in its distribution between the coarse and fine aerosol fractions. Although nitrate was present predominantly in the coarse fraction throughout the sampling period, the continental air masses sampled in the

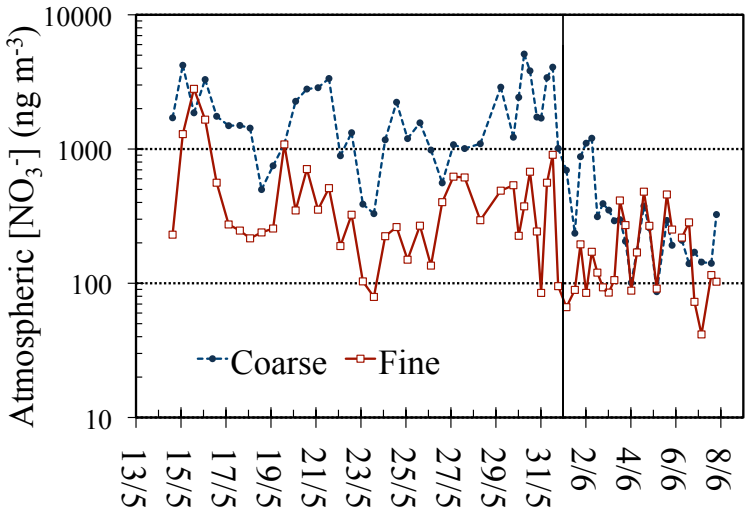

FIGURE 4.3 - Temporal variability in the atmospheric concentration of nitrate in the coarse (supermicron) and fine (submicron) particle fractions. The solid black line indicates the period of transit between the South and the Central Coast regions (1 June).

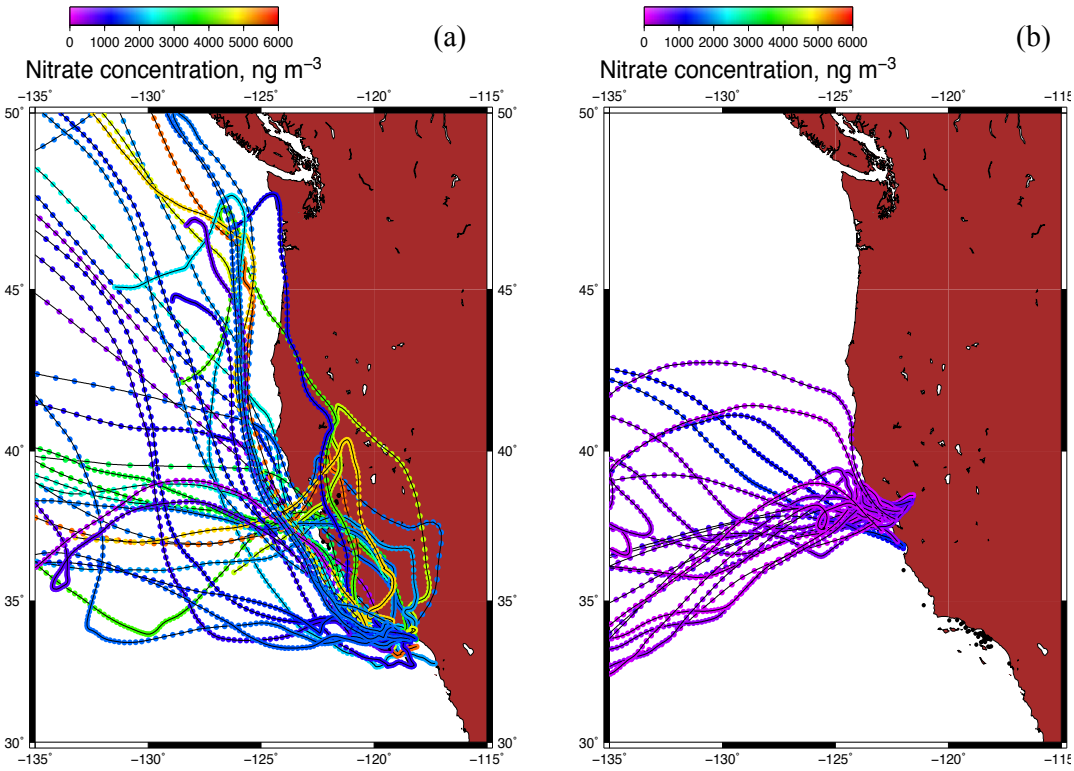

FIGURE 4.4 - Backward trajectories of the air masses reaching the R/V Atlantis during the South Coast **(a)** and Central Coast **(b)** segments of the cruise. AMBT data was obtained from the National Oceanic and Atmospheric Administration (NOAA) GDAS database using the hybrid single-particle Lagrangian integrated trajectory (HYSPLIT) model (Draxier and Hess, 1998). The trajectories are color-coded based on the average concentration of atmospheric nitrate during each sampling period.

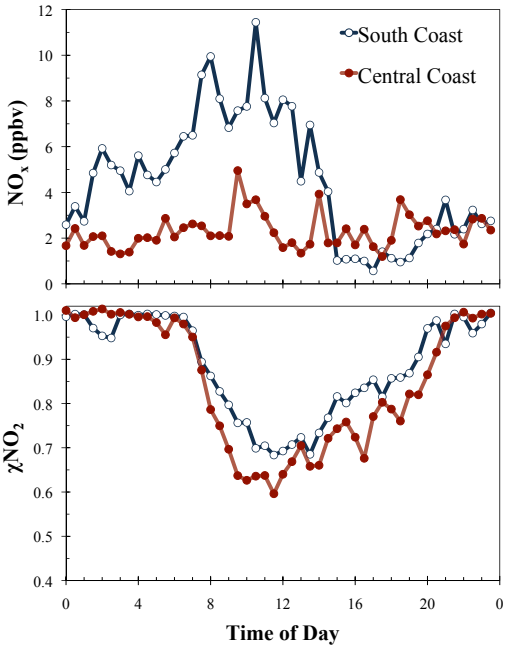

FIGURE 4.5 - Diurnally averaged values for total NO_x concentration and NO_2 molar ratio ($\chi NO_2 = [NO_2] / [NO] + [NO_2]$) during the two major segments of the cruise on R/V Atlantis. The values shown were computed from 30-minute averages of the NO and NO_2 concentration measurements conducted onboard.

South Coast region were characterized by a smaller proportion of nitrate in the fine aerosol fraction 20 ± 12% as compared to the Central Coast 38 ± 17%. In agreement with previous studies of the size distribution of atmospheric nitrate (Virkkula *et al.*, 2006; Morin *et al.*, 2009), a negative linear relationship was observed between the proportion of nitrate in the fine mode and ambient air temperature; however, the strength of this anticorrelation is higher when considering only the samples collected from predominantly marine air masses (r = 0.79) and neglecting those with AMBT showing influence of continental outflow.

The dissimilarity observed in air mass history between the South and Central Coast regions is also reflected in the gas-phase atmospheric chemistry measurements conducted onboard R/V *Atlantis*. The average NO_x concentrations observed during the South and Central Coast segments of the cruise were 6.4 (or nmol mol^{-1}) and 3.0 ppb, respectively, and the concentration differed by approximately a factor of two during both daytime and nighttime hours (**Figure 4.5**). NO was largely absent during the night, and the molar ratio of NO_2 ($\chi NO_2 = [NO_2]/[NO_x]$) exhibited a nighttime average of 0.99 throughout the campaign, which reflects the complete titration of NO to NO_2 by ozone at the end of the photochemical day. Daytime NO_2 molar ratios averaged 0.78 and 0.72 in the South and Central coast regions, respectively, and typically reached their lowest values during the period 09:00 – 15:00.

The diurnally averaged mixing ratios of ozone and N_2O_5 for the South and Central

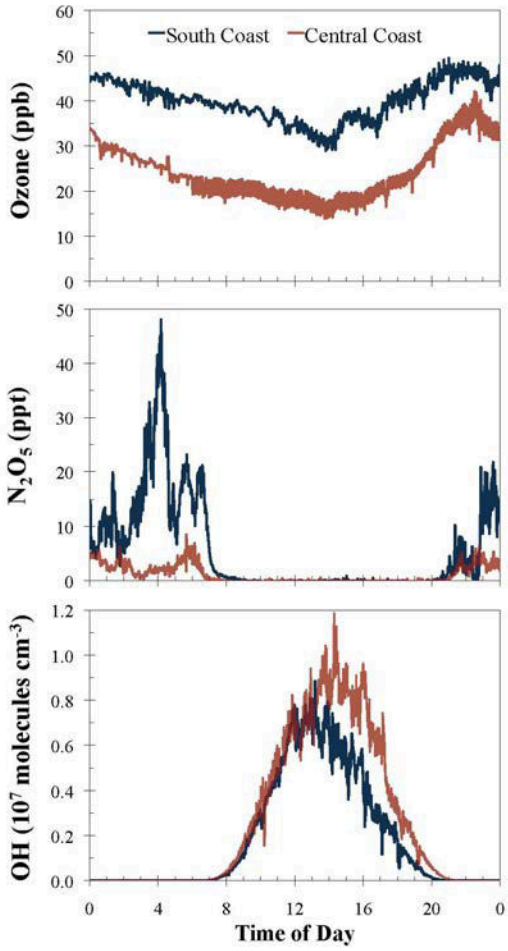

FIGURE 4.6 - Diurnally averaged mixing ratios of ozone (*upper*) and N_2O_5 (*middle*) during the South and Central coast segments of the cruise.

Coast regions of the campaign are shown in **Figure 4.6**. Also shown is the diurnally averaged OH concentration, which has been calculated from spectral radiometer measurements of the photolysis rate coefficient of ozone to produce $O(^1D)$ using the parameterization developed by Ehhalt and Rohrer (2000), which is not strictly valid for application to the coastal MBL, but should produce estimates within ± 30% of more sophisticated model calculations (Sommariva *et al.*, 2009). Ozone was consistently present at higher mixing ratios in the South Coast region, averaging 40.4 ± 8.4 ppb while averaging 25.1 ± 8.2 ppb in the Central Coast region. N_2O_5 reached significant concentrations only during nighttime hours (approximately 20:00 - 08:00) reflecting the rapid daytime loss of the NO_3 radical, which is an essential N_2O_5 precursor (**Figure 4.1**). Nighttime N_2O_5 mixing ratios averaged 11.4 and 2.3 ppt (or pmol mol^{-1}) for the South and Central coast regions, respectively. Collectively, the aerosol and gas-phase chemistry data reported here suggest a greater anthropogenic

impact on the air masses sampled during the southern portion of the cruise (Ryerson *et al.*, 2012).

4.3.2 Isotopic composition of nitrate

4.3.2.1 Size-segregated isotopic measurements

Size-resolved measurements of the comprehensive isotopic composition of atmospheric nitrate during the R/V *Atlantis* cruise are presented in **Figure 4.7**, which shows the $\delta^{18}O$, $\Delta^{17}O$, and $\delta^{15}N$ values obtained for the coarse (D_a > 1 μm) and fine (D_a < 1 μm) aerosol fractions.

In agreement with previous measurements of the oxygen isotopic composition of nitrate (Hastings *et al.*, 2003; Michalski *et al.*, 2003; Morin *et al.*, 2009), $\delta^{18}O(NO_3^-)$ was observed to vary in the range of approximately 50 - 90‰. When considering $\delta^{18}O(NO_3^-)$ values averaged over the duration of the campaign, no clear difference can be detected between the coarse and fine nitrate fractions, which possessed mean values of 66.3 ± 7.6‰ and 67.1 ± 8.3‰, respectively. However, significant deviations (~ 20‰) in $\delta^{18}O(NO_3^-)$ between size fractions occurred for individual samples and the average absolute difference between coarse and fine nitrate (8.0‰) was equal to 21% of the total variance. Conversely, measurements of the ^{17}O-excess of nitrate, $\Delta^{17}O(NO_3^-)$, reveal significantly different patterns in the two size fractions: $\Delta^{17}O$ was systematically higher in the supermicron mode, particularly in the South Coast region, where $\Delta^{17}O(NO_3^-)$ averaged 25.8 ± 1.7‰ and 23.3 ± 1.8‰ for the coarse and fine aerosol fractions, respectively, with an average difference of 2.6‰ (21% of the total variance). This observation is consistent with the results obtained by *Morin et al.* (2009) for atmospheric nitrate in the Atlantic MBL and is also in agreement with *Patris et al.* (2007) who reported a $\Delta^{17}O(NO_3^-)$ difference of approximately 1.5‰ between the coarse and fine fractions at a coastal site in northern California (Trinidad Head) during April/May. This asymmetrical size distribution of $\Delta^{17}O(NO_3^-)$ suggests that the oxidative pathways leading to the conversion of NO_2 to nitrate are sensitive to particle size, a trend that was less pronounced in the Central Coast region, where nitrate in the supermicron and submicron fractions exhibited similar $\Delta^{17}O(NO_3^-)$ values, averaging 22.6 ± 2.2‰ and 22.2 ± 2.0‰, respectively.

$\delta^{15}N(NO_3^-)$ values obtained in this study are in good agreement with previous size-

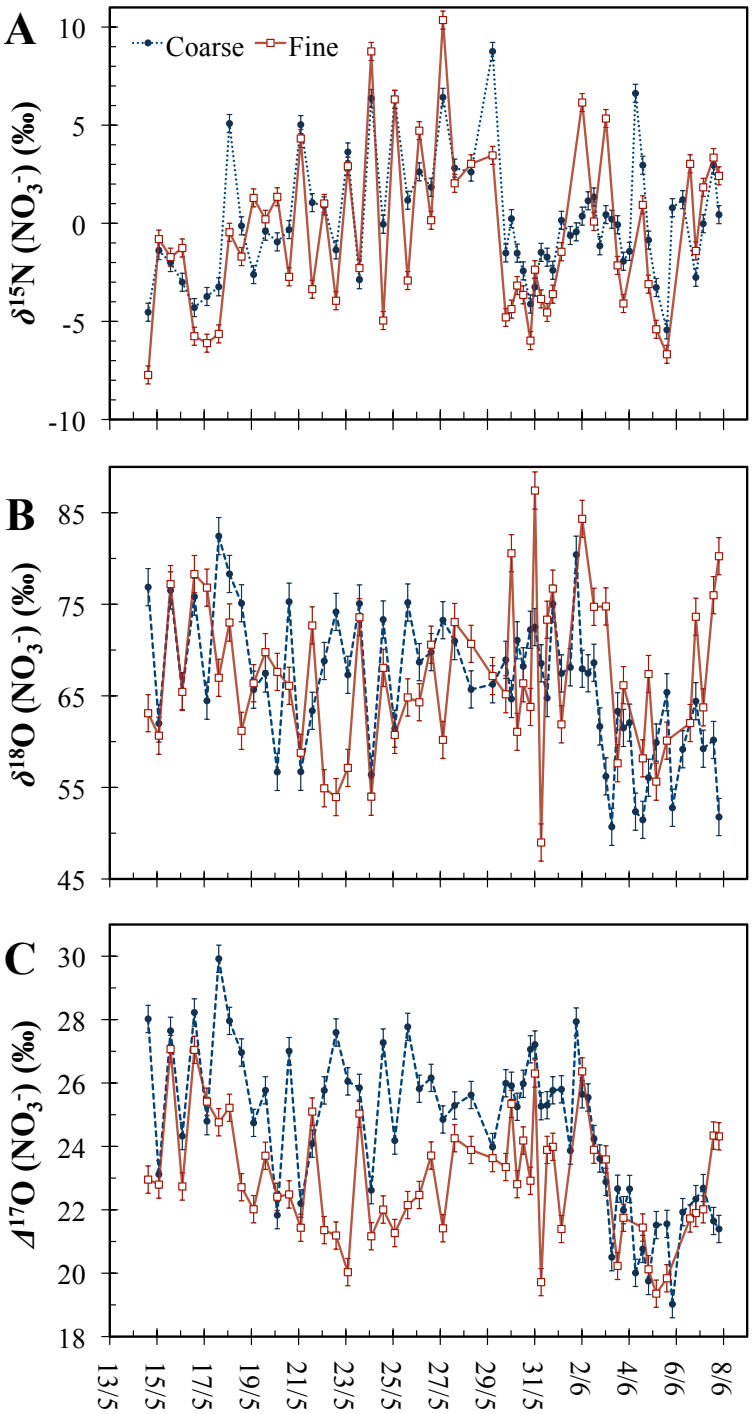

FIGURE 4.7 - Size-distributed isotope ratios for atmospheric nitrate collected during the cruise on R/V *Atlantis*: **(a)** $\delta^{15}N$, **(b)** $\delta^{18}O$, and **(c)** $\Delta^{17}O$. Coarse and fine isotopic values are represented by dashed and solid lines, respectively. Error bars indicate the analytical uncertainty of the measurements (2.0‰, 0.43‰, and 0.46‰ for $\delta^{18}O$, $\Delta^{17}O$, and $\delta^{15}N$, respectively.

resolved measurements of aerosol nitrate in non-polar regions (Yeatman *et al.*, 2001; Morin *et al.*, 2009). Contrary to the trend observed for oxygen isotopes, no clear tendency can be distinguished between the nitrogen isotope ratios of nitrate in the two aerosol size fractions. $\delta^{15}N(NO_3^-)$ in the supermicron mode ranged between -5.4 and 8.8‰ with an average of 0.1 ± 3.1‰, while submicron $\delta^{15}N(NO_3^-)$ values, although exhibiting a somewhat larger level of overall variability (-7.7 - 10.4‰), were of a comparable average value of -0.8 ± 4.1‰. The average $\delta^{15}N(NO_3^-)$ difference between the supermicron and submicron modes was only 2.2‰ for the duration of the campaign, 12% of the total range of variability. Furthermore, the correlation between $\delta^{15}N(NO_3^-)$ in the coarse and fine aerosol modes (r = 0.78) was much more robust than that observed for $\Delta^{17}O$ (r = 0.45).

4.3.2.2 Bulk isotopic measurements

Bulk values of $\delta^{18}O$, $\Delta^{17}O$, and $\delta^{15}N$ for atmospheric nitrate collected during the R/V *Atlantis* cruise have been computed by mass-weighting the values obtained for the coarse and fine aerosol fractions and are presented for each sampling period in **Table 4.1** (end of text) together with details regarding ship position, air mass origin, and atmospheric nitrate concentration and size distribution. Bulk $\Delta^{17}O$ and $\delta^{15}N$ values and their mass-weighted 24-hour averages are also shown as a time-series in **Figure 4.8**.

Bulk $\Delta^{17}O(NO_3^-)$ varied in the range of 19.0 to 29.2‰ during the sampling period with an average value of 24.1 ± 2.2‰. A clear distinction between the South and Central Coast segments of the campaign can be observed in the $\Delta^{17}O(NO_3^-)$ record: in the South Coast region, $\Delta^{17}O(NO_3^-)$ averaged 25.3 ± 1.6‰, reaching values as high as 29‰; in contrast, samples collected from marine air masses in the Central Coast region exhibited significantly reduced ^{17}O-excess, with values decreasing markedly after the Central Coast transit (1 June) and averaging 22.3 ± 1.8‰ during the last week of the cruise. These values are in the same general range as those previously reported for mid-latitude and coastal regions (see Alexander *et al.* (2009) and references therein), although the absolute range is somewhat larger than that previously observed. However, care should be taken in comparing our $\Delta^{17}O(NO_3^-)$ measurements to those found in the literature. Previous studies have typically employed sampling durations greater than 24 hours in order to ensure the collection of an adequate amount of nitrate for isotopic analysis, a strategy that effectively masks

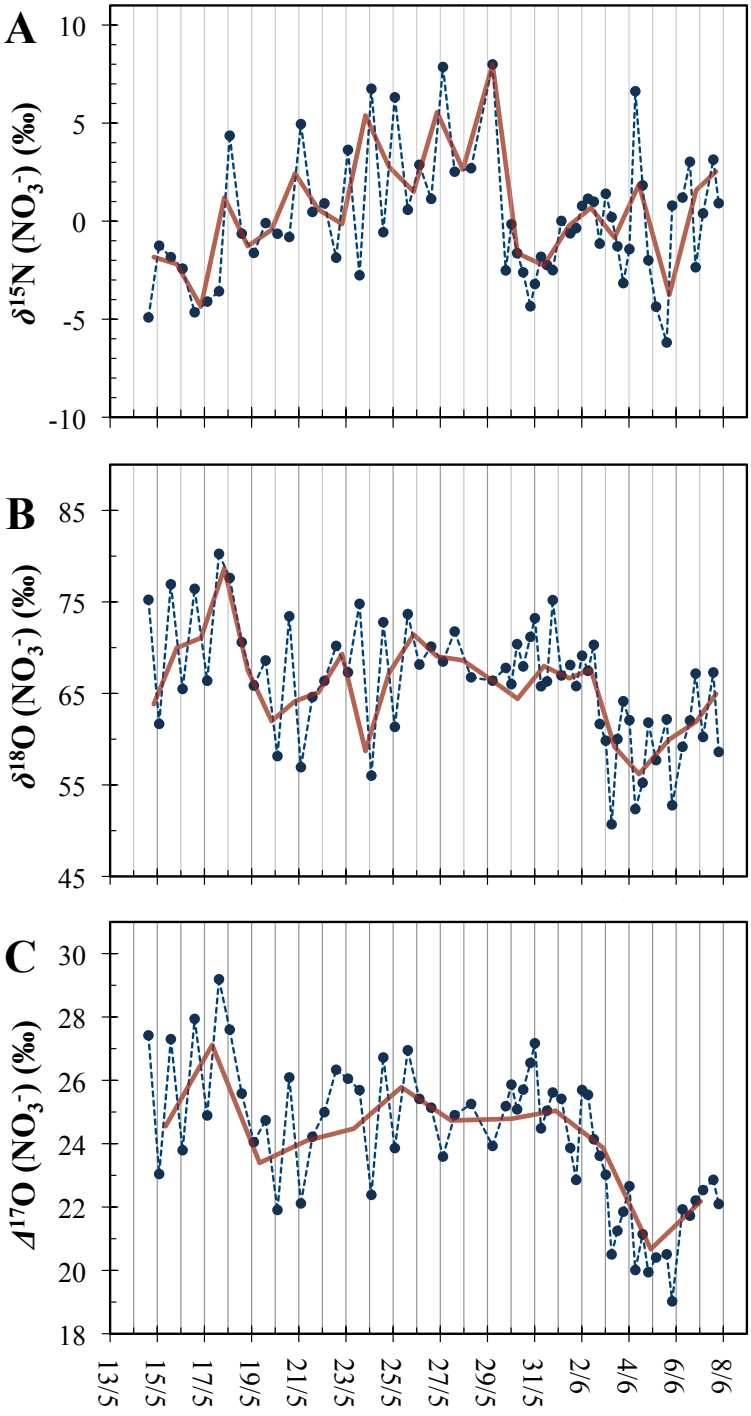

FIGURE 4.8 - Bulk isotope ratios for atmospheric nitrate collected during the cruise on R/V *Atlantis*: **(a)** $\delta^{18}O$, **(b)** $\Delta^{17}O$, and **(c)** $\delta^{15}N$. 24-hour averages are indicated by solid red lines.

any high-frequency variations in $\Delta^{17}O(NO_3^-)$. For example, in a one-year study of seasonal trends in $\Delta^{17}O(NO_3^-)$ in coastal California (La Jolla), Michalski *et al.* (2003) measured values ranging from 20 to 30‰ for samples spanning several days of collection time. Similarly, in an investigation of the isotopic composition of atmospheric nitrate over a time period similar to this study, Morin *et al.* (2009) measured bulk $\Delta^{17}O(NO_3^-)$ values ranging between 24 and 33‰ for samples collected at a daily time resolution along a ship-borne latitudinal transect (approximately 28° S - 52° N) in the Atlantic MBL. The detection of an equal magnitude of variability (~ 10‰) in the present study, which covered only a limited temporal and latitudinal extent (24 days and 5.8 degrees, respectively), is thus a significant result because it indicates the presence of high-frequency variations that are superimposed on the broad temporal and spatial features of the ^{17}O-excess of nitrate. This observation can be unambiguously attributed to the strong diurnal tendency observed in the nitrate $\Delta^{17}O$ record: for the 27 samples collected on a 12-hour frequency (14 – 27 May), $\Delta^{17}O(NO_3^-)$ averaged 24.1 ± 1.6‰ for samples collected during the night and 26.3 ± 1.4‰ for those collected during the day. This diurnal pattern is counterintuitive given that $\Delta^{17}O$ transfer is expected to be more significant during the night due to the instability of the NO_3 radical and absence of N_2O_5 during the day (**Figure 4.6**); however, when considering the relatively long lifetime of nitrate against deposition (Liang *et al.*, 1998), this observation can be reconciled in terms of the expected ^{17}O transfer associated with daytime and nighttime reactions (i.e., atmospheric nitrate collected during the night is likely to have been produced from NO_x oxidation occurring during the preceding day and *vice versa*). This impact of lifetime on $\Delta^{17}O(NO_3^-)$ dynamics has been recently observed at a coastal site in the UK (Bateman and Kaiser, 2010) and has also been predicted by numerical modeling studies that account for the diurnality of nitrate production (Morin *et al.*, 2011); however, the present report represents, to the best of our knowledge, the first detailed observational account of diurnal variations in the $\Delta^{17}O$ of nitrate.

The phase shift between the $\Delta^{17}O$ of nitrate and its precursor molecules was likely magnified in the present study due to a persistent diurnal sea breeze-land breeze recirculation in the South Coast air basin, which has been inferred from Doppler wind profile measurements at Los Angeles International Airport as described by *Wagner et al.* (2012). This thermally induced recirculation is a well known meso-scale phenomenon in which a strong daytime sea breeze brings marine air into the Los

Angeles basin, driving polluted urban air masses eastward (Gentner *et al.*, 2009), while a weaker land breeze transports urban emissions and their accumulated secondary species out of the basin and over Santa Monica Bay during the night (Cass and Shair, 1984). The impact of this recirculation on the temporal evolution of nitrate concentration and $\Delta^{17}O$ is most evident for the period 29 – 31 May, when 9 consecutive samples were collected at relatively short sampling frequencies (3 – 6 hour) under sea breeze-land breeze transitions in Santa Monica Bay. $\Delta^{17}O(NO_3^-)$ was linked with the wind direction measured onboard R/V *Atlantis* during this period with values decreasing during the land breeze phase (easterly wind) of recirculation, which typically began at midnight and continued until approximately 06:00, and increasing during the sea breeze phase (westerly wind), reaching maximum daily values at midnight. The atmospheric concentration of nitrate exhibited an opposite trend with respect to wind direction during this time, reaching maximum values (~ 4 – 5 μg m^{-3}) during the nocturnal land breeze and decreasing rapidly upon the transition to westerly marine flow. This observation suggests that the land breeze was likely dominated by nitrate produced through OH channel (R4.7) that had accumulated within the Los Angeles Basin during the day, while samples collected from the sea breeze were composed mostly of nitrate that had been produced through nocturnal reactions (R4.9 – R4.10) over water and returned to the coastal sampling location with the sea breeze in the morning.

Bulk aerosol $\delta^{15}N(NO_3^-)$ values ranged between -6.2 and 8.0‰ during the campaign with an average value of 0.0 ± 3.2‰. This mean and range of values is typical for $\delta^{15}N(NO_3^-)$ measurements in extra-polar regions (Freyer, 1991; Yeatman *et al.*, 2001; Hastings *et al.*, 2003; Baker *et al.*, 2007; Morin *et al.*, 2009); however, in disagreement with some of these studies, where large ^{15}N enrichments have been observed for nitrate of anthropogenic origin, there is no apparent correlation between $\delta^{15}N(NO_3^-)$ and air mass origin in the present study. For example, despite the significant differences in back trajectories and atmospheric nitrate concentration (**Figure 4.4**) observed in the two major sampling regions, no systematic difference can be detected in the nitrogen isotopic composition of nitrate collected during the South and Central Coast cruise legs, where $\delta^{15}N(NO_3^-)$ averaged 0.0 ± 3.5‰ and 0.0 ± 2.6‰, respectively; although, when considering the mass-weighted 24-hour averages, a small difference can be detected (averages of 0.8‰ for the South Coast and -0.1‰ for the Central Coast).

A particularly remarkable feature of the $\delta^{15}N(NO_3^-)$ record is the diurnal pattern observed, which is suggestive of isotopic effects associated with either the photolytic cycling of NO_2 or the conversion of NO_2 to nitrate. This is a surprising and significant result considering the long standing debate over the relative importance of NO_x sources, ^{15}N partitioning within the NO_x cycle, and the effect of atmospheric transport in determining temporal variations in the $\delta^{15}N$ of atmospheric nitrate (Hastings *et al.*, 2003; Jarvis *et al.*, 2008; Morin *et al.*, 2008). For the 27 diurnal samples (14 - 27 May), $\delta^{15}N(NO_3^-)$ averaged 2.1 ± 3.9‰ for nighttime collections and -1.2 ± 2.2‰ for samples collected during the day. Considering the temporal offset between NO_x cycling and nitrate production suggested by the $\Delta^{17}O(NO_3^-)$ record, this observation indicates that increased ^{15}N values are associated with daytime nitrate production (i.e., OH channel). Similar to the case with $\Delta^{17}O(NO_3^-)$, this is the first study to report direct observational evidence of diurnal variations in atmospheric $\delta^{15}N(NO_3^-)$.

4.4 Discussion

4.4.1 Interpretation of $\Delta^{17}O(NO_3^-)$ measurements

The general mass-balance equation (also termed the "continuity equation") governing the temporal evolution of the concentration of nitrate in a given air parcel is given by:

$$\frac{d}{dt}\left[NO_3^-\right] = \sum_i P_i - L \qquad (4.2)$$

where the atmospheric concentration of nitrate, denoted $[NO_3^-]$, is expressed in cm^{-3}. P_i and L represent the individual source rates and total sink rate of nitrate (in $cm^{-3}\ s^{-1}$), respectively, which include both chemical reactions within the parcel and fluxes at its boundaries.

The implementation of $\Delta^{17}O$ into the mass balance equation follows from the conservation of mass applied to the ^{17}O-excess. The key assumption behind this approach is that sink reactions do not induce a specific non-mass dependent fractionation and that every source reaction induces the transfer of a given $\Delta^{17}O$ value to the nitrate produced. This assumption would not be applicable to isotopic enrichment (δ) values or fractionation effects would have to be taken into account for every reaction considered. Therefore, while $\delta^{18}O(NO_3^-)$ results have been provided (**Table 4.1**) for comparison to previous studies and to allow for the computation of

$\delta^{17}O(NO_3^-)$, they are not discussed in the following analysis. The continuity equation for $\Delta^{17}O(NO_3^-)$ can be stated as follows:

$$\frac{d}{dt}\left[NO_3^-\right] \times \Delta^{17}O(NO_3^-) = \sum_i P_i \times \Delta^{17}O(NO_3^-)_i - L \times \Delta^{17}O(NO_3^-) \quad (4.3)$$

where $\Delta^{17}O(NO_3^-)_i$ is the specific $\Delta^{17}O$ signature induced by the nitrate production channel P_i (R4.7 - R4.10) (Morin *et al.*, 2011). In practice, $\Delta^{17}O(NO_3^-)_i$ values are estimated as a function of the $\Delta^{17}O$ of the precursors involved in a given nitrate production channel using mass balance calculations that trace the origin of oxygen atoms transferred during the chemical transformation of NO_x in the atmosphere. This approach, which springs from the pioneering work of Lyons (2001) and Michalski *et al*. (2003), has been applied in several studies to assess seasonal variations in NO_x transformation processes at regional to global scales (Alexander *et al.*, 2004; 2009; Michalski *et al.*, 2005; McCabe *et al.*, 2007; Morin *et al.*, 2007; 2008; 2009; 2012; Patris *et al.*, 2007; Savarino *et al.*, 2007; 2013; Kunasek *et al.*, 2008). In this study, we have estimated $\Delta^{17}O(NO_3^-)_i$ values for the nitrate production reactions previously discussed using the diurnally-integrated isotopic signature (DIIS) values modeled by Morin *et al.* (2011) for 45 °N. DIIS values implicitly integrate seasonal variations in the $\Delta^{17}O$ of NO_2 that occur due to changes in the activity of ozone (R4.3) relative to the peroxy radicals (R4.4), which are derived from O_2 and possess negligible ^{17}O-excess (Savarino and Thiemens, 1999). Estimates of $\Delta^{17}O(NO_3^-)_i$ are highly sensitive to the value used for $\Delta^{17}O(O_3^*)$, the transferrable $\Delta^{17}O$ of ozone (Morin *et al.*, 2011). We have scaled the DIIS functions to a $\Delta^{17}O(O_3^*)$ of 41‰, an average of measurements in the equatorial Atlantic MBL during a cruise in the spring of 2012 (Savarino *et al.*, 2013), obtained using a recently developed analytical technique with an uncertainty of ± 3‰ (see Chapters 2 and 3). This value is consistent in terms of $\Delta^{17}O(O_3)_{bulk}$ with the average of existing measurements of ozone isotopic composition obtained using the traditional "cryogenic technique" (Krankowsky *et al.*, 1995; Johnston and Thiemens, 1997); furthermore, this value is similar to that used in the landmark study of atmospheric nitrate isotopes by Michalski *et al.* (2003) who adopted an effective $\Delta^{17}O(O_3^*)$ value of 35‰ (Morin *et al.*, 2007). By adopting a $\Delta^{17}O(O_3^*)$ value of 41‰, we have calculated the $\Delta^{17}O$ signatures of the R4.7, R4.9, and R4.10 nitrate production pathways (see Introduction) to be 18.6‰, 36.6‰, and 30.2‰, respectively.

Solving numerically the system of equations formed by Equations 4.2 and 4.3 simultaneously yields the time evolution of the concentration and $\Delta^{17}O$ of atmospheric nitrate. By decomposing the left-hand side of Equation 4. 3 and reorganizing, we obtain:

$$\left[NO_3^-\right]\times\frac{d}{dt}\Delta^{17}O(NO_3^-)=\sum_i P_i\times\Delta^{17}O(NO_3^-)_i-\Delta^{17}O(NO_3^-)\times\left(L+\frac{d}{dt}\left[NO_3^-\right]\right) \quad (4.4)$$

Substituting the last term using Equation 4.2, we have:

$$\left[NO_3^-\right]\times\frac{d}{dt}\Delta^{17}O(NO_3^-)=\sum_i P_i\times\Delta^{17}O(NO_3^-)_i-\Delta^{17}O(NO_3^-)\times\sum_i P_i \quad (4.5)$$

After a final organization, we obtain:

$$\frac{d}{dt}\Delta^{17}O(NO_3^-)=\sum_i\frac{P_i}{\left[NO_3^-\right]}\times\left[\Delta^{17}O(NO_3^-)_i-\Delta^{17}O(NO_3^-)\right] \quad (4.6)$$

In plain words, we find that the time derivative of $\Delta^{17}O(NO_3^-)$ should scale as the sum of nitrate production rates multiplied by the deviation of their isotopic signature to the current $\Delta^{17}O$ value. Equation 6 can be further modified by introducing P_{total}, the total nitrate production rate:

$$\frac{d}{dt}\Delta^{17}O(NO_3^-)=\frac{P_{total}}{\left[NO_3^-\right]}\times\sum_i\frac{P_i}{P_{total}}\times\left[\Delta^{17}O(NO_3^-)_i-\Delta^{17}O(NO_3^-)\right] \quad (4.7)$$

Note that when nitrate is in steady state with respect to chemical production and loss:

$$\frac{P_{total}}{\left[NO_3^-\right]}=\frac{1}{\tau} \quad (4.8)$$

where τ is the atmospheric lifetime of nitrate.

Equation 4.7 thus provides a general mathematical formalism to evaluate temporal variations in $\Delta^{17}O(NO_3^-)$ in terms of the relative proportions of the production channels and atmospheric lifetime of nitrate. Until now, quantitative interpretations of $\Delta^{17}O(NO_3^-)$ measurements have been dependent on the implicit assumption of isotopic steady state. This assumption is equivalent to setting the left-hand side of Equation 4.7 to zero (i.e., hypothesized static $\Delta^{17}O(NO_3^-)$ time derivative), which results in the steady state formalism developed by *Michalski et al.* (2003):

$$\Delta^{17}O(NO_3^-)=\sum_i\frac{P_i}{P_{total}}\times\Delta^{17}O(NO_3^-)_i \quad (4.9)$$

The steady state approach has proven useful in the interpretation of seasonal-scale dynamics using $\Delta^{17}O(NO_3^-)$ observations averaged over several days; however, Equation 4.9 does not adequately address variations at temporal scales smaller than

the atmospheric lifetime of nitrate (e.g., diurnal variations). In the case of high frequency $\Delta^{17}O(NO_3^-)$ observations, the physical loss of nitrate through deposition must be explicitly taken into account using Equation 4.7. In the analysis that follows, we will utilize both approaches in their appropriate contexts. First, $\Delta^{17}O(NO_3^-)$ measurements aggregated over 48-hour periods (i.e., a time period greater than or equal to the lifetime of nitrate) will be interpreted using the traditional steady state formalism, which allows for a semi-quantitative assessment of the differences in nitrate formation pathways between the South and Central Coast segments of the cruise (Section 4.4.1.1). The steady state assumption will then be relaxed and the general mass balance equation will be applied in a detailed analysis of the diurnal variations observed during the period 14 - 27 May (Section 4.4.1.2).

4.4.1.1 Steady state evaluation of $\Delta^{17}O(NO_3^-)$

If the average contributions from at least two of the R4.7-R4.10 pathways are known or can be neglected, the relative contributions from the remaining two pathways can be derived using the steady state mass balance equation (Equation 4.9). The impact of halogen mediated nitrate production from the heterogeneous XNO_3 pathway (R4.8) is difficult to assess in the present study due to the absence of reactive halogen measurements during the cruise on R/V *Atlantis*. However, while this pathway can be quite significant in some environmental contexts (Morin *et al.*, 2007; Savarino *et al.*, 2013), reactions involving halogens are generally not expected to account for a considerable fraction of nitrate production in mid-latitude regions impacted by anthropogenic NO_x emissions (Sander *et al.*, 1999; Parrella *et al.*, 2012). Therefore, we will neglect for now the R4.8 channel and consider only the R4.7, R4.9, and R4.10 pathways. Of these three major nitrate formation channels, direct H abstraction by the NO_3 radical via reaction with DMS (R4.9), which was the overwhelmingly dominant NO_3 + RH reaction during the cruise on R/V *Atlantis* (Wagner *et al.*, 2012), is thought to play the least significant role in nitrate production. For example, using a global aerosol-oxidant model, *Alexander et al.* (2009) obtained an average annual contribution from the R4.9 pathway equal to only 4% of total nitrate production and Michalski *et al.* (2003) modeled a contribution from this pathway that varied between 1 and 10 % on an annual basis at La Jolla. If $P_{R4.9}/P_{total}$ is assumed to account for a 7.5 ± 5% of total nitrate production during this study, the same range adopted by Patris *et al.* (2007), Equation 4.9 can be rearranged

TABLE 4.2 - Mass-Weighted 48-Hour Averages of $\Delta^{17}O(NO_3^-)$ for the Coarse, Fine, and Bulk Aerosol Fractions.

Collection Dates	$\Delta^{17}O(NO_3^-)$ (‰)			$P_{R4.10}/P_{total}$ (%)[a]		
	Bulk	*Coarse*	*Fine*	*Bulk*	*Coarse*	*Fine*
14 - 15 May	24.6	24.6	24.4	40	40	39
16 - 17 May	27.1	27.4	25.9	62	64	51
18 - 19 May	23.4	23.5	23.0	30	31	26
20 - 21 May	24.1	24.3	22.8	36	38	24
22 - 23 May	24.5	25.0	21.3	39	43	12
24 - 25 May	25.8	26.3	22.0	50	55	17
26 - 28 May	24.7	25.4	23.2	41	47	28
29 - 30 May	24.8	25.0	23.7	42	43	32
31 May - 1 June	25.0	25.8	22.4	44	50	21
2 - 3 June	23.9	24.3	22.0	34	38	17
4 - 5 June	20.7	20.9	20.5	6	9	4
6 - 7 June	22.2	22.1	22.5	19	18	22

[a]The estimated relative production from the nocturnal N_2O_5 pathway has been calculated using the steady state approximation of Equation 4.9 and assuming $\Delta^{17}O(O_3^*) = 41‰$ and the relative importance of the NO_3-DMS pathway to nitrate production averages 7.5%.

and solved for the fractional contribution of the nocturnal N_2O_5 pathway ($P_{R4.10}/P_{total}$) by using 48-hour averages of $\Delta^{17}O(NO_3^-)$ as input. The results of this computation for the coarse, fine, and bulk (weighted) aerosol fractions are presented in **Table 4.2**.

Mass-weighting the subdiurnal isotopic measurements over 48-hour periods eliminates much of the temporal variability observed in the time-series and reveals an average $\Delta^{17}O(NO_3^-)$ of ~ 25‰ for the South Coast region, a seasonal signature for coastal California that is consistent with previous measurements and modeling (Michalski *et al.*, 2003; Alexander *et al.*, 2009). Individual 48-hour averages generate estimates of relative nitrate production via the N_2O_5 pathway ($P_{R4.10}/P_{total}$) that vary between 30 - 62%, with an average of 42 ± 10%, suggesting that this pathway played a quantitatively significant and sometimes dominant role in terms of NO_x removal in the air masses sampled in this region. This finding is consistent with recent studies that have found nocturnal processes to have a significant impact on the reactive nitrogen budget, converting a comparable amount of NO_x as daytime reactions in air masses impacted by anthropogenic emissions (Brown *et al.*, 2004; 2006); furthermore, the range of inferred $P_{R4.10}/P_{total}$ values obtained here is in excellent quantitative agreement with estimates for La Jolla during May/June (~ 30 - 50%)

based on atmospheric box modeling by Michalksi *et al.* (2003). Patris *et al.* (2007) derived somewhat higher contributions from the R4.10 pathway (~ 50 - 80%) from $\Delta^{17}O(NO_3^-)$ measurements in the MBL at Trinidad Head during April-May, although we suspect that the significance of the R4.10 pathway was likely overestimated in this study due to the use of a low $\Delta^{17}O$ signature for N_2O_5 hydrolysis in the mass-balance calculations (25.7‰).

The largest relative contributions from the N_2O_5 channel are attributed to the period 16 - 17 May, when the R/V *Atlantis* was stationed overnight in the Santa Monica Bay and sustained sea breeze-land breeze recirculation resulted in nitrate concentration maxima in both the coarse and fine modes (**Figure 4.3**). Daytime (sea breeze) nitrate collections during this period exhibited considerably elevated $\Delta^{17}O(NO_3^-)$ values (> 27‰), corresponding to a 48-hour average $P_{R4.10}/P_{total}$ estimate of 62%. Subsequent peaks in nocturnal nitrate production occurred when the R/V *Atlantis* had returned to Santa Monica Bay (20 - 21, 24 - 25, 29 - 31 May) and are also associated with periods of persistent nighttime outflow from the Los Angeles metropolitan region (Wagner *et al.*, 2012). Conversely, periods of predominantly onshore atmospheric transport (e.g., 18 - 19, 22 - 23, and 26 - 28 May) correspond to relatively low atmospheric nitrate concentrations and reduced contributions from the R4.10 channel. Similarly, the low 48-hour average $\Delta^{17}O(NO_3^-)$ values obtained for samples collected in the Central Coast region (1 - 7 June) correspond to estimates of contributions from the N_2O_5 pathway that vary between 6 and 34%, indicating that the daytime OH + NO_2 channel was the dominant NO_x sink in the marine air masses sampled in this region (60 - 85%). The observation of significant contributions from N_2O_5 hydrolysis in polluted air masses from continental outflow, as well as the broad differences in $\Delta^{17}O(NO_3^-)$ and air mass origin detected between the two main sampling regions, suggests a strong spatial coupling of anthropogenic emissions and nighttime chemistry (Andreae and Crutzen, 1997).

Due to the relatively long lifetime of nitrate (~ 1 or more days) (Liang *et al.*, 1998; Levy *et al.*, 1999; Brown *et al.*, 2004), the *in-situ* atmospheric chemistry data obtained during the cruise on R/V *Atlantis* is not directly reflective of the nitrate collected during any individual sampling period. For example, it appears that nitrate concentration gradients during periods of sea breeze-land breeze recirculation were determined primarily by source variability and mixing rather than *in-situ* chemical production. In this case, a robust evaluation of nitrate isotope measurements in terms

of parallel atmospheric measurements would require the use of a chemical transport model (CTM) to predict the evolution of nitrate along the trajectories of the air masses sampled, a modeling effort that is beyond the scope of this study. However, the general trends observed in precursor gas concentrations are broadly indicative of the differences in daytime and nighttime NO_x processing between the two main sampling regions. The average nighttime N_2O_5 mixing ratio in the Central Coast (2.3 ppt) was significantly lower than that observed during the southern section of the cruise (11.4 ppt) and also much lower than previous observations of N_2O_5 in the MBL reported in the literature (Brown *et al.*, 2004; Sommariva *et al.*, 2009; McLaren *et al.*, 2010). N_2O_5 concentrations were typically below the limit of detection (~1 ppt) during the period 4 - 5 June, when $\Delta^{17}O(NO_3^-)$ reached its lowest values and the inferred contributions from the heterogeneous pathway amount to 6%. Furthermore, while the inferred OH radical production is similar for the two sampling regions, ozone was present at significantly higher nighttime concentrations in the South Coast (**Figure 4.6**). Considering that the average concentrations of NO_x observed in the South and Central Coast regions differed by approximately a factor of two during both nighttime and daytime hours, the disproportionality in OH and ozone concentrations implies a larger potential for nighttime NO_3 radical chemistry to play a significant role in nitrate production in the South Coast. Therefore, the broad spatial variability in the relative importance of nocturnal NO_x processing inferred from the South and Central Coast $\Delta^{17}O(NO_3^-)$ records seem to be largely supported by the *in-situ* atmospheric chemistry data obtained during the cruise on R/V *Atlantis*.

The systematically elevated $\Delta^{17}O(NO_3^-)$ observed in the supermicron aerosol fraction in the South Coast region amounts to a large difference in terms of the resulting nitrate budget calculations (**Table 4.2**): on average, 49% of nitrate in the coarse mode is attributed to the N_2O_5 pathway in this region as compared to 32% in the submicron mode. This observation is consistent with all previous size-distributed measurements of the $\Delta^{17}O$ of atmospheric nitrate in the MBL (Patris *et al.*, 2007; Morin *et al.*, 2009) and suggests that the size distribution of $\Delta^{17}O$ is determined largely by the physical characteristics of the individual precursor gases (HNO_3, NO_3, N_2O_5, etc.), with heterogeneous N_2O_5 reactions occurring preferentially on the surface of supermicron particles. This greater relative importance of the coarse aerosol fraction as a sink for N_2O_5 in coastal and marine regions may indicate an increased efficiency of N_2O_5 hydrolysis on deliquesced sea salt particles, which typically

represent a large fraction of total aerosol surface area in the MBL. However, increased $\Delta^{17}O(NO_3^-)$ values in the coarse fraction could also result from the reaction between N_2O_5 and particulate chloride (Cl^-), which is abundant in coarse marine aerosol (Bertram and Thornton, 2009):

$$N_2O_5 + Cl^-_{(aq)} \rightarrow ClNO_2 + NO_3^-{}_{(aq)} \quad \text{(R4.11)}$$

Most previous studies of nocturnal NO_x transformations have assumed that N_2O_5 reactions on particles proceed solely through the hydrolysis channel to form two HNO_3 molecules. However, reaction with Cl^- may compete with N_2O_5 hydrolysis in the case of marine aerosols, with recent studies suggesting that this pathway represents a significant fraction of total N_2O_5 consumption in some polluted coastal environments (Thornton *et al.*, 2010; Phillips *et al.*, 2012). This N_2O_5 loss mechanism has important implications for air quality because it results in the production of nitryl chloride ($ClNO_2$) and only one HNO_3 molecule, thereby decreasing the magnitude of the nocturnal NO_x sink from HNO_3 formation while also forming a reactive halogen species that may subsequently influence ozone chemistry (Knipping and Dabdub, 2003; Osthoff *et al.*, 2008). Reactive chlorine measurements during the R/V *Atlantis* cruise suggest that the R4.11 pathway represented a significant N_2O_5 loss mechanism in the South Coast region, particularly during nights spent in Santa Monica Bay (e.g., 16, 21, 24, and 25 May) when $ClNO_2$ concentrations greater than 500 ppt were observed during the land breeze circulation phase between approximately 03:00 and 06:00 (Riedel *et al.*, 2012; Wagner *et al.*, 2012). Coarse fraction $\Delta^{17}O(NO_3^-)$ values were greater than 27‰ for samples collected on the days following these high nighttime $ClNO_2$ events; furthermore, coarse $\Delta^{17}O(NO_3^-)$ was enriched 4 - 6‰ over the fine fraction for these samples. *Hayes et al.* (2012) note that sea salt aerosol measured in the Los Angeles Basin was substantially depleted in Cl^- during the cruise on R/V *Atlantis*, presumably due to nocturnal atmospheric processing involving reactive uptake of N_2O_5; they further noted a parallel increase in supermicron aerosol nitrate, consistent with our findings. Based on these observations, we tentatively suggest that the association of higher $\Delta^{17}O(NO_3^-)$ values with coarse aerosol observed in this study and others results from an enhanced importance of the R4.11 pathway in the MBL; furthermore, our results suggest that high frequency size-distributed $\Delta^{17}O(NO_3^-)$ measurements could be a useful tool for evaluating the magnitude and spatiotemporal variability of this sink, a potential application of nitrate stable isotopes that is deserving of further study.

$\Delta^{17}O(NO_3^-)$ did not vary widely with particle size for samples collected in the Central Coast region (**Figure 4.7**), corresponding to estimates of contributions from the R4.10 pathway of 22% and 15% for coarse and fine particles, respectively. This observation is similar to that of Patris *et al*. (2007), who reported comparable contributions from the N_2O_5 pathway for coarse and fine aerosol in air masses transported to the California coast from Asia and attributed this observation to the redistribution of nitrate during long-range transport. The difference in air mass origin and $\Delta^{17}O(NO_3^-)$ observed between the South and Central Coast regions offers a potential explanation for these observations: atmospheric residence time declines sharply as a function of diameter for particles > 1 μm, while fine particle nitrate exhibits a lower deposition velocity and remains suspended in the atmosphere for longer periods (Chen *et al.*, 2007). Atmospheric deposition during long-range transport may thus result in the disproportionate removal of nitrate produced through the N_2O_5 pathway when it accumulates preferentially in the coarse fraction (e.g., due to the R4.11 pathway). Therefore, the observation of a constant size distribution for both mass (**Figure 4.3**) and $\Delta^{17}O(NO_3^-)$ (**Figure 4.7**) in the Central Coast can be interpreted as further evidence that the nitrate sampled in this region was likely transported long distances across the ocean, providing a background source of nitrate with a low $\Delta^{17}O(NO_3^-)$ value that disrupted the variability induced by emissions from the continent.

It should be recognized that the estimates of $P_{R4.10}/P_{total}$ shown in **Table 4.2** are only semi-quantitative due to potential biases resulting from the assumptions drawn regarding the isotopic composition of ozone ($\Delta^{17}O(O_3^*)$ = 41 ‰) and the relative proportions of nitrate production from the halogen ($P_{R4.8}/P_{total}$ = 0 %) and DMS ($P_{R4.9}/P_{total}$ = 7.5 %) channels. Variations in the R4.8 and R4.9 pathways introduce modest uncertainties. For example, variability in the DMS pathway induces an error of ± 8% in terms of the resulting estimate of $P_{R4.10}/P_{total}$ when $P_{R4.9}/P_{total}$ is allowed to fluctuate in the range of 2.5 - 12.5% (i.e., ± 5 %), although variations in DMS concentration that are larger than those assumed in coarse global or regional models could introduce larger uncertainty (Osthoff *et al.*, 2009). Furthermore, we estimate a relatively small 6 - 12 % decrease in $P_{R4.10}/P_{total}$ when 5 - 10% of total nitrate production is attributed to the daytime halogen pathway in Equation 4.9, assuming an isotope transfer similar to that proposed for $BrNO_3$ hydrolysis by *Morin et al.* (2009). However, quantitative estimates of contributions from the N_2O_5 pathway are

exceptionally sensitive to the $\Delta^{17}O(O_3^*)$ value chosen in the calculation: for example, allowing $\Delta^{17}O(O_3^*)$ to vary by ± 3‰ (the analytical uncertainty of the method used for ozone isotope analysis (see Chapter 2) results in a recalculation of $P_{R4.10}/P_{total}$ on the order of ± 15%. If we consider a relatively large 34 - 48‰ range of potential $\Delta^{17}O(O_3^*)$ values, the higher end of the 25 - 48‰ range evaluated in a global model by Alexander *et al.* (2009), the resulting average P_{R10}/P_{total} estimate for the South Coast region varies between 7 and 82%, thus inverting the potential atmospheric interpretation resulting from the same $\Delta^{17}O(NO_3^-)$ value. Clearly, the quantification of the nitrate production budget from $\Delta^{17}O(NO_3^-)$ is highly dependent on the value of $\Delta^{17}O(O_3^*)$ adopted in the mass-balance calculation, which underscores the need for further field measurements to better constrain the ^{17}O-excess of ozone. In the next section, we will demonstrate how the diurnal variations observed for $\Delta^{17}O(NO_3^-)$ in this study can be used to eliminate unrealistic assumptions regarding the quantity of $\Delta^{17}O(O_3^*)$.

4.4.1.2 Diurnal variations in $\Delta^{17}O(NO_3^-)$

One of the most remarkable features of the $\Delta^{17}O(NO_3^-)$ record obtained for the cruise on R/V *Atlantis* is the pronounced diurnal variability observed during the period 14 – 27 May, when samples were collected at a 12-hour frequency allowing for direct daytime/nighttime comparisons. These diurnal cycles indicate that the lifetime of atmospheric nitrate is sufficiently short in some cases that $\Delta^{17}O(NO_3^-)$ reflects variations in the relative contributions of daytime and nighttime oxidation pathways. Such variations cannot be interpreted within the traditional steady state framework used in the previous section; however, the general mass balance equation (continuity equation) repeated below can be used to evaluate these diurnal fluctuations in $\Delta^{17}O(NO_3^-)$ by accounting for nitrate sinks (i.e., the atmospheric lifetime of nitrate against wet and dry deposition at chemical steady state):

$$\frac{d}{dt}\Delta^{17}O(NO_3^-) = \frac{1}{\tau} \times \sum_i \frac{P_i}{P_{total}} \times \left[\Delta^{17}O(NO_3^-)_i - \Delta^{17}O(NO_3^-)\right] \qquad (4.10)$$

In the following analysis, we will consider the same three nitrate production pathways introduced in Section 4.4.1.1, namely the R4.7, R4.9, and R4.10 channels, and apply the same assumptions regarding $\Delta^{17}O(O_3^*)$ and $P_{R4.9}/P_{total}$. The rate of the R4.7 reaction is negligible during the night due to the rapid loss of the OH radical after 20:00 (**Figure 4.6**) and can therefore be considered only during daytime hours

(08:00 – 20:00). Due to the instability of the NO_3 radical during the day, the rate of nitrate production through the R4.9 and R4.10 channels can be considered only for nighttime hours (20:00 – 08:00). It is possible that the lifetime of the NO_3 radical against photolysis can be sufficiently long in some cases to lead to the daytime production of HNO_3 (Brown *et al.*, 2005); however, the assumption of a negligible daytime contribution from this pathway seems to be substantiated by the *in-situ* measurements of N_2O_5 (**Figure 4.6**), which was found to be largely absent during the day. Because the R4.7 and R4.9/R4.10 production channels are restricted to daytime and nighttime hours, respectively, the values of P_i/P_{total} can be assumed *a priori* in the case of samples collected on a diurnal frequency (collections periods were approximately 08:00 – 19:00 and 19:00 – 08:00 for daytime and nighttime collections, respectively). This greatly simplifies the mass-balance calculation and allows for an evaluation of the temporal evolution of $\Delta^{17}O(NO_3^-)$ solely in terms of the atmospheric lifetime of nitrate.

The lifetime of nitrate in the troposphere can vary widely and it cannot be calculated directly from the gas-phase measurements made onboard. If we assume a constant τ value of 24 hours and ignore for now any potential variability in atmospheric lifetime, we can compare the time derivative of $\Delta^{17}O(NO_3^-)$ observed in this study with that predicted by the continuity equation as shown in **Figure 4.9**. Linear regression analysis reveals a robust correlation between these two variables ($r = 0.84$, $n = 27$), indicating that the continuity equation accurately describes the general trend observed in the data; furthermore, the absolute magnitude of the observed variability is in good agreement with that computed by constraining the continuity equation to our $\Delta^{17}O(NO_3^-)$ measurements, suggesting that the adopted value of τ (24 hours) is appropriate in many cases. The calculated values are more consistent with the observations during periods of sustained sea breeze-land breeze recirculation in the Los Angeles Basin, such as during the period 14 - 17 May, when both the concentration and $\Delta^{17}O$ of nitrate reached maximum values; conversely, periods of predominantly onshore flow (e.g., 18 - 19 May, 23 May, 26 - 27 May) seem to cause a disruption in the temporal evolution of $\Delta^{17}O(NO_3^-)$, presumably by delivering nitrate from the remote MBL to the coastal sampling location and displacing continental air masses laden with anthropogenic nitrate, an assertion that is consistent with the decreased atmospheric concentrations observed during these

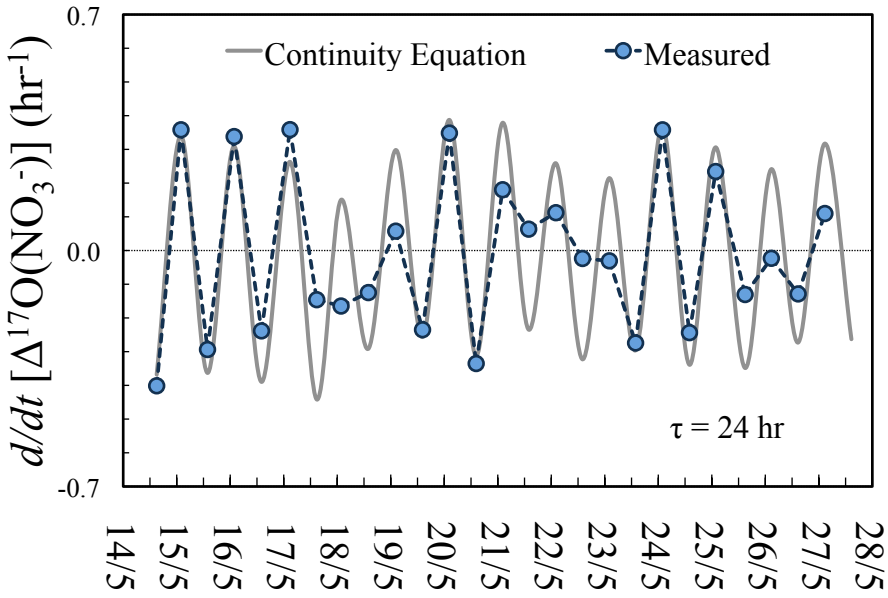

FIGURE 4.9 - Comparison of the $\Delta^{17}O(NO_3^-)$ derivatives observed in this study with those generated by constraining the continuity equation to our measurements. The linear fit between these variables is given by m = 1.11, b = -0.011, where y = mx + b (r = 0.84).

periods (**Figure 4.3**). Because the magnitudes of the observed variations in $\Delta^{17}O$ are much smaller than that predicted by the continuity equation during periods of marine transport, it seems likely that the nitrate sampled at these times possessed a longer atmospheric lifetime, thus partially masking the extent of diurnal variability, consistent with the arguments developed in Section 4.4.1.1 regarding the size distribution of nitrate and atmospheric lifetime.

By using the measured $\Delta^{17}O(NO_3^-)$ values as input, we have quantified the atmospheric lifetime of the nitrate sampled during the period 14 - 27 May by rearranging Equation 4.10 and solving directly for τ. The results of this computation are shown in **Figure 4.10** along with the total atmospheric nitrate concentration. It should be borne in mind that our estimates of τ likely represent "apparent" lifetimes as the continuity equation produces unreliable results during episodes of instability in air mass origin as the underlying assumption of following a given air parcel is violated. For example, changes in $\Delta^{17}O$ that are in the opposite direction than predicted by the continuity equation result in negative τ values for five samples (data not shown in **Figure 4.10**) and occur in conjunction with transitions from continental to marine atmospheric transport in all cases. However, the τ values obtained for the majority of samples are in good agreement with those typically encountered in the literature. For example, Liang *et al.* (1998) used a photochemical model to simulate NO_x cycling in

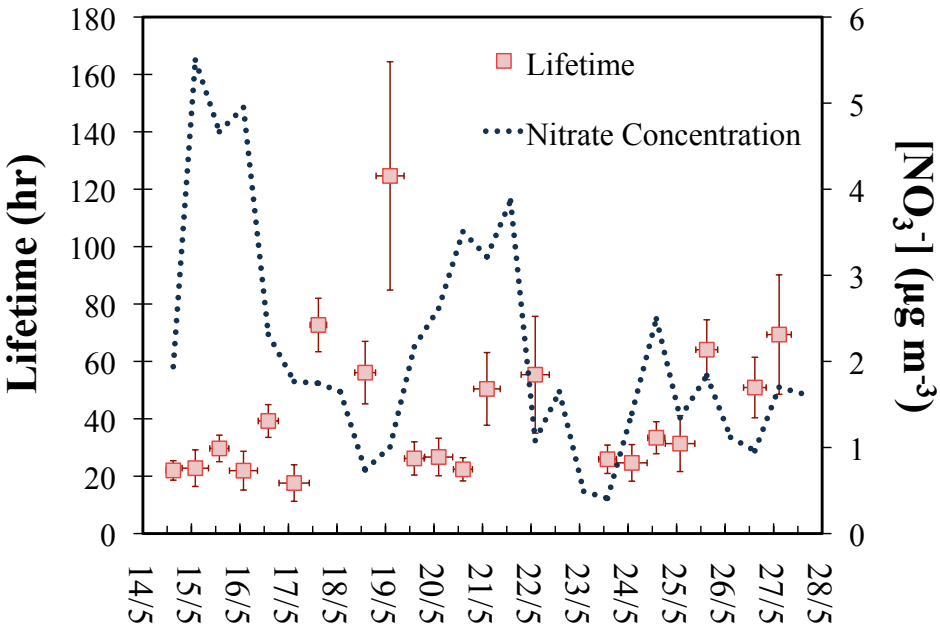

FIGURE 4.10 - Time series showing the lifetime of atmospheric nitrate (squares) as calculated using Equation 4.10 for the period 14 - 27 May. Error bars represent the uncertainty induced by allowing $\Delta^{17}O(O_3^*)$ to vary by ± 3‰ in the calculation. The total atmospheric nitrate concentration (secondary y-axis) is indicated by a dotted line.

the industrialized eastern U.S. and obtained average τ values for nitrate ranging from 12 hours in the spring to 26 hours in the fall. The τ values estimated in this study, which vary within the range of 18 to 39 hours during periods of nighttime continental outflow to the Santa Monica Bay (Wagner *et al.*, 2012), are largely consistent with these findings. Furthermore, these values substantiate the assumption made in Section 4.4.1.1 regarding the lifetime of nitrate (i.e., 12 hours < τ < 48 hours). Estimates of τ are higher for samples collected during periods of marine transport, typically ranging from 2 to 3 days and reaching values as high as 5 days. Millet *et al.* (2004) used a variability-lifetime approach to estimate the lifetime of submicron particulate nitrate in air masses arriving at the California coast (Trinidad Head) from the Pacific Ocean and obtained average values of 3 to 7 days, consistent with our estimates for onshore flow periods. Assuming a boundary layer depth of 900 m over the California coast (Wood and Bretherton, 2004), the atmospheric lifetimes inferred in this study correlate to deposition velocities of 0.4 - 1.4 cm s^{-1}, in excellent agreement with the estimates commonly encountered in the literature for submicron and supermicron particulate nitrate (0.1 and 2.0 cm s^{-1}, respectively) and gaseous HNO_3 (1.0 cm s^{-1}) (Duce *et al.*, 1991; Hauglustaine *et al.*, 1994; Baker *et al.*, 2007; Chen *et al.*, 2007).

In addition to allowing for an estimation of the atmospheric lifetime of nitrate, the application of the continuity equation to the diurnal variations observed in this study also provides a unique opportunity to evaluate different assumptions regarding the quantity of $\Delta^{17}O(O_3^*)$. **Figure 4.11** compares the observed $\Delta^{17}O(NO_3^-)$ time derivatives to output produced by constraining the continuity equation to our $\Delta^{17}O(NO_3^-)$ measurements at $\Delta^{17}O(O_3^*)$ values of 34, 41, and 48‰ (the same range discussed in Section 4.4.1.1). Each panel represents a different assumption in the equation regarding τ. From inspection of **Figure 4.11**, it is clear that changes in the assumed τ value are associated with changes in the slopes of the regression lines, while changes in the $\Delta^{17}O(O_3^*)$ value result in changes to the intercepts. Slopes are closest to unity (i.e., proportionality between the calculated and measured values) when τ is taken to be 24 hours, while τ values of 12 and 48 hours result in slopes of approximately 2.0 and 0.5, respectively. This strongly suggests that 24 hours was indeed the average atmospheric lifetime of nitrate during the period 14 - 27 May. However, assuming $\Delta^{17}O(O_3^*) = 48‰$ and $\tau = 24$ hours leads to a significant overestimation of the magnitude of peaks in $\Delta^{17}O(NO_3^-)$ occurring as a result of nighttime nitrate production (i.e., the amplification of the continuity equation curve shown in **Figure 4.9**). Conversely, assuming $\Delta^{17}O(O_3^*) = 34$ ‰ and $\tau = 24$ hours overestimates the downward movement of $\Delta^{17}O(NO_3^-)$ resulting from the OH + NO_2 pathway during the day. $\Delta^{17}O(O_3^*)$ and τ values of 41‰ and 24 hours, respectively, provide the best agreement between the calculated and measured values, with a best fit line almost identical to the 1:1 line (m = 1.11, b = -0.011, where y = mx + b). Furthermore, the assumption of $\Delta^{17}O(O_3^*) = 41‰$ results in a best fit line that passes through the origin regardless of the value chosen for τ. These observations argue strongly that the appropriate $\Delta^{17}O(O_3^*)$ value is indeed in the range of 41 ± 3‰ ($\Delta^{17}O(O_3)_{bulk} \approx 25$ - 29‰), an assumption that has formed the basis of quantitative interpretations derived from isotope ratio measurements in many previous studies (Röckmann *et al.*, 2001; Michalski *et al.*, 2003; 2004; 2005; Alexander *et al.*, 2004; Morin *et al.*, 2007; 2009; 2012; Patris *et al.*, 2007; Savarino *et al.*, 2007; Kunasek *et al.*, 2008). Furthermore, these findings lend credence to the existing measurements of ozone ^{17}O-excess reported in the literature (Krankowsky *et al.*, 1995; Johnston and Thiemens, 1997), including the most recent results obtained with the nitrite-coated filter method (see Chapters 2 and 3), and substantiate the quantitative conclusions drawn in Section 4.4.1.1 regarding the average contributions from the N_2O_5 pathway.

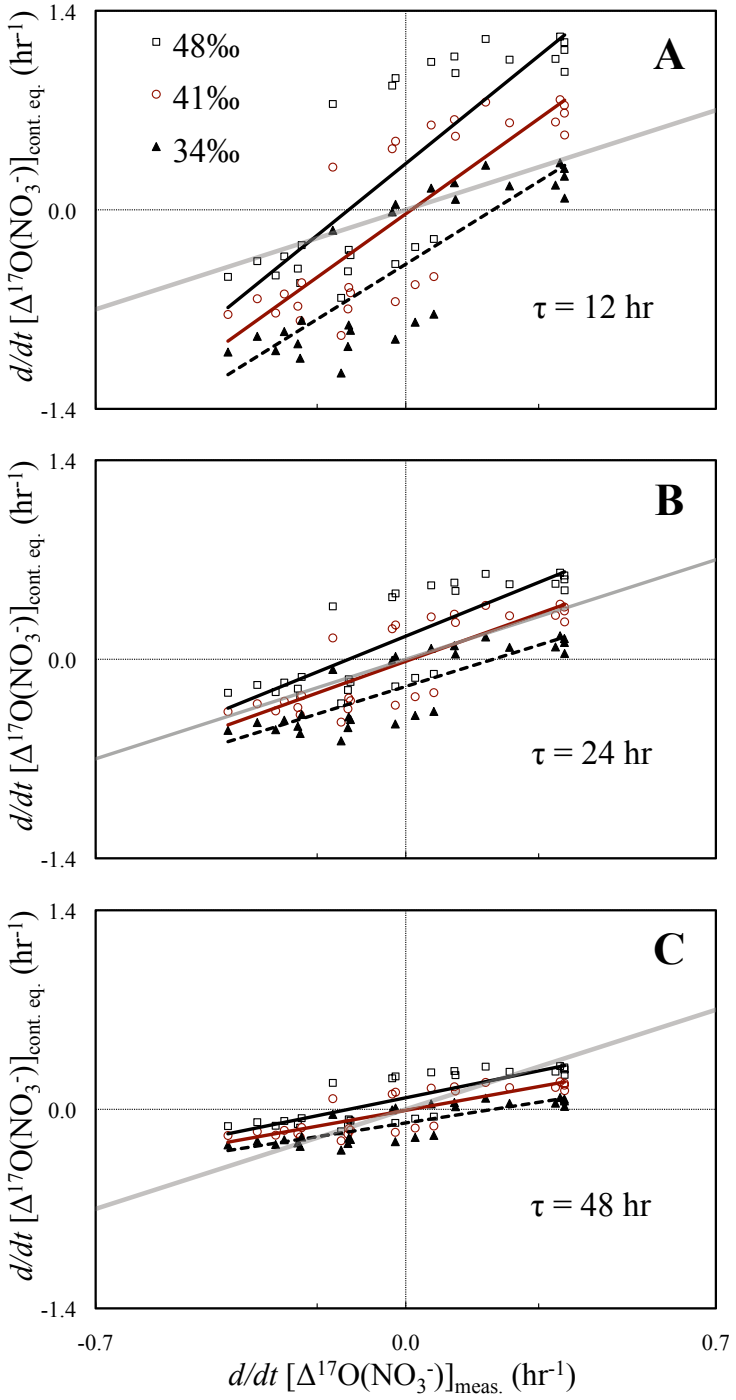

FIGURE 4.11 - Comparison of the $\Delta^{17}O(NO_3^-)$ time derivatives observed in this study with those generated by constraining Equation 4.10 to our measurements at $\Delta^{17}O(O_3^*)$ values of 34, 41, and 48‰. Each panel represents a different assumption in the equation regarding τ: **(a)** 12 hours, **(b)** 24 hours, and **(c)** 48 hours. The best linear fit between observations and calculated values is represented by a solid black line, solid red line, and dashed black line for $\Delta^{17}O(O_3^*)$ = 34, 41, and 48‰, respectively. The 1:1 line is displayed in each panel as a solid gray line.

4.4.2 Interpretation of $\delta^{15}N(NO_3^-)$ measurements

Variations in the $\delta^{15}N$ of atmospheric nitrate could plausibly be attributed to four different causes: (i) variations in the $\delta^{15}N$ value of the NO_x emission, or the "source signature;" (ii) partitioning of ^{15}N between NO and NO_2; (iii) isotopic fractionations associated with the conversion of NO_x to nitrate (R1 – R3 channels); or (iv) isotopic effects occurring during the transport of nitrate in the atmosphere (e.g., deposition, gas-particle partitioning of HNO_3, etc.) (Morin *et al.*, 2009). There remains a great deal of uncertainty regarding the potential quantitative impacts of these processes. Isotopic fractionations associated with the atmospheric NO_x cycle have been proposed (e.g., Freyer (1991) and Freyer *et al.* (1993)); however, there is very little experimental or observational evidence that supports these assertions. Isotopic fractionation during atmospheric transport is typically thought to be negligible due to the relatively short lifetime of nitrate against wet and dry deposition; therefore, it is often assumed in the literature that the $\delta^{15}N$ value of NO_x is conserved from source to sink and natural spatial and temporal variations in the $\delta^{15}N$ of atmospheric nitrate are thus typically attributed to NO_x source variability (Freyer, 1991; Hastings *et al.*, 2003; 2009; Elliott *et al.*, 2007; 2009; Savarino *et al.*, 2007; Wankel *et al.*, 2010; Fang *et al.*, 2011).

The framework commonly applied in the interpretation of atmospheric $\delta^{15}N(NO_3^-)$ values can be generalized as follows: anthropogenic NO_x emissions resulting from fuel combustion are enriched relative to atmospheric N_2. Therefore, positive $\delta^{15}N$ values in atmospheric nitrate are often taken to represent a combustion source signal. For example, Elliott *et al.* (2009) observed a strong spatial correlation between the $\delta^{15}N$ of nitrate in atmospheric dry deposition, which averaged 3.2 ‰, and the magnitude of NO_x emissions from stationary sources (e.g., power plants) in the eastern U.S.; in another study, Fang *et al.* (2011) used $\delta^{15}N$ measurements of precipitation nitrate, which averaged 3.6 ‰ over a two-year period, to estimate the relative contributions of nitrate originating from fossil fuel NO_x emissions at an industrialized site in China. Lower atmospheric $\delta^{15}N(NO_3^-)$ values, such as those reported by Baker *et al.* (2007) and Morin *et al.* (2009) for the remote Atlantic MBL (-6 – 0 ‰), are generally assumed to indicate a mostly natural background NO_x source, such as emission from soils ($\delta^{15}N$ < -20 ‰) (Freyer, 1991) or production during lighting strikes ($\delta^{15}N$ ~ 0) (Hoering, 1957).

It is difficult to reconcile our observations of $\delta^{15}N(NO_3^-)$ to the commonly applied interpretive framework discussed above. Considering the large variations often observed between subsequent daytime and nighttime samples (7 - 10‰), it would seem that $\delta^{15}N(NO_3^-)$ was largely driven by diurnal variations associated with photochemical NO_x cycling rather than source variability. Furthermore, the only sustained periods of relative stability in $\delta^{15}N$ occurred during the nitrate concentration maxima observed under sea breeze-land breeze recirculation in the Los Angeles metropolitan region on 14 - 17 May and 29 - 31 May, when $\delta^{15}N(NO_3^-)$ averaged -3.2 ± 1.4‰ and -2.3 ± 1.1‰, respectively. If it can be assumed that the nitrate budget was most impacted by anthropogenic emissions during these periods (see Section 4.4.1.2), the observation of negative $\delta^{15}N(NO_3^-)$ values seems to be inconsistent with studies that have found atmospheric nitrate derived from anthropogenic sources to possess a significantly higher $\delta^{15}N$ value than that derived from natural sources (Hastings *et al.*, 2003; Elliott *et al.*, 2009; Morin *et al.*, 2009). However, this apparent contradiction can be resolved by considering the two main classes of combustion-related NO_x emissions: "fuel" NO_x, which is produced directly through the release and subsequent oxidation of fuel-bound nitrogen, and "thermal" NO_x, which is produced via high-temperature oxidation of O_2 and N_2 gas in combustion air, are known to possess different $\delta^{15}N$ signatures. For example, Heaton (1990) and Snape *et al.* (2003) obtained relatively high $\delta^{15}N$ values (6 - 18‰) for fuel NO_x derived from coal combustion and negative values for thermal NO_x. The production of anthropogenic NO_x proceeds through both of these processes and their relative importance determines the $\delta^{15}N$ of the NO_x produced. Coal-fired energy production most likely results in positive $\delta^{15}N(NO_x)$ values (Elliott *et al.*, 2009; Fang *et al.*, 2011); however, there is some indication that the $\delta^{15}N$ signature of NO_x derived from transport fuel combustion is negative and can induce negative $\delta^{15}N(NO_3^-)$ values in the atmosphere (Hastings *et al.*, 2003; 2009; Widory, 2007). Heaton (1990) determined the $\delta^{15}N$ of NO_x in vehicle exhaust and obtained values ranging from -2‰ for vehicles carrying heavy loads to -13‰ for idling engines. It should be noted that there are some conflicting reports regarding the $\delta^{15}N$ of road-traffic NO_x from dendrological studies near motorways (Ammann *et al.*, 1999; Saurer *et al.*, 2004); however, it seems that there is good evidence that transport fuel combustion leads to a large relative proportion of thermal NO_x production in some cases. Therefore, we tentatively conclude that the atmospheric nitrate concentration peaks occurring during the periods

14 - 17 May and 29 - 31 May were induced by emissions from vehicles and other sources of thermal NO_x in the Los Angeles metropolitan region. This conclusion is consistent with air pollution inventories prepared by the California Air Resources Board (CARB), which attribute over 50% of all NO_x emissions in the South Coast air basin to on-road motor vehicles (CARB, 2009). Furthermore, there is presently very little coal combustion in California relative to the eastern U.S. However, we acknowledge that the $\delta^{15}N$ of NO_x from vehicle emissions cannot be fully resolved by the present study and identify this as an important topic for future research.

4.4.2.1. Diurnal variations in $\delta^{15}N(NO_3^-)$

The diurnal features of the $\delta^{15}N(NO_3^-)$ record can be summarized by considering the time derivatives determined for $\delta^{15}N(NO_3^-)$ as a function of those determined for $\Delta^{17}O(NO_3^-)$ during the period 14 - 27 May, as is shown in **Figure 4.12**. The largest daily variations in $\Delta^{17}O$ occurred in conjunction with maximum atmospheric nitrate concentrations, while diurnal variations in $\delta^{15}N$ were primarily restricted to periods of low or stable concentrations (i.e., significant variations in both $\Delta^{17}O$ and $\delta^{15}N$ were rarely observed in the same sample sets) and thus the correlation between these two variables is rather weak ($r = 0.54$). However, the general relationship between $\delta^{15}N$ and $\Delta^{17}O$ is unambiguous: ^{15}N enrichment is clearly associated with nitrate produced through the daytime OH channel (decreasing $\Delta^{17}O$), while nocturnal nitrate production (increasing $\Delta^{17}O$) is clearly associated with ^{15}N depletion. From a purely phenomenological perspective, this relationship suggests the possibility of opposing kinetic isotopic effects associated with the OH and N_2O_5 pathways, which have been previously proposed by Freyer *et al* (1991). However, we can reject this hypothesis in the present case based on three lines of reasoning: i) the fractionation effects proposed by Freyer *et al* (1991) would suggest an opposite diurnal trend to that observed here (i.e., negative fractionation from the OH channel and positive fractionation from N_2O_5 hydrolysis); (ii) nitrate produced through the OH and N_2O_5 pathways was detected in different size fractions in this study (see Section 4.4.1.2), while $\delta^{15}N$ exhibited no apparent trend with respect to particle size (**Figure 4.7**), suggesting that the isotopic effects inducing diurnal variations in $\delta^{15}N$ occurred within the NO_x pool prior to conversion to nitrate; and (iii) as previously mentioned, large diurnal variations in $\delta^{15}N$ and $\Delta^{17}O$ did not occur simultaneously and exhibited opposite trends with respect to atmospheric nitrate concentration.

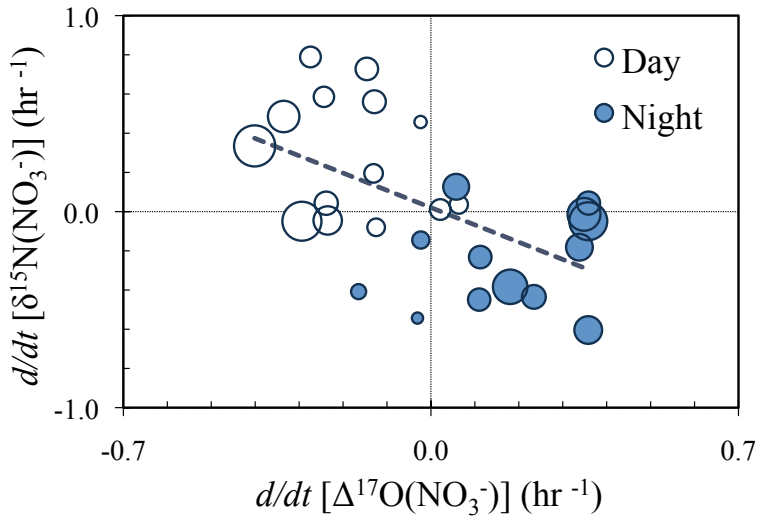

FIGURE 4.12 - Bubble plot showing the time derivatives determined for $\delta^{15}N(NO_3^-)$ as a function of those determined for $\Delta^{17}O(NO_3^-)$ during the period 14 - 27 May. The size of the bubbles corresponds to the average atmospheric concentration of nitrate during each sampling period, which ranged from 409 to 5500 ng m^{-3}. Day-night (14:00 - 02:00) and night-day (02:00 - 14:00) time derivatives are indicated by open and solid bubbles, respectively.

If the diurnal variations observed in the $\delta^{15}N(NO_3^-)$ record cannot be attributed to NO_x source variability or fractionation effects associated with NO_x to nitrate conversion, then it stands to reason that they result from either ^{15}N partitioning within NO_x or isotopic effects occurring during atmospheric transport. Given the short time scale of these variations (~12 hours) and their apparent insensitivity to particle size, isotopic effects from transport (e.g., depositional effects) can almost certainly be ruled out. However, isotopic exchange between NO and NO_2, which is known to promote ^{15}N enrichment in the more oxidized form (Sharma *et al.*, 1970), is capable of explaining our observations. This isotopic partitioning proceeds through the formation and subsequent disassociation of N_2O_3 and occurs wherever NO and NO_2 coexist. The effective isotopic exchange constant (K') for this reaction was originally defined for standard tropospheric conditions by Freyer *et al.* (1993) as follows:

$$K' = \frac{[NO_x] \times k^+ + \frac{1}{\chi NO_2} \times [O_3] \times k_1}{[NO_x] \times k^- + \frac{1}{\chi NO_2} \times [O_3] \times k_1} \tag{4.11}$$

where k^+ and k^- are the forward and backward rate constants of the isotopic exchange reaction ($k^+ / k^- = K$, the thermodynamic equilibrium constant), both equal to approximately 8.1×10^{-14} cm^3 $molecules^{-1}$ s^{-1} at 298 K (Sharma *et al.*, 1970), and k_1 is the rate constant for the reaction between NO and O_3, equal to approximately 1.8 ×

10^{-14} cm^3 $molecules^{-1}$ s^{-1} (Atkinson *et al.*, 1997). In plain words, Eq. (11) predicts that when NO and NO_2 occur in the same air mass ($\chi NO_2 < 1$), isotopic exchange will occur at a rate that is proportional to the ratio of NO_x to O_3 and inversely proportional to χNO_2. The dependence of K' on O_3 concentration arises from the photolytic cycling of NO_2, which tends to counteract the isotopic exchange and promotes isotopic equilibrium between NO_2 and NO_x; however, when concentrations of NO_x and O_3 are comparable, the rate of the isotopic exchange is significant and NO_2 becomes enriched in ^{15}N. The photochemical steady state operates only during daytime hours and thus the isotopic exchange between NO and NO_2 faces no opposing effect during the night; however, in regions that are remote from NO_x sources, the NO pool is normally titrated completely to NO_2 during the night and the isotopic exchange becomes insignificant as χNO_2 approaches 1. The overall quantitative effect of the isotopic exchange in terms of the $\delta^{15}N$ of NO_2 over that of the total NO_x reservoir, denoted $[\delta^{15}N(NO_2) - \delta^{15}N(NO_x)]$, can be assessed as follows:

$$\left[\delta^{15}N(NO_2) - \delta^{15}N(NO_x)\right] = (K' - 1) \times (1 - \chi NO_2) \qquad (4.12)$$

By applying 30-minute averages of the $[O_3]$, $[NO_x]$, and χNO_2 values determined *in-situ* to Equation 4.11, we have computed the diurnally averaged trend in $[\delta^{15}N(NO_2) - \delta^{15}N(NO_x)]$ over the entire period of this study (**Figure 4.13**). The value of the thermodynamic equilibrium constant, K, which sets the quantitative upper-limit for the isotopic exchange, is not presently well constrained. For example, Freyer *et al.* (1993) determined $K = 1.022$ in a study of NO_x in the ambient troposphere over the German city of Jülich, while other authors have determined higher values from both *ad-hoc* calculations and direct measurements. Considering the uncertainty in this parameter, we have computed K' over the range of K values reported in the literature (1.022 to 1.046) (Begun and Melton, 1956; Begun and Fletcher, 1960; Richet *et al.*, 1977).

From inspection of **Figure 4.13**, it is clear that the isotopic exchange between NO and NO_2 would have been capable of producing a qualitatively similar trend to that observed for $\delta^{15}N(NO_3^-)$ during the cruise on R/V *Atlantis*. During daytime hours, NO_x was normally present at a sufficiently high concentration relative to O_3 for isotopic exchange to lead to a significant increase in the $\delta^{15}N$ of NO_2 over that of the total NO_x pool. Therefore, nitrate production through the OH + NO_2 channel would have resulted in increasing $\delta^{15}N(NO_3^-)$ values during the day. However, due to the

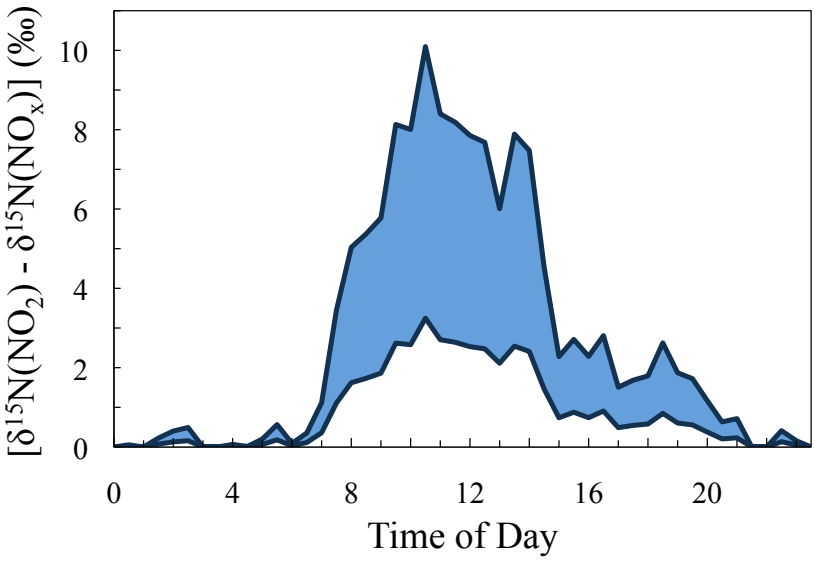

FIGURE 4.13 - The diurnally averaged trend in $[\delta^{15}N(NO_2) - \delta^{15}N(NO_x)]$ calculated using the O_3 and NO_x mixing ratios determined *in-situ* and Equations 4.11 and 4.12. The shaded surface represents estimates computed over a range of *K* values (1.022 to 1.046) for the isotopic exchange between NO and NO_2.

rapid loss of NO in the absence of photochemistry, χNO_2 was typically equal to 1 during nighttime hours (**Figure 4.5**) and thus the rate of isotopic exchange would have been negligible. Therefore, nocturnal nitrate production via the NO_3 radical would have resulted in decreasing $\delta^{15}N(NO_3^-)$ values as $\delta^{15}N(NO_2)$ approached $\delta^{15}N(NO_x)$. If we consider the average $[O_3]$, $[NO_x]$, and χNO_2 values during the South Coast segment of the cruise, we estimate average daytime $[\delta^{15}N(NO_2) - \delta^{15}N(NO_x)]$ values of 2.1‰ and 4.5‰ for *K* values of 1.022 and 1.046, respectively. For the 27 diurnal samples collected during the period 14 - 27 May, $\delta^{15}N(NO_3^-)$ exhibited an average difference of 3.3‰ between daytime and nighttime collections, quantitatively consistent with our estimates of the exchange between NO and NO_2.

Our findings regarding the role of isotopic exchange in determining the $\delta^{15}N$ of nitrate have important implications for the interpretation of this variable in the atmosphere. As previously discussed, positive $\delta^{15}N$ values in atmospheric nitrate are typically taken to reflect the source signal of NO_x derived from fuel combustion. However, in air masses where NO and NO_2 occur at sufficiently high concentrations relative to O_3 during both daytime and nighttime hours (e.g., NO_x plumes from urban sources and power plants), NO_2 may become progressively enriched relative to NO_x, resulting in $\delta^{15}N(NO_3^-)$ values that increase continuously prior to deposition. In this case, highly positive $\delta^{15}N(NO_3^-)$ values would indeed reflect anthropogenic NO_x sources, although not for the reasons commonly assumed. Such a mechanism would

be largely consistent with the observations of Elliott *et al.* (2007; 2009) regarding the spatial correlation between positive $\delta^{15}N(NO_3^-)$ values in atmospheric deposition and stationary source NO_x emissions. Furthermore, in the case of aged urban air masses where the NO_x/O_3 ratio is low during the day but NO and NO_2 coexist during the night due to the proximity of fresh NO_x sources, isotopic exchange between NO and NO_2 would also be capable of producing a diurnal trend opposite in phase to the one observed in this study (i.e., $\delta^{15}N(NO_3^-)$ increasing from nighttime chemistry and decreasing during the day). The impact of isotopic exchange observed in this study suggests that the $\delta^{15}N$ of atmospheric nitrate does not necessarily reflect a NO_x source signature, similar to the conclusions of Savarino *et al.* (2013) regarding $\delta^{15}N(NO_3^-)$ variations in the remote marine boundary layer. $\delta^{15}N(NO_3^-)$ measurements should therefore be carefully interpreted with regards to regional atmospheric context (i.e., NO, NO_2, O_3), particularly in cases where source induced variations in ^{15}N are small relative to the potential variability due to isotopic exchange.

4.5 Summary and conclusions

Nocturnal reactions involving the NO_3 radical and N_2O_5 represent important NO_x sinks leading to the formation of nitrate in the atmosphere; however, the magnitude of these sinks and their variability in different atmospheric contexts remain a significant area of uncertainty. The ^{17}O-excess ($\Delta^{17}O$) of nitrate may provide a useful tracer for the relative activities of daytime and nighttime nitrate formation mechanisms at different temporal and spatial scales; however, while the interpretive power of $\Delta^{17}O(NO_3^-)$ has been demonstrated at the seasonal scale, isotopic effects associated with diurnal changes in photochemistry are presently not well constrained. In order to address these knowledge gaps, we measured the size-resolved concentration and isotopic composition of atmospheric nitrate at a diurnal/subdiurnal resolution during a research cruise along the coast of California. This cruise was organized as a component of the CalNex 2010 field study and provided a unique opportunity to combine the isotopic analysis of atmospheric nitrate with *in-situ* measurements of the gas-phase precursors involved in its production (O_3, NO_x, N_2O_5).

Our results indicate that nocturnal processes were responsible for a significant proportion of nitrate production (30 – 62%) in air masses sampled in the South Coast

region during periods of continental outflow from the Los Angeles air basin, suggesting a spatial coupling of anthropogenic emissions and nighttime chemistry. The N_2O_5 channel induced a strong diurnality in the $\Delta^{17}O$ of atmospheric nitrate during these periods, which was evident for samples collected at a 12-hour frequency (i.e.; daytime/nighttime comparisons); however, the observed $\Delta^{17}O(NO_3^-)$ variations were out of phase with the diurnal O_3 and N_2O_5 profiles, an effect that is attributable to the lifetime of nitrate and persistent sea breeze-land breeze recirculation in the South Coast. Sustained onshore transport lead to a disruption in the diurnal pattern by delivering fine particle nitrate with a relatively long atmospheric lifetime and low $\Delta^{17}O$ to the coastal sampling location. Samples collected under a strictly marine transport regime in the Central Coast region exhibited no diurnal trend and possessed uniformly low $\Delta^{17}O$ values, indicating relatively insignificant nitrate contributions from nighttime chemistry. This broad spatial variability in the relative importance of nocturnal NO_x processing inferred from our isotopic measurements is largely consistent with the *in-situ* observations of O_3, NO_x, and N_2O_5 during the cruise.

Spatiotemporal dynamics in $\Delta^{17}O(NO_3^-)$ were driven largely by the coarse (> 1 μm) aerosol fraction, which is composed predominantly of sea salt in the MBL and was consistently enriched in nitrate during the South Coast segment of the cruise. In agreement with previous studies, coarse particle nitrate samples exhibited $\Delta^{17}O$ values that were considerably higher than those found in the fine fraction, suggesting that the products of the N_2O_5 pathway accumulate preferentially in the supermicron mode. This observation seems to be attributable to the heterogeneous reaction of N_2O_5 with the chloride ion, which was observed to account for a large proportion of N_2O_5 loss during the South Coast segment of the cruise (Riedel *et al.*, 2012; Wagner *et al.*, 2012) and led to substantial chloride depletion in sea salt aerosol measured in the Los Angeles Basin (Hayes, 2012). The association of high $\Delta^{17}O$ values with the coarse particle fraction indicates the potential for an isotopic effect of deposition on the bulk $\Delta^{17}O$ value of atmospheric nitrate (i.e., decreasing $\Delta^{17}O(NO_3^-)$ values with long-range transport). Such an effect could provide an explanation for the relatively low $\Delta^{17}O(NO_3^-)$ observed in marine air masses during both segments of the cruise. These observations should be integrated into atmospheric models of nitrate isotope dynamics, which could be modified to account for both the size-distribution of $\Delta^{17}O(NO_3^-)$ and the atmospheric lifetimes of particles in different size fractions.

The magnitude and proportionality of the diurnal variability observed for $\Delta^{17}O(NO_3^-)$ during this study was accurately reproduced by constraining a continuity equation for $\Delta^{17}O(NO_3^-)$ to our measurements. This analysis represents the first direct observational evidence for the fluctuations in $\Delta^{17}O(NO_3^-)$ that have been hypothesized to result from diurnal changes in the relative activities of nitrate production pathways (Morin *et al.*, 2011). The quantitative approach adopted in this study allowed for an estimation of the atmospheric lifetime of nitrate, which is difficult to evaluate directly in the ambient troposphere. Lifetime was estimated to vary in the range of 18 to 39 hours and 2 to 5 days for nitrate in continental and marine air masses, respectively, corresponding to particle deposition velocities of 0.4 - 1.4 cm s^{-1}, estimates that are all in good agreement with the values typically encountered in the literature. The application of the continuity equation to the diurnal variations observed in this study also provided a unique opportunity to evaluate different quantitative assumptions regarding the ^{17}O-excess of ozone. Our analysis suggests that the appropriate value for $\Delta^{17}O(O_3^*)$ is in the range of 38 - 44‰ (41 ± 3‰), a conclusion that lends credence to the existing ambient measurements of ozone isotopes as well as the numerous studies that have adopted $\Delta^{17}O(O_3^*)$ values in this range.

The nitrogen isotopic composition ($\delta^{15}N$) of nitrate also exhibited a clear diurnal trend during this study, typically increasing through daytime production via the OH channel and decreasing through nocturnal production. This observation is difficult to reconcile to the traditional interpretive framework in which natural spatial and temporal variations in $\delta^{15}N(NO_3^-)$ are typically attributed to NO_x source variability. While $\delta^{15}N(NO_3^-)$ did appear to reflect the $\delta^{15}N$ signature of vehicle NO_x emissions during periods of nitrate concentration maxima, the diurnal pattern was the dominant feature of the $\delta^{15}N(NO_3^-)$ record, suggesting that isotopic effects associated with diurnal changes in the NO_x cycling exert primary control on $\delta^{15}N(NO_3^-)$ at the time scale of this study. A quantitative evaluation of the *in-situ* O_3 and NO_x measurements suggests that this diurnal pattern can be explained by the isotopic exchange equilibrium between NO and NO_2, which would have resulted in increasing $\delta^{15}N(NO_2)$ values during the day in the air masses sampled in the South Coast due to a relatively high NO_x/O_3 ratio in the Los Angeles Basin. Therefore, our results indicate that the $\delta^{15}N$ of atmospheric nitrate does not necessarily reflect a source signature under high NO_x conditions, a finding that has important implications for the use $\delta^{15}N(NO_3^-)$ as tracer for anthropogenic NO_x emissions.

TABLE 4.1 - Summary of the Bulk Isotopic Composition, Concentration, and Size Distribution of Atmospheric Nitrate.

Sampling Midpoint	*Lat.*	*Long.*	*Air Temp.*	*Average* $[NO_3^-]$	*Mass < 1 μm*	$\delta^{18}O$ (NO_3^-)	$\Delta^{17}O$ (NO_3^-)	$\delta^{15}N$ (NO_3^-)
(PST)	**(°N)**	**(°W)**	**(°C)**	**(ng m^{-3})**	**(%)**	**(‰)**	**(‰)**	**(‰)**
14/5 15:01	32.8	117.3	14.4	1939	12	75.2	27.4	-4.9
15/5 1:55	33.4	118.1	13.4	5500	23	61.7	23.0	-1.3
15/5 13:49	33.9	118.5	13.2	4668	60	76.9	27.3	-1.8
16/5 1:45	33.8	118.6	13.0	4950	33	65.5	23.8	-2.4
16/5 14:01	33.5	118.8	12.4	2315	24	76.4	27.9	-4.6
17/5 2:49	34.0	118.9	11.8	1767	16	66.4	24.9	-4.1
17/5 14:48	34.2	119.4	11.8	1746	14	80.3	29.2	-3.6
18/5 1:42	34.1	119.2	12.0	1648	13	77.6	27.6	4.4
18/5 13:57	34.0	119.1	13.6	738	32	70.6	25.6	-0.6
19/5 2:15	33.7	118.3	13.6	1006	25	65.9	24.0	-1.6
19/5 14:15	33.7	118.2	13.5	2169	50	68.6	24.7	-0.1
20/5 2:18	33.7	118.2	14.3	2617	13	58.1	21.9	-0.6
20/5 14:19	33.7	118.1	16.1	3507	20	73.4	26.1	-0.8
21/5 2:11	33.8	118.7	14.9	3216	11	56.9	22.1	4.9
21/5 13:52	33.9	118.6	14.8	3865	13	64.6	24.2	0.5
22/5 2:04	33.7	118.3	14.7	1080	18	66.4	25.0	0.9
22/5 14:01	33.7	118.3	16.1	1648	20	70.2	26.3	-1.9
23/5 2:02	33.4	118.2	12.8	492	21	67.3	26.1	3.6
23/5 13:49	33.4	118.2	13.0	409	19	74.8	25.7	-2.8
24/5 1:52	33.8	118.4	12.8	1396	16	56.0	22.4	6.8
24/5 13:59	33.9	118.5	13.3	2494	11	72.8	26.7	-0.6
25/5 1:44	33.8	118.5	12.5	1346	11	61.3	23.9	6.3
25/5 14:56	33.9	118.8	13.3	1836	15	73.7	27.0	0.6
26/5 2:42	33.6	118.4	13.8	1118	12	68.2	25.4	2.9
26/5 14:43	33.8	118.3	17.5	961	42	70.1	25.1	1.1
27/5 2:43	33.8	118.3	15.4	1700	37	68.5	23.6	7.9
27/5 14:37	33.7	118.4	14.8	1622	38	71.8	24.9	2.5
28/5 7:20	33.7	118.2	14.6	1390	21	66.8	25.3	2.7
29/5 5:10	33.8	118.4	14.1	3380	14	66.4	23.9	8.0
29/5 18:37	33.9	118.5	17.5	1762	31	67.8	25.2	-2.5
30/5 0:21	33.6	118.6	16.3	2654	9	66.0	25.9	-0.2

TABLE 4.1 (*continued*) - Summary of the Bulk Isotopic Composition, Concentration, and Size Distribution of Atmospheric Nitrate.

Sampling Midpoint	*Lat.*	*Long.*	*Air Temp.*	*Average* $[NO_3^-]$	*Mass* $< 1\ \mu m$	$\delta^{18}O$ (NO_3^-)	$\Delta^{17}O$ (NO_3^-)	$\delta^{15}N$ (NO_3^-)
(PST)	**(°N)**	**(°W)**	**(°C)**	**(ng m^{-3})**	**(%)**	**(‰)**	**(‰)**	**(‰)**
30/5 6:10	33.6	118.5	15.1	5475	7	70.4	25.1	-1.6
30/5 12:21	33.9	118.7	14.6	4505	15	67.9	25.7	-2.6
30/5 19:42	33.9	119.2	14.7	1973	12	71.2	26.6	-4.3
31/5 0:15	34.1	119.2	13.4	1785	5	73.2	27.2	-3.2
31/5 6:30	34.3	119.4	14.0	3965	14	65.8	24.5	-1.8
31/5 12:36	34.3	119.6	14.4	4979	18	66.3	25.0	-2.2
31/5 18:25	34.3	120.0	13.1	1106	9	75.2	25.6	-2.5
1/6 3:12	34.9	121.1	12.0	762	9	67.0	25.4	0.0
1/6 12:13	36.1	122.0	11.4	325	27	68.1	23.9	-0.6
1/6 18:14	36.8	122.0	12.4	1072	18	65.8	22.9	-0.4
2/6 0:17	36.9	122.0	12.5	1190	7	69.1	25.7	0.8
2/6 6:17	36.9	122.0	11.5	1376	12	67.5	25.5	1.1
2/6 12:14	37.0	122.2	11.3	433	28	70.3	24.1	1.0
2/6 18:12	37.8	122.5	13.8	485	19	61.7	23.6	-1.1
3/6 0:23	38.0	122.2	15.4	436	20	59.8	23.0	1.4
3/6 6:21	38.0	122.2	15.5	398	27	50.7	20.5	0.2
3/6 12:16	38.2	121.8	20.8	712	58	60.0	21.2	-1.3
3/6 18:13	38.6	121.6	25.0	477	57	64.1	21.9	-3.2
4/6 0:26	38.6	121.6	19.1	189	47	62.1	22.7	-1.4
4/6 6:28	38.6	121.6	17.3	343	49	52.4	20.0	6.6
4/6 13:53	38.5	121.6	21.7	857	56	55.2	21.1	1.8
4/6 19:42	38.3	121.6	23.0	527	51	61.8	19.9	-2.0
5/6 3:35	38.6	121.6	17.7	178	51	57.7	20.4	-4.4
5/6 14:24	38.4	121.7	25.3	752	61	62.2	20.5	-6.2
5/6 19:58	38.1	122.1	23.7	443	57	52.8	19.0	0.8
6/6 6:28	38.1	122.1	16.7	428	51	59.2	21.9	1.2
6/6 14:01	37.8	122.7	14.6	424	67	62.0	21.7	3.0
6/6 19:49	37.7	123.0	13.3	243	30	67.2	22.2	-2.4
7/6 3:21	37.4	123.0	12.1	185	22	60.2	22.5	0.4
7/6 13:50	37.7	122.6	13.4	256	45	67.3	22.9	3.1
7/6 19:19	37.8	122.3	14.4	428	24	58.6	22.1	0.9

Chapter 5

Nitrogen and oxygen isotope dynamics of nitrate in the surface snow and boundary layer of the East Antarctic plateau

---

This chapter incorporates data published in:

Erbland, J., **Vicars, W. C.**, Savarino, J., Morin, S., Frosini, D., Frey, M. M., Vince, E. and Martins, J. M. F., **2013**. Air-snow transfer of nitrate on the East Antarctic plateau, Part 1: Isotopic evidence for a photolytically driven dynamic equilibrium. *Atmospheric Chemistry and Physics* **(in press)**.

Abstract

Here we present measurements of the nitrogen ($\delta^{15}N$) and triple-oxygen ($\delta^{17}O$ and $\delta^{18}O$) isotopic composition of nitrate year-round in the atmosphere and snow "skin layer" (surface 3-4 mm) at Dome C, Antarctica during 2009 - 2010. This dataset is further complimented by additional atmospheric nitrate samples collected during December 2011 within the framework of the OPALE (Oxidant Production over Antarctic Land and its Export) field campaign. The dual isotopic composition of nitrate ($\delta^{15}N$ and $\Delta^{17}O$) obtained throughout this full annual cycle is presented and compared to other seasonal-scale measurements carried out in Antarctica and extra-polar locations. Similar to previous investigations at South Pole, the oxygen isotope composition of nitrate in the atmosphere and surface snow reflects stratospheric chemistry during the winter and tropospheric chemistry in summer. The ^{17}O-excess ($\Delta^{17}O$) of nitrate in the skin layer maintained an approximate equilibrium with the atmospheric phase for most of the year, although significant deviations were observed in spring, when nitrate in the skin layer exhibited $\Delta^{17}O$ values as much as 6‰ higher than the atmospheric reservoir. Conversely, skin layer nitrate was consistently enriched in ^{15}N by approximately 20 - 30‰ over the atmospheric signal during all

seasons, which is suggestive of an equilibrium fractionation effect associated with the deposition and physical release of nitrate at the snow surface. For both the $\delta^{15}N$ and $\Delta^{17}O$ of nitrate, a photolytically-driven isotopic equilibrium imposed by nitrate recycling (i.e., removal, atmospheric processing, and redeposition) at the air-snow interface was achieved in the late spring/early summer, when atmospheric nitrate concentrations reached their annual maxima (> 100 ng m^{-3}). An isotope mass balance based on *in-situ* measurements of the gas-phase precursors involved in nitrate production (NO_x, O_3, OH, HO_2, etc.) predicts a $\Delta^{17}O(NO_3^-)$ signature during the OPALE campaign that is approximately 5 - 8‰ lower than the direct observations. Much of this disagreement can be resolved by accounting for the ^{17}O-excess of the OH radical, which is expected to be increased over the Antarctic plateau due to the extremely low ambient humidity and the enhanced contribution of HONO photolysis to OH production. However, a consideration of the $\Delta^{17}O$ transfer associated with this pathway cannot fully reconcile the discrepancy between predicted and measured values, which suggests the existence of an unexpected process that contributes significantly to the atmospheric nitrate budget over Dome C. While the exact nature of this process cannot be identified unambiguously, the strong correlation observed between the $\delta^{15}N$ and $\Delta^{17}O$ values of atmospheric nitrate during this time suggests a NO_x transformation mechanism that is tightly coupled in time and space with the intensity of snowpack emissions. Further information on the connection between snow photochemistry and nitrate production on the Antarctic plateau is critical to the development of ice-core proxies of paleo-oxidation chemistry based on the ^{17}O-excess of nitrate.

5.1 Introduction

Oxidation by ozone (O_3) and the related free radical species (e.g., OH, HO_2, etc.) is the primary sink for most atmospheric trace species that contribute to reduced air quality and climate change (e.g., CH_4, CO, NO_x, SO_x, etc.) (Fowler *et al.*, 2009; Isaksen *et al.*, 2009; Monks *et al.*, 2009). Global mean concentrations of OH, the most significant oxidizing agent in the atmosphere, provide a metric for assessing the processes and rates by which trace species are transformed via oxidation (i.e., the "oxidative capacity" of the atmosphere) (Lelieveld *et al.*, 2004a; Bloss *et al.*, 2005).

Human activities, such as fossil fuel combustion, agriculture, biomass burning, and deforestation, result in strong emissions of OH precursors and sink reactants, thereby altering tropospheric oxidative capacity (Wang and Jacob, 1998; Lelieveld *et al.*, 2004b). However, as air pollution and greenhouse gas reduction policies drive changes in anthropogenic emissions, a new equilibrium between OH source and sink reactions could alter oxidative capacity, which could lead to significant changes in the concentrations and lifetimes of reduced trace gases. Such changes could subsequently result in feedbacks that either amplify or dampen the impact of emissions changes on climate forcing and air pollution (Thompson, 1992; Prinn *et al.*, 2001; 2005). There is an urgent need to understand this intricate coupling between atmospheric chemistry and radiative forcing in order to better predict the evolution of climate under global change.

Reconstructions of historic variations in atmospheric oxidative capacity could potentially allow for an assessment of the link between global atmospheric composition and climate. Current estimates of past variations in the concentrations of ozone and OH are derived primarily from atmospheric chemical-transport models. The models consistently indicate that ozone concentrations have increased since the preindustrial period, with modeled estimates for this increase ranging from 20% to over 100%; however, estimates of accompanying changes in OH concentration vary in both sign and magnitude (Thompson and Cicerone, 1986; Wang and Jacob, 1998; Lelieveld and Dentener, 2000; Hauglustaine and Brasseur, 2001; Lelieveld *et al.*, 2002). Reconstructing oxidation chemistry through glacial-interglacial climate changes presents an even greater challenge due to the more limited constraints on the composition and chemistry of the paleo-atmosphere. Similar to the case with modeling of the preindustrial-industrial transition, models agree on the change in ozone from the Last Glacial Maximum (LGM) to preindustrial time (20 - 30% increase), while estimates of LGM-preindustrial changes in OH concentration vary over a wider range (Thompson *et al.*, 1993; Kaplan *et al.*, 2006).

Development of ice core proxies for variations in paleo-oxidation chemistry could offer independent validation of model estimates of ozone and OH changes over preindustrial-industrial and glacial-interglacial timescales. Early ice core reconstructions of oxidation chemistry based on H_2O_2 (Sigg and Neftel, 1991) and HCHO (Staffelbach *et al.*, 1991) measurements were confounded due to the post-depositional alteration of H_2O_2 and HCHO concentrations in the upper snowpack

prior to preservation in the ice (Hutterli *et al.*, 2003). More recently, the ^{17}O-excess ($\Delta^{17}O = \delta^{17}O - 0.52 \times \delta^{18}O$) of nitrate, a unique isotopic signature inherited from ozone via bimolecular chemical reactions in the atmosphere, has shown promise as a conserved proxy for past oxidant concentrations (Alexander *et al.*, 2004; McCabe *et al.*, 2005). The $\Delta^{17}O$ signal of nitrate reflects the relative importance of NO_x transformation mechanisms and recent studies suggest that the measurement of this isotopic signal in ice cores and ancient sediments may provide relevant information regarding the role of ozone in the overall oxidative capacity of the paleo-atmosphere (Michalski *et al.*, 2003; 2004; Thiemens, 2006; McCabe *et al.*, 2007; Savarino *et al.*, 2007). Parallel studies of the nitrogen isotope ratios ($\delta^{15}N$) of nitrate in polar ice and snow suggest that this isotopic tracer may serve as a proxy for past variations in natural sources of atmospheric reactive nitrogen ($NO_x = NO + NO_2$) (Hastings *et al.*, 2005; 2009; Jarvis *et al.*, 2008). However, the chemical and physical factors governing the oxygen and nitrogen isotopic composition of atmospheric nitrate and its precursor gases are not fully understood (Alexander *et al.*, 2009; Morin *et al.*, 2009). This is particularly true for the polar troposphere, where the UV-photolysis of trace species in the snowpack initiates complex boundary layer oxidation processes involving reactive halogen species (Grannas *et al.*, 2007; Wang *et al.*, 2007; Bloss *et al.*, 2010) and results in distinctive $\Delta^{17}O$ and $\delta^{15}N$ signatures in atmospheric nitrate (Morin *et al.*, 2007; 2008; 2012). Furthermore, before relevant information can be derived from the ice core record, it is critical to first understand the air-snow transfer function of nitrogen and oxygen isotope ratios of nitrate (Legrand and Mayewski, 1997; Legrand *et al.*, 1999) and to determine the impact of post-depositional processes in snow that may result in redistribution of nitrate stable isotopes (Freyer *et al.*, 1996). While the nitrogen isotopic signature of nitrate photolysis is better understood from laboratory and field studies (Blunier *et al.*, 2005; Frey *et al.*, 2009), the isotope dynamics associated with nitrate deposition and physical release are currently undocumented (Jarvis *et al.*, 2009). It is hypothesized that the upper-most snow layer maintains an approximate equilibrium with the lower atmosphere and that the atmospheric isotopic signal is preserved in this "skin layer," (Wolff *et al.*, 2002; Hastings *et al.*, 2004; Frey *et al.*, 2009); however, this has yet to be established in field studies.

Here we present measurements of the nitrogen ($\delta^{15}N$) and triple-oxygen ($\delta^{17}O$ and $\delta^{18}O$) isotopic composition of nitrate in the atmosphere and snow skin layer (surface 3

- 4 mm) at Dome C, Antarctica during 2009 - 2010. This dataset is further complimented by additional atmospheric nitrate samples conducted during November 2011 - January 2012 within the framework of the OPALE (Oxidant Production over Antarctic Land and its Export) project, which has provided an opportunity to combine nitrate isotopic observations with a wealth of meteorological and chemical data, including *in-situ* concentration measurements of the gas-phase precursors involved in nitrate production (NO_x, O_3, OH, HO_2, etc.) (see Preunkert *et al.* (2012) for a description of the OPALE 2010 - 2011 campaign at Dumont d'Urville). The primary goals of this study were: (i) to characterize the annual evolution of atmospheric nitrate concentration and isotopic composition at Dome C with regards to seasonal variations in NO_x sources and sinks; (ii) to establish the air-snow transfer function of nitrate stable isotope ratios and investigate the seasonal dynamics of the isotopic equilibrium at the air-snow interface; and (iii) to reconcile observations of $\Delta^{17}O$ for atmospheric nitrate at Dome C with quantitative predictions based on nitrate isotope mass balance and atmospheric chemistry parameters.

5.1.1 Site description and scientific background

Measurements discussed in this chapter were conducted at the Dome Concordia station (hereafter referred to as "Dome C"), located 3233 m above sea level on the East Antarctic Plateau (75°06' S, 123°23' E), approximately 1100 km from the coastal research station Dumont d'Urville and 560 km from the Vostok station (**Figure 5.1**). Dome C is one of the coldest places on Earth, with an average annual temperature of -54.5 °C. Temperatures frequently fall below -80 °C during the winter. In summer (December-January), the Sun is above the horizon throughout the day; however, Dome C is far enough from the South Pole that there are significant differences in solar elevation angle during the 24-hour cycle. Consequently, there is a pronounced diurnal temperature range of ~15 °C during this period, with a mean temperature of about -30 °C. Being located at the top of the Antarctic plateau, the world's largest desert, Dome C is exceptionally dry, with very little precipitation throughout the year and a present-day snow accumulation rate of 25 kg m^{-2} yr^{-1}. Due to its elevation and relative distance from the edges of the plateau, Dome C does not

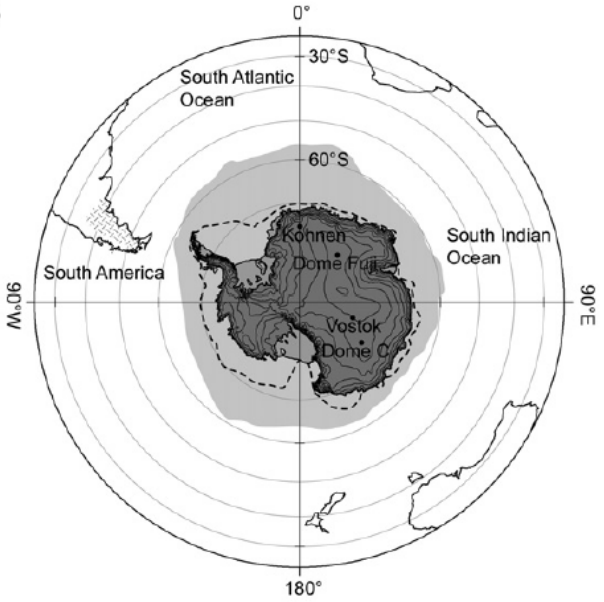

FIGURE 5.1 - Map of Antarctica showing the Dome C site and the surrounding southern hemisphere. The extent of sea ice is indicated by a grey shaded area and a broken line for winter and summer, respectively (Bigler *et al.*, 2010).

experience the katabatic winds typical of other coastal and inland regions of Antarctica. In fact, wind speeds observed at Dome C are among the lightest on the continent, with a mean annual value of ~3 m s^{-1} and no apparent annual cycle (Wendler and Kodama, 1984). The low level of turbulence in the boundary layer above Dome C, along with the high elevation of the site and the low water vapor and aerosol content of the atmosphere, provide ideal conditions for ground-based astronomical observations (Lawrence *et al.*, 2004).

Beginning in 1995, several ice core retrieval campaigns have been carried out at Dome C within the framework of the European Project for Ice Coring in Antarctica (EPICA). The core samples obtained from the Dome C drill site in the intervening years have provided highly resolved paleo-records of climate signals (e.g., δD), greenhouse gas concentrations (e.g., CO_2 and CH_4), and aerosol chemical composition extending over eight glacial cycles, the age of the oldest recovered ice being approximately 800,000 yr at a depth of 3200 m (Augustin *et al.*, 2004; Barbante *et al.*, 2006; Jouzel *et al.*, 2007; Luthi *et al.*, 2008; Bigler *et al.*, 2010). Many parallel studies have been conducted at Dome C and the surrounding regions in an effort to understand the meteorological, chemical, and physical factors governing the variability of trace constituents preserved in the ice. For example, a number of aerosol measurement campaigns have been carried out to investigate the sources and seasonality of sea salt transport to Dome C (Jourdain *et al.*, 2008; Udisti *et al.*, 2012).

Other studies have focused on the boundary layer chemistry of the Dome C site, particularly with regards to the photochemical oxidation of dimethylsulfide (DMS), an important aerosol production mechanism whose intensity is recorded in ice (Preunkert *et al.*, 2008; Becagli *et al.*, 2012). Findings from Dome C have been largely analogous to those obtained from measurement campaigns at South Pole and reveal several interesting features. Firstly, although the Antarctic plateau is extraordinarily dry, cold, and far removed from sources of anthropogenic emissions, atmospheric measurements conducted in 1998 - 1999 during the ISCAT (Investigation of Sulfur Chemistry in the Antarctic Troposphere) field campaign demonstrated a surprisingly high level of photochemical activity. For example, the average summertime OH concentration (2×10^6 cm^{-3}) over the South Pole was found to be similar to that in the tropical marine boundary layer (MBL) (Mauldin *et al.*, 2001). Unexpectedly high levels of nitric oxide (NO) were also detected, with concentrations one to two orders of magnitude higher than that typically observed in other remote regions (Davis *et al.*, 2001). Model simulations revealed that the large and variable OH concentrations observed at South Pole were a result of the elevated NO level, which catalyzes a rapid cycling of HO_2 to OH (Chen *et al.*, 2001; 2004). The high concentrations of NO_x were also inferred to drive *in-situ* photochemical production of ozone during the ISCAT campaign (Crawford *et al.*, 2001). The high oxidative capacity observed in the atmosphere over South Pole was initially assumed to be associated with shallow boundary layers of less than 50 m (Davis *et al.*, 2004); however, subsequent aircraft and balloon-based measurements revealed that elevated NO_x and OH levels are common throughout the Antarctic plateau at elevations of 50 - 150 m (Davis *et al.*, 2008; Helmig *et al.*, 2008). Surface ozone and NO_x measurements at Dome C suggest a similar level of enhanced oxidant production during November - January (Legrand *et al.*, 2009; Frey *et al.*, 2013).

The high levels of photochemical activity observed at South Pole and Dome C are now understood in terms of NO_x release from the snowpack (Honrath *et al.*, 1999; 2000; Jones *et al.*, 2000; 2001; Zhou *et al.*, 2001). This process is initiated by the photolysis of nitrate, which can lead to large fluxes of NO_2, NO, and HONO from permanently sunlit snow (Grannas *et al.*, 2007; Jacobi and Hilker, 2007; Anastasio and Chu, 2009). Observed and modeled NO_x production rates are largely capable of explaining the high levels of photochemical activity observed on the Antarcitc plateau during spring (Wang *et al.*, 2007; Helmig *et al.*, 2008; Liao and Tan, 2008; France *et*

al., 2011). In addition to its impact on boundary layer chemistry, the seasonal photo-denitrification of the snowpack also has important implications for the stability and preservation of nitrate in the snow. Nitrate concentration profiles in ice cores have long been thought to convey information regarding atmospheric NO_x source and sink variations in ancient atmospheres (Legrand *et al.*, 1988; 1999; Legrand and Kirchner, 1990; Mayewski and Legrand, 1990; Dibb *et al.*, 1998). However, photochemical release from the snowpack can results in extensive loss of nitrate mass and thus the amount of nitrate preserved in the ice may not be directly indicative of past variations in atmospheric NO_x concentrations (Röthlisberger *et al.*, 2000; 2002; Wolff *et al.*, 2008; Jones *et al.*, 2011). This process is unambiguously reflected in the nitrogen isotopic composition ($\delta^{15}N$) of snowpack nitrate (Freyer *et al.*, 1996), particularly at sites with low snow accumulation rates where the $\delta^{15}N(NO_3^-)$ is driven strongly by post-depositional mass loss processes and information regarding NO_x sources is generally lost in favor of the nitrate photolysis signature (Blunier *et al.*, 2005). In an effort to constrain the impact of this process on nitrate preserved in the EPICA ice core, Frey *et al.* (2009) measured the isotopic composition of nitrate from two snow pits (50 and 70 cm depth) at Dome C and observed extraordinary ^{15}N enrichments of > 300‰ in the top decimeters. Assuming a Rayleigh-type distillation process, the authors of this study calculated a ε value of -60 ± 15‰ for nitrate photolysis, consistent with previous laboratory and field studies. They concluded that photolysis is an important process driving nitrate mass loss in surface snow and the most important process determining the $\delta^{15}N$ signal of nitrate archived at depth. Recent measurements of snowpack optical properties at Dome C (France *et al.*, 2011) suggest that the light attenuation depth is ~ 10 - 20 cm, significantly higher than previously assumed, leading Erbland (2012) to conclude that up to 80% of the nitrate mass loss observed at Dome C can be attributed to photolysis, contrary to the earlier 40% estimate of Wolff *et al.* (2002). While the nitrate remaining in the snow becomes considerably enriched in ^{15}N through photolytic loss, conservation of mass implies that the NO_x emissions produced from these photochemical reactions are depleted, which is reflected in the negative $\delta^{15}N$ values commonly observed for atmospheric nitrate in the polar boundary layer (Morin *et al.*, 2007; 2008; 2009; 2012; Savarino *et al.*, 2007), including at Dome C (Frey *et al.*, 2009).

5.2 Methods

5.2.1 Snow and atmospheric sampling

The experimental procedures employed in this study are similar to those previously described for the 2004 and 2007 sampling campaigns at the DC station by Frey *et al* (2009); however, the primary focus of the present study was not variations with depth in the snowpack, but rather the seasonality of nitrate stable isotopes in the snow skin layer. This uppermost snow layer is susceptible to wind transport and is in the most direct contact with the atmosphere. The first 3 - 4 mm of this non-adhesive surface snow was collected approximately every three days throughout the campaign (January 2009 - January 2010). Additionally, an intensive hourly collection was conducted during the period 28 - 29 December 2009. Approximately 300 grams of snow was secured for each sample to ensure the collection of an adequate amount of nitrate for multiple (if necessary) isotopic analyses at a 100-nmol target (see Chapter 2). Snow samples sealed in 1-liter Whirl-Pak™ plastic bags were allowed to melt at room temperature. Nitrate concentrations were then determined for each sample using a colorimetric method employed routinely at DC for the continuous flow analysis of nitrate (Frey *et al.*, 2006; Frey *et al.*, 2009), similar to the method described in Chapters 2 and 4. Nitrate concentrations for the snow samples were found to range from 62 - 1425 ng g^{-1} (1.0 - 22.9 μmol L^{-1}), with a mean and standard deviation of 363 ± 342 ng g^{-1} (6.0 ± 5.4 μmol L^{-1}). In order to obtain a nitrate concentration range high enough for the isotopic analysis of each sample (> 20 μmol L^{-1}), all samples were pre-concentrated in the warm lab at DC following the procedure of Silva *et al.* (2000). Briefly, nitrate in the melted snow samples was concentrated via quantitative trapping using 0.3 mL of anion exchange resin (BioRad™ AG 1-X8), followed by elution with 10 mL of a 1.0 mol L^{-1} NaCl solution. The pre-concentrated samples were then shipped frozen to our laboratory in Grenoble for isotopic analysis.

Bulk atmospheric particulate matter samples were collected at Dome C on glass fiber filters using a high-volume air sampler (HVAS), which was installed on a platform 1 m above the ground. The HVAS was operated at an average flow rate of 0.7 m^3 min^{-1}, necessary to ensure the collection of a sufficient amount of nitrate for isotopic analysis. Samples were collected for 37 separate five to seven day periods

throughout the 2009 - 2010 sampling campaign. In addition to the samples collected throughout the year during 2009 - 2010, 11 HVAS samples were also obtained during the OPALE field campaign at Dome C from November 2011 - January 2012. After each collection period, filters were removed from the HVAS and placed in clean 50 mL centrifuge tubes, which were sealed in plastic bags and stored at -20 ˚C. Upon arrival at our laboratory in Grenoble, atmospheric filter samples were extracted in 40 mL of ultra-pure water via centrifugation using Millipore Centricon™ filter units. Nitrate concentration was then determined for each filter extract solution using a colorimetric method (see Chapter 2). Atmospheric nitrate concentrations were calculated as the quotient of the total nitrate filter loading and the total volume of air pumped through the filter at standard temperature and pressure.

5.2.2 Isotopic analysis

The comprehensive isotopic composition of nitrate ($^{15}N/^{14}N$, $^{17}O/^{16}O$, $^{18}O/^{16}O$) was measured on a Finnigan™ MAT253 isotope ratio mass spectrometer (IRMS), equipped with a GasBench II™ and coupled to an in-house built nitrate interface (Morin *et al.*, 2009). Nitrate in both the pre-concentrated surface snow samples and the aerosol filter extracts was prepared for isotopic analysis by conversion to N_2O via the bacterial denitrifier method (Casciotti *et al.*, 2002; Kaiser *et al.*, 2007; Michalski *et al.*, 2002). The details of our analytical procedure have been described thoroughly in Chapter 2 and elsewhere in the literature (for example, by Morin *et al.* (2009)) and will be only briefly outlined here.

Denitrifying bacteria (*Pseudomonas aureofaciens*) were cultured in nitrate-amended soy broth and incubated for 5 days in stoppered glass bottles. Bacterial cultures, after concentration by centrifugation and re-suspension, were dispensed as 2 mL aliquots into 20 mL glass vials, which were then crimped and purged with helium for 3 hours. Approximately 100 nmol of sample nitrate was then injected into the purged vials and conversion of the sample nitrate to nitrous oxide (N_2O) via bacterial denitrification was allowed to proceed overnight. The N_2O sample was then cryo-focused in a liquid nitrogen trap and introduced into a gold furnace where it was thermally decomposed at 900 °C to O_2 and N_2. Following separation via gas chromatography, the O_2 and N_2 sample gases were directed into the ionization chamber of the IRMS. All analytical steps were simultaneously performed on nitrate

isotopic standards and their equimolar mixtures (International Atomic Energy Agency USGS 32, USGS 34, and USGS 35, see Chapter 2), which were prepared in an identical background matrix as the samples (ultrapure water and 1.0 mol L^{-1} NaCl solution prepared in Dome C water for aerosol and surface snow samples, respectively). Individual analyses were normalized through comparison with these three nitrate reference materials (Werner and Brand, 2001; Coplen, 2011). All isotopic enrichment values for nitrate are reported relative to VSMOW and air N_2 for oxygen and nitrogen, respectively. The overall accuracy of the method is estimated as the reduced standard deviation of the residuals from the linear regression between the measured reference materials and their expected values. For the results described here, the average uncertainty values obtained for $\delta^{18}O$, $\Delta^{17}O$, and $\delta^{15}N$ were 1.6‰, 0.5‰, and 1.0‰, respectively.

5.3 Results

5.3.1 Nitrate concentrations in the atmosphere and skin layer

Figure 5.2 presents the atmospheric and skin layer nitrate concentrations observed at Dome C during February 2009 - January 2010. Atmospheric nitrate levels remained relatively low and stable for most of the year, with an average (±1σ) value of 5.9 ± 4.1 ng m^{-3} during polar night (i.e., from March to September 2009). Sporadic concentration maxima (> 90 ng m^{-3}) occurred in the spring, concurrent with the return of continuous sunlight (polar day) at Dome C. During this period of enhanced photochemical activity initiated by NO_x and HONO emissions from the snow (Frey *et al.*, 2009; 2013; Legrand *et al.*, 2009; France *et al.*, 2011), nitrate concentrations increased markedly, averaging 61.9 ±19.2 ng m^{-3} during October-December, then decreased sharply to values lower than 30 ng m^{-3} in early summer (January 2010). The magnitude and seasonality of the atmospheric nitrate concentrations observed here is consistent with previous observations at Dome C in 2007 (Frey *et al.*, 2009) and at South Pole (McCabe *et al.*, 2007).

Skin layer nitrate concentrations exhibited a similar seasonal trend to that observed in the atmosphere, with low and stable concentrations (161 ± 50 ng g^{-1}) during polar

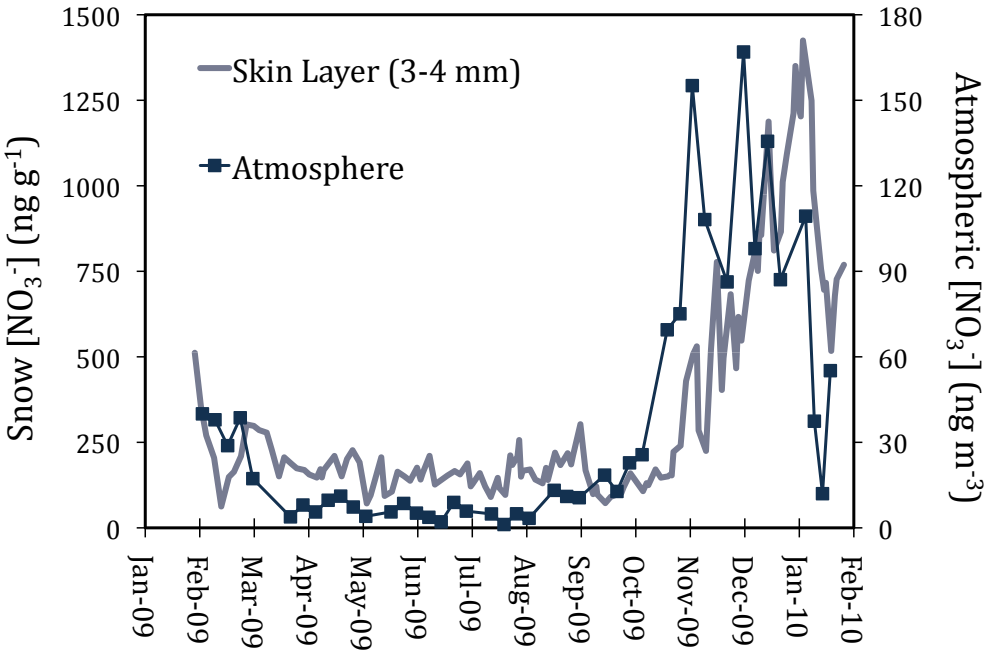

FIGURE 5.2 - Annual record of nitrate concentrations in the atmosphere and snow skin layer at Dome C during 2009 - 2010.

night, followed by a sharp increase to values in the 600 - 1400 ng g^{-1} range in the spring and early summer, similar to results obtained for daily surface snow collections at Halley, Antarctica (Wolff *et al.*, 2008). The observed temporal variations of nitrate mass in the skin layer were offset from those observed in the atmosphere by a period of approximately 3 - 4 weeks. For instance, while atmospheric nitrate concentration increased above its background level in mid-October, nitrate accumulation in the skin layer did not begin to increase until mid-November; in fact, nitrate concentrations decreased to minimum annual values in the skin layer during October, suggesting strong mass loss of nitrate from the skin layer during this period of peak UV irradiance (France *et al.*, 2011).

5.3.2 Isotopic measurements

Annual variations in the $\delta^{15}N$, $\delta^{18}O$, and $\Delta^{17}O$ values of nitrate in the atmosphere and snow skin layer at Dome C during 2009 - 2010 are shown in **Figure 5.3** along with the isotope ratio values for the aerosol samples collected during November 2011 - January 2012. Atmospheric $\delta^{15}N(NO_3^-)$ exhibited the same general seasonal features during 2009 - 2010 as those reported for Dome C during 2007 - 2008 by Frey *et al.*

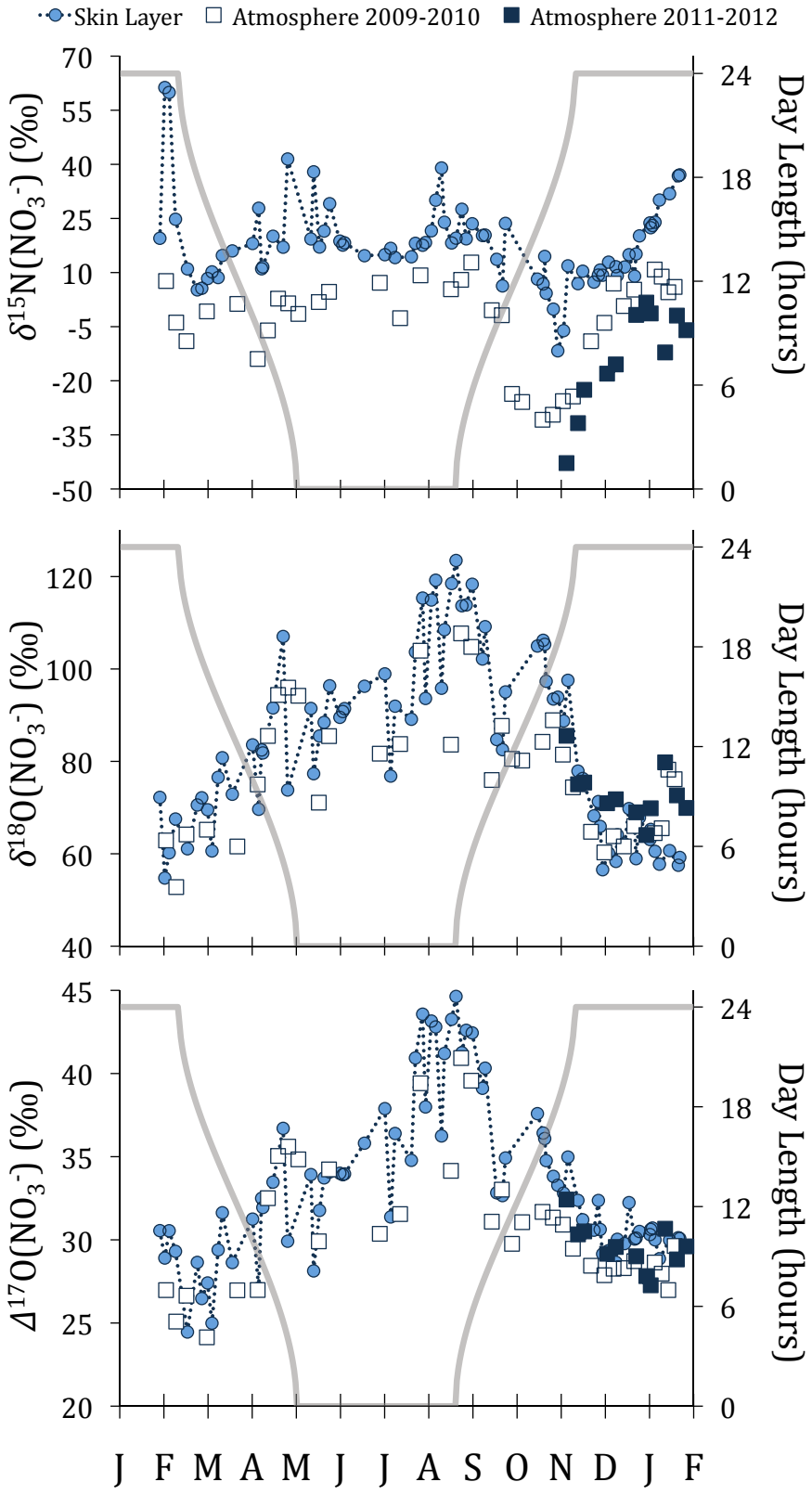

FIGURE 5.3 - Isotopic composition of atmospheric and skin layer nitrate obtained from Dome C during 2009 - 2010 and atmospheric values from 2011 - 2012: $\delta^{15}N$ (*upper panel*), $\delta^{18}O$ (*center panel*), and $\Delta^{17}O$ (*lower panel*). The day length at Dome C is indicated in each panel by a solid grey line (secondary y-axis).

(2009). For most of the year, atmospheric $\delta^{15}N(NO_3^-)$ varied within the global annual mean range of approximately -10 - 10 ‰ (Morin *et al.*, 2009), with an average value of 1.3 ± 6.2‰ during January-September. However, $\delta^{15}N$ values for atmospheric nitrate dropped sharply at the onset of spring (mid-September), reaching minimum values during the month of October (-27 ± 2.7‰). Such depleted atmospheric $\delta^{15}N(NO_3^-)$ values, while much lower than those reported in the literature for the mid-latitudes, are a typical seasonal feature of the atmospheric boundary layer over snow-covered regions (Morin *et al.*, 2007; 2008; 2009; 2012; Savarino *et al.*, 2007). In the skin layer, $\delta^{15}N(NO_3^-)$ exhibited an annual weighted mean of 18.2‰. Minimum values (< -10‰) occurred in spring, at the end of October. After this minimum, $\delta^{15}N$ steadily increased to reach values above 30‰ by the end of the summer. While the skin layer nitrate possessed an average $\delta^{15}N$ value of 21.1 ± 7.7‰, drastic variations of more than 40‰ were often observed between two consecutive samples. On average, $\delta^{15}N(NO_3^-)$ in the skin layer was approximately 25‰ higher than $\delta^{15}N(NO_3^-)$ in the atmosphere.

$\Delta^{17}O$ values for atmospheric nitrate sampled at Dome C during 2009 - 2010 are consistent with previous measurements during 2007 - 2008 (Frey *et al.*, 2009). Maximum values (> 40‰) were observed during late winter (August). After this period, $\Delta^{17}O(NO_3^-)$ decreased steadily throughout the summer, reaching minimum values of 27‰ in mid-January 2010, similar to the low values observed at the beginning of the campaign in February - March 2009 (24 - 27‰). $\Delta^{17}O(NO_3^-)$ in the skin layer exhibited a similar seasonal trend, but with a reduced degree of variability and an average offset from the atmospheric $\Delta^{17}O(NO_3^-)$ signal of ~ 2‰. The mass-weighted $\Delta^{17}O$ averages calculated for atmospheric and skin layer nitrate are 29.4‰ and 31.7‰, respectively, consistent with $\Delta^{17}O$ measurements of nitrate at depth in the snowpack at Dome C and South Pole (McCabe *et al.*, 2007; Frey *et al.*, 2009) and mineral nitrate collected from McMurdo Dry Valley soils (Michalski *et al.*, 2005).

5.3.3 Intensive snow collections

Results of the 30-hour intensive skin layer collection carried out at Dome C during the period 28 - 29 December 2009 are presented in **Figure 5.4**. Nitrate concentrations and

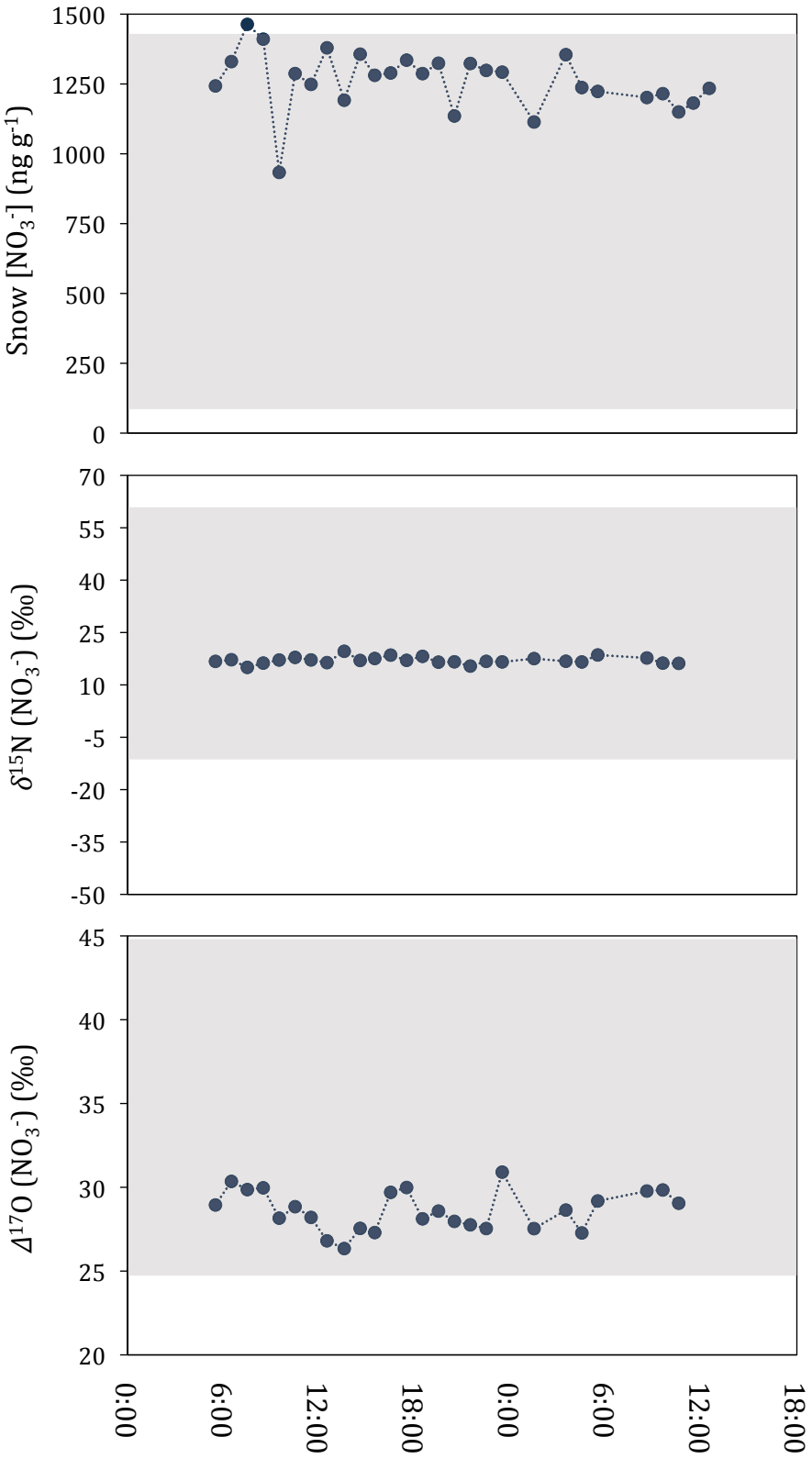

FIGURE 5.4 - Hourly variations in skin layer nitrate concentration (*upper panel*), $\delta^{15}N$ (*center panel*), and $\Delta^{17}O$ (*lower panel*) at Dome C during the period 28 - 29 December 2009. The shaded areas represent the measured ranges observed for the entire 2009 - 2010 time series. The analytical uncertainty for each measurement is smaller than the size of the symbols.

$\delta^{15}N$ and $\Delta^{17}O$ values for the hourly collections are shown on identical y-axes as in **Figure 5.2** and **Figure 5.3**, respectively. The grey shaded areas represent the total annual range observed in the skin layer time series. The average (±1σ) concentration, $\delta^{15}N$, and $\Delta^{17}O$ values for nitrate in the skin layer snow during this time were 1261 ± 105 ng g^{-1}, 17.0 ± 1.0‰, and 28.6 ± 1.2‰ respectively, consistent with the annual data obtained for this period. The degree of scatter observed in the $\delta^{15}N$ and $\Delta^{17}O$ data is close to the typical analytical uncertainties obtained for these measurements (approximately 0.5‰ and 1.0‰, respectively, for nitrate in pre-concentrated surface snow samples). Therefore, the observed level of variability in $\delta^{15}N$ and $\Delta^{17}O$ for the hourly skin layer nitrate collections is not quantitatively significant at the precision of our methodological approach and thus does not reflect true isotopic variability. The chosen sampling method (i.e., one skin layer sample collection every 3 days on average) is therefore an appropriate approach for tracking annual variations in the isotopic composition of nitrate in this reservoir.

5.4 Discussion

5.4.1 Seasonal variations

The dual-isotope ($\delta^{15}N$ and $\Delta^{17}O$) composition of the atmospheric samples obtained at Dome C during 2009 - 2010 indicates the existence of distinct seasonal NO_x source/sink regimes throughout the year (**Figure 5.5**). To facilitate the discussion of the seasonal co-variations observed in the $\delta^{15}N$ and $\Delta^{17}O$ of nitrate, we have divided the observations into three different periods, similar to the approach of Savarino *et al.* (2007) in a study of the isotopic composition of atmospheric nitrate at Dumont d'Urville. Period 1 encompasses the late spring and summer seasons (February - March 2009 and December 2009 - January 2010) and is characterized by $\delta^{15}N$ and $\Delta^{17}O$ values of 0.8 ± 7.4‰ and 27.4 ± 1.4‰, respectively. $\delta^{15}N$ values in this range are similar to those reported in the literature for aerosol nitrate in mid-latitude regions and indicate atmospheric NO_x from a mixture of natural sources including soil emissions, biomass burning, and formation from lighting (Kendall *et al.*, 2007; Morin *et al.*, 2009). Furthermore, the observed range in $\Delta^{17}O$ is typical for measurements and model simulations of atmospheric nitrate in mid-latitude regions (see Alexander *et al.*

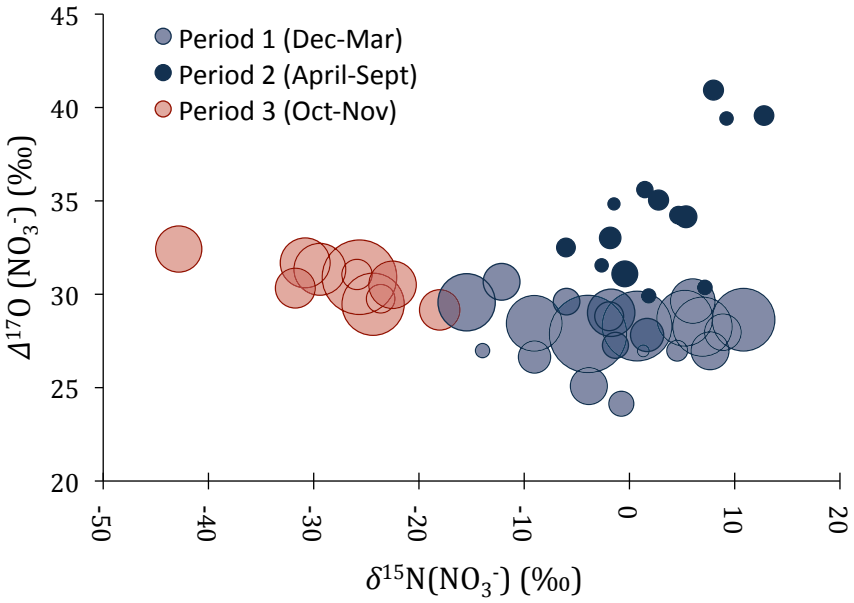

FIGURE 5.5 - Plot of $\delta^{15}N$ against $\Delta^{17}O$ for the atmospheric nitrate samples collected at Dome C during 2009 - 2010 and 2011 - 2012, showing the seasonal co-variations observed. The size of the circles corresponds to the atmospheric concentration during the individual sampling periods. Three periods of distinct isotopic signatures are indicated. Period 1 can be understood in terms of isotope transfers associated with tropospheric chemistry. Period 2 corresponds to increased contributions of nitrate from the stratosphere and from nocturnal NO_x transformation processes in the troposphere. Period 3 can be explained in terms of nitrate produced from the re-oxidation of local snowpack NO_x emissions.

(2009) and references therein). For example, Morin *et al.* (2009) measured bulk aerosol nitrate $\Delta^{17}O$ values ranging from 24‰ to 33‰ for samples collected along a ship-borne latitudinal transect (approximately 45 °S - 45 °N) in the Atlantic MBL. This suggests that the $\Delta^{17}O(NO_3^-)$ values obtained for the Period 1 aerosol filter samples resulted largely from the same NO_x transformation processes prevalent in the global troposphere (Alexander *et al.*, 2009). In Section 5.4.3, the $\Delta^{17}O$ measurements for the samples collected in Period 1 (December -January) during the OPALE 2011 - 2012 campaign will be compared to values predicted from an isotopic mass balance calculated using simultaneous local measurements of O_3, NO_x, OH, and HO_2.

Period 2 includes the majority of the fall and winter months (April - September). During this time, the concentration of nitrate in the boundary layer over Dome C decreased abruptly to reach a low and stable level (~ 10 ng m^{-3}) relative to Period 1, while $\Delta^{17}O(NO_3^-)$ increased steadily to its maximum annual values (39 - 41‰) in August. Extreme levels of nitrate ^{17}O-excess such as these are observed only in the Antarctic atmosphere and are strongly suggestive of a stratospheric source of nitrate during winter (McCabe *et al.*, 2007; Savarino *et al.*, 2007). Particulate nitrate and nitric acid in the stratosphere are largely the result of nitrous oxide (N_2O) oxidation

via $O(^1D)$ followed by the oxidation of the NO product by ozone according to the following reactions:

$$N_2O + O(^1D) \rightarrow NO + O \quad \text{(R5.1)}$$

$$NO + O_3 \rightarrow NO_2 + O_2 \quad \text{(R5.2)}$$

$$NO_2 + O_3 \rightarrow NO_3 + O_2 \quad \text{(R5.3)}$$

In the dark polar stratosphere, NO_x is converted to reservoir species and stable nitrate end-product through the following processes (Kull *et al.*, 2002):

$$NO_3 + NO_2 \leftrightarrow N_2O_5 \quad \text{(R5.4a)}$$

$$N_2O_5 + H_2O_{(liquid)} \rightarrow 2HNO_{3\,(aq)} \quad \text{(R5.4b)}$$

$$NO_2 + ClO + M \rightarrow ClNO_3 + O_2 + M \quad \text{(R5.5a)}$$

$$ClNO_3 + HCl \rightarrow HNO_3 + Cl_2 \quad \text{(R5.5b)}$$

The winter denitrification of the Antarctic stratosphere is well described in the literature (Fahey *et al.*, 1990; Santee *et al.*, 1995; Van Allen *et al.*, 1995). As day length decreases in the fall, gas-phase HNO_3 accumulates in the Antarctic stratosphere, primarily via hydrolysis of dinitrogen pentoxide (N_2O_5) on preexisting aerosol particles (R5.4b). At the end of winter, when stratospheric temperatures decline to < 195K, the decomposition of $ClNO_3$, either via hydrolysis or from reaction with HCl (R5.5b) (Finlayson-Pitts *et al.*, 1989) also becomes a significant source of gaseous nitric acid (Brasseur *et al.*, 1997). When the vapor pressure of HNO_3 reaches the threshold for formation of polar stratospheric clouds (PSCs), condensation into the solid phase yields nitric acid trihydrate (NAT) (Voigt *et al.*, 2000).

The hydrolysis of N_2O_5 and the reaction of $ClNO_3$ with HCl yield nitrate with $\Delta^{17}O$ values that can be calculated as follows:

$$\Delta^{17}O(NO_3^-)_{R5.4} = \frac{\alpha \times \Delta^{17}O(O_3^*)_{strat.}}{3} + \frac{\frac{2}{3}\alpha \times \Delta^{17}O(O_3^*)_{strat.} + \frac{1}{3}\Delta^{17}O(O_3^*)_{strat.}}{2} \quad (5.1)$$

$$\Delta^{17}O(NO_3^-)_{R5.5} = \frac{2}{3}\alpha \times \Delta^{17}O(O_3^*)_{strat.} + \frac{1}{3}\Delta^{17}O(O_3^*)_{strat.} \quad (5.2)$$

where $\Delta^{17}O(O_3^*)_{strat.}$ is the transferrable ^{17}O-excess of stratospheric ozone and α represents the fraction of the stratospheric NO_2 reservoir produced via $NO + O_3$ (R5.2). Assuming a bulk $\Delta^{17}O$ value for stratospheric ozone of 33 ± 4‰, the average and standard deviation of the observational record obtained via balloon-borne cryosampling (n = 42) (Krankowsky *et al.*, 2007), an average $\Delta^{17}O(O_3^*)_{strat.}$ value of approximately 50 ± 6‰ can be estimated based on a 3/2 relationship linking the bulk and terminal O-atom $\Delta^{17}O$ values of ozone (see Chapter 2). If α is taken to be 1.0 (i.e.,

a ^{17}O-excess in NO_2 equal to 100% of the effect in the terminal O-atoms of ozone), a reasonable assumption for the dark polar stratosphere (Alexander *et al.*, 2009; Morin *et al.*, 2011), the specific $\Delta^{17}O$ signatures induced by the stratospheric N_2O_5 and $ClNO_3$ pathways are 42 ± 5‰ and 50 ± 6‰, respectively. Conversely, using an α value of 1.0 and a $\Delta^{17}O(O_3^*)$ value of 40 ± 3‰ for average tropospheric conditions (see Chapter 3), the $\Delta^{17}O$ signature of the heterogeneous N_2O_5 pathway is 33 ± 2‰ (the $ClNO_3$ pathway can likely be neglected for the polar troposphere in winter). Therefore, while the samples collected early in Period 2 (April - June) are quantitatively consistent with the $\Delta^{17}O$ transferred via nocturnal nitrate production in the troposphere, the peak $\Delta^{17}O$ values observed in August can be rationalized only in the context of the elevated ^{17}O-excess of stratospheric ozone. Stratospheric denitrification must therefore contribute significantly to total atmospheric nitrate loading during this time, consistent with arguments developed by several previous authors (Legrand and Kirchner, 1990; Mayewski and Legrand, 1990; Wagenbach *et al.*, 1998; Michalski *et al.*, 2005; McCabe *et al.*, 2007; Savarino *et al.*, 2007).

Period 3 corresponds to the rising limb of the atmospheric concentration maxima observed during spring 2009 (28 September - 9 November), which coincides with the return of continuous sunlight at Dome C. The level of UV-radiation received at the surface maximizes during this period owing to reduced ozone column densities associated with the seasonal appearance of the Antarctic stratospheric "ozone hole" (Solomon, 1990; 1999). Atmospheric nitrate concentration maxima observed at this time can be understood in the context of NO_x emissions resulting from nitrate/nitrite photochemistry (Mack and Bolton, 1999), which proceeds on the Antarctic plateau according to the following simplified reaction scheme (Grannas *et al.*, 2007):

$$NO_3^- + h\nu \rightarrow NO_2 + O^- \quad \text{(R5.8)}$$

$$NO_3^- + h\nu \rightarrow NO_2^- + O \quad \text{(R5.9)}$$

$$NO_2^- + h\nu \rightarrow NO + O^- \quad \text{(R5.10)}$$

$$NO_2^- + OH \rightarrow NO_2 + OH^- \quad \text{(R5.11)}$$

At wavelengths > 290 nm, nitrate photolyzes with an absorption band centered at 302 nm (Chu and Anastasio, 2007), yielding NO_2 (R5.8) and nitrite (NO_2^-) (R5.9). Nitrite undergoes either photolysis with UV absorption maxima of approximately 318 nm and 354 nm (R5.10) or reacts with the hydroxyl radical (OH) (R5.11) to yield NO and NO_2, respectively (Boxe and Saiz-Lopez, 2008). The oxide radical ions (O^-) produced in Reactions R5.8 and R5.10 are rapidly protonated, which contributes significantly to

the photo-formation of OH in snow (Anastasio *et al.*, 2007). Additionally, nitrous acid (HONO) is formed at pH < 7:

$NO_2^- + H^+ \rightarrow HONO$ (R5.12)

The rate of the R5.8 pathway exceeds that for R5.9 by nearly an order of magnitude; therefore, the most abundant emission resulting from nitrate photolysis is NO_2, followed in relative importance by NO and HONO (Grannas *et al.*, 2007).

The photochemical reactions shown above proceed through the preferential removal of light isotopologues, leading to an enrichment in the $\delta^{15}N$ of the nitrate remaining in the snow and a corresponding depletion in $\delta^{15}N$ for the NO_x emitted to the atmosphere (Blunier *et al.*, 2005; Frey *et al.*, 2009). The extremely low $\delta^{15}N$ values (< -20‰) observed for atmospheric nitrate during the Period 3 peak concentration events thus indicate that the re-oxidation of snowpack NO_x emissions was the dominant source of atmospheric nitrate during this time (Morin *et al.*, 2008). Atmospheric $\delta^{15}N(NO_3^-)$ began to steadily increase after reaching its minimum values in mid-October, eventually returning to background levels in mid-November. This increase is likely an effect of the reduced nitrate mass fraction remaining in the snow photic zone, which results in increasingly enriched NO_x emissions as nitrate concentrations in the upper snowpack are reduced via photochemistry. Based on the annual accumulation rate at Dome C (25 kg m^{-2} yr^{-1}), and an estimated photolytic fractionation constant ($^{15}\varepsilon_{air\text{-}snow}$) for $\delta^{15}N$ of 48‰ (Frey *et al.*, 2009), nitrate mass concentration in the photic zone is expected to decrease by approximately 90% during October-December, with an accompanying 35‰ increase in the $\delta^{15}N$ of NO_x emissions. The measurements of atmospheric $\delta^{15}N(NO_3^-)$ obtained in this study are consistent with these expectations and provide further evidence of the relevance of snow photochemistry to the budget of reactive nitrogen and nitrate over the Antarctic plateau.

5.4.2 Dynamic equilibrium at the air-snow interface

The photochemical release of reactive nitrogen from snow has important implications for oxidative capacity and local N cycling above the Antarctic plateau. NO_x emitted into the polar boundary layer from the UV-photolysis of nitrate (R5.8 - R5.11) initiates a complex and rapid recycling of nitrogen characterized by high rates of oxidant production from the photolysis of NO_2 and HONO, which results in a

relatively short photochemical lifetime for NO_x ($\tau \approx 15$ h for the South Pole) (Huey *et al.*, 2004; Davis *et al.*, 2008; Frey *et al.*, 2009; 2013). This rapid recycling may drive an isotopic equilibrium between the atmospheric and skin layer nitrate reservoirs, as previously suggested by Frey *et al.* (2009). Here we test this hypothesis in light of our observations at the air-snow interface at Dome C.

Skin layer $\delta^{15}N(NO_3^-)$ values were consistently enriched by approximately 20‰ over the atmospheric signal for most of the year at Dome C (**Figure 5.3**). During polar day, a ^{15}N depletion in atmospheric nitrate can be interpreted as resulting from the production of nitrate from reactive nitrogen emissions from surface snow as discussed above; however, nitrate photolysis can clearly not be invoked to explain the isotopic disequilibrium between the atmosphere and skin layer observed during polar night. This shift in $\delta^{15}N(NO_3^-)$ may result from an equilibrium isotope effect associated with the physical exchange of HNO_3 between the surface snow and atmosphere. Our data suggest that the $\delta^{15}N$ fractionation factor associated with the reversible deposition reaction $H^{15}NO_{3(snow)} + H^{14}NO_{3(air)} \rightarrow H^{14}NO_{3(snow)} + H^{15}NO_{3(air)}$ (denoted $^{15}\varepsilon_{snow\text{-}air}$) is on the order of -18‰ during Periods 1 and 2 (**Table 5.1**).

The $\Delta^{17}O$ values for nitrate in the snow skin layer and atmosphere were in approximate equilibrium at Dome C throughout most of the year, suggesting that the atmospheric signal is transferred quantitatively to the snow surface via deposition. However, a significant and persistent offset (with respect to the analytical uncertainty) on the order of 2‰ was observed between atmospheric and skin layer nitrate, with the latter reservoir possessing slightly higher $\Delta^{17}O$ values (**Table 5.1**). This almost constant shift in $\Delta^{17}O$ is not incompatible with the hypothesis of isotopic equilibrium at the Dome C air-snow interface; nevertheless, the difference in $\Delta^{17}O(NO_3^-)$ observed between the atmosphere and skin layer indicates that this equilibrium proceeds with an apparent mass-independent fractionation effect. The deposition process itself can be assumed to proceed in a strictly mass-dependent fashion (Michalski *et al.*, 2004); furthermore, this difference cannot be explained by our choice of a 0.52 slope on the definition of $\Delta^{17}O$. Therefore, our results seems to indicate a nitrate production mechanism occurring at the snow surface that induces a higher $\Delta^{17}O$ than the pathways operating in the atmosphere. For example, the primary products of nitrate photolysis are likely to recombine within the ice lattice to form nitrate. However, nitrate photo-products produced at or near the air-ice interface are more mobile and are likely to be stabilized (Boxe and Saiz-Lopez, 2008). NO_2 at the snow surface has

TABLE 5.1 - Seasonal Variations in the Isotopic Composition of Atmospheric and Snow Skin Layer Nitrate at Dome C for the 2009 - 2010 Campaign.

	Period 1	*Period 2*	*Period 3*
Atmosphere	**n = 15**	**n = 14**	**n = 6**
$[NO_3^-]$ (ng m^{-3})	60.0 ± 48.7	9.1 ± 3.9	76.1 ± 50.4
$\delta^{15}N$ (‰)	0.8 ± 7.4	2.9 ± 5.2	-26.6 ± 2.9
$\Delta^{17}O$ (‰)	27.4 ± 1.4	34.4 ± 3.5	30.7 ± 0.9
Skin Layer	**n = 33**	**n = 34**	**n = 12**
$[NO_3^-]$ (ng g^{-1})	655.4 ± 392.2	166.4 ± 48.9	297.2 ± 214.9
$\delta^{15}N$ (‰)	19.3 ± 13.7	21.0 ± 7.4	6.2 ± 9.3
$\Delta^{17}O$ (‰)	29.6 ± 1.7	36.6 ± 4.8	34.2 ± 1.9
$\varepsilon_{snow\text{-}air}$			
$\delta^{15}N$ (‰)	-18.4	-18.1	-32.9
$\Delta^{17}O$ (‰)	-2.1	-2.1	-3.5

been proposed to undergo the following heterogeneous reaction (Zhou *et al.*, 2001; Kinugawa *et al.*, 2011):

$$2NO_2 + H_2O \rightarrow NO_3^- + NO_2^- + 2H^+ \quad \text{(R5.13)}$$

The significance of this reaction may be enhanced on the surface of ice due to the temperature dependence of the NO_2-N_2O_4 equilibrium, with N_2O_4 formation being over 100 times more favorable at -30 °C as compared to room temperature (Finlayson-Pitts et al., 2003). Such a reaction could be expected to result in a higher $\Delta^{17}O(NO_3^-)$ at the snow surface relative to the atmosphere, where the $\Delta^{17}O$ of nitrate is diluted due to interactions among NO_x and the OH and peroxy (HO_2) radicals, which possess lower levels of ^{17}O-excess (Dubey *et al.*, 1997; Savarino and Thiemens, 1999). However, there is currently insufficient observational data from Dome C to assess the potential for this reaction to impact the $\Delta^{17}O$ of nitrate.

During Period 3, the dramatic order of magnitude increase observed in nitrate aerosol concentration was accompanied by a significant reduction in atmospheric $\Delta^{17}O(NO_3^-)$ values relative to the skin layer. This offset, which exceeded 6‰ during mid-October, cannot be understood in the context of *in-situ* photochemical isotope effects (e.g., cage recombination of photo-products) (McCabe *et al.*, 2005), and is better explained by the relatively low $\Delta^{17}O$ signature of the nitrate production mechanisms active in the boundary layer over Dome C during this time relative to the high $\Delta^{17}O$ of the snow nitrate that has accumulated in the photic zone during polar

night. Surface snow integrates the depositional $\Delta^{17}O(NO_3^-)$ signature over extended periods of time, while the aerosol filter collections can be expected to record oxidation and source conditions only during the period of collection. The presence of a strong disequilibrium in $\Delta^{17}O(NO_3^-)$ between the atmosphere and skin layer at the onset of polar spring is therefore possible evidence that stratospheric nitrate deposited during the winter is the primary source for nitrate photochemically released from surface snow in spring.

The concentration maximum in atmospheric nitrate precedes that in the skin layer by a period of approximately three weeks. This temporal offset is likely attributable to the dominance of fluxes from the snow to the atmosphere via photolysis over the relatively minor transfer from the atmosphere to the snow through atmospheric deposition during this period. To test this hypothesis, we have assumed a dry depositional flux (F_d expressed in ng m^{-2} s^{-1}) of nitrate from the atmosphere to the snow with a constant deposition velocity (V_d expressed in m s^{-1}):

$$F_d = V_d \times [NO_3^-] \quad (5.3)$$

where $[NO_3^-]$ is the atmospheric nitrate concentration in ng m^{-3}. We have then calculated the cumulative nitrate mass deposited from the atmosphere to the snow starting from the end of the winter and compare this quantity to the nitrate mass in the skin layer over the same period of time. The temporal shift in nitrate concentration observed between the two reservoirs can be quantitatively reproduced using a V_d value of approximately 0.005 m s^{-1} (0.5 cm s^{-1}) (**Figure 5.6**). This value is somewhat lower than the 0.8 cm s^{-1} value calculated for dry deposition of HNO_3 from flux measurements at South Pole (Huey et al., 2004), and also lower than the average value estimated for the coastal California MBL in Chapter 4 (~ 1.0 cm s^{-1}). However, it should be borne in mind that our estimate likely represents an "apparent" deposition velocity for summer conditions at DC, as a reemission flux of reactive nitrogen from the skin layer to the atmosphere also occurs. For example, if the pure deposition velocity of nitrate is actually 1.0 cm s^{-1} at Dome C, consistent with the estimates commonly encountered in the literature for gaseous HNO_3 (Hauglustaine *et al.*, 1994; Liang *et al.*, 1998), including in Chapter 4 of this manuscript, then the finding of an apparent deposition velocity of 0.5 cm s^{-1} implies the existence of an upward nitrate flux that is approximately half of the depositional flux on an annual basis.

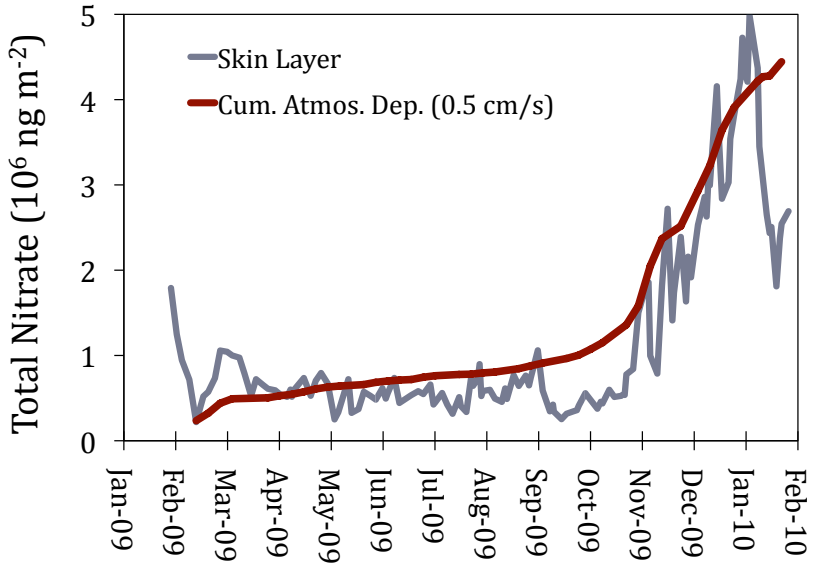

FIGURE 5.6 - Cumulative annual dry deposition from the atmosphere to the skin layer for an apparent deposition velocity of 0.5 cm s^{-1}.

The accumulation of nitrate in the skin layer through atmospheric deposition became increasingly dominant during mid-December to early January, a time of the year when the stratospheric ozone column typically recovers over the Antarctic continent and UV flux to the surface begins to wane (Solomon, 1999). The total skin layer nitrate reservoir became quantitatively equivalent to the cumulative estimated atmospheric nitrate deposition during this period. This peak in skin layer concentrations was accompanied by the development of a rapid isotopic equilibrium at the air-snow interface, with both $\delta^{15}N$ and $\Delta^{17}O$ becoming approximately equal in the atmospheric and skin layer nitrate reservoirs for a period of ~ 2 weeks. Skin layer nitrate concentration then decreased by a factor of two in mid-January, concurrent with a shift in meteorological conditions at Dome C from stable clear-sky weather to windy and cloudy conditions. The $\delta^{15}N$ value of nitrate in the skin layer increased steadily during this period, presumably due to a reestablishment of the equilibrium effect imposed by the physical deposition and release of HNO_3, which had been overwhelmed during the spring and early summer due to the strong fluxes of NO_x and nitrate between the snow and overlying boundary layer.

5.4.3 Nitrate isotope mass balance during OPALE 2011 - 2012

The availability of a large database of trace species measurements at Dome C during the OPALE 2010-2011 field campaign presents a unique opportunity to compare

observations of $\Delta^{17}O(NO_3^-)$ in the atmosphere (**Figure 5.3**) to estimated values calculated using direct observations of the complete suite of relevant gas-phase precursors. As discussed in Section 4.4.1, the ^{17}O-excess transfer functions associated with the various nitrate production pathways (i.e., $\Delta^{17}O(NO_3^-)_i$ values) can be estimated as a function of the $\Delta^{17}O$ of nitrate precursor gases (i.e., NO_x, O_3, OH, etc.) using mass balance calculations that trace the origin of oxygen atoms transferred during the chemical transformation of NO_x in the atmosphere. In each atmospheric nitrate production channel, the main reactant is either NO_2 or a NO_x reservoir species derived from NO_2 (e.g., N_2O_5); therefore, the first step in determining the $\Delta^{17}O$ signature of each pathway is a quantitative assessment of the steady state $\Delta^{17}O$ value of NO_2. As previously discussed in relation to stratospheric nitrate inputs (Section 5.4.1), $\Delta^{17}O(NO_2)$ is typically calculated as a function of the $\Delta^{17}O$ value of ozone and the reaction dynamics involved in the conversion of NO to NO_2. At photochemical steady state, an assumption that can be reasonably applied throughout the day at Dome C during summer:

$$\Delta^{17}O(NO_2) = \alpha \times \Delta^{17}O(O_3^*) \tag{5.4}$$

where $\Delta^{17}O(O_3^*)$ represents the ^{17}O-excess transferred by ozone through bimolecular chemical reactions and α represents the fraction of the atmospheric NO_2 reservoir that has been produced through oxidation by ozone rather than HO_2/RO_2 at photochemical equilibrium (Röckmann *et al.*, 2001; Michalski *et al.*, 2003; Alexander *et al.*, 2009; Morin *et al.*, 2011):

$$\alpha = \frac{k_{NO+O_3}[NO][O_3]}{k_{NO+O_3}[NO][O_3] + k_{NO+HO_2}[NO][HO_2] + k_{NO+RO_2}[NO][RO_2]} \tag{5.5}$$

Using 15-minute average measurements of NO_x, O_3, OH and HO_2/RO_2 (OPALE consortium, personal communication, 2012), along with temperature dependent reaction kinetics data obtained from Atkinson *et al.* (2004), we have calculated the diurnally averaged trend in α for the month of December 2011 at Dome C. Measurements of $\Delta^{17}O(O_3^*)$ at Dome C during the OPALE campaign averaged 34‰; however, the results were inconclusive. In the absence of dependable observations at Dome C, an issue that will soon be resolved in a forthcoming field campaign, we have tentatively assumed a $\Delta^{17}O(O_3^*)$ value of 40‰ in this analysis, consistent with nitrite-coated filter measurements from other locations (see Chapter 3). The trend in $\Delta^{17}O(NO_2)$ calculated using Equation 5.4 is shown in **Figure 5.7**. Maximum values of

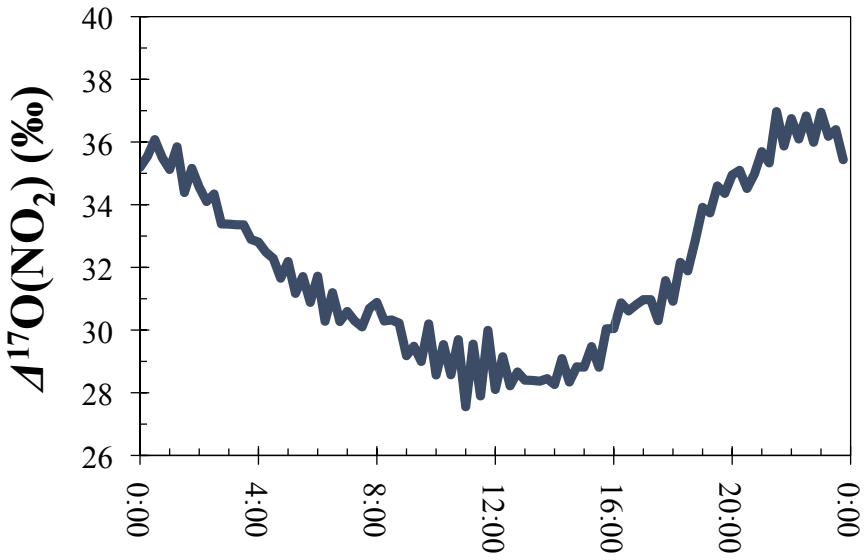

FIGURE 5.7 - Quantitative assessment of the diurnally averaged trend in the $\Delta^{17}O$ of NO_2 at Dome C during December 2011 derived from *in-situ* measurements of ozone, NO, and HO_2/RO_2.

33 - 36‰ are predicted for "nighttime" hours at Dome C (20:00 - 03:00), when the photochemical production of peroxy radicals is diminished due to reduced actinic flux and the NO + O_3 pathway (R5.2) dominates the NO to NO_2 conversion ($\alpha > 0.85$). Conversely, $\alpha = 0.75 - 0.85$ during the rest of the day, corresponding to steady state $\Delta^{17}O(NO_2)$ values of 28 - 33‰.

By accounting for the origin of the oxygen atom transferred during the conversion of NO_2 to nitrate, the $\Delta^{17}O$ signature of the nitrate produced through different reaction mechanisms can be calculated. For summer conditions at Dome C, it is reasonable to assume that the dominant atmospheric nitrate formation pathway is the gas-phase association of NO_2 and the OH radical (Alexander *et al.*, 2009):

$$NO_2 + OH + M \rightarrow HNO_3 + M \qquad \text{(R5.14)}$$

In order to predict the $\Delta^{17}O$ value of the nitrate produced through this reaction by mass balance, the isotopic composition of tropospheric OH must be known. Although it is formed primarily from the reaction H_2O with $O(^1D)$ produced from ozone photolysis and thus initially possesses a significant level of ^{17}O-excess, the OH radical participates in a rapid isotopic exchange with atmospheric water vapor, which represents a very large oxygen reservoir relative to OH, with a $\Delta^{17}O$ that is negligible compared to ozone or nitrate (Luz and Barkan, 2010). This exchange tends to erase the ^{17}O-excess of OH under humidity and temperature conditions typical of the mid-latitudes (Dubey *et al.*, 1997); therefore, the $\Delta^{17}O$ of OH is normally assumed to be

zero in modeling studies and the nitrate produced through the R5.14 channel is calculated with the following equation (Michalski *et al.*, 2003):

$$\Delta^{17}O(NO_3^-)_{R5.14} = \frac{2}{3}\Delta^{17}O(NO_2) \quad (5.6)$$

Using Equation 5.6 and the diurnal range of $\Delta^{17}O(NO_2)$ shown in **Figure 5.7**, calculated values for the $\Delta^{17}O$ signature induced by R5.14 vary between 20 - 22‰, significantly lower than the direct observations of atmospheric $\Delta^{17}O(NO_3^-)$ during the month of December (27 - 30‰, **Figure 5.3**). However, as discussed by Morin *et al.* (2007), the assumption of $\Delta^{17}O(OH) = 0$ is likely to fail under the low humidity conditions typical of the polar atmosphere and must therefore be quantitatively assessed. The degree of isotopic equilibration between OH and H_2O can be determined as a function of the relative rates of the isotope exchange reaction and the main OH sink reactions:

$$\beta = \frac{L}{L + k_{H_2O+OH}[H_2O]} \quad (5.6)$$

where L represents the total chemical loss rate of OH via CO and CH_4 oxidation:

$$L = k_{OH+CO}[CO] + k_{OH+CH_4}[CH_4] \quad (5.7)$$

and β is the factor relating the initial $\Delta^{17}O$ transferred to OH upon its formation, denoted $\Delta^{17}O(OH)_{prod.}$, to its steady state $\Delta^{17}O$ value (Morin *et al.*, 2007):

$$\Delta^{17}O(OH) = \beta \times \Delta^{17}O(OH)_{prod.} \quad (5.8)$$

In plain words, Equations 5.6 - 5.8 predict that when the isotopic exchange reaction dominates over net chemical losses (i.e., $\beta << 1$), the steady state $\Delta^{17}O$ value of OH will be equal to that of water (i.e., $\Delta^{17}O \approx 0$‰). Conversely, when water vapor concentrations are low and the rate of chemical loss is large relative to the rate of the isotopic exchange, then $\Delta^{17}O(OH) = \Delta^{17}O(OH)_{prod.}$. To assess the value of $\Delta^{17}O(OH)$, we have computed β using temperature, pressure, and humidity data (OPALE consortium, personal communication, 2012), temperature dependent kinetic rates (Dubey *et al.*, 1997; Atkinson *et al.*, 2004), and approximate tropospheric CO and CH_4 mixing ratios of 55 and 1800 ppb, respectively (Isaksen *et al.*, 2009). The results of this calculation, which are shown in **Figure 5.8**, indicate that $\beta = 0.45 \pm 0.18$ at Dome C during the month of December, suggesting that approximately half of the $\Delta^{17}O$ value originally present in OH is preserved from exchange with H_2O, consistent with estimates for an Arctic site described by Morin *et al.* (2007). The value of

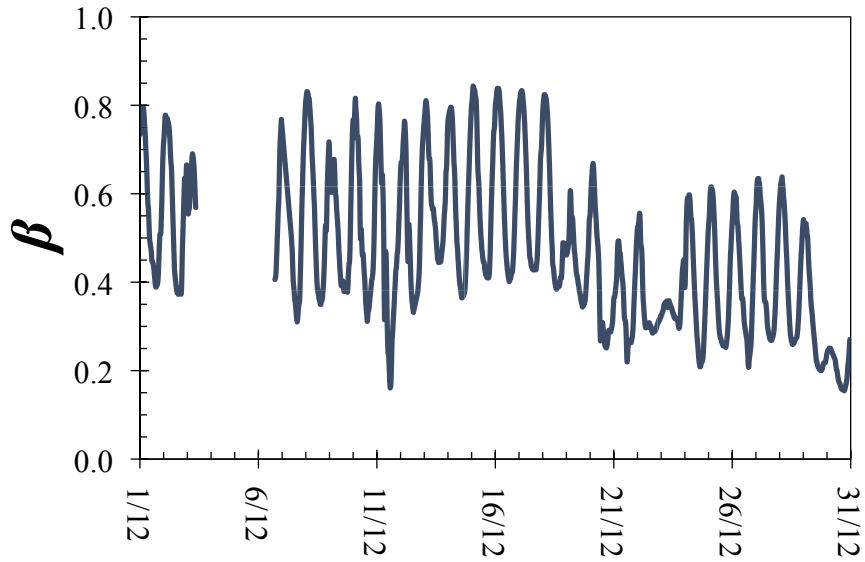

FIGURE 5.8 - December time-series for β, the proportion of the ^{17}O-excess originally associated with the OH radical that is preserved against isotopic exchange with water.

$\Delta^{17}O(OH)_{prod.}$ is more difficult to assess. For the $O(^1D) + H_2O$ pathway, $\Delta^{17}O(OH)_{prod.} \approx 20‰$, as the $\Delta^{17}O$ of $O(^1D)$ can be assumed to be approximately equivalent to that of a terminal O-atom of ozone (i.e., $\Delta^{17}O(O_3^*) = 40‰$) (Janssen, 2005), which is diluted in the OH product by the incorporation of one oxygen atom inherited from water. However, very recent observations at Dome C during the OPALE 2011 - 2012 campaign indicate that the photolysis of HONO may represent the most significant source of OH at Dome C during the period of seasonal snowpack emissions (A. Kukui, personal communication, 2012). The major process leading to the emission of HONO from the snowpack is the photolysis of nitrate (R5.12, Section 5.4.1), which possesses a $\Delta^{17}O$ value of approximately 30 - 35‰, both in the skin layer (**Figure 5.3**) and in the top 10 cm of snow (Frey *et al.*, 2009). However, the ultimate fate of nitrate oxygen isotopes during photolysis and subsequent release as NO_x and HONO is not well understood (McCabe *et al.*, 2005). As a first-order approximation, we can assume $\Delta^{17}O(OH)_{prod.} = 20‰$, which is equivalent to the $\Delta^{17}O$ value of OH produced via $O(^1D) + H_2O$, while keeping in mind that this value may be higher or lower than the actual $\Delta^{17}O(OH)_{prod.}$ value at Dome C, depending on $\Delta^{17}O(HONO)$ and the relative importance of the HONO photolysis pathway to total OH formation. A re-estimation of the $\Delta^{17}O$ signature for the $NO_2 + OH$ channel, $\Delta^{17}O(NO_3^-)_{R5.14}$, that accounts for the ^{17}O-excess carried by the OH radical results in values that range from 21 to 27‰. By accounting for the diurnal trend in the production rate from R5.14,

Table 5.2 - Comparison of Measured and Calculated $\Delta^{17}O(NO_3)$ Values.

Sampling Period	**Measured**	**Calculated**				
		$\Delta^{17}O(OH) = 0$ [XO] = 0	$\Delta^{17}O(OH) = \beta \times 20‰$ [XO] = 0	$\Delta^{17}O(OH) = \beta \times 30‰$ [XO] = 0	$\Delta^{17}O(OH) = \beta \times 20‰$, [XO] = 5 ppt	$\Delta^{17}O(OH) = \beta \times 30‰$, [XO] = 5 ppt
10 Dec - 16 Dec	**29.6**	21.8	25.2	27.4	27.0	29.2
16 Dec - 23 Dec	**29.0**	21.3	24.3	26.2	26.3	28.3
23 Dec - 30 Dec	**27.8**	21.5	23.8	25.2	25.7	27.1
30 Dec - 02 Jan	**27.3**	21.6	23.1	24.0	24.9	25.8

which has been inferred from OH and NO_2 concentration measurements (OPALE consortium, personal communication, 2012) and the temperature-dependent rate constant for the reaction (Atkinson *et al.*, 2004), diurnally-integrated average $\Delta^{17}O(NO_3^-)$ values of 23 - 25‰ can be estimated for December (**Table 5.2**). While these values are higher than the previous estimates, they are still 4 - 5‰ lower than the observed values for $\Delta^{17}O(NO_3^-)$. Alternatively, if the $\Delta^{17}O$ of HONO is assumed to be roughly equivalent to that of nitrate in the surface snow and $\Delta^{17}O(OH)_{prod.}$ = 30‰, average $\Delta^{17}O(NO_3^-)$ values of 24 - 27‰ are calculated for $\Delta^{17}O(NO_3^-)$, which is much more compatible with the observed range of 27 - 30‰, but still systematically lower. However, given the significant uncertainty surrounding the isotopic composition of HONO and its relative contribution to total OH production at Dome C, it is not possible to make a firm conclusion in this regard. Furthermore, there are several other processes that could conceivably produce the observed disagreement between the measurements and mass balance calculations. For example, the heterogeneous hydrolysis of N_2O_4, which was previously offered as a possible explanation for the 2‰ offset in $\Delta^{17}O(NO_3^-)$ observed between the atmosphere and skin layer (Section 5.4.2), could also potentially explain the difference between the calculated and measured atmospheric $\Delta^{17}O(NO_3^-)$ values. This channel would represent a source of nitrate with a $\Delta^{17}O$ value roughly equivalent to the nitrate originally present in the surface snow (i.e., 30 - 35‰), a signature significantly higher than that induced by R5.14. If this production mechanism is active at the air-snow

interface at Dome C and results in the slow emission of nitrate to the atmosphere via physical release after its formation, it would act to increase the $\Delta^{17}O$ value of nitrate in the boundary layer relative to the local $\Delta^{17}O(NO_3^-)_{R5.14}$ oxidation signature. Furthermore, the stratospheric nitrate deposited to the surface snow during winter, which possessed $\Delta^{17}O(NO_3^-)$ values in the range of 35 - 41‰ (**Figure 5.3**), may act to buffer the $\Delta^{17}O$ of the atmospheric nitrate reservoir via evaporation late into the spring and summer. However, this seems unlikely given the rapidity of NO_x cycling and oxidative loss at Dome C during this time (Legrand *et al.*, 2009; Frey *et al.*, 2013).

Another possible explanation for the underestimation of $\Delta^{17}O(NO_3^-)$ involves the potential role of reactive halogen chemistry in the troposphere over the Antarctic plateau (Bloss *et al.*, 2010). Reactive halogen oxides (XO = BrO, ClO, IO, etc.) are produced through the reaction of halogen radicals (X) with ozone, a pathway that plays an important role in the catalytic process responsible for ozone depletion events (ODEs) observed in the Arctic boundary layer since the 1980s (Fan and Jacob, 1992; Simpson *et al.*, 2007):

$$X + O_3 \rightarrow XO + O_2 \qquad \text{(R5.15)}$$

In terms of the chemical budget of NO_x, the impact of XO can occur via two chemical mechanisms. First, XO can oxidize NO to NO_2, a pathway that competes with the NO + O_3 and NO + HO_2/RO_2 reactions in terms of NO oxidation:

$$XO + NO \rightarrow X + NO_2 \qquad \text{(R5.16)}$$

For conditions typical of the Antarctic boundary layer, 1 ppt of XO has roughly the same oxidizing power as 4 ppb of ozone in terms of NO oxidation (Atkinson *et al.*, 1997). Therefore, when halogen oxides are present at relevant levels, the R5.16 pathway can result in concentrations of NO_2 that are higher than that predicted from the balance between NO_2 destruction via photolysis and production through the reaction of NO with O_3 or HO_2/RO_2 (i.e., the extended Leighton mechanism):

$$\frac{[NO_2]}{[NO]} = \frac{k_{NO+O_3}[O_3] + k_{NO+HO_2}[NO][HO_2] + k_{NO+RO_2}[NO][RO_2]}{j_{NO_2}} \qquad (5.9)$$

Observations of NO_x, ozone, and peroxy radicals during the CHABLIS field campaign at Halley, Antarctica (Jones *et al.*, 2008; 2011) suggest that NO_2 concentrations are significantly higher at this coastal site during summer than predicted from Equation 5.9. Co-measurements of halogen oxide radicals during CHABLIS revealed average surface concentrations of BrO and IO of 2.5 ppt and 3.3

ppt, respectively (Saiz-Lopez *et al.*, 2007b; 2008), which are quantitatively consistent with the shift in NO_x partitioning observed during this study (Bloss *et al.*, 2010; Bauguitte *et al.*, 2012). In a recent study at Dome C, Frey *et al.* (2013) observed an even larger deviation of the NO_2/NO ratio from the extended Leighton relationship, which strongly suggests the existence of an unexpected pathway converting NO to NO_2. The authors of this study proposed that reactive halogen radicals could potentially explain this discrepancy, although they acknowledged that this would require a concentration of XO much greater than that observed at Halley.

The interaction of XO in the NO_x cycle at Dome C would have important implications for the $\Delta^{17}O$ of atmospheric nitrate. The production of halogen oxide radicals proceeds through a direct transfer of a terminal oxygen atom from ozone to the XO product (Zhang *et al.*, 1997). Therefore, it is expected that the $\Delta^{17}O$ of XO is equal to $\Delta^{17}O(O_3^*)$, which means that the reaction of NO with XO is equivalent to the NO + O_3 reaction terms of $\Delta^{17}O$ transfer to NO_2. The participation of XO species in the oxidation of NO thus leads to a greater $\Delta^{17}O$ transfer to NO_2 by effectively increasing the value of α (**Figure 5.7**). Direct ground-based measurements of reactive halogen species are currently lacking at Dome C. However, based on satellite observations (Richter *et al.*, 1998; Saiz-Lopez *et al.*, 2007a) and the surface measurements conducted at Halley, it seems reasonable to assume that 5 ppt of XO may be present in the boundary layer above Dome C during the summer. Estimates of $\Delta^{17}O(NO_3^-)$ that account for the impact of [XO] = 5 ppt on α range from 25 - 27‰ and 26 - 29‰ at $\Delta^{17}O(OH)_{prod.}$ values of 20‰ and 30‰, respectively, in much better agreement with the observations as compared to the calculations that neglect the potential NO + XO pathway (**Table 5.2**).

In addition to its impact on NO_x cycling through the R5.16 pathway, an increasing body of evidence points towards reactive halogen chemistry as a major NO_x sink and source of nitrate via the production and subsequent hydrolysis of XNO_3 species (Vogt *et al.*, 1996; Sander *et al.*, 1999; Savarino *et al.*, 2013):

$$XO + NO_2 + M \rightarrow XNO_3 + M \qquad \text{(R5.17)}$$

$$XNO_3 + H_2O_{(liquid)} \rightarrow HNO_{3\,(aq)} + HOX \qquad \text{(R5.18)}$$

A critical analysis of the CHABLIS data led Bauguitte *et al.* (2012) to conclude that the R5.18 pathway exerted predominant control over the chemical loss rate of NO_x during the campaign, despite the significant uncertainties involved in the parameterization of the uptake processes involved (Finlayson-Pitts, 2009). This

implies that XNO_3 uptake may also represent a significant source of nitrate at Dome C should halogen oxide radicals be present at a concentration comparable to Halley (i.e., ~ 5 ppt). Experimental (Gane *et al.*, 2001) and theoretical (McNamara and Hillier, 2001) studies suggest that the oxygen atom initially associated with XO combines with the N atom of NO_2 to form nitrate, thus transferring the isotopic signature of both XO and NO_2. The specific $\Delta^{17}O$ value induced by XNO_3 hydrolysis can thus be expressed as follows (Morin *et al.*, 2007):

$$\Delta^{17}O(NO_3^-)_{R5.18} = \frac{2}{3}\alpha \times \Delta^{17}O(O_3^*) + \frac{1}{3}\Delta^{17}O(O_3^*) \quad (5.10)$$

Through consideration of the increased $\Delta^{17}O$ transfer associated with R5.18, the observations of $\Delta^{17}O(NO_3^-)$ during December can be reconciled with the values calculated by mass-balance if approximately 10 - 20% of total nitrate production is assumed to occur via XNO_3 hydrolysis.

While it is presently difficult to determine the exact nature of the process or processes leading to the relatively large ^{17}O-excess values observed for atmospheric nitrate at Dome C, the results presented here provide at least one direct line of evidence that the high $\Delta^{17}O(NO_3^-)$ values observed during spring and early summer are associated with snowpack emissions of NO_x. If only the samples collected during October - December are considered (i.e., Period 3 and the transition into Period 1 during December), a strong anticorrelation (r = 0.90) is observed between the $\delta^{15}N$ and $\Delta^{17}O$ values of atmospheric nitrate (**Figure 5.9**). In other words, the atmospheric nitrate sampled in early spring (i.e., Period 1, October - November), which was heavily depleted in ^{15}N due its formation from snowpack NO_x emissions, also possessed consistently higher $\Delta^{17}O$ values than the nitrate sampled directly after this period of maximum snow photochemistry. This finding suggests that the mechanism producing enhanced $\Delta^{17}O(NO_3^-)$ values observed during this time is tightly coupled in time and space with the intensity of NO_x emissions from the snowpack, an observation very similar to that of Morin *et al.* (2012), who detected a similar relationship between $\delta^{15}N$ and $\Delta^{17}O$ for atmospheric nitrate in the springtime boundary layer over Barrow, Alaska (71 °N). The authors of this study attributed the observed correlation to the coupling of snowpack NO_x emissions and reactive halogen chemistry, suggesting that these two processes were interrelated and mutually reinforcing. In the case of the OPALE 2011 - 2012 data, the correlation between $\delta^{15}N$ and $\Delta^{17}O$ could arise from any of the potential pathways previously discussed. For

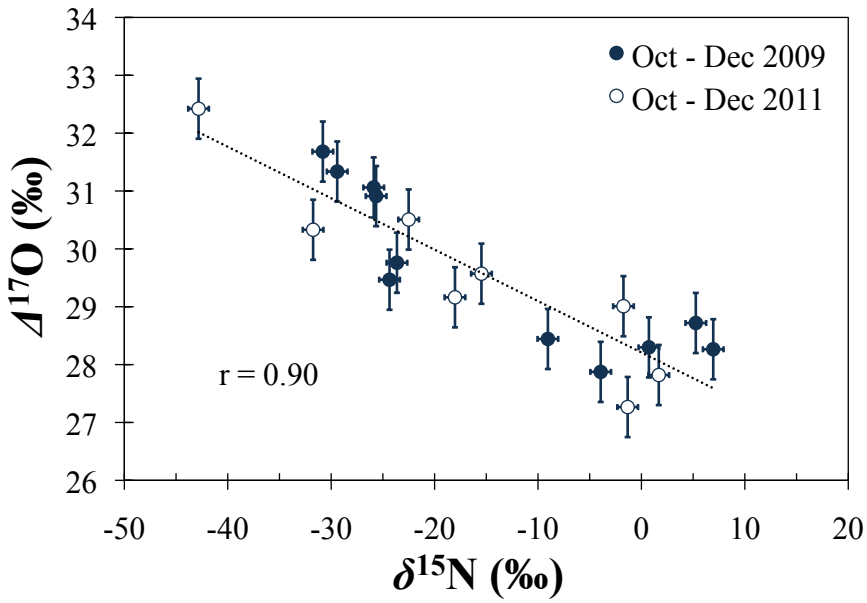

FIGURE 5.9 - Linear correlation observed between the $\delta^{15}N$ and $\Delta^{17}O$ values of atmospheric nitrate at Dome C during the October - December period of both the 2009 and 2011 sampling campaigns. Error bars indicate the typical analytical uncertainties associated with the measurements.

example, as proposed by Morin *et al.* (2012), the R5.17 and R5.18 pathways may be enhanced under periods of intense snowpack emissions. Alternatively, a correlation could result from an increased contribution to total OH production from the photolysis of HONO, which is co-emitted with NO_x via nitrate photochemistry (R5.12) and may induce a larger ^{17}O-excess in OH as compared to the conventional $O(^1D) + H_2O$ pathway. Furthermore, the hydrolysis of N_2O_4 in snow, should it contribute significantly to nitrate production at Dome C, is likely amplified during periods when concentrations NO_2 are high in the snowpack interstitial air due to nitrate/nitrite photochemistry (R5.8 and R5.11). Therefore, while the processes responsible for driving the formation of atmospheric nitrate at Dome C during spring cannot be unambiguously identified in the absence of reactive halogen measurements or detailed modeling efforts, the isotopic results presented here clearly indicate that snowpack emissions result in enhanced $\Delta^{17}O$ transfer to nitrate. Our understanding of NO_x chemistry above snow surface is therefore incomplete.

5.5 Summary and conclusions

Constraining the propagation of ozone's ^{17}O-excess signature within the NO_x cycle is critical in polar areas where there exists the possibility of extending atmospheric

interpretations based on $\Delta^{17}O$ measurements to the glacial/interglacial time scale using deep ice core records of nitrate. However, the factors governing the isotopic composition of atmospheric nitrate over the Antarctic plateau remain poorly understood, primarily due to the complex nature of the boundary layer photochemistry initiated during spring by NO_x emissions from the snowpack. Furthermore, significant uncertainty exists regarding the air-snow transfer of nitrate and the overall impact of post-depositional processes that alter the concentration and isotope ratios of nitrate both in the atmosphere and in the snowpack.

In order to investigate these air/snow dynamics, we measured the nitrogen ($\delta^{15}N$) and triple-oxygen ($\delta^{17}O$ and $\delta^{18}O$) isotope composition of nitrate year-round in the atmosphere and snow "skin layer" (surface 3 - 4 mm) at Dome C, Antarctica during 2009 - 2010. The dual isotopic composition of nitrate ($\delta^{15}N$ and $\Delta^{17}O$) in the atmosphere indicates three distinct seasonal NO_x source/sink regimes at Dome C. During the summer (Period 1), the $\Delta^{17}O$ values of nitrate are indicative of troposheric NO_x chemistry, with nighttime production becoming more relevant during the fall (beginning of Period 2). In later winter (August, Period 2), the $\Delta^{17}O$ values obtained for nitrate in the surface snow and atmosphere can only be explained in terms of stratospheric ozone chemistry, suggesting that the deposition of PSCs likely represents the dominant source of nitrate at Dome C during this time. Extremely depleted $\delta^{15}N(NO_3^-)$ values observed in the atmosphere in spring (Period 3) can be unambiguously attributed to the transformation of local snowpack NO_x emissions via photochemistry in the boundary layer, which led to peaks in atmospheric nitrate concentration during the period October - December. An isotopic mass balance performed for atmospheric nitrate during this period, informed by *in-situ* oxidant concentration measurements conducted within the framework of the OPALE field study, suggests the existence of an unexpected process that contributes significantly to the atmospheric nitrate budget over Dome C. The strong correlation observed between the $\delta^{15}N$ and $\Delta^{17}O$ values of nitrate during the peak concentration events in October - December suggests that this unknown process is enhanced during periods of intense emissions from the snowpack. Potential explanations for this observation include: (i) an increased $\Delta^{17}O$ transfer from OH due to its formation from the photolysis of HONO released from the snowpack; (ii) heterogeneous hydrolysis of N_2O_4 formed due to the high concentrations of NO_2 in the snowpack interstitial air; and (iii) the co-

emission of reactive halogen species that act as an intermediate in the transfer of $\Delta^{17}O$ from ozone to nitrate.

Seasonal variations in the oxygen isotopic composition of nitrate in the skin layer closely followed those in the atmosphere during this study, suggesting that the upper-most snow layer acts as an integrator of the atmospheric signal. Conversely, skin layer $\delta^{15}N(NO_3^-)$ values were consistently enriched by approximately 20‰ over the atmospheric signal throughout most the year. This observation is indicative of the fractionation of nitrate isotopes during deposition or subsequent processing; however, the persistence of this offset through the winter months can only be explained in terms of an equilibrium isotope effect associated with physical exchange between the atmosphere and surface snow. For both the $\delta^{15}N$ and $\Delta^{17}O$ of nitrate, an approximate equilibrium between the atmosphere and skin layer is achieved in the late spring/early summer, when atmospheric nitrate concentrations reach their annual maxima (> 90 ng m^{-3}). This suggests that nitrate removal and subsequent recycling is very intense and most likely composed of more than one cycle (i.e., removal, atmospheric processing, re-deposition and/or export).

Chapter 6

Conclusions and outlook

The primary goal of thesis has been to further our understanding of the propagation of the ^{17}O-excess ($\Delta^{17}O$) signature of ozone (O_3) throughout the atmospheric reactive nitrogen ($NO_x = NO + NO_2$) cycle. This unique and distinctive isotopic quantity is preserved in nitrate (NO_3^-) aerosols and mineral deposits, providing a conservative tracer for the relative importance of ozone and other key oxidants involved in NO_x cycling. Measurements of $\Delta^{17}O(NO_3^-)$ can thus be used to identify and apportion NO_x sinks and assess the oxidative capacity of the atmosphere. There also exists the possibility of extending these interpretations into the past using deep ice core records of nitrate, which could allow for an evaluation of the link between climate and atmospheric oxidation chemistry over glacial/interglacial time scales and during rapid climate change events. However, despite the intense research effort dedicated to the interpretation of $\Delta^{17}O(NO_3^-)$ measurements, the atmospheric processes responsible for the transfer of $\Delta^{17}O$ to nitrate and their overall influence on nitrate isotopic composition on different spatial and temporal scales are not well understood. Furthermore, the utility of ozone's $\Delta^{17}O$ signature as a quantitative tracer of atmospheric chemistry is contingent upon a precise and accurate knowledge of its magnitude and the extent of its natural spatial and temporal variability, which is currently lacking, a problem that has confounded the interpretation of $\Delta^{17}O$ measurements for over a decade. The research questions that have been pursued in the preceding chapters were formulated to address these knowledge gaps.

The primary analytical tool used to address these questions was the bacterial denitrifier method followed by continuous-flow isotope ratio mass spectrometry (CF-IRMS), which allows for the comprehensive isotopic analysis of nitrate (i.e., the simultaneous measurement of all its stable isotope ratios: $^{17}O/^{16}O$, $^{18}O/^{16}O$, and $^{15}N/^{14}N$). This method was applied to the isotopic analysis of nitrate samples in two case studies: (i) an investigation of the diurnal and spatial features of atmospheric nitrate isotopic composition in coastal California; and (ii) a study of the seasonality and air-snow transfer of nitrate stable isotopes on the Antarctic plateau. Furthermore,

the method was adapted to the isotopic characterization of ozone via chemical conversion of its terminal oxygen atoms to nitrate. During the course of this thesis, a large dataset of tropospheric $\Delta^{17}O(O_3)$ measurements has been obtained, including a full annual record from Grenoble, France (45 °N) and a ship-based latitudinal profile from 50 °S to 50 °N in the Atlantic marine boundary layer (MBL). In this closing chapter, we relate the results of these various studies to the original scientific questions posed in the introduction.

6.1 Can the aqueous-phase reaction of ozone with nitrite (NO_2^-) be applied as a chemical probe for measuring $\Delta^{17}O(O_3)$ in ambient air?

Based on the internal consistency of our large observational record of $\Delta^{17}O(O_3)$, as well as the strong agreement between our data and that previously obtained using the cryogenic collection technique (Krankowsky *et al.*, 1995; Johnston and Thiemens, 1997), we feel confident in offering a resounding "yes" to this question. However, our endorsement does not come without caveats. Despite the apparent simplicity of the nitrite-based collection technique, several analytical obstacles are associated with this approach. Most significantly, the nitrite reagent used to trap ozone will invariably possess a certain level of background nitrate contamination. The quantitative impact of this blank can be accounted for through calibration of the samples to nitrate standard reference materials prepared in an identical background "matrix" of filter coating reagents (i.e., application of the identical treatment principal); however, an implicit assumption underlying this automatic blank correction is that the blank to sample ratio does not vary widely between individual ozone collections. This assumption appears to be a valid in the case of the ozone collections performed in Grenoble; however, filter samples collected at Dome C and during a research cruise in the Atlantic suffered to varying degrees from blank accumulation and loss during sampling, handling, or storage (see Chapter 3). The calibration of such samples to standards prepared in an average matrix blank (i.e., the level of nitrate blank expected from 100% recovery of coating reagents) is not be strictly valid, as variations in blank to sample ratio are associated with changes in the slopes and intercepts of the linear regressions used to calibrate the raw isotopic measurements (see Chapter 2). Therefore, unexpected variability in blank/sample mixing can compromise the efficacy of the calibration process and result in erroneous conclusions regarding the

isotopic composition of the ozone sampled. However, the $\delta^{15}N$ of the nitrate formed on the sample filters acts as a sensitive indicator of the accuracy of the $\Delta^{17}O$ calibration. Samples with enhanced blank levels (i.e., increased blank to sample ratio) exhibit systematically higher $\delta^{15}N$ and lower $\Delta^{17}O$ values and *vice versa*. The strong anticorrelation observed between these two variables provided a means for correcting the measured $\Delta^{17}O$ values in this study. Therefore, we recommend that $\delta^{15}N$ be always measured along with the oxygen stable isotope ratios of nitrate in order to screen the data for this effect. To reduce the potential for blank/sample mixing variability to impact the results, extra caution must be taken in the use of reagents for the normalization of nitrate isotopic data. Because the reagent nitrate blank is large and may vary between batches of reagents, it is absolutely necessary that samples and standard references are processed in batches; i.e., groups of filter samples sharing the same coating date, storage and transport conditions, etc., must be normalized to standards prepared with the same reagents used to coat the filters from that batch. Additionally, coated filters should be protected at all times from excessive exposure to light, which was found to lead to an accumulation of nitrate background. In order to reduce the potential for this interference to impact the isotopic results, we recommend that the sampling filter holder be covered in aluminum foil during sample collection.

For the samples collected in Grenoble throughout 2012, a very clear trend is apparent when comparing the $\Delta^{17}O(O_3)$ values obtained for samples smaller and larger than 150 ppb•hr (n = 24 and 47, respectively), with the vast majority of variability in the measurements associated with the former, smaller group of samples (see Chapter 3). This effect can be understood in terms of the quantitative impact of the volume of filter extract that is injected with the bacteria. When total sample sizes are low, a greater volume of filter extract must be injected with the bacterial denitirifiers to obtain a sufficient mass for the analysis; therefore, a larger proportion of the nitrate will originate from the blank present in the reagents, which will increase the analytical uncertainty of the measurement. While this blank size effect does not appear to have a very large quantitative impact on the calibration parameters generated using the nitrate isotopic reference materials (see Chapter 2), it will certainly increase the opportunity for the blank/sample mixing effect to degrade the comparability between the samples and standards, as discussed above. Based on the sum of the observations reported and discussed in Chapters 2 and 3, we recommend the collection of at least 0.5 - 1.0 μmol of nitrate on each filter (25 - 50 μmol L^{-1} in

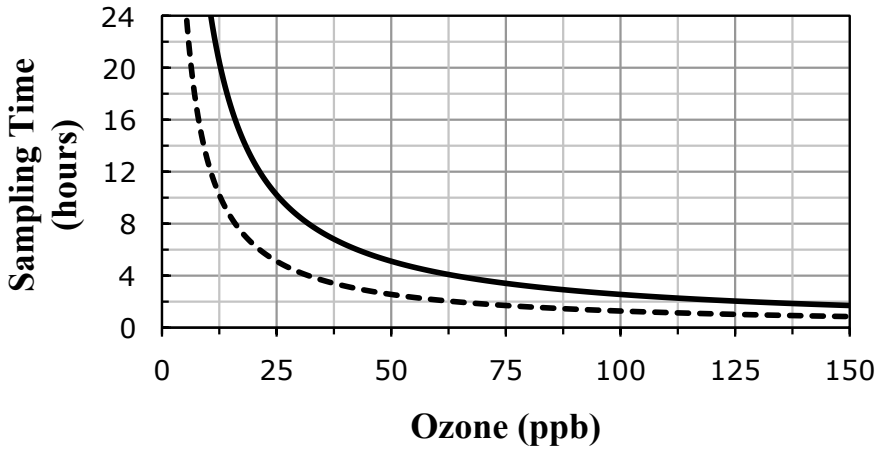

FIGURE 6.1 - Required sampling durations for the collection of 0.5 μmol (broken line) to 1.0 μmol (solid line) of nitrate for various ozone mixing ratios. Sampling time is estimated assuming a flow rate of 3.0 L min^{-1} and the overall ozone collection efficiency reported in Chapter 2 (58%).

the 20 mL filter extract solution, corresponding to 2 - 4 mL total injection volumes at a 100 nmol nitrate analysis target). This corresponds to a sampling intensity of approximately 150 - 300 ppb•hr at the flow rate and collection efficiency of the sampler used in this thesis. In order to ensure the collection of this minimum amount, ozone mixing ratio should always be monitored at the site of collection in order to adjust the sampling duration accordingly (**Figure 6.1**). Considering that tropospheric ozone mixing ratios typically exceed 20 ppb in most locations (Vingarzan, 2004), the recommended sample size can normally be achieved within 8 hours of sampling time. For ambient concentrations as low as 10 ppb, such as those observed in Grenoble during fall and winter and in other urban settings (Zhang *et al.*, 2004), sampling intervals of up to 15 - 30 hours are necessary. However, due to the large variability observed in the results for samples collected at ozone concentrations less than 5 ppb, we do not recommend the application of the method to such atmospheric environments. All things considered, we recommend that, when balancing the time resolution of the measurements with sample size, maximizing the sample size should take priority. Further studies of diurnal variations, which were not detected in Grenoble, could be conducted during ozone pollution episodes in highly impacted environments, such as the Los Angeles Basin, where ozone often exceeds 24-hour average concentrations of 100 ppb during summer (Johnston and Thiemens, 1997).

6.2 What is the transferrable $\Delta^{17}O$ signature of ozone in the troposphere and how does it vary over different spatial and temporal scales?

The most conspicuous feature of the comparison between our results and those obtained using the cryogenic collection technique is the greatly reduced level of variability in $\Delta^{17}O(O_3)$ in the nitrite-coated filter record (see Chapter 3). For both the annual record at Grenoble and the latitudinal profile from the R/V *Polarstern*, the observed level of variability (1σ = 1.3‰ and 1.1%, respectively, in terms of bulk ozone) is less than the analytical uncertainty estimated in Chapter 2 (1.7‰). This indicates that the ^{17}O-excess of ozone is spatially and seasonally homogeneous within the analytical uncertainty of the technique. This finding is largely consistent with the theoretical considerations of the factors influencing $\Delta^{17}O(O_3)$ discussed in Chapter 3; however, it is contrary to the results of Johnston and Thiemens (1997), who detected a systematic variability in $\Delta^{17}O(O_3)$ that was attributed to differences in the intensity of local photochemical cycling among three different sites. Our observations suggest that measurements of $\Delta^{17}O(O_3)$ using the nitrite-coated filter method are unlikely to provide relevant information regarding the tropospheric ozone budget. However, the observational record compiled during the course of this thesis represents an invaluable constraint on the transferrable ^{17}O-excess of tropospheric ozone. The consistent use of a $\Delta^{17}O(O_3^*)$ value of 39 ± 2‰ (the average value and standard deviation for both the Grenoble and R/V *Polarstern* records) should aid significantly in the further application of this tracer in studies of atmospheric oxidation pathways.

6.3 Does the isotopic composition of nitrate exhibit diurnal variability analogous to its large-scale seasonal trend?

In Chapter 4, we have seen that, in some cases, the isotopic composition of atmospheric nitrate does indeed vary on a diurnal basis. The magnitude and proportionality of the diurnal variability observed for $\Delta^{17}O(NO_3^-)$ during the CalNex study, which was driven by diurnal changes in atmospheric chemistry coupled with the amplifying effect of sea breeze-land breeze recirculation, was accurately reproduced by constraining a continuity equation for $\Delta^{17}O(NO_3^-)$ to our measurements. This analysis represents the first direct observational evidence for the fluctuations in $\Delta^{17}O(NO_3^-)$ that have been hypothesized to result from diurnal changes

in the relative activities of nitrate production pathways (Morin *et al.*, 2011) and provides a framework for the interpretation of such variations in future studies. The quantitative approach developed in Chapter 4 allowed for an estimation of the atmospheric lifetime of nitrate, which is difficult to evaluate directly in the ambient troposphere. Furthermore, the application of the continuity equation to the observed diurnal variations also provided a unique opportunity to evaluate different quantitative assumptions regarding the ^{17}O-excess of ozone. Our analysis suggests that the appropriate value for $\Delta^{17}O(O_3^*)$ is on the order of 41 ± 3‰, a conclusion that lends credence to the $\Delta^{17}O(O_3^*)$ range recommended based on our nitrite-coated filter measurements.

The nitrogen isotopic composition ($\delta^{15}N$) of nitrate also exhibited a clear diurnal trend during the CalNex study on R/V *Atlantis*, typically increasing through daytime production and decreasing through nocturnal production. A quantitative evaluation of the *in-situ* O_3 and NO_x measurements conducted during the cruise suggests that this diurnal pattern can be explained by the isotope exchange equilibrium between NO and NO_2, which would have resulted in increasing $\delta^{15}N(NO_2)$ values during the day due to the relatively high NO_x/O_3 ratio in the Los Angeles Basin. Therefore, our results indicate that the $\delta^{15}N$ of atmospheric nitrate does not necessarily reflect a source signature under high NO_x conditions, a finding that has important implications for the use $\delta^{15}N(NO_3^-)$ as tracer for anthropogenic NO_x emissions (Elliott *et al.*, 2009).

6.4 How is the complex oxidation chemistry resulting from snow photo-denitrification reflected in the isotopic composition of nitrate in the surface snow and atmosphere of the Antarctic plateau?

Nitrate concentration profiles in ice cores have long been thought to convey information regarding atmospheric NO_x source and sink variations in ancient atmospheres (Legrand *et al.*, 1988). However, photochemical release from the snowpack can result in extensive loss of nitrate mass and thus the amount of nitrate preserved in the ice may not be directly indicative of past variations in atmospheric NO_x concentrations (Frey *et al.*, 2009). This process is unambiguously reflected in the nitrogen isotopic composition of snowpack nitrate (Freyer *et al.*, 1996), particularly at sites with low snow accumulation rates where the $\delta^{15}N(NO_3^-)$ is driven strongly by post-depositional mass loss processes and information regarding NO_x sources is

generally lost in favor of the nitrate photolysis signature (Blunier *et al.*, 2005). However, as we have seen in Chapter 5, the photodenitrification of snow at Dome C is also recorded in the $\Delta^{17}O$ of atmospheric nitrate: periods of intense emissions from the snow, which have been delineated using the $\delta^{15}N$ measurements, are consistently associated with elevated $\Delta^{17}O(NO_3^-)$ values. Potential explanations for this observation include: (i) an increased $\Delta^{17}O$ transfer from OH due to its formation from the photolysis of HONO released from the snowpack; (ii) heterogeneous hydrolysis of N_2O_4 formed due to the high concentrations of NO_2 in the snowpack interstitial air; and (iii) the co-emission of reactive halogen species that act as an intermediate in the transfer of $\Delta^{17}O$ from ozone to nitrate. Future studies should attempt to determine the relative impacts of these processes on the $\Delta^{17}O$ of nitrate in the atmosphere and snow of the Antarctic plateau. These processes may be particularly relevant in light of the recent interest in developing ice core proxies for variations in paleo-oxidation chemistry based on $\Delta^{17}O(NO_3^-)$, as they will impact the $\Delta^{17}O$ signal preserved at depth in the ice.

6.5 Application to modeling studies

Coupled observations and modeling of the $\Delta^{17}O$ of nitrate can be used to investigate the relative importance of various nitrate formation pathways and could provide both qualitative and quantitative constraints on the atmospheric NO_x budget. Furthermore, comparisons of measured and modeled values can provide a means for testing the physical and chemical codes and parameterizations used to simulate atmospheric chemistry in the models.

The $\Delta^{17}O(NO_3^-)$ tracer has been recently implemented into the global atmospheric chemistry model GEOS-Chem (Alexander *et al.*, 2009). This effort has allowed for a detailed analysis of global variations in $\Delta^{17}O(NO_3^-)$. However, a truly robust evaluation of the comparison between initial model runs and existing observations (**Figure 6.2**) has been difficult for two primary reasons: (i) uncertainty regarding $\Delta^{17}O(O_3^*)$, as discussed at length in this manuscript; and (ii) as suggested by Alexander *et al.* (2009), an absence of reactive halogen chemistry in the model. The results presented in Chapters 2 and 3 of this thesis suggest that $\Delta^{17}O(O_3^*)$ is on the order of 39 ± 2‰, significantly lower than the 48‰ value used in the original model

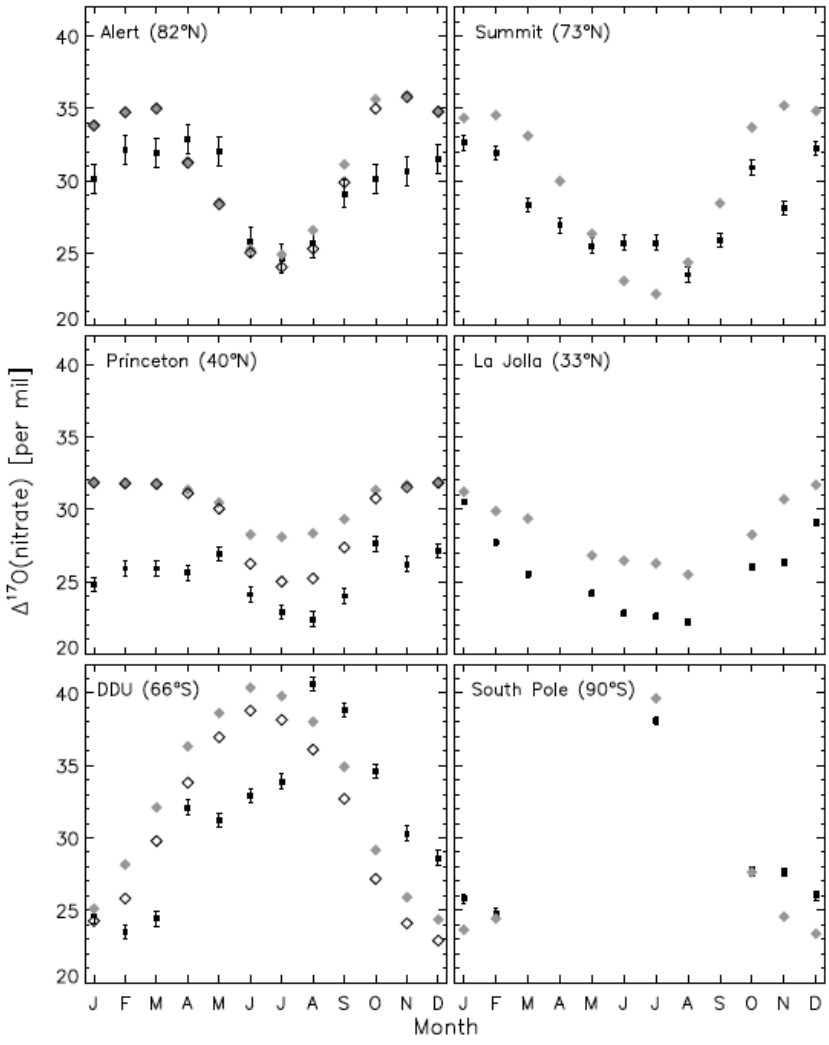

FIGURE 6.2 - Averaged measurements of $\Delta^{17}O(NO_3^-)$ reported in the literature (black squares with ±1‰ error bars) compared to values simulated using the GEOS-Chem model (gray and open diamonds) assuming a $\Delta^{17}O(O_3^*)$ value of 48‰. The largest discrepancies are in polar regions during spring and summer (0–5‰ underestimate) and in the mid- to high latitudes in winter (1–7‰ overestimate), hypothesized to result from the absence of reactive bromine chemistry in the model and the importance of long-range transport to the nitrate budget during boreal winter, respectively (Alexander *et al.*, 2009).

runs described by Alexander *et al.* (2009). A recalculation of $\Delta^{17}O(NO_3^-)$ using a $\Delta^{17}O(O_3^*)$ value of 39‰, will lead to an approximate 3 - 5‰ decrease from the simulated values shown in **Figure 6.2**. This decrease should thus result in a close agreement between measured and modeled $\Delta^{17}O(NO_3^-)$ values for the annual record at Princeton, New Jersey, which would suggest that GEOS-Chem accurately represents seasonal variations in NO_x sinks over mid-latitude continental sites where the impact of halogen chemistry is minimized. However, a decrease of 3 - 5‰ is also likely to result in large underestimates of $\Delta^{17}O(NO_3^-)$ in some cases, particularly for high-latitude sites in the northern hemisphere during spring and summer, but also during

winter in La Jolla, a coastal mid-continental site, and at the two Antarctic sites in winter and spring. It is possible that many of these discrepancies can be resolved through the consideration of the impact of reactive halogen chemistry on $\Delta^{17}O(NO_3^-)$, as discussed in Chapter 5. In order to test this hypothesis, isotope transfer functions for the reactions involving NO_x, halogen radicals (X and XO), and the reservoir species XNO_2 and XNO_3, could be implemented into a reactive halogen mechanism coupled to the GEOS-Chem model, such as the reactive bromine mechanism recently developed by Parrella *et al.* (2012). The inclusion of both halogen chemistry and our new observational constraints on $\Delta^{17}O(O_3^*)$ into GEOS-Chem could potentially produce a more realistic representation of $\Delta^{17}O(NO_3^-)$, which would further the use of $\Delta^{17}O$ for addressing specific questions regarding pathways of the NO_x cycle.

Bibliography

Adon, M.*, et al.*, **2010**. Long term measurements of sulfur dioxide, nitrogen dioxide, ammonia, nitric acid and ozone in Africa using passive samplers. *Atmospheric Chemistry and Physics* 10, 7467-7487.

Alexander, B., Allman, D. J., Amos, H. M., Fairlie, T. D., Dachs, J., Hegg, D. A., and Sletten, R. S., **2012**. Isotopic constraints on the formation pathways of sulfate aerosol in the marine boundary layer of the subtropical northeast Atlantic Ocean. *Journal of Geophysical Research-Atmospheres* 117.

Alexander, B., Hastings, M. G., Allman, D. J., Dachs, J., Thornton, J. A., and Kunasek, S. A., **2009**. Quantifying atmospheric nitrate formation pathways based on a global model of the oxygen isotopic composition (delta O-17) of atmospheric nitrate. *Atmospheric Chemistry and Physics* 9, 5043-5056.

Alexander, B., Savarino, J., Barkov, N. I., Delmas, R. J., and Thiemens, M. H., **2002**. Climate driven changes in the oxidation pathways of atmospheric sulfur. *Geophysical Research Letters* 29, 30-4.

Alexander, B., Savarino, J., Kreutz, K. J., and Thiemens, M. H., **2004**. Impact of preindustrial biomass-burning emissions on the oxidation pathways of tropospheric sulfur and nitrogen. *Journal of Geophysical Research-Atmospheres* 109.

Alexander, B., Thiemens, M. H., Farquhar, J., Kaufman, A. J., Savarino, J., and Delmas, R. J., **2003**. East Antarctic ice core sulfur isotope measurements over a complete glacial-interglacial cycle. *Journal of Geophysical Research* 108, ACH18-1-7.

Allan, B. J., Carslaw, N., Coe, H., Burgess, R. A., and Plane, J. M. C., **1999**. Observations of the nitrate radical in the marine boundary layer. *Journal of Atmospheric Chemistry* 33, 129-154.

Amberger, A. and Schmidt, H. L., **1987**. The natural isotope content of nitrate as an indicator of its origin. *Geochimica Et Cosmochimica Acta* 51, 2699-2705.

Ammann, M., Siegwolf, R., Pichlmayer, F., Suter, M., Saurer, M., and Brunold, C., **1999**. Estimating the uptake of traffic-derived NO2 from N-15 abundance in Norway spruce needles. *Oecologia* 118, 124-131.

Anastasio, C. and Chu, L., **2009**. Photochemistry of nitrous acid (HONO) and nitrous acidium ion (H2ONO+) in aqueous solution and ice. *Environmental Science & Technology* 43, 1108-1114.

Anastasio, C., Galbavy, E. S., Hutterli, M. A., Burkhart, J. F., and Friel, D. K., **2007**. Photoformation of hydroxyl radical on snow grains at Summit, Greenland. *Atmospheric Environment* 41, 5110-5121.

Andreae, M. O. and Crutzen, P. J., **1997**. Atmospheric aerosols: Biogeochemical sources and role in atmospheric chemistry. *Science* 276, 1052-1058.

Arnold, J. R. and Luke, W. T., **2007**. Nitric acid and the origin and size segregation of aerosol nitrate aloft during BRACE 2002. *Atmospheric Environment* 41, 4227-4241.

Assonov, S. S. and Brenninkmeijer, C. A. M., **2003**. On the O-17 correction for CO2 mass spectrometric isotopic analysis. *Rapid Communications in Mass Spectrometry* 17, 1007-1016.

Atkinson, R.*, et al.*, **2004**. Evaluated kinetic and photochemical data for atmospheric chemistry: Volume I - gas phase reactions of O-x, HOx, NOx and SOx species. *Atmospheric Chemistry and Physics* 4, 1461-1738.

Augustin, L.*, et al.*, **2004**. Eight glacial cycles from an Antarctic ice core. *Nature* 429, 623-628.

Austin, J. F. and Follows, M. J., **1991**. The ozone record at Payerne: an assessment of the cross-tropopause flux. *Atmospheric Environment Part a-General Topics* 25, 1873-1880.

Bains-Sahota, S. K. and Thiemens, M. H., **1987**. Mass-independent oxygen isotopic fractionation in a microwave plasma. *Journal of Physical Chemistry* 91, 4370-4374.

Baker, A. R., Weston, K., Kelly, S. D., Voss, M., Streu, P., and Cape, J. N., **2007**. Dry and wet deposition of nutrients from the tropical Atlantic atmosphere: Links to primary productivity and nitrogen fixation. *Deep-Sea Research* 54, 1704-1720.

Bao, H. M., Lyons, J. R., and Zhou, C. M., **2008**. Triple oxygen isotope evidence for elevated CO(2) levels after a Neoproterozoic glaciation. *Nature* 453, 504-506.

Bao, H. M., Thiemens, M. H., Farquhar, J., Campbell, D. A., Lee, C. C. W., Heine, K., and Loope, D. B., **2000**. Anomalous O-17 compositions in massive sulphate deposits on the Earth. *Nature* 406, 176-178.

Barbante, C.*, et al.*, **2006**. One-to-one coupling of glacial climate variability in Greenland and Antarctica. *Nature* 444, 195-198.

Barrie, L. A., Bottenheim, J. W., Schnell, R. C., Crutzen, P. J., and Rasmussen, R. A., **1988**. Ozone destruction and photochemical-reactions at polar sunrise in the lower arctic atmosphere. *Nature* 334, 138-141.

Bateman, A. and Kaiser, J., **2010**. Diurnal variations in the nitrogen and oxygen isotope composition of aerosol nitrate*EGU General Assembly*.

Bauguitte, S. J. B.*, et al.*, **2012**. Summertime NOx measurements during the CHABLIS campaign: can source and sink estimates unravel observed diurnal cycles? *Atmospheric Chemistry and Physics* 12, 989-1002.

Becagli, S.*, et al.*, **2012**. Study of present-day sources and transport processes affecting oxidised sulphur compounds in atmospheric aerosols at Dome C (Antarctica) from year-round sampling campaigns. *Atmospheric Environment* 52, 98-108.

Beekmann, M., Ancellet, G., and Megie, G., **1994**. Climatology of tropospheric ozone in southern Europe and its relation to potential vorticity. *Journal of Geophysical Research-Atmospheres* 99, 12841-12853.

Begun, G. M. and Fletcher, W. H., **1960**. Partition function ratios for molecules containing nitrogen isotopes. *Journal of Chemical Physics* 33, 1083-1085.

Begun, G. M. and Melton, C. E., **1956**. Nitrogen isotopic fractionation between NO and NO2 and mass discrimination in mass analysis of NO2. *Journal of Chemical Physics* 25, 1292-1293.

Berhanu, T. A., Savarino, J., Bhattacharya, S. K., and Vicars, W. C., **2012**. O-17 excess transfer during the NO2 + O-3 -> NO3 + O-2 reaction. *Journal of Chemical Physics* 136.

Bertram, T. H. and Thornton, J. A., **2009**. Toward a general parameterization of N2O5 reactivity on aqueous particles: The competing effects of particle liquid water, nitrate and chloride. *Atmospheric Chemistry and Physics* 9, 8351-8363.

Bhattacharya, S. K., Pandey, A., and Savarino, J., **2008**. Determination of intramolecular isotope distribution of ozone by oxidation reaction with silver metal. *Journal of Geophysical Research-Atmospheres* 113.

Bhattacharya, S. K., Savarino, J., and Luz, B., **2009**. Mass-dependent isotopic fractionation in ozone produced by electrolysis. *Analytical Chemistry* 81, 5226-5232.

Bhattacharya, S. K. and Thiemens, M. H., **1988**. Isotopic fractionation in ozone decomposition. *Geophysical Research Letters* 15, 9-12.

Bigeleisen, J., **1965**. Chemistry of isotopes. *Science* 147, 463-+.

Bigeleisen, J. and Mayer, M. G., **1947**. Calculation of equilibrium constants for isotopic exchange reactions. *Journal of Chemical Physics* 15, 261-267.

Bigler, M.*, et al.*, **2010**. Atmospheric decadal variability from high-resolution Dome C ice core records of aerosol constituents beyond the Last Interglacial. *Quaternary Science Reviews* 29, 324-337.

Bloss, W. J.*, et al.*, **2010**. Coupling of HOx, NOx and halogen chemistry in the antarctic boundary layer. *Atmospheric Chemistry and Physics* 10, 10187-10209.

Bloss, W. J., Evans, M. J., Lee, J. D., Sommariva, R., Heard, D. E., and Pilling, M. J., **2005**. The oxidative capacity of the troposphere: Coupling of field measurements of OH and a global chemistry transport model. *Faraday Discussions* 130, 425-436.

Blunier, T., Barnett, B., Bender, M. L., and Hendricks, M. B., **2002**. Biological oxygen productivity during the last 60,000 years from triple oxygen isotope measurements. *Global Biogeochemical Cycles* 16.

Blunier, T., Floch, G. L., Jacobi, H. W., and Quansah, E., **2005**. Isotopic view on nitrate loss in Antarctic surface snow. *Geophysical Research Letters* 32.

Boering, K. A., Jackson, T., Hoag, K. J., Cole, A. S., Perri, M. J., Thiemens, M., and Atlas, E., **2004**. Observations of the anomalous oxygen isotopic composition of carbon dioxide in the lower stratosphere and the flux of the anomaly to the troposphere. *Geophysical Research Letters* 31.

Böhlke, J. K., Ericksen, G. E., and Revesz, K., **1997**. Stable isotope evidence for an atmospheric origin of desert nitrate deposits in northern Chile and southern California, USA. *Chemical Geology* 136, 135-152.

Böhlke, J. K., Mroczkowski, S. J., and Coplen, T. B., **2003**. Oxygen isotopes in nitrate: new reference materials for 18O:17O:16O measurements and observations on nitrate-water equilibration. *Rapid Communications in Mass Spectrometry* 17, 1835-1846.

Böhlke, J. K., Smith, R. L., and Hannon, J. E., **2007**. Isotopic analysis of N and O in nitrite and nitrate by sequential selective bacterial reduction to N2O. *Analytical Chemistry* 79, 5888-5895.

Bowen, G. J. and Wilkinson, B., **2002**. Spatial distribution of delta O-18 in meteoric precipitation. *Geology* 30, 315-318.

Boxe, C. S. and Saiz-Lopez, A., **2008**. Multiphase modeling of nitrate photochemistry in the quasi-liquid layer (QLL): implications for NO(x) release from the Arctic and coastal Antarctic snowpack. *Atmospheric Chemistry and Physics* 8, 4855-4864.

Brasseur, G. P., Tie, X. X., Rasch, P. J., and Lefevre, F., **1997**. A three-dimensional simulation of the Antarctic ozone hole: Impact of anthropogenic chlorine on the lower stratosphere and upper troposphere. *Journal of Geophysical Research-Atmospheres* 102, 8909-8930.

Brenninkmeijer, C. A. M., Janssen, C., Kaiser, J., Röckmann, T., Rhee, T. S., and Assonov, S. S., **2003**. Isotope effects in the chemistry of atmospheric trace compounds. *Chemical Reviews* 103, 5125-5161.

Brown, S. S.*, et al.*, **2004**. Nighttime removal of NOx in the summer marine boundary layer. *Geophysical Research Letters* 31.

Brown, S. S.*, et al.*, **2005**. Aircraft observations of daytime NO3 and N2O5 and their implications for tropospheric chemistry. *Journal of Photochemistry and Photobiology* 176, 270-278.

Brown, S. S.*, et al.*, **2006**. Variability in nocturnal nitrogen oxide processing and its role in regional air quality. *Science* 311, 67-70.

Brown, S. S. and Stutz, J., **2012**. Nighttime radical observations and chemistry. *Chemical Society Reviews* 41, 6405-6447.

Brunekreef, B. and Holgate, S. T., **2002**. Air pollution and health. *Lancet* 360, 1233-1242.

Bunton, C. A., Llewellyn, D. R., and Stedman, G., **1955**. Oxygen exchange between nitrous acid and water. *Nature* 175, 83-84.

Bunton, C. A., Llewellyn, D. R., and Stedman, G., **1959**. Oxygen exchange between nitrous acid and water. *Journal of the Chemical Society*, 568-573.

Calvert, J. G. and Lindberg, S. E., **2003**. A modeling study of the mechanism of the halogen-ozone-mercury homogeneous reactions in the troposphere during the polar spring. *Atmospheric Environment* 37, 4467-4481.

CARB, **2009**. Emission Data by Region (Statewide). California Air Resources Board.

Casciotti, K. L., Böhlke, J. K., McIlvin, M. R., Mroczkowski, S. J., and Hannon, J. E., **2007**. Oxygen isotopes in nitrite: Analysis, calibration, and equilibration. *Analytical Chemistry* 79, 2427-2436.

Casciotti, K. L., Sigman, D. M., Hastings, M. G., Böhlke, J. K., and Hilkert, A., **2002**. Measurement of the oxygen isotopic composition of nitrate in seawater and freshwater using the denitrifier method. *Analytical Chemistry* 74, 4905-4912.

Cass, G. R. and Shair, F. H., **1984**. Sulfate accumulation in a sea breeze land breeze circulation system. *Journal of Geophysical Research-Atmospheres* 89, 1429-1438.

Chakraborty, S., **2003**. Isotopic fractionation of the O(3)-nitric oxide reaction. *Current Science* 85, 1210-1212.

Chakraborty, S. and Bhattacharya, S. K., **2003a**. Mass-independent isotopic fractionation: Recent developments. *Current Science* 84, 766-774.

Chakraborty, S. and Bhattacharya, S. K., **2003b**. Oxygen isotopic anomaly in surface induced ozone dissociation. *Chemical Physics Letters* 369, 662-667.

Chakraborty, S. and Bhattacharya, S. K., **2003c**. Oxygen isotopic fractionation during UV and visible light photodissociation of ozone. *Journal of Chemical Physics* 118, 2164-2172.

Chakraborty, S. and Bhattacharya, S. K., **2003d**. Reply to 'Comment on 'Oxygen isotopic anomaly in surface induced ozone dissociation' Chem. Phys. Lett. 369 (2003) 662. *Chemical Physics Letters* 379, 592-594.

Chang, W. L., Bhave, P. V., Brown, S. S., Riemer, N., Stutz, J., and Dabdub, D., **2011**. Heterogeneous atmospheric chemistry, ambient measurements, and model calculations of N2O5: A review. *Aerosol Science and Technology* 45, 665-695.

Chapman, S., **1930**. A theory of upper-atmosphere ozone. *Mem. Roy. Meteorol. Soc.* 3, 103-125.

Chaxel, E. and Chollet, J. P., **2009**. Ozone production from Grenoble city during the August 2003 heat wave. *Atmospheric Environment* 43, 4784-4792.

Chen, G.*, et al.*, **2004**. A reassessment of HOx South Pole chemistry based on observations recorded during ISCAT 2000. *Atmospheric Environment* 38, 5451-5461.

Chen, G.*, et al.*, **2001**. An investigation of South Pole HOx chemistry: Comparison of model results with ISCAT observations. *Geophysical Research Letters* 28, 3633-3636.

Chen, Y., Mills, S., Street, J., Golan, D., Post, A., Jacobson, M., and Paytan, A., **2007**. Estimates of atmospheric dry deposition and associated input of nutrients to Gulf of Aqaba seawater. *Journal of Geophysical Research-Atmospheres* 112.

Chu, L. and Anastasio, C., **2007**. Temperature and wavelength dependence of nitrite photolysis in frozen and aqueous solutions. *Environmental Science & Technology* 41, 3626-3632.

Clayton, R. N., Grossman, L., and Mayeda, T. K., **1973**. A component of primitive nuclear composition in carbonaceous meteorites. *Science* 182, 485-488.

Cliff, S. S. and Thiemens, M. H., **1994**. High-precision isotopic determination of the O-18/O-16 and O-17/O-16 ratios in nitrous-oxide. *Analytical Chemistry* 66, 2791-2793.

Cole, A. S. and Boering, K. A., **2006**. Mass-dependent and non-mass-dependent isotope effects in ozone photolysis: Resolving theory and experiments. *Journal of Chemical Physics* 125.

Cooper, O. R.*, et al.*, **2010**. Increasing springtime ozone mixing ratios in the free troposphere over western North America. *Nature* 463, 344-348.

Coplen, T. B., **2011**. Guidelines and recommended terms for expression of stable-isotope-ratio and gas-ratio measurement results. *Rapid Communications in Mass Spectrometry* 25, 2538-2560.

Costa, A. W., Michalski, G., Schauer, A. J., Alexander, B., Steig, E. J., and Shepson, P. B., **2011**. Analysis of atmospheric inputs of nitrate to a temperate forest ecosystem from Delta(17)O isotope ratio measurements. *Geophysical Research Letters* 38.

Couach, O.*, et al.*, **2003**. An investigation of ozone and planetary boundary layer dynamics over the complex topography of Grenoble combining measurements and modeling. *Atmospheric Chemistry and Physics* 3, 549-562.

Craig, H., **1961**. Standard for reporting concentrations of deuterium and oxygen-18 in natural waters. *Science* 133, 1833-1834.

Crawford, J. H., *et al.*, **2001**. Evidence for photochemical production of ozone at the South Pole surface. *Geophysical Research Letters* 28, 3641-3644.

Crutzen, P. J., **1970**. Influence of nitrogen oxides on atmospheric ozone content. *Quarterly Journal of the Royal Meteorological Society* 96, 320-&.

Dansgaard, W., **1964**. Stable isotopes in precipitation. *Tellus* 16, 436-468.

Davis, D., *et al.*, **2004**. South Pole NOx chemistry: an assessment of factors controlling variability and absolute levels. *Atmospheric Environment* 38, 5375-5388.

Davis, D., *et al.*, **2001**. Unexpected high levels of NO observed at South Pole. *Geophysical Research Letters* 28, 3625-3628.

Davis, D. D., *et al.*, **2008**. A reassessment of Antarctic plateau reactive nitrogen based on ANTO 2003 airborne and ground based measurements. *Atmospheric Environment* 42, 2831-2848.

De Santis, F., Vazzana, C., Menichelli, S., Allegrini, I., and Morimoto, S., **2003**. Ozone monitoring in the polar troposphere using a new diffusive sampler. *Physics and Chemistry of the Earth* 28, 1213-1216.

Dentener, F. J. and Crutzen, P. J., **1993**. Reaction of N2O5 on tropospheric aerosols: Impact on the global distributions of NOx, O3, and OH. *Journal of Geophysical Research-Atmospheres* 98, 7149-7163.

Dibb, J. E., Talbot, R. W., Munger, J. W., Jacob, D. J., and Fan, S. M., **1998**. Air-snow exchange of HNO3 and NOy at Summit, Greenland. *Journal of Geophysical Research-Atmospheres* 103, 3475-3486.

Draxier, R. R. and Hess, G. D., **1998**. An overview of the HYSPLIT 4 modelling system for trajectories, dispersion and deposition. *Australian Meteorological Magazine* 47, 295-308.

Dubey, M. K., Mohrschladt, R., Donahue, N. M., and Anderson, J. G., **1997**. Isotope specific kinetics of hydroxyl radical (OH) with water (H2O): Testing models of reactivity and atmospheric fractionation. *Journal of Physical Chemistry* 101, 1494-1500.

Duce, R. A., *et al.*, **2008**. Impacts of atmospheric anthropogenic nitrogen on the open ocean. *Science* 320, 893-897.

Duce, R. A., *et al.*, **1991**. The atmospheric input of trace species to the world ocean. *Global Biogeochemical Cycles* 5, 193-259.

Ehhalt, D. H. and Rohrer, F., **2000**. Dependence of the OH concentration on solar UV. *Journal of Geophysical Research-Atmospheres* 105, 3565-3571.

Elliott, E. M., *et al.*, **2009**. Dual nitrate isotopes in dry deposition: Utility for partitioning NOx source contributions to landscape nitrogen deposition. *Journal of Geophysical Research-Biogeosciences* 114.

Elliott, E. M.*, et al.*, **2007**. Nitrogen isotopes as indicators of NO(x) source contributions to atmospheric nitrate deposition across the Midwestern and northeastern United States. *Environmental Science & Technology* 41, 7661-7667.

Erbland, J., **2012**. Constraintes isotopiques sur l'interprétation de l'enregistrement en nitrate dans la carotte de glace de Vostok. Ph.D. Thesis, Université Joseph Fourier.

Erbland, J.*, et al.*, **2013**. Air-snow transfer of nitrate on the East Antarctic plateau – Part 1: Isotopic evidence for a photolytically driven dynamic equilibrium. *Atmospheric Chemistry and Physics (in press)* 12.

Evans, M. J.*, et al.*, **2003**. Coupled evolution of BrO(x)-ClO(x)-HO(x)-NO(x) chemistry during bromine-catalyzed ozone depletion events in the arctic boundary layer. *Journal of Geophysical Research-Atmospheres* 108.

Fahey, D. W., Kelly, K. K., Kawa, S. R., Tuck, A. F., Loewenstein, M., Chan, K. R., and Heidt, L. E., **1990**. Observations of denitrification and dehydration in the winter polar stratospheres. *Nature* 344, 321-324.

Fan, S. M. and Jacob, D. J., **1992**. Surface ozone depletion in arctic spring sustained by bromine reactions on aerosols. *Nature* 359, 522-524.

Fang, Y. T.*, et al.*, **2011**. Anthropogenic imprints on nitrogen and oxygen isotopic composition of precipitation nitrate in a nitrogen-polluted city in southern China. *Atmospheric Chemistry and Physics* 11, 1313-1325.

Felix, J. D., Elliott, E. M., and Shaw, S. L., **2012**. Nitrogen Isotopic Composition of Coal-Fired Power Plant NOx: Influence of Emission Controls and Implications for Global Emission Inventories. *Environmental Science & Technology* 46, 3528-3535.

Fenn, M. E.*, et al.*, **2003**. Ecological effects of nitrogen deposition in the western United States. *Bioscience* 53, 404-420.

Finlayson-Pitts, B. J., **2009**. Reactions at surfaces in the atmosphere: integration of experiments and theory as necessary (but not necessarily sufficient) for predicting the physical chemistry of aerosols. *Physical Chemistry Chemical Physics* 11, 7760-7779.

Finlayson-Pitts, B. J., Ezell, M. J., and Pitts, J. N., **1989**. Formation of chemically active chlorine compounds by reactions of atmospheric NaCl particles with gaseous N2O5 and ClONO2. *Nature* 337, 241-244.

Finlayson-Pitts, B. J. and Pitts, J. N., **1997**. Tropospheric air pollution: Ozone, airborne toxics, polycyclic aromatic hydrocarbons, and particles. *Science* 276, 1045-1052.

Finlayson-Pitts, B. J. and Pitts, J. N., **2000**. *Chemistry of the Upper and Lower Atmosphere: Theory, Experiments and Applications*. Academic, San Diego, Calif.

Finlayson-Pitts, B. J., Wingen, L. M., Sumner, A. L., Syomin, D., and Ramazan, K. A., **2003**. The heterogeneous hydrolysis of NO2 in laboratory systems and in outdoor and indoor atmospheres: An integrated mechanism. *Physical Chemistry Chemical Physics* 5, 223-242.

Fischer, M. and Warneck, P., **1996**. Photodecomposition of nitrite and undissociated nitrous acid in aqueous solution. *Journal of Physical Chemistry* 100, 18749-18756.

Fowler, D.*, et al.*, **2009**. Atmospheric composition change: Ecosystems-Atmosphere interactions. *Atmospheric Environment* 43, 5193-5267.

France, J. L.*, et al.*, **2011**. Snow optical properties at Dome C (Concordia), Antarctica: Implications for snow emissions and snow chemistry of reactive nitrogen. *Atmospheric Chemistry and Physics* 11, 9787-9801.

Frey, M. M., Bales, R. C., and McConnell, J. R., **2006**. Climate sensitivity of the century-scale hydrogen peroxide (H2O2) record preserved in 23 ice cores from West Antarctica. *Journal of Geophysical Research* 111, D21301.

Frey, M. M.*, et al.*, **2013**. The diurnal variability of atmospheric nitrogen oxides (NO and NO2) above the Antarctic Plateau driven by atmospheric stability and snow emissions. *Atmospheric Chemistry and Physics (in press)*.

Frey, M. M., Savarino, J., Morin, S., Erbland, J., and Martins, J. M. F., **2009**. Photolysis imprint in the nitrate stable isotope signal in snow and atmosphere of East Antarctica and implications for reactive nitrogen cycling. *Atmospheric Chemistry and Physics* 9, 8681-8696.

Freyer, H. D., **1991**. Seasonal variation of N-15/N-14 ratios in atmospheric nitrate species. *Tellus* 43B, 30-44.

Freyer, H. D., Kley, D., Volzthomas, A., and Kobel, K., **1993**. On the interaction of isotopic exchange processes with photochemical reactions in atmospheric oxides of nitrogen. *Journal of Geophysical Research-Atmospheres* 98, 14791-14796.

Freyer, H. D., Kobel, K., Delmas, R. J., Kley, D., and Legrand, M. R., **1996**. First results of N-15/N-14 ratios in nitrate from alpine and polar ice cores. *Tellus* 48B, 93-105.

Galloway, J. N., Aber, J. D., Erisman, J. W., Seitzinger, S. P., Howarth, R. W., Cowling, E. B., and Cosby, B. J., **2003**. The nitrogen cascade. *Bioscience* 53, 341-356.

Gane, M. P., Williams, N. A., and Sodeau, J. R., **2001**. A reflection-absorption infrared spectroscopy (RAIRS) investigation of the low-temperature heterogeneous hydrolysis of bromine nitrate. *Journal of Physical Chemistry* 105, 4002-4009.

Gao, Y. Q. and Marcus, R. A., **2001**. Strange and unconventional isotope effects in ozone formation. *Science* 293, 259-263.

Gellene, G. I., **1996**. An explanation for symmetry-induced isotopic fractionation in ozone. *Science* 274, 1344-1346.

Gentner, D. R., Harley, R. A., Miller, A. M., and Goldstein, A. H., **2009**. Diurnal and seasonal variability of gasoline-related volatile organic compound emissions in Riverside, California. *Environmental Science & Technology* 43, 4247-4252.

Geyh, A. S., Wolfson, J. M., Koutrakis, P., Mulik, J. D., and Avol, E. L., **1997**. Development and evaluation of a small active ozone sampler. *Environmental Science & Technology* 31, 2326-2330.

Granger, J. and Sigman, D. M., **2009**. Removal of nitrite with sulfamic acid for nitrate N and O isotope analysis with the denitrifier method. *Rapid Communications in Mass Spectrometry* 23, 3753-3762.

Granger, J., Sigman, D. M., Prokopenko, M. G., Lehmann, M. F., and Tortell, P. D., **2006**. A method for nitrite removal in nitrate N and O isotope analyses. *Limnology and Oceanography-Methods* 4, 205-212.

Grannas, A. M.*, et al.*, **2007**. An overview of snow photochemistry: Evidence, mechanisms and impacts. *Atmospheric Chemistry and Physics* 7, 4329-4373.

Gromov, S., Jockel, P., Sander, R., and Brenninkmeijer, C. A. M., **2010**. A kinetic chemistry tagging technique and its application to modelling the stable isotopic composition of atmospheric trace gases. *Geoscientific Model Development* 3, 337-364.

Hastings, M. G., Jarvis, J. C., and Steig, E. J., **2009**. Anthropogenic impacts on nitrogen isotopes of ice-core nitrate. *Science* 324, 1288.

Hastings, M. G., Sigman, D. M., and Lipschultz, F., **2003**. Isotopic evidence for source changes of nitrate in rain at Bermuda. *Journal of Geophysical Research-Atmospheres* 108.

Hastings, M. G., Sigman, D. M., and Steig, E. J., **2005**. Glacial/interglacial changes in the isotopes of nitrate from the Greenland Ice Sheet Project 2 (GISP2) ice core. *Global Biogeochemical Cycles* 19.

Hastings, M. G., Steig, E. J., and Sigman, D. M., **2004**. Seasonal variations in N and O isotopes of nitrate in snow at Summit, Greenland: Implications for the study of nitrate in snow and ice cores. *Journal of Geophysical Research-Atmospheres* 109.

Hauglustaine, D. A. and Brasseur, G. P., **2001**. Evolution of tropospheric ozone under anthropogenic activities and associated radiative forcing of climate. *Journal of Geophysical Research-Atmospheres* 106, 32337-32360.

Hauglustaine, D. A., Granier, C., Brasseur, G. P., and Megie, G., **1994**. The importance of atmospheric chemistry in the calculation of radiative forcing on the climate system. *Journal of Geophysical Research-Atmospheres* 99, 1173-1186.

Hayes, P. L., **2012**. Aerosol composition and sources in Los Angeles during the 2010 CalNex campaign. *Journal of Geophysical Research-Atmospheres (in review)*.

Heaton, T. H. E., **1990**. 15N/14N ratios of NOx from vehicle engines and coal-fired power stations. *Tellus* 42B, 304-307.

Heidenreich, J. E. and Thiemens, M. H., **1983**. A non-mass-dependent isotope effect in the production of ozone from molecular oxygen. *Journal of Chemical Physics* 78, 892-895.

Heidenreich, J. E. and Thiemens, M. H., **1985**. The non-mass-dependent oxygen isotope effect in the electrodissociation of carbon-dioxide: a step toward understanding nomad chemistry. *Geochimica Et Cosmochimica Acta* 49, 1303-1306.

Helaleh, M. I. H., Ngudiwaluyo, S., Korenaga, T., and Tanaka, K., **2002**. Development of passive sampler technique for ozone monitoring. Estimation of indoor and outdoor ozone concentration. *Talanta* 58, 649-659.

Helmig, D., Johnson, B., Oltmans, S. J., Neff, W., Eisele, F., and Davis, D. D., **2008**. Elevated ozone in the boundary layer at South Pole. *Atmospheric Environment* 42, 2788-2803.

Hill-Falkenthal, J., Priyadarshi, A., and Thiemens, M., **2012**. Differentiating sulfate aerosol oxidation pathways for varying source altitudes using S-35 and Delta O-17 tracers. *Journal of Geophysical Research-Atmospheres* 117.

Hoering, T., **1957**. The isotopic composition of the ammonia and the nitrate ion in rain. *Geochimica Et Cosmochimica Acta* 12, 97-102.

Holland, E. A*., et al.*, **1997**. Variations in the predicted spatial distribution of atmospheric nitrogen deposition and their impact on carbon uptake by terrestrial ecosystems. *Journal of Geophysical Research-Atmospheres* 102, 15849-15866.

Honrath, R. E., Guo, S., Peterson, M. C., Dziobak, M. P., Dibb, J. E., and Arsenault, M. A., **2000**. Photochemical production of gas phase NOx from ice crystal NO3. *Journal of Geophysical Research-Atmospheres* 105, 24183-24190.

Honrath, R. E., Peterson, M. C., Guo, S., Dibb, J. E., Shepson, P. B., and Campbell, B., **1999**. Evidence of NOx production within or upon ice particles in the Greenland snowpack. *Geophysical Research Letters* 26, 695-698.

Houston, P. L., Suits, A. G., and Toumi, R., **1996**. Isotopic enrichment of heavy ozone in the stratosphere. *Journal of Geophysical Research-Atmospheres* 101, 18829-18834.

Huey, L. G*., et al.*, **2004**. CIMS measurements of HNO3 and SO2 at the South Pole during ISCAT 2000. *Atmospheric Environment* 38, 5411-5421.

Hutterli, M. A., McConnell, J. R., Bales, R. C., and Stewart, R. W., **2003**. Sensitivity of hydrogen peroxide (H2O2) and formaldehyde (HCHO) preservation in

snow to changing environmental conditions: Implications for ice core records. *Journal of Geophysical Research-Atmospheres* 108.

Isaksen, I. S. A.*, et al.*, **2009**. Atmospheric composition change: Climate-Chemistry interactions. *Atmospheric Environment* 43, 5138-5192.

Jacobi, H. W. and Hilker, B., **2007**. A mechanism for the photochemical transformation of nitrate in snow. *Journal of Photochemistry and Photobiology* 185, 371-382.

Janssen, C., **2003**. Comment on "Oxygen isotopic anomaly in surface induced ozone dissociation" Chem. Phys. Lett. 369 (2003) 662. *Chemical Physics Letters* 379, 588-591.

Janssen, C., **2005**. Intramolecular isotope distribution in heavy ozone ((OOO)-O-16-O-18-O-16 and (OOO)-O-16-O-16-O-18). *Journal of Geophysical Research-Atmospheres* 110.

Janssen, C., Guenther, J., Krankowsky, D., and Mauersberger, K., **2003**. Temperature dependence of ozone rate coefficients and isotopologue fractionation in O-16-O-18 oxygen mixtures. *Chemical Physics Letters* 367, 34-38.

Janssen, C., Guenther, J., Mauersberger, K., and Krankowsky, D., **2001**. Kinetic origin of the ozone isotope effect: a critical analysis of enrichments and rate coefficients. *Physical Chemistry Chemical Physics* 3, 4718-4721.

Janssen, C. and Tuzson, B., **2006**. A diode laser spectrometer for symmetry selective detection of ozone isotopomers. *Applied Physics B-Lasers and Optics* 82, 487-494.

Jarvis, J. C., Hastings, M. G., Steig, E. J., and Kunasek, S. A., **2009**. Isotopic ratios in gas-phase HNO3 and snow nitrate at Summit, Greenland. *Journal of Geophysical Research-Atmospheres* 114.

Jarvis, J. C., Steig, E. J., Hastings, M. G., and Kunasek, S. A., **2008**. Influence of local photochemistry on isotopes of nitrate in Greenland snow. *Geophysical Research Letters* 35.

Jenkin, M. E., Watson, L. A., Utembe, S. R., and Shallcross, D. E., **2008**. A Common Representative Intermediates (CRI) mechanism for VOC degradation - Part 1: Gas phase mechanism development. *Atmospheric Environment* 42, 7185-7195.

Johnson, D. G., Jucks, K. W., Traub, W. A., and Chance, K. V., **2000**. Isotopic composition of stratospheric ozone. *Journal of Geophysical Research-Atmospheres* 105, 9025-9031.

Johnson, M. S., Feilberg, K. L., von Hessberg, P., and Nielsen, O. J., **2002**. Isotopic processes in atmospheric chemistry. *Chemical Society Reviews* 31, 313-323.

Johnston, J. C. and Thiemens, M. H., **1997**. The isotopic composition of tropospheric ozone in three environments. *Journal of Geophysical Research-Atmospheres* 102, 25395-25404.

Jones, A. E., Weller, R., Anderson, P. S., Jacobi, H. W., Wolff, E. W., Schrems, O., and Miller, H., **2001**. Measurements of NOx emissions from the Antarctic snowpack. *Geophysical Research Letters* 28, 1499-1502.

Jones, A. E., Weller, R., Wolff, E. W., and Jacobi, H. W., **2000**. Speciation and rate of photochemical NO and NO2 production in Antarctic snow. *Geophysical Research Letters* 27, 345-348.

Jones, A. E.*, et al.*, **2011**. The multi-seasonal NOy budget in coastal Antarctica and its link with surface snow and ice core nitrate: results from the CHABLIS campaign. *Atmospheric Chemistry and Physics* 11, 9271-9285.

Jones, A. E.*, et al.*, **2008**. Chemistry of the Antarctic boundary layer and the interface with snow: An overview of the CHABLIS campaign. *Atmospheric Chemistry and Physics* 8, 3789-3803.

Jourdain, B., Preunkert, S., Cerri, O., Castebrunet, H., Udisti, R., and Legrand, M., **2008**. Year-round record of size-segregated aerosol composition in central Antarctica (Concordia station): Implications for the degree of fractionation of sea-salt particles. *Journal of Geophysical Research* 113, D14308.

Jouzel, J.*, et al.*, **2007**. Orbital and millennial Antarctic climate variability over the past 800,000 years. *Science* 317, 793-796.

Kaiser, J., **2009**. Reformulated O-17 correction of mass spectrometric stable isotope measurements in carbon dioxide and a critical appraisal of historic 'absolute' carbon and oxygen isotope ratios (vol 72, pg 1312, 2008). *Geochimica Et Cosmochimica Acta* 73, 4616-4616.

Kaiser, J., Hastings, M. G., Houlton, B. Z., Röckmann, T., and Sigman, D. M., **2007**. Triple oxygen isotope analysis of nitrate using the denitrifier method and thermal decomposition of N2O. *Analytical Chemistry* 79, 599-607.

Kaiser, J., Rockmann, T., and Brenninkmeijer, C. A. M., **2004**. Contribution of mass-dependent fractionation to the oxygen isotope anomaly of atmospheric nitrous oxide. *Journal of Geophysical Research-Atmospheres* 109.

Kaplan, J. O., Folberth, G., and Hauglustaine, D. A., **2006**. Role of methane and biogenic volatile organic compound sources in late glacial and Holocene fluctuations of atmospheric methane concentrations. *Global Biogeochemical Cycles* 20.

Kaye, J. A., **1987**. Mechanisms and observations for isotope fractionation of molecular-species in planetary-atmospheres. *Reviews of Geophysics* 25, 1609-1658.

Kendall, C., Elliott, E. M., and Wankel, S. D., **2007**. Tracing anthropogenic inputs of nitrogen to ecosystems. In: *Stable Isotopes in Ecology and Environmental Science*. Blackwell Publishing.

Kinugawa, T., Enami, S., Yabushita, A., Kawasaki, M., Hoffmann, M. R., and Colussi, A. J., **2011**. Conversion of gaseous nitrogen dioxide to nitrate and

nitrite on aqueous surfactants. *Physical Chemistry Chemical Physics* 13, 5144-5149.

Knipping, E. M. and Dabdub, D., **2003**. Impact of chlorine emissions from sea-salt aerosol on coastal urban ozone. *Environmental Science & Technology* 37, 275-284.

Komatsu, D. D., Ishimura, T., Nakagawa, F., and Tsunogai, U., **2008**. Determination of the N-15/N-14, O-17/O-16, and O-18/O-16 ratios of nitrous oxide by using continuous-flow isotope-ratio mass spectrometry. *Rapid Communications in Mass Spectrometry* 22, 1587-1596.

Koutrakis, P., Wolfson, J. M., Bunyaviroch, A., Froehlich, S. E., Hirano, K., and Mulik, J. D., **1993**. Measurement of ambient ozone using a nitrite-coated filter. *Analytical Chemistry* 65, 209-214.

Krankowsky, D., Bartecki, F., Klees, G. G., Mauersberger, K., Schellenbach, K., and Stehr, J., **1995**. Measurement of heavy isotope enrichment in tropospheric ozone. *Geophysical Research Letters* 22, 1713-1716.

Krankowsky, D., Lammerzahl, P., and Mauersberger, K., **2000**. Isotopic measurements of stratospheric ozone. *Geophysical Research Letters* 27, 2593-2595.

Krankowsky, D., Lammerzahl, P., Mauersberger, K., Janssen, C., Tuzson, B., and Rockmann, T., **2007**. Stratospheric ozone isotope fractionations derived from collected samples. *Journal of Geophysical Research-Atmospheres* 112.

Kroopnick, P. and Craig, H., **1972**. Atmospheric oxygen: isotopic composition and solubility fractionation. *Science* 175, 54-&.

Krzyzanowski, J., **2004**. Ozone variation with height in a forest canopy - results from a passive sampling field campaign. *Atmospheric Environment* 38, 5957-5962.

Kull, V., Riese, M., Tie, X., Wiemert, T., Eidmann, G., Offermann, D., and Brasseur, G. P., **2002**. NOy partitioning and aerosol influences in the stratosphere. *Journal of Geophysical Research-Atmospheres* 107.

Kunasek, S. A., Alexander, B., Steig, E. J., Hastings, M. G., Gleason, D. J., and Jarvis, J. C., **2008**. Measurements and modeling of delta O-17 of nitrate in snowpits from Summit, Greenland. *Journal of Geophysical Research-Atmospheres* 113.

Kunasek, S. A.*, et al.*, **2010**. Sulfate sources and oxidation chemistry over the past 230 years from sulfur and oxygen isotopes of sulfate in a West Antarctic ice core. *Journal of Geophysical Research-Atmospheres* 115.

Lal, D. and Baskaran, M., **2011**. Applications of Cosmogenic Isotopes as Atmospheric Tracers. In: *Handbook of Environmental Isotope Geochemistry*. Springer Berlin Heidelberg.

Lammerzahl, P., Rockmann, T., Brenninkmeijer, C. A. M., Krankowsky, D., and Mauersberger, K., **2002**. Oxygen isotope composition of stratospheric carbon dioxide. *Geophysical Research Letters* 29.

Landais, A., Barkan, E., and Luz, B., **2008**. Record of delta(18)O and (17)O-excess in ice from Vostok Antarctica during the last 150,000 years. *Geophysical Research Letters* 35.

Lawrence, J. S., Ashley, M. C. B., Tokovinin, A., and Travouillon, T., **2004**. Exceptional astronomical seeing conditions above Dome C in Antarctica. *Nature* 431, 278-281.

Lee, C. C. W., Savarino, J., and Thiemens, M. H., **2001**. Mass independent oxygen isotopic composition of atmospheric sulfate: Origin and implications for the present and past atmosphere of earth and mars. *Geophysical Research Letters* 28, 1783-1786.

Lee, J. D., Moller, S. J., Read, K. A., Lewis, A. C., Mendes, L., and Carpenter, L. J., **2009**. Year-round measurements of nitrogen oxides and ozone in the tropical North Atlantic marine boundary layer. *Journal of Geophysical Research-Atmospheres* 114.

Legrand, M. and Mayewski, P., **1997**. Glaciochemistry of polar ice cores: A review. *Reviews of Geophysics* 35, 219-243.

Legrand, M., Preunkert, S., Jourdain, B., Gallee, H., Goutail, F., Weller, R., and Savarino, J., **2009**. Year-round record of surface ozone at coastal (Dumont d'Urville) and inland (Concordia) sites in East Antarctica. *Journal of Geophysical Research-Atmospheres* 114.

Legrand, M., Wolff, E., and Wagenbach, D., **1999**. Antarctic aerosol and snowfall chemistry: Implications for deep Antarctic ice-core chemistry. *Annals of Glaciology* 29, 66-72.

Legrand, M. R. and Kirchner, S., **1990**. Origins and variations of nitrate in south polar precipitation. *Journal of Geophysical Research-Atmospheres* 95, 3493-3507.

Legrand, M. R., Lorius, C., Barkov, N. I., and Petrov, V. N., **1988**. Vostok (Antarctica) ice core: Atmospheric chemistry changes over the last climatic cycle (160,000 years). *Atmospheric Environment* 22, 317-331.

Lelieveld, J. and Dentener, F. J., **2000**. What controls tropospheric ozone? *Journal of Geophysical Research-Atmospheres* 105, 3531-3551.

Lelieveld, J., Dentener, F. J., Peters, W., and Krol, M. C., **2004a**. On the role of hydroxyl radicals in the self-cleansing capacity of the troposphere. *Atmospheric Chemistry and Physics* 4, 2337-2344.

Lelieveld, J., Peters, W., Dentener, F. J., and Krol, M. C., **2002**. Stability of tropospheric hydroxyl chemistry. *Journal of Geophysical Research-Atmospheres* 107.

Lelieveld, J., van Aardenne, J., Fischer, H., de Reus, M., Williams, J., and Winkler, P., **2004b**. Increasing ozone over the Atlantic Ocean. *Science* 304, 1483-1487.

Lerdau, M. T., Munger, L. J., and Jacob, D. J., **2000**. Atmospheric chemistry - The NO2 flux conundrum. *Science* 289, 2291-+.

Lerner, B. M., Murphy, P. C., and Williams, E. J., **2009**. Field Measurements of Small Marine Craft Gaseous Emission Factors during NEAQS 2004 and TexAQS 2006. *Environmental Science & Technology* 43, 8213-8219.

Levy, H., Moxim, W. J., Klonecki, A. A., and Kasibhatla, P. S., **1999**. Simulated tropospheric NOx: Its evaluation, global distribution and individual source contributions. *Journal of Geophysical Research-Atmospheres* 104, 26279-26306.

Liang, J. Y.*, et al.*, **1998**. Seasonal budgets of reactive nitrogen species and ozone over the United States, and export fluxes to the global atmosphere. *Journal of Geophysical Research-Atmospheres* 103, 13435-13450.

Liang, M. C., Irion, F. W., Weibel, J. D., Miller, C. E., Blake, G. A., and Yung, Y. L., **2006**. Isotopic composition of stratospheric ozone. *Journal of Geophysical Research-Atmospheres* 111.

Liao, W. and Tan, D., **2008**. 1-D Air-snowpack modeling of atmospheric nitrous acid at South Pole during ANTCI 2003. *Atmospheric Chemistry and Physics* 8, 7087-7099.

Likens, G. E., Driscoll, C. T., and Buso, D. C., **1996**. Long-term effects of acid rain: Response and recovery of a forest ecosystem. *Science* 272, 244-246.

Liu, Q., Schurter, L. M., Muller, C. E., Aloisio, S., Francisco, J. S., and Margerum, D. W., **2001**. Kinetics and mechanisms of aqueous ozone reactions with bromide, sulfite, hydrogen sulfite, iodide, and nitrite ions. *Inorganic Chemistry* 40, 4436-4442.

Luthi, D.*, et al.*, **2008**. High-resolution carbon dioxide concentration record 650,000-800,000 years before present. *Nature* 453, 379-382.

Luz, B. and Barkan, E., **2010**. Variations of O-17/O-16 and O-18/O-16 in meteoric waters. *Geochimica Et Cosmochimica Acta* 74, 6276-6286.

Luz, B., Barkan, E., Bender, M. L., Thiemens, M. H., and Boering, K. A., **1999**. Triple-isotope composition of atmospheric oxygen as a tracer of biosphere productivity. *Nature* 400, 547-550.

Lyons, J. R., **2001**. Transfer of mass-independent fractionation in ozone to other oxygen-containing radicals in the atmosphere. *Geophysical Research Letters* 28, 3231-3234.

Mack, J. and Bolton, J. R., **1999**. Photochemistry of nitrite and nitrate in aqueous solution: a review. *Journal of Photochemistry and Photobiology* 128, 1-13.

MacPherson, G. J. and Thiemens, M. H., **2011**. Cosmochemistry: Understanding the Solar System through analysis of extraterrestrial materials. *Proceedings of the National Academy of Sciences of the United States of America* 108, 19130-19134.

Malm, W. C., Schichtel, B. A., Pitchford, M. L., Ashbaugh, L. L., and Eldred, R. A., **2004**. Spatial and monthly trends in speciated fine particle concentration in the United States. *Journal of Geophysical Research-Atmospheres* 109.

Manning, W. J., Krupa, S. V., Bergweiler, C. J., and Nelson, K. I., **1996**. Ambient ozone (O-3) in three class I wilderness areas in the northeastern USA: Measurements with Ogawa passive samplers. *Environmental Pollution* 91, 399-403.

Marcus, R. A., **2008**. Mass-independent oxygen isotope fractionation in selected systems: Mechanistic considerations. In: *Advances in Quantum Chemistry, Vol. 55: Applications of Theoretical Methods to Atmospheric Science*. Elsevier Academic Press Inc., San Diego.

Mark, G., Korth, H. G., Schuchmann, H. P., and vonSonntag, C., **1996**. The photochemistry of aqueous nitrate ion revisited. *Journal of Photochemistry and Photobiology* 101, 89-103.

Marshall, J. D., **1992**. Climatic and oceanographic isotopic signals from the carbonate rock record and their preservation. *Geological Magazine* 129, 143-160.

Mauersberger, K., **1981**. Measurement of heavy ozone in the stratosphere. *Geophysical Research Letters* 8, 935-937.

Mauersberger, K., **1987**. Ozone isotope measurements in the stratosphere. *Geophysical Research Letters* 14, 80-83.

Mauersberger, K., Erbacher, B., Krankowsky, D., Gunther, J., and Nickel, R., **1999**. Ozone isotope enrichment: Isotopomer-specific rate coefficients. *Science* 283, 370-372.

Mauersberger, K., Krankowsky, D., and Janssen, C., **2003**. Oxygen isotope processes and transfer reactions. *Space Science Reviews* 106, 265-279.

Mauersberger, K., Krankowsky, D., Janssen, C., and Schinke, R., **2005**. Assessment of the ozone isotope effect. In: *Advances in Atomic, Molecular, and Optical Physics, Vol 50*.

Mauersberger, K., Lammerzahl, P., and Krankowsky, D., **2001**. Stratospheric ozone isotope enrichments-revisited. *Geophysical Research Letters* 28, 3155-3158.

Mauldin, R. L*., et al.*, **2001**. Measurements of OH, H2SO4, and MSA at the South Pole during ISCAT. *Geophysical Research Letters* 28, 3629-3632.

Mayewski, P. A. and Legrand, M. R., **1990**. Recent increase in nitrate concentration of Antarctic snow. *Nature* 346, 258-260.

McCabe, J. R., Boxe, C. S., Colussi, A. J., Hoffmann, M. R., and Thiemens, M. H., **2005**. dOxygen isotopic fractionation in the photochemistry of nitrate in water and ice. *Journal of Geophysical Research-Atmospheres* 110.

McCabe, J. R., Thiemens, M. H., and Savarino, J., **2007**. A record of ozone variability in South Pole Antarctic snow: Role of nitrate oxygen isotopes. *Journal of Geophysical Research-Atmospheres* 112.

McIlvin, M. R. and Altabet, M. A., **2005**. Chemical conversion of nitrate and nitrite to nitrous oxide for nitrogen and oxygen isotopic analysis in freshwater and seawater. *Analytical Chemistry* 77, 5589-5595.

McIlvin, M. R. and Casciotti, K. L., **2011**. Technical updates to the bacterial method for nitrate isotopic analyses. *Analytical Chemistry* 83, 1850-1856.

McLaren, R., Wojtal, P., Majonis, D., McCourt, J., Halla, J. D., and Brook, J., **2010**. NO3 radical measurements in a polluted marine environment: links to ozone formation. *Atmospheric Chemistry and Physics* 10, 4187-4206.

McLinden, C. A., Prather, M. J., and Johnson, M. S., **2003**. Global modeling of the isotopic analogues of N2O: Stratospheric distributions, budgets, and the O-17-O-18 mass-independent anomaly. *Journal of Geophysical Research-Atmospheres* 108.

McNamara, J. P. and Hillier, I. H., **2001**. Mechanism of the hydrolysis of halogen nitrates in small water clusters studied by electronic structure methods. *Journal of Physical Chemistry* 105, 7011-7024.

Meijer, H. A. J. and Li, W. J., **1998**. The use of electrolysis for accurate delta O-17 and delta O-18 isotope measurements in water. *Isotopes in Environmental and Health Studies* 34, 349-369.

Michalski, G. and Bhattacharya, S. K., **2009**. The role of symmetry in the mass independent isotope effect in ozone. *Proceedings of the National Academy of Sciences of the United States of America* 106, 5493-5496.

Michalski, G., Bockheim, J. G., Kendall, C., and Thiemens, M., **2005**. Isotopic composition of Antarctic Dry Valley nitrate: Implications for NO(y) sources and cycling in Antarctica. *Geophysical Research Letters* 32.

Michalski, G., Bohlke, J. K., and Thiemens, M., **2004**. Long term atmospheric deposition as the source of nitrate and other salts in the Atacama Desert, Chile: New evidence from mass-independent oxygen isotopic compositions. *Geochimica Et Cosmochimica Acta* 68, 4023-4038.

Michalski, G., Savarino, J., Böhlke, J. K., and Thiemens, M., **2002**. Determination of the total oxygen isotopic composition of nitrate and the calibration of a Delta O-17 nitrate reference material. *Analytical Chemistry* 74, 4989-4993.

Michalski, G., Scott, Z., Kabiling, M., and Thiemens, M. H., **2003**. First measurements and modeling of delta O-17 in atmospheric nitrate. *Geophysical Research Letters* 30.

Miller, C. E., Onorato, R. M., Liang, M.-C., and Yung, Y. L., **2005a**. Extraordinary isotopic fractionation in ozone photolysis. *Geophysical Research Letters* 32, L14814.

Miller, K. G.*, et al.*, **2005b**. The phanerozoic record of global sea-level change. *Science* 310, 1293-1298.

Miller, M. F., **2002**. Isotopic fractionation and the quantification of O-17 anomalies in the oxygen three-isotope system: an appraisal and geochemical significance. *Geochimica Et Cosmochimica Acta* 66, 1881-1889.

Millet, D. B.*, et al.*, **2004**. Volatile organic compound measurements at Trinidad Head, California, during ITCT 2K2: Analysis of sources, atmospheric composition, and aerosol residence times. *Journal of Geophysical Research-Atmospheres* 109.

Mollner, A. K.*, et al.*, **2010**. Rate of gas phase association of hydroxyl radical and nitrogen dioxide. *Science* 330, 646-649.

Monks, P. S., **2000**. A review of the observations and origins of the spring ozone maximum. *Atmospheric Environment* 34, 3545-3561.

Monks, P. S., **2005**. Gas-phase radical chemistry in the troposphere. *Chemical Society Reviews* 34, 376-395.

Monks, P. S.*, et al.*, **2009**. Atmospheric composition change: Global and regional air quality. *Atmospheric Environment* 43, 5268-5350.

Monks, P. S., Salisbury, G., Holland, G., Penkett, S. A., and Ayers, G. P., **2000**. A seasonal comparison of ozone photochemistry in the remote marine boundary layer. *Atmospheric Environment* 34, 2547-2561.

Morin, S., **2008**. Analyse de la composition isotopique de l'ion nitrate dans la basse atmosphère polaire et marine. Ph.D. Thesis, Université Joseph Fourier.

Morin, S.*, et al.*, **2012**. An isotopic view on the connection between photolytic emissions of NO(x) from the Arctic snowpack and its oxidation by reactive halogens. *Journal of Geophysical Research-Atmospheres* 117, R8-R8.

Morin, S., Sander, R., and Savarino, J., **2011**. Simulation of the diurnal variations of the oxygen isotope anomaly (Delta(17)O) of reactive atmospheric species. *Atmospheric Chemistry and Physics* 11, 3653-3671.

Morin, S., Savarino, J., Bekki, S., Cavender, A., Shepson, P. B., and Bottenheim, J. W., **2007a**. Major influence of BrO on the NOx and nitrate budgets in the Arctic spring, inferred from Delta O-17(NO3-) measurements during ozone depletion events. *Environmental Chemistry* 4, 238-241.

Morin, S., Savarino, J., Bekki, S., Gong, S., and Bottenheim, J. W., **2007b**. Signature of Arctic surface ozone depletion events in the isotope anomaly (Delta O-17) of atmospheric nitrate. *Atmospheric Chemistry and Physics* 7, 1451-1469.

Morin, S., Savarino, J., Frey, M. M., Domine, F., Jacobi, H. W., Kaleschke, L., and Martins, J. M. F., **2009**. Comprehensive isotopic composition of atmospheric nitrate in the Atlantic Ocean boundary layer from 65 degrees S to 79 degrees N. *Journal of Geophysical Research-Atmospheres* 114.

Morin, S., Savarino, J., Frey, M. M., Yan, N., Bekki, S., Bottenheim, J. W., and Martins, J. M. F., **2008**. Tracing the origin and fate of NOx in the arctic atmosphere using stable isotopes in nitrate. *Science* 322, 730-732.

Morton, J., Barnes, J., Schueler, B., and Mauersberger, K., **1990**. Laboratory studies of heavy ozone. *Journal of Geophysical Research-Atmospheres* 95, 901-907.

Ndengue, S. A., Schinke, R., Gatti, F., Meyer, H. D., and Jost, R., **2012a**. Comparison of the Huggins band for six ozone isotopologues: vibrational levels and absorption cross section. *Journal of Physical Chemistry A* 116, 12260-12270.

Ndengue, S. A., Schinke, R., Gatti, F., Meyer, H. D., and Jost, R., **2012b**. Ozone photodissociation: isotopic and electronic branching ratios for symmetric and asymmetric isotopologues. *Journal of Physical Chemistry A* 116, 12271-12279.

Occupational Safety and Health Administration Salt Lake Technical Center, **1995**. Ozone (IGFF) in Workplace Atmospheres (USDOL/OSHA-SLCAL Method No. ID-214). Occupational Safety and Health Administration, Salt Lake City, UT.

Osthoff, H. D.*, et al.*, **2009**. Regional variation of the dimethyl sulfide oxidation mechanism in the summertime marine boundary layer in the Gulf of Maine. *Journal of Geophysical Research-Atmospheres* 114.

Osthoff, H. D.*, et al.*, **2008**. High levels of nitryl chloride in the polluted subtropical marine boundary layer. *Nature Geoscience* 1, 324-328.

Park, J. and Lin, M. C., **1997**. A mass spectrometric study of the NH2+NO2 reaction. *Journal of Physical Chemistry* 101, 2643-2647.

Parrella, J. P.*, et al.*, **2012**. Tropospheric bromine chemistry: implications for present and pre-industrial ozone and mercury. *Atmospheric Chemistry and Physics* 12, 6723-6740.

Patris, N., Cliff, S. S., Quinn, P. K., Kasem, M., and Thiemens, M. H., **2007**. Isotopic analysis of aerosol sulfate and nitrate during ITCT-2k2: Determination of different formation pathways as a function of particle size. *Journal of Geophysical Research-Atmospheres* 112.

Peìro-Garcìa, J. and Nebot-Gil, I., **2003**. Ab initio study of the mechanism of the atmospheric reaction: NO2+O-3 -> NO3+O-2. *Journal of Computational Chemistry* 24, 1657-1663.

Phillips, G. J.*, et al.*, **2012**. Significant concentrations of nitryl chloride observed in rural continental Europe associated with the influence of sea salt chloride and anthropogenic emissions. *Geophysical Research Letters* 39.

Preunkert, S., *et al.*, **2012**. Oxidant Production over Antarctic Land and its Export (OPALE) project: An overview of the 2010-2011 summer campaign. *Journal of Geophysical Research-Atmospheres* 117.

Preunkert, S., Jourdain, B., Legrand, M., Udisti, R., Becagli, S., and Cerri, O., **2008**. Seasonality of sulfur species (dimethyl sulfide, sulfate, and methanesulfonate) in Antarctica: Inland versus coastal regions. *Journal of Geophysical Research-Atmospheres* 113.

Prinn, R. G., *et al.*, **2005**. Evidence for variability of atmospheric hydroxyl radicals over the past quarter century. *Geophysical Research Letters* 32.

Prinn, R. G., *et al.*, **2001**. Evidence for substantial variations of atmospheric hydroxyl radicals in the past two decades. *Science* 292, 1882-1888.

Priyadarshi, A., Dominguez, G., Savarino, J., and Thiemens, M., **2011**. Cosmogenic (35)S: A unique tracer to Antarctic atmospheric chemistry and the polar vortex. *Geophysical Research Letters* 38.

Prospero, J. M. and Savoie, D. L., **1989**. Effect of continental sources on nitrate concentrations over the Pacific Ocean. *Nature* 339, 687-689.

Rayleigh, J. W. S., **1896**. Theoretical considerations respecting the separation of gases by diffusion and similar processes. *Philos. Mag.* 42.

Revesz, K. and Bohlke, J. K., **2002**. Comparison of O-delta 18 measurements in nitrate by different combustion techniques. *Analytical Chemistry* 74, 5410-5413.

Revesz, K., Bohlke, J. K., and Yoshinari, T., **1997**. Determination of delta O-18 and delta N-15 in nitrate. *Analytical Chemistry* 69, 4375-4380.

Richet, P., Bottinga, Y., and Javoy, M., **1977**. Review of hydrogen, carbon, nitrogen, oxygen, sulfur, and chlorine stable isotope fractionation among gaseous molecules. *Annual Review of Earth and Planetary Sciences* 5, 65-110.

Richter, A., Wittrock, F., Eisinger, M., and Burrows, J. P., **1998**. GOME observations of tropospheric BrO in northern hemispheric spring and summer 1997. *Geophysical Research Letters* 25, 2683-2686.

Riedel, T. P., *et al.*, **2012**. Nitryl chloride and molecular chlorine in the coastal marine boundary layer. *Environmental Science & Technology* 46, 10463-10470.

Röckmann, T., Kaiser, J., Crowley, J. N., Brenninkmeijer, C. A. M., and Crutzen, P. J., **2001**. The origin of the anomalous or "mass-independent" oxygen isotope fractionation in tropospheric N2O. *Geophysical Research Letters* 28, 503-506.

Roelofs, G.-J. and Lelieveld, J. O. S., **1997**. Model study of the influence of cross-tropopause O3 transports on tropospheric O3 levels. *Tellus* 49, 38-55.

Röthlisberger, R., Hutterli, M. A., Sommer, S., Wolff, E. W., and Mulvaney, R., **2000**. Factors controlling nitrate in ice cores: Evidence from the Dome C deep ice core. *Journal of Geophysical Research-Atmospheres* 105, 20565-20572.

Röthlisberger, R.*, et al.*, **2002**. Nitrate in Greenland and Antarctic ice cores: A detailed description of post-depositional processes. *Annals of Glaciology* 35, 209-216.

Russell, K. M., Galloway, J. N., Macko, S. A., Moody, J. L., and Scudlark, J. R., **1998**. Sources of nitrogen in wet deposition to the Chesapeake Bay region. *Atmospheric Environment* 32, 2453-2465.

Ryerson, T. B.*, et al.*, **2012**. The 2010 California Research at the Nexus of Air Quality and Climate Change (CalNex) field study. *Journal of Geophysical Research-Atmospheres (in review)*.

Saiz-Lopez, A., Chance, K., Liu, X., Kurosu, T. P., and Sander, S. P., **2007a**. First observations of iodine oxide from space. *Geophysical Research Letters* 34.

Saiz-Lopez, A., Mahajan, A. S., Salmon, R. A., Bauguitte, S. J. B., Jones, A. E., Roscoe, H. K., and Plane, J. M. C., **2007b**. Boundary layer halogens in coastal Antarctica. *Science* 317, 348-351.

Saiz-Lopez, A.*, et al.*, **2008**. On the vertical distribution of boundary layer halogens over coastal Antarctica: implications for O-3, HOx, NOx and the Hg lifetime. *Atmospheric Chemistry and Physics* 8, 887-900.

Sander, R.*, et al.*, **2003**. Inorganic bromine in the marine boundary layer: a critical review. *Atmospheric Chemistry and Physics* 3, 1301-1336.

Sander, R., Rudich, Y., von Glasow, R., and Crutzen, P. J., **1999**. The role of BrNO3 in marine tropospheric chemistry: A model study. *Geophysical Research Letters* 26, 2857-2860.

Santee, M. L.*, et al.*, **1995**. Interhemispheric differences in polar stratospheric HNO3, H2O, ClO, and O3. *Science* 267, 849-852.

Sarwar, G., Simon, H., Bhave, P., and Yarwood, G., **2012**. Examining the impact of heterogeneous nitryl chloride production on air quality across the United States. *Atmospheric Chemistry and Physics* 12, 6455-6473.

Saurer, M., Cherubini, P., Ammann, M., De Cinti, B., and Siegwolf, R., **2004**. First detection of nitrogen from NOx in tree rings: A N-15/N-14 study near a motorway. *Atmospheric Environment* 38, 2779-2787.

Savarino, J., Alexander, B., Darmohusodo, V., and Thiemens, M. H., **2001**. Sulfur and oxygen isotope analysis of sulfate at micromole levels using a pyrolysis technique in a continuous flow system. *Analytical Chemistry* 73, 4457-4462.

Savarino, J., Bekki, S., Cole-Dai, J. H., and Thiemens, M. H., **2003**. Evidence from sulfate mass independent oxygen isotopic compositions of dramatic changes in

atmospheric oxidation following massive volcanic eruptions. *Journal of Geophysical Research-Atmospheres* 108.

Savarino, J., Bhattacharya, S. K., Morin, S., Baroni, M., and Doussin, J. F., **2008**. The NO+O3 reaction: A triple oxygen isotope perspective on the reaction dynamics and atmospheric implications for the transfer of the ozone isotope anomaly. *Journal of Chemical Physics* 128.

Savarino, J., Kaiser, J., Morin, S., Sigman, D. M., and Thiemens, M. H., **2007**. Nitrogen and oxygen isotopic constraints on the origin of atmospheric nitrate in coastal Antarctica. *Atmospheric Chemistry and Physics* 7, 1925-1945.

Savarino, J., Lee, C. C. W., and Thiemens, M. H., **2000**. Laboratory oxygen isotopic study of sulfur (IV) oxidation: Origin of the mass-independent oxygen isotopic anomaly in atmospheric sulfates and sulfate mineral deposits on Earth. *Journal of Geophysical Research-Atmospheres* 105, 29079-29088.

Savarino, J.*, et al.*, **2013**. Bromine chemistry in a tropical marine boundary layer (Cape Verde) revealed by the stable isotope ratios of atmospheric nitrate. *Proceedings of the National Academy of Sciences of the United States of America (in press)*.

Savarino, J. and Thiemens, M. H., **1999**. Mass-independent oxygen isotope (O-16, O-17, O-18) fractionation found in H-x, O-x reactions. *Journal of Physical Chemistry* 103, 9221-9229.

Schueler, B., Morton, J., and Mauersberger, K., **1990**. Measurement of isotopic abundances in collected stratospheric ozone samples. *Geophysical Research Letters* 17, 1295-1298.

Seinfeld, J. H. and Pandis, S. N., **2006**. *Atmospheric Chemistry and Physics: From Air Pollution to Climate Change*. Wiley Interscience, New York.

Shaheen, R., Abramian, A., Horn, J., Dominguez, G., Sullivan, R., and Thiemens, M. H., **2010**. Detection of oxygen isotopic anomaly in terrestrial atmospheric carbonates and its implications to Mars. *Proceedings of the National Academy of Sciences of the United States of America* 107, 20213-20218.

Sharma, H. D., Jervis, R. E., and Wong, K. Y., **1970**. Isotopic exchange reactions in nitrogen oxides. *Journal of Physical Chemistry* 74, 923-933.

Sigg, A. and Neftel, A., **1991**. Evidence for a 50-percent increase in H2O2 over the past 200 years from a Greenland ice core. *Nature* 351, 557-559.

Sigman, D. M., Casciotti, K. L., Andreani, M., Barford, C., Galanter, M., and Böhlke, J. K., **2001**. A bacterial method for the nitrogen isotopic analysis of nitrate in seawater and freshwater. *Analytical Chemistry* 73, 4145-4153.

Sillman, S., **1999**. The relation between ozone, NOx and hydrocarbons in urban and polluted rural environments. *Atmospheric Environment* 33, 1821-1845.

Silva, S. R., Kendall, C., Wilkison, D. H., Ziegler, A. C., Chang, C. C. Y., and Avanzino, R. J., **2000**. A new method for collection of nitrate from fresh water and the analysis of nitrogen and oxygen isotope ratios. *Journal of Hydrology* 228, 22-36.

Simpson, W. R.*, et al.*, **2007**. Halogens and their role in polar boundary-layer ozone depletion. *Atmospheric Chemistry and Physics* 7, 4375-4418.

Snape, C. E., Sun, C. G., Fallick, A. E., Irons, R., and Haskell, J., **2003**. Potential of stable nitrogen isotope ratio measurements to resolve fuel and thermal NOx in coal combustion. *Abstracts of Papers of the American Chemical Society* 225, U843-U843.

Sofen, E. D., Alexander, B., and Kunasek, S. A., **2011**. The impact of anthropogenic emissions on atmospheric sulfate production pathways, oxidants, and ice core Delta O-17(SO42-). *Atmospheric Chemistry and Physics* 11, 3565-3578.

Solomon, S., **1990**. Progress towards a quantitative understanding of antarctic ozone depletion. *Nature* 347, 347-354.

Solomon, S., **1999**. Stratospheric ozone depletion: A review of concepts and history. *Reviews of Geophysics* 37, 275-316.

Sommariva, R.*, et al.*, **2009**. Radicals in the marine boundary layer during NEAQS 2004: a model study of day-time and night-time sources and sinks. *Atmospheric Chemistry and Physics* 9, 3075-3093.

Staffelbach, T., Neftel, A., Stauffer, B., and Jacob, D., **1991**. A record of the atmospheric methane sink from formaldehyde in polar ice cores. *Nature* 349, 603-605.

Stark, H.*, et al.*, **2007**. Influence of nitrate radical on the oxidation of dimethyl sulfide in a polluted marine environment. *Journal of Geophysical Research-Atmospheres* 112.

Stehr, J., Krankowsky, D., and Mauersberger, K., **1996**. Collection and analysis of atmospheric ozone samples. *Journal of Atmospheric Chemistry* 24, 317-325.

Stohl, A.*, et al.*, **2003**. Stratosphere-troposphere exchange: A review, and what we have learned from STACCATO. *Journal of Geophysical Research-Atmospheres* 108.

Thiemens, M. H., **1999**. Mass-independent isotope effects in planetary atmospheres and the early solar system. *Science* 283, 341-345.

Thiemens, M. H., **2006**. History and applications of mass-independent isotope effects. *Annual Review of Earth and Planetary Sciences* 34, 217-262.

Thiemens, M. H. and Heidenreich, J. E., **1983**. The mass-independent fractionation of oxygen - a novel isotope effect and its possible cosmochemical implications. *Science* 219, 1073-1075.

Thiemens, M. H. and Jackson, T., **1987**. Production of isotopically heavy ozone by ultraviolet-light photolysis of O2. *Geophysical Research Letters* 14, 624-627.

Thiemens, M. H. and Jackson, T., **1988**. New experimental evidence for the mechanism for production of isotopically heavy O3. *Geophysical Research Letters* 15, 639-642.

Thiemens, M. H. and Jackson, T., **1990**. Pressure dependency for heavy isotope enhancement in ozone formation. *Geophysical Research Letters* 17, 717-719.

Thiemens, M. H., Jackson, T. L., and Brenninkmeijer, C. A. M., **1995**. Observation of a mass-independent oxygen isotopic composition in terrestrial stratospheric CO2, the link to ozone chemistry, and the possible occurrence in the martian atmosphere. *Geophysical Research Letters* 22, 255-257.

Thomas, J. L.*, et al.*, **2012**. Modeling chemistry in and above snow at Summit, Greenland - Part 2: Impact of snowpack chemistry on the oxidation capacity of the boundary layer. *Atmospheric Chemistry and Physics* 12, 6537-6554.

Thompson, A. M., **1992**. The oxidizing capacity of the earths atmosphere - probable past and future changes. *Science* 256, 1157-1165.

Thompson, A. M., Chappellaz, J. A., Fung, I. Y., and Kucsera, T. L., **1993**. The atmospheric CH4 increase since the last glacial maximum, 2: Interactions with oxidants. *Tellus* 45B, 242-257.

Thompson, A. M. and Cicerone, R. J., **1986**. Atmospheric CH4, CO and OH from 1860 to 1985. *Nature* 321, 148-150.

Thompson, A. M.*, et al.*, **2003**. Southern Hemisphere Additional Ozonesondes (SHADOZ) 1998-2000 tropical ozone climatology - 2. Tropospheric variability and the zonal wave-one. *Journal of Geophysical Research-Atmospheres* 108.

Thornton, J. A.*, et al.*, **2010**. A large atomic chlorine source inferred from mid-continental reactive nitrogen chemistry. *Nature* 464, 271-274.

Udisti, R.*, et al.*, **2012**. Sea spray aerosol in central Antarctica. Present atmospheric behaviour and implications for paleoclimatic reconstructions. *Atmospheric Environment* 52, 109-120.

Urey, H. C., **1947**. The thermodynamic properties of isotopic substances. *Journal of the Chemical Society*, 562-581.

Urey, H. C., Brickwedde, F. G., and Murphy, G. M., **1932**. A hydrogen isotope of mass 2. *Physical Review* 39, 164-165.

Van Allen, R., Liu, X., and Murcray, F. J., **1995**. Seasonal variation of atmospheric nitric acid over the South Pole in 1992. *Geophysical Research Letters* 22, 49-52.

van der A, R. J.*, et al.*, **2008**. Trends, seasonal variability and dominant NO(x) source derived from a ten year record of NO(2) measured from space. *Journal of Geophysical Research-Atmospheres* 113.

VanHaver, P., DeMuer, D., Beekmann, M., and Mancier, C., **1996**. Climatology of tropopause folds at midlatitudes. *Geophysical Research Letters* 23, 1033-1036.

Vingarzan, R., **2004**. A review of surface ozone background levels and trends. *Atmospheric Environment* 38, 3431-3442.

Virkkula, A.*, et al.*, **2006a**. Chemical composition of boundary layer aerosol over the Atlantic Ocean and at an Antarctic site. *Atmospheric Chemistry and Physics* 6, 3407-3421.

Virkkula, A.*, et al.*, **2006b**. Chemical size distributions of boundary layer aerosol over the Atlantic Ocean and at an Antarctic site. *Journal of Geophysical Research-Atmospheres* 111.

Vogt, R., Crutzen, P. J., and Sander, R., **1996**. A mechanism for halogen release from sea-salt aerosol in the remote marine boundary layer. *Nature* 383, 327-330.

Voigt, C.*, et al.*, **2000**. Nitric acid trihydrate (NAT) in polar stratospheric clouds. *Science* 290, 1756-1758.

Wagenbach, D., Legrand, M., Fischer, H., Pichlmayer, F., and Wolff, E. W., **1998**. Atmospheric near-surface nitrate at coastal Antarctic sites. *Journal of Geophysical Research-Atmospheres* 103, 11007-11020.

Wagner, N. L., Dube, W. P., Washenfelder, R. A., Young, C. J., Pollack, I. B., Ryerson, T. B., and Brown, S. S., **2011**. Diode laser-based cavity ring-down instrument for NO(3), N(2)O(5), NO, NO(2) and O(3) from aircraft. *Atmospheric Measurement Techniques* 4, 1227-1240.

Wagner, N. L.*, et al.*, **2012**. The sea breeze / land breeze circulation in Los Angeles and its influence on nitryl chloride production in this region. *Journal of Geophysical Research-Atmospheres (in review)*.

Wang, Y. H., Choi, Y., Zeng, T., Davis, D., Buhr, M., Huey, L. G., and Neff, W., **2007**. Assessing the photochemical impact of snow NOx emissions over Antarctica during ANTCI 2003. *Atmospheric Environment* 41, 3944-3958.

Wang, Y. H. and Jacob, D. J., **1998**. Anthropogenic forcing on tropospheric ozone and OH since preindustrial times. *Journal of Geophysical Research-Atmospheres* 103, 31123-31135.

Wankel, S. D., Chen, Y., Kendall, C., Post, A. F., and Paytan, A., **2010**. Sources of aerosol nitrate to the Gulf of Aqaba: Evidence from delta N-15 and delta O-18 of nitrate and trace metal chemistry. *Marine Chemistry* 120, 90-99.

Wen, J. and Thiemens, M. H., **1990**. An apparent new isotope effect in a molecular decomposition and implications for nature. *Chemical Physics Letters* 172, 416-420.

Wen, J. and Thiemens, M. H., **1991**. Experimental and theoretical-study of isotope effects on ozone decomposition. *Journal of Geophysical Research-Atmospheres* 96, 10911-10921.

Wen, J. and Thiemens, M. H., **1993**. Multi-isotope study of the O((1)D)+CO2 exchange and stratospheric consequences. *Journal of Geophysical Research-Atmospheres* 98, 12801-12808.

Wendler, G. and Kodama, Y., **1984**. On the climate of Dome C, Antarctica, in relation to its geographical setting. *Journal of Climatology* 4, 495-508.

Werner, R. A. and Brand, W. A., **2001**. Referencing strategies and techniques in stable isotope ratio analysis. *Rapid Communications in Mass Spectrometry* 15, 501-519.

Weston, R. E., **1999**. Anomalous or mass-independent isotope effects. *Chemical Reviews* 99, 2115-2136.

Widory, D., **2007**. Nitrogen isotopes: Tracers of origin and processes affecting PM10 in the atmosphere of Paris. *Atmospheric Environment* 41, 2382-2390.

Williams, E. J., Fehsenfeld, F. C., Jobson, B. T., Kuster, W. C., Goldan, P. D., Stutz, J., and McCleanny, W. A., **2006**. Comparison of ultraviolet absorbance, chemiluminescence, and DOAS instruments for ambient ozone monitoring. *Environmental Science & Technology* 40, 5755-5762.

Wolff, E. W., Jones, A. E., Bauguitte, S. J. B., and Salmon, R. A., **2008**. The interpretation of spikes and trends in concentration of nitrate in polar ice cores, based on evidence from snow and atmospheric measurements. *Atmospheric Chemistry and Physics* 8, 5627-5634.

Wolff, E. W., Jones, A. E., Martin, T. J., and Grenfell, T. C., **2002**. Modelling photochemical NOX production and nitrate loss in the upper snowpack of Antarctica. *Geophysical Research Letters* 29.

Wood, R. and Bretherton, C. S., **2004**. Boundary layer depth, entrainment, and decoupling in the cloud-capped subtropical and tropical marine boundary layer. *Journal of Climate* 17, 3576-3588.

Xue, D. M., De Baets, B., Vermeulen, J., Botte, J., Van Cleemput, O., and Boeckx, P., **2010**. Error assessment of nitrogen and oxygen isotope ratios of nitrate as determined via the bacterial denitrification method. *Rapid Communications in Mass Spectrometry* 24, 1979-1984.

Yeatman, S. G., Spokes, L. J., Dennis, P. F., and Jickells, T. D., **2001**. Can the study of nitrogen isotopic composition in size-segregated aerosol nitrate and ammonium be used to investigate atmospheric processing mechanisms? *Atmospheric Environment* 35, 1337-1345.

Yung, Y. L., Demore, W. B., and Pinto, J. P., **1991**. Isotopic exchange between carbon-dioxide and ozone via O(1D) in the stratosphere. *Geophysical Research Letters* 18, 13-16.

Yung, Y. L., Lee, A. Y. T., Irion, F. W., DeMore, W. B., and Wen, J., **1997**. Carbon dioxide in the atmosphere: Isotopic exchange with ozone and its use as a tracer in the middle atmosphere. *Journal of Geophysical Research-Atmospheres* 102, 10857-10866.

Zahn, A., Franz, P., Bechtel, C., Grooss, J. U., and Rockmann, T., **2006**. Modelling the budget of middle atmospheric water vapour isotopes. *Atmospheric Chemistry and Physics* 6, 2073-2090.

Zanis, P., Ganser, A., Zellweger, C., Henne, S., Steinbacher, M., and Staehelin, J., **2007**. Seasonal variability of measured ozone production efficiencies in the lower free troposphere of Central Europe. *Atmospheric Chemistry and Physics* 7, 223-236.

Zhang, J. S., Miau, T. T., and Lee, Y. T., **1997**. Crossed molecular beam study of the reaction Br+O-3. *Journal of Physical Chemistry* 101, 6922-6930.

Zhang, R. Y., Lei, W. F., Tie, X. X., and Hess, P., **2004**. Industrial emissions cause extreme urban ozone diurnal variability. *Proceedings of the National Academy of Sciences of the United States of America* 101, 6346-6350.

Zhou, X. L., Beine, H. J., Honrath, R. E., Fuentes, J. D., Simpson, W., Shepson, P. B., and Bottenheim, J. W., **2001**. Snowpack photochemical production of HONO: a major source of OH in the Arctic boundary layer in springtime. *Geophysical Research Letters* 28, 4087-4090.

Summary of activities

This section aims to present succinctly the scientific and academic activities I have pursued during the three years of my doctoral work.

Publications

During the course of this thesis, I have contributed to five scientific articles that have been published or accepted by the date of the defense:

Erbland, J., **Vicars, W. C.**, Savarino, J., Morin, S., Frosini, D., Frey, M. M., Vince,E. and Martins, J. M. F., **2013**. Air-snow transfer of nitrate on the East Antarctic plateau, Part 1: Isotopic evidence for a photolytically driven dynamic equilibrium. *Atmospheric Chemistry and Physics* **(in press)**.

Savarino, J., Morin, S., Erbland, J., Grannec, F., Patey, M. D., **Vicars, W. C.**, Alexander, B., and Achterberg, E. P., 2013. Isotopic composition of atmospheric nitrate in a tropical marine boundary layer. *Proceedings of the National Academy of Sciences of the United States of America* (**in press**).

Vicars, W. C., Bhattacharya, S. K., Erbland, J., and Savarino, J., **2012**. Measurement of the ^{17}O-excess (Δ^{17}O) of tropospheric ozone using a nitrite-coated filter. *Rapid Communications in Mass Spectrometry* 26, 1219-1231.

Berhanu, T. A., Savarino, J., Bhattacharya, S. K., and **Vicars, W. C.**, **2012**. ^{17}O-excess transfer during the $NO_2 + O_3 \rightarrow NO_3 + O_2$ reaction. *Journal of Chemical Physics* 136, 044311.

Vicars, W. C., Morin, S., Savarino, J., Wagner, N. L., Erbland, J., Vince, E., Martins, J. M. F., Lerner, B. M., Williams, E. J., and Brown, S. S., Spatial and diurnal variability in reactive nitrogen oxide chemistry as reflected in the isotopic

composition of atmospheric nitrate: Results from the CalNex 2010 field study. *Journal of Geophysical Research-Atmospheres* **(accepted)**.

Three additional manuscripts are in preparation for submission:

Vicars, W. C. and Savarino, J., The role of combined $^{15}N/^{14}N$ measurements in the nitrite-coated filter method: Ambient measurements of the ^{17}O-excess of ozone from 50 °S to 50 °N in the Atlantic marine boundary layer. *Rapid Communications in Mass Spectrometry* **(to be submitted)**.

Vicars, W. C. and Savarino, J., Quantitative constraints on the ^{17}O-excess ($\Delta^{17}O$) signature of surface ozone. *Geophysical Research Letters* **(to be submitted)**.

Savarino, J., **Vicars, W. C.**, Erbland, J., Preunkert, S., Jourdain, B., Kukui, A., Frey, M. M., Gil, J. E., and Legrand, M. Isotopic composition of atmospheric nitrate at Dome C, Antarctica: Results from the OPALE 2011 - 2012 field study. *Journal of Geophysical Research-Atmospheres* **(to be submitted)**.

Conferences

During the course of this thesis, I have attended several informal meetings and international scientific conferences, which are listed below along with the my first author contributions:

American Geophysical Union Fall Meeting, San Francisco, December 2012
Vicars, W. C., Morin, S., Wagner, N. L., Savarino, J., Erbland, J., Brown, S. S., and Williams, E. J., Diurnal variations in the isotopic composition of atmospheric nitrate in coastal California: $\Delta^{17}O$ and $\delta^{15}N$ as tracers of daytime and nighttime nitrogen oxide chemistry (**oral presentation**).

6th International Symposium on Isotopomers, Washington, D. C., June 2012
Vicars, W. C., Bhattacharya, S.K., Erbland, J., and Savarino, J., Spatial and temporal variability in the ^{17}O-excess ($\Delta^{17}O$) of surface ozone: Ambient

measurements using the nitrite-coated filter method (**oral presentation**).

10th Informal Conference on Atmospheric and Molecular Science, Copenhagen, June 2011
Vicars, W. C., Bhattacharya, S. K., Erbland, J., and Savarino, J., Measurement of the oxygen isotope anomaly ($\Delta^{17}O$) of tropospheric ozone using a nitrite-coated filter (**oral presentation**).

Comité National Français des Recherches Arctiques et Antarctiques 7èmes Journées Scientifiques, Paris, May 2011
Vicars W. C., Erbland, J., and Savarino, J., Comprehensive isotopic composition of nitrate in the Antarctic atmosphere and surface snow: Towards interpretation of the polar ice core record (**oral presentation**).

European Geosciences Union General Assembly, Vienna, April 2011
Vicars, W. C., Bhattacharya, S. K., Erbland, J., and Savarino, J., Measurement of the oxygen isotope anomaly ($\Delta^{17}O$) of tropospheric ozone using a nitrite-coated filter (**oral presentation**).
Vicars W. C., Erbland, J., and Savarino, J., Comprehensive isotopic composition of nitrate in Antarctic snow and atmospheric aerosol samples: Towards interpretation of the polar ice core record (**poster**).

Summer Schools

During the course of this thesis, I have attended three summer schools:

European Research Course on Atmospheres (ERCA), Grenoble, Jan. - Feb. 2011
INTRAMIF Summer School "Science and Society," Paris, Aug. 2011
INTRAMIF Summer School on Mass Independent Isotope Fractionation (MIF), Norwich, Aug. 2010